

THE NATURE OF FLUIDS IN HYDROTHERMAL  
COPPER AND MOLYBDENUM ORE DEPOSITS

An experimental and analytical study

**Dissertation**

zur Erlangung der Würde eines  
Doktors der Naturwissenschaften  
- Dr. rer. nat. -

der Fakultät für Biologie, Chemie und Geowissenschaften  
der Universität Bayreuth

vorgelegt von

**Mag. rer. nat. Linda Lerchbaumer**

aus Mallnitz (Österreich)

Bayreuth, Mai 2012

Die vorliegende Arbeit wurde von September 2008 bis Mai 2012 am Bayerischen Geoinstitut, Universität Bayreuth unter der Leitung von Dr. Andreas Audétat und Prof. Dr. Hans Keppler angefertigt.

Vollständiger Abdruck der von der Fakultät für Chemie, Biologie und Geowissenschaften der Universität Bayreuth genehmigten Dissertation zur Erlangung des Grades eines Doktors der Naturwissenschaften (Dr. rer. nat.).

Einreichung der Dissertation am 11. Mai 2012

Zulassung durch die Promotionskommission am 16. Mai 2012

Tag des wissenschaftlichen Kolloquiums: 6. August 2012

Prüfungsausschuss:

*Prof. Dr. J. Brey (Vorsitzender)*

*Prof. Dr. H. Keppler (1. Gutachter)*

*Prof. Dr. F. Seifert (2. Gutachter)*

*Prof. Dr. T. Katsura*

*Prof. Dr. B. Planer-Friedrich*

*Für*  
*meine Familie*



## TABLE of CONTENTS

ABSTRACT.....	H
ZUSAMMENFASSUNG .....	J
<b>1 INTRODUCTION.....</b>	<b>12</b>
1.1 PORPHYRY ORE DEPOSITS .....	12
1.1.1 <i>Tectonic setting and classification</i> .....	12
1.1.2 <i>Geometry of porphyry deposits</i> .....	13
1.1.2.1 Mineralization and hydrothermal alteration.....	15
1.1.3 <i>Porphyry Cu deposits</i> .....	16
1.1.4 <i>Granite-related (porphyry) Mo deposits</i> .....	17
1.1.5 <i>The role of sulfur</i> .....	20
1.1.6 <i>The source magma</i> .....	22
1.1.6.1 The partitioning of Cu and Mo between melt and fluid.....	26
1.1.7 <i>The magmatic-hydrothermal fluid</i> .....	27
1.1.8 <i>Metal transport and deposition of Cu and Mo</i> .....	31
1.2 GENETIC MODEL .....	34
1.3 OPEN QUESTIONS AND SCOPE OF THIS THESIS .....	36
1.3.1 <i>Porphyry Cu deposits</i> .....	36
1.3.2 <i>Granite-related Mo deposits</i> .....	37
<b>2 EXPERIMENTAL AND ANALYTICAL METHODS.....</b>	<b>39</b>
2.1 HYDROTHERMAL EXPERIMENTS .....	39
2.1.1 <i>Design of experiments</i> .....	39
2.1.2 <i>Starting material</i> .....	40
2.1.3 <i>Preparation of sample capsules</i> .....	40
2.1.4 <i>Cold-seal pressure vessels</i> .....	42
2.2 ANALYTICAL METHODS.....	44
2.2.1 <i>Optical microscopy</i> .....	44
2.2.2 <i>Microthermometry</i> .....	45
2.2.3 <i>Raman Spectroscopy</i> .....	48
2.2.4 <i>LA-ICP-MS</i> .....	50
<b>3 RESULTS AND DISCUSSION .....</b>	<b>53</b>
3.1 CU PARTITIONING BETWEEN VAPOR AND BRINE.....	53
3.2 RE-EQUILIBRATION OF SYNTHETIC FLUID INCLUSIONS.....	54
3.3 RE-EQUILIBRATION OF NATURAL FLUID INCLUSIONS .....	57
3.4 COMPOSITION OF MELTS AND FLUIDS IN MO-MINERALIZED GRANITES .....	59
<b>4 REFERENCES .....</b>	<b>64</b>
<b>5 LIST OF MANUSCRIPTS AND STATEMENT OF THE AUTHOR' S CONTRIBUTION .....</b>	<b>79</b>

<b>6</b>	<b>MANUSCRIPTS .....</b>	<b>80</b>
6.1	THE 'QUARTZ CAPSULE' – A NEW METHOD TO AVOID ALLOYING PROBLEMS WITH NOBLE METAL CAPSULES IN HYDROTHERMAL EXPERIMENTS.....	80
6.1.1	<i>Abstract</i> .....	80
6.1.2	<i>Introduction</i> .....	81
6.1.3	<i>Methods</i> .....	83
6.1.4	<i>Results</i> .....	86
6.1.5	<i>Concluding Remarks</i> .....	98
6.1.6	<i>Acknowledgements</i> .....	99
6.1.7	<i>References</i> .....	99
6.2	HIGH CU CONCENTRATIONS IN VAPOR-TYPE FLUID INCLUSIONS: AN ARTIFACT? .....	103
6.2.1	<i>Abstract</i> .....	103
6.2.2	<i>Introduction</i> .....	104
6.2.3	<i>Methods</i> .....	106
6.2.3.1	Experimental procedure .....	106
6.2.3.2	Raman spectroscopy.....	108
6.2.3.3	Microthermometry .....	109
6.2.3.4	Laser Ablation-Inductively Coupled Plasma-Mass Spectrometry .....	109
6.2.4	<i>Results and Discussion</i> .....	110
6.2.4.1	Regular vapor-brine partitioning experiments .....	110
6.2.4.1.1	Reproduction of Nagaseki and Hayashi's (2008) experiments .....	110
6.2.4.1.2	New vapor-brine partitioning experiments.....	119
6.2.4.2	Re-equilibration experiments.....	120
6.2.4.3	Equilibration of a natural sample from the Erongo Granite.....	126
6.2.4.4	Diffusion of Cu <sup>+</sup> at lower temperatures .....	129
6.2.5	<i>Implications for porphyry Cu ore formation</i> .....	131
6.2.6	<i>Acknowledgements</i> .....	133
6.2.7	<i>References</i> .....	134
6.3	THE METAL CONTENT OF SILICATE MELTS AND AQUEOUS FLUIDS IN SUB-ECONOMICALLY MO-MINERALIZED GRANITES: IMPLICATIONS FOR PORPHYRY MO GENESIS.....	140
6.3.1	<i>Abstract</i> .....	140
6.3.2	<i>Introduction</i> .....	141
6.3.3	<i>Samples</i> .....	142
6.3.3.1	Treasure Mountain Dome (Colorado, USA).....	143
6.3.3.2	Drammen granite (Norway) .....	145
6.3.3.3	Glitrevann granite (Norway).....	148
6.3.4	<i>Methods</i> .....	149
6.3.4.1	Microthermometry .....	149
6.3.4.2	Raman spectroscopy.....	150
6.3.4.3	Laser ablation-inductively coupled-mass spectrometry .....	150
6.3.4.4	Re-equilibration experiments.....	151
6.3.5	<i>Results</i> .....	152
6.3.5.1	Treasure Mountain Dome.....	152
6.3.5.2	Drammen granite .....	158
6.3.5.3	Glitrevann granite.....	166

6.3.5.4	Re-equilibration of fluid inclusions from the Drammen granite .....	166
6.3.6	<i>Comparison with other intrusions</i> .....	170
6.3.6.1	Molybdenum concentrations in silicate melts.....	170
6.3.6.2	Metal concentrations in magmatic fluids.....	173
6.3.6.3	Size, depth, and structure of magma chambers .....	176
6.3.7	<i>Summary and conclusions</i> .....	182
6.3.8	<i>Acknowledgements</i> .....	184
6.3.9	<i>References</i> .....	184
6.4	RAPID NA, CU EXCHANGE BETWEEN SYNTHETIC FLUID INCLUSIONS AND EXTERNAL AQUEOUS SOLUTIONS: EVIDENCE FROM LA-ICP-MS ANALYSIS .....	193
6.4.1	<i>Abstract</i> .....	193
6.4.2	<i>Introduction</i> .....	194
6.4.3	<i>Experimental and analytical methods</i> .....	195
6.4.4	<i>Results</i> .....	197
6.4.5	<i>Discussion</i> .....	201
6.4.5.1	Accuracy of LA-ICP-MS quantification.....	201
6.4.5.2	Cu, Na diffusion in primary fluid inclusions .....	202
6.4.6	<i>Implications</i> .....	205
6.4.7	<i>Conclusions</i> .....	207
6.4.8	<i>Acknowledgements</i> .....	207
6.4.9	<i>References</i> .....	208
<b>ACKNOWLEDGEMENTS</b> .....		<b>CCXI</b>
<b>ERKLÄRUNG</b> .....		<b>CCXII</b>

## ABSTRACT

The evolution of magmatic-hydrothermal fluids in porphyry Cu and porphyry Mo deposits was studied using synthetic and natural fluid inclusions by optical microscopy, microthermometry, Raman spectroscopy, and LA-ICP-MS.

The partitioning of Cu between vapor and brine in aqueous NaCl-S ± KCl ± FeCl<sub>2</sub>-rich fluids was investigated by means of hydrothermal experiments in rapid quench autoclaves at 600–800°C, 70–130 MPa and at both oxidizing and reducing fO<sub>2</sub>, covering all geologically relevant conditions. Resulting partition coefficients ( $D_{\text{Cu}^{\text{vap/brine}}}$ ) are between 0.2 and 0.4 for the range of studied S-concentrations, fluid pH, fO<sub>2</sub>, and P-T conditions. These values indicate that Cu does not partition into the vapor phase at any plausible condition in contrast to data from natural quartz-hosted vapor and brine inclusions which appear to indicate Cu enrichment in the vapor.

The formation of such Cu-rich vapor-type fluid inclusions was investigated in hydrothermal re-equilibration experiments. For this purpose, coexisting vapor and brine inclusions of known composition were re-equilibrated in a fluid of slightly different composition and lower pH than the trapped one at 800°C, 70–130 MPa. This procedure led to a dramatic increase in Cu concentrations in the vapor phase from  $0.3 \pm 0.03$  to  $5.7 \pm 3.3$  wt% after re-equilibration and the change of  $D_{\text{Cu}^{\text{vap/brine}}}$  from a true value of  $0.4 \pm 0.05$  to an apparent value of  $8.3 \pm 4.9$ . This post-entrapment modification can be traced back to the difference in fluid pH between the trapped and the surrounding fluid, inducing diffusion of H<sup>+</sup> out of the inclusion and the diffusion of Cu<sup>+</sup> (and Na<sup>+</sup>, Ag<sup>+</sup>) into the inclusion in order to maintain charge balance. Moreover, the presence of larger amounts of S within vapor inclusions as compared to brine inclusions can bind larger amounts of Cu. The re-equilibration of trails of vapor and brine inclusions in a natural quartz sample in a fluid similar to the trapped one, yet more acidic, showed that this modification process can be reversed, resulting in the loss of major amounts of Cu from natural vapor inclusions.

The composition of metal-bearing melts and magmatic fluids of Mo-mineralized granites resembling porphyry Mo deposits was investigated using natural melt-, fluid-, and solid-inclusions in quartz crystals found in miarolitic cavities from minor Mo-occurrences in Colorado and Norway. Melt inclusions from the Treasure Mountain Dome are highly H

enriched in Mo (4-43 ppm), also melt inclusions from the Drammen and Glitrevann granites (5-32 ppm, and 12 ppm, respectively), resembling highly fractionated melts. Copper concentrations are low (<1-30 ppm) in the melts, but high in the fluids: intermediate density, supercritical fluid inclusions of these three locations host 6-1900 ppm, 8-3500 ppm, and 5-180 ppm Cu, respectively. The comparison of these results with data from economic porphyry Mo and porphyry Cu (Mo, Au) deposits shows no difference in Mo concentrations in the particular melts and fluids. Hence, other factors probably control the evolution of a granitic intrusion into large, economic Mo deposits, minor Mo occurrences, or just into barren plutons. These may be mainly the size, position, and geometry of the parental magma chamber, the multiplicity of intrusions maintaining a constant flux of metalliferous, S-rich, hot melts, and the extent of fluid focusing within small rock volumes forming high-grade ore shells.

## ZUSAMMENFASSUNG

Magmatisch-hydrothermale Fluide in porphyrischen Kupfer- und Molybdänlagerstätten wurden anhand von synthetischen und natürlichen Flüssigkeitseinschlüssen mit Hilfe von Auf- und Durchlichtmikroskopie, Mikrothermometrie, Raman Spektroskopie und Laser-Ablations-ICP-MS untersucht.

Es wurden Hydrothermal-Experimente in ‚rapid-quench‘ Autoklaven, bei Temperaturen von 600 bis 800°C und Drücken von 70 bis 130 MPa unter sowohl oxidierenden als auch reduzierenden Bedingungen durchgeführt, um die Verteilung von Kupfer zwischen der Dampf- und Flüssigkeitsphase in wässrigen, NaCl-S ± KCl ± FeCl<sub>2</sub>-reichen Fluiden zu studieren. Die gemessenen Dampf/Flüssigkeits-Verteilungskoeffizienten von Kupfer liegen zwischen 0.2 und 0.4, so dass Kupfer unter den simulierten, naturnahen Bedingungen nicht in der Dampfphase angereichert wird. Dieses Resultat steht in klarem Widerspruch zu Daten aus natürlichen Flüssigkeitseinschlüssen in Quarz, die eine Anreicherung von Kupfer in der Dampfphase zeigen.

Die Bildung solch kupferreicher, Dampfphasen-dominiertes Flüssigkeitseinschlüsse wurde in Reequilibrierungs-Experimenten untersucht. Dazu wurden zunächst Einschlüsse der koexistierenden Dampf- und Flüssigkeitsphase bei 800°C, 70-130 MPa synthetisiert und der Inhalt von einigen der entstandenen Einschlüsse analysiert. In einem zweiten Schritt wurden die verbleibenden Einschlüsse in einem neuen Fluid ähnlicher Zusammensetzung, aber mit neutralerem pH-Wert abermals equilibriert. Dadurch stiegen die Kupferkonzentrationen in den Einschlüssen der Dampfphase von  $0.3 \pm 0.03$  auf  $5.7 \pm 3.3$  wt%, was auch eine Modifikation des Verteilungskoeffizienten von Kupfer zur Folge hatte; dieser stieg durch die Reequilibrierung vom ursprünglichen, echten Wert von  $0.4 \pm 0.05$  auf den scheinbaren Wert von  $8.3 \pm 4.9$ . Diese Modifikation des Elementgehalts eigentlich verschlossener Flüssigkeitseinschlüsse kann auf die Diffusion einzelner Ionen durch den Quarz-Wirtskristall zurückgeführt werden: Der pH-Unterschied zwischen dem eingeschlossenen und dem umgebenden Fluid löst eine Wanderung von H<sup>+</sup> aus den Flüssigkeitseinschlüssen aus. Das entstehende Ladungsdefizit wird durch die Diffusion von Cu<sup>+</sup> (und Na<sup>+</sup>, Ag<sup>+</sup>) in die Flüssigkeitseinschlüsse hinein kompensiert. Hinzu kommt, dass

die Einschlüsse der Dampfphase, im Gegensatz zu Einschlüssen der Flüssigkeit, stark mit Schwefel angereichert sind und dadurch größere Mengen Kupfer binden können. Die Reequilibration natürlicher Dampf- und Flüssigkeitseinschlüsse in einem, dem eingeschlossenen ähnlichen, jedoch deutlich saurerem Fluid zeigte, dass die Diffusion von Kupfer auch wieder rückgängig gemacht werden kann: Ein Großteil des Kupfers, das in der Dampfphase angereichert war, ging verloren.

Die Eigenschaften der metallreichen Schmelzen und Fluide, die zur Bildung porphyrischer Molybdänlagerstätten führten, wurde anhand von natürlichen Schmelz- und Flüssigkeitseinschlüssen aus molybdänreichen Graniten von Colorado und Norwegen untersucht. Schmelzeinschlüsse sowohl des Treasure Mountain Dome, als auch der Drammen und Glitrevann Granite sind Mo-reich (4-43 ppm, 5-32 ppm, und 12 ppm) und stellen stark fraktionierte Schmelzen dar. Die Kupfergehalte der Schmelzen sind eher gering (<1-30 ppm). Die Analyse von Einschlüssen superkritischer magmatischer Fluide mittlerer Dichte ergibt hingegen hohe Kupferwerte für alle drei oben genannten Vorkommen (Treasure Mountain Dome: 6-1900 ppm; Drammen: 8-3500 ppm; Glitrevann: 5-180 ppm). Der Vergleich dieser Ergebnisse von nicht wirtschaftlich nutzbaren Molybdänvorkommen mit Daten porphyrischer Molybdän- und Kupfer-(Molybdän-, Gold-)lagerstätten zeigt, dass sich die Schmelzen und primären Fluide in ihrem Mo-Gehalt nicht unterscheiden. Folglich müssen andere Faktoren ausschlaggebend sein, damit sich eine einfache granitische Intrusion zu einer Molybdänlagerstätte entwickeln kann. Diese Faktoren sind wahrscheinlich die Größe, Lage und Geometrie der ursprünglichen Magmenkammer, die stete Zufuhr heißer, metall- und schwefelreicher Schmelzen und der Grad der Fokussierung von daraus entstandenen metallreichen Fluiden in kleineren Gesteinsvolumina, die zur Bildung hochgradiger Stockwerksvererzungen führen.

# 1 INTRODUCTION

## *1.1 Porphyry ore deposits*

An ore deposit is defined as an accumulation of metalliferous minerals of economic importance whose concentration is rich enough to justify mining. Minor occurrences of ore minerals may contribute to a general understanding of this geologic feature. Magmatic-hydrothermal ore deposits originated from hot (~250-700°C), aqueous solutions, usually a mixture of magmatic and smaller portions of meteoric water that flowed through definite pathways in the Earth's crust, transported metals, and deposited them in localized areas within the crust or close to the surface (e.g. Skinner, 1997).

Porphyry type deposits are linked to tectonic active regions and the subsequent emplacement of granitic rocks within the Earth's crust. The sequestering of metal-rich hydrothermal fluids from these plutons leads to the deposition of high grade Cu and Mo ore within small areas. Porphyry Cu systems supply almost 75% of the world's Cu, 50% of the Mo, ~20% of the Au, most of the Re, and minor amounts of Ag, Pb, Te, Se, Bi, Zn, and Pb (Sillitoe, 2010).

### **1.1.1 Tectonic setting and classification**

Porphyry ore deposits may be classified according to their relation to major tectonic processes that are subduction of oceanic lithosphere and intracontinental rifting. Both ocean-ocean and ocean-continent collisions and subsequent subduction could lead to the formation of porphyry ore deposits. Porphyry deposits within continental arcs are associated with calc-alkaline granodioritic rocks (I-type granites; Ishihara, 1981) and show higher ore grades and larger tonnages of ore as compared to deposits within island arcs, probably due to more intense crustal thickening, which aids the formation of large mid-upper crustal magma chambers (Takada, 1994). A prominent example for the first type is the Bingham Canyon deposit (Utah), for the latter type related to island-arcs the Panguna deposit (Papua New Guinea). These island arc-related deposits in general show higher Au/Cu ratios and lower Mo/Cu (e.g. Richards, 2005). Apart from the primary magma source

and the formation of plutons, other tectonic structures like large fault zones are of major importance as they facilitate the ascent of magma (Clark, 1993; Richards, 2000). Such zones can be found in all major porphyry regions, for example within the Colorado Mineral Belt (Colorado) where Precambrian fault structures were reactivated in the Early Tertiary due to the Laramide orogeny and the formation of the Cordillera in western North America (e.g. Tweto and Sims, 1963).

Rifting processes, on the other hand, often occur in back-arc settings as consequence of previous subduction. Magmas associated with rifting are alkaline and of A-type affinity (e.g. White et al., 1981; Carten et al., 1993) leading to the formation of porphyry Mo deposits which are characterized by a Mo/Cu-ratio greater than 1. Examples are the large deposits at Climax and Henderson (both Colorado, USA) which postdate Laramide subduction and are associated with the formation of the Rio Grande Rift (White et al., 1981; Bookstrom, 1989).

### 1.1.2 Geometry of porphyry deposits

The “parents” of porphyry Cu and Mo systems are large, multiphase batholiths of dioritic to granitic composition which were established ~1-2 Ma before the onset of the intrusion of porphyry stocks (e.g. Dilles and Wright, 1988; Mortensen et al., 1995; Dilles et al., 1997; Deckart et al., 2005; Campbell et al., 2006) at depths of ~5 km (e.g. Sillitoe, 2010; Richards, 2011). But unless a deposit was tilted, no tracks of these parental magma chambers would be visible within the deposit. Some porphyry Cu systems are furthermore associated with calc-alkaline volcanism of intermediate to felsic composition (Sillitoe, 1973) that usually took place 0.5 to 3 Ma prior to stock intrusion as it is recorded at Bingham (Waite et al., 1997). However, erosion usually eliminated all volcanic marks from the surface. Subsurface witnesses of volcanic evolution though could be maar-diatreme complexes. The volcanic activity in total is rather limited as intense explosive eruptions would lead to the loss of metal-rich magmatic volatiles thus hampering the formation of large deposits within the crust (e.g. Sillitoe, 1980; Pasteris, 1996; Cloos, 2001; Richards, 2005).

The center of a porphyry system is formed by the porphyry stock itself which in its ideal shape is elongated and cylindrical (e.g. Seedorff et al., 2005) partly reaching shallow levels

>2 km below the surface (e.g. Richards, 2011), (Figure 1.1). The porphyries are made up of variable amounts of phenocrysts and a fine-grained aplitic groundmass produced by pressure quenching during rapid ascent and loss of volatiles (Burnham, 1967). Along with this main igneous body, magmatic-hydrothermal and phreatic breccias as well as diatremes may occur. Hydrothermal breccias may contain more metals than the surrounding stockwork due to their high permeability. Phreatic breccias on the other hand, are mostly barren because of their late-stage appearance after the main mineralization events (Sillitoe, 2010). Diatremes represent long volcanic vents generated mainly by phreatomagmatic eruptions and usually measure more than 1 km in diameter (e.g. Sillitoe, 1985).

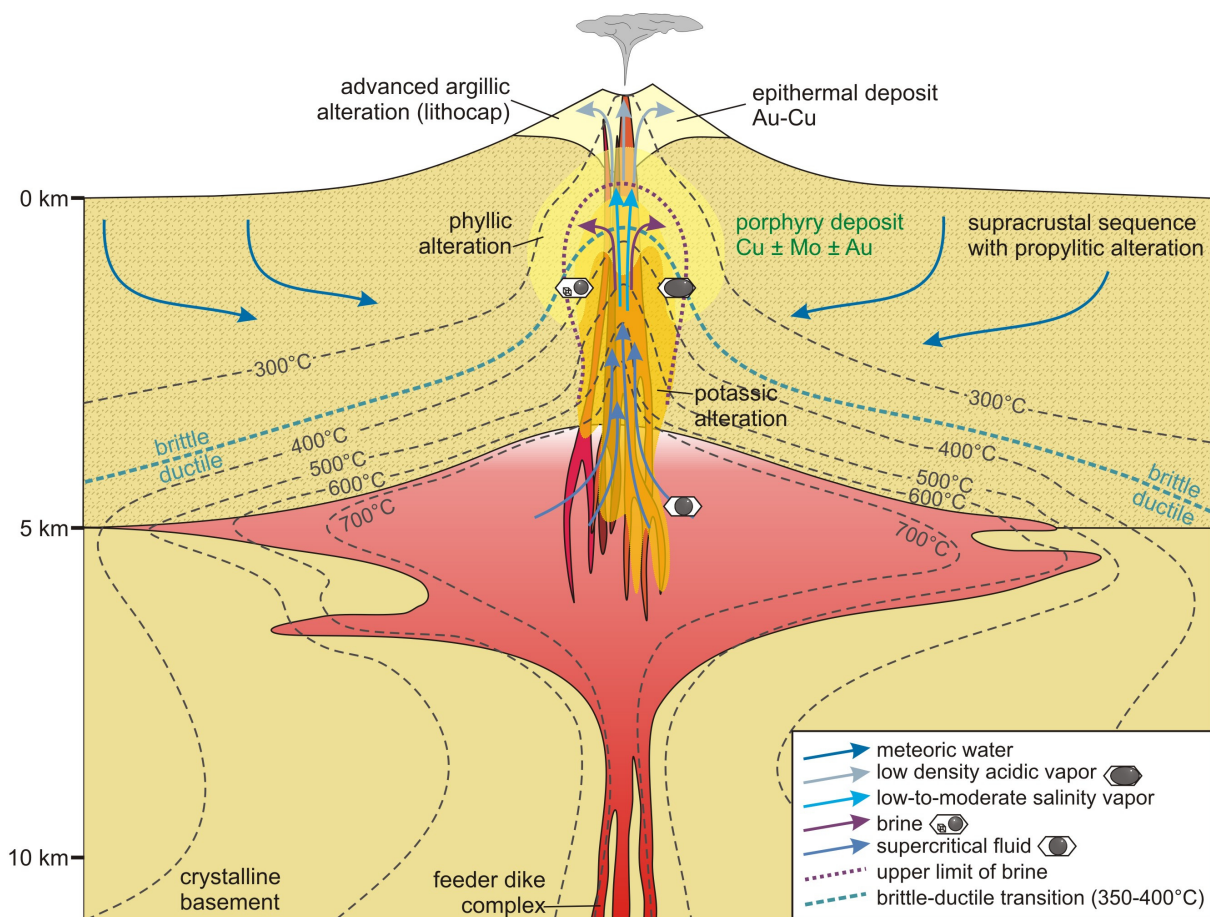


**Figure 1.1**

Idealized section through a porphyry system illustrating the hydrothermal alteration pattern, thermal structure, and fluid flow pathways (modified from Richards, 2011). Fluid evolution starts with a primary single-phase, supercritical fluid at depth, which separates into vapor and brine at the Cu-Mo-porphyry stage and finally reaches the surface in form of low density, acidic vapor leading to the formation of epithermal Au (Cu) deposits.

The majority of ore minerals is concentrated in the so-called stockwork, an intensively cracked area situated on top of the porphyry stock. Such mineralized stockwork breccias are characteristic of all porphyry metal systems (Fournier, 1968; Cunningham, 1978; Westra, 1979).

#### *1.1.2.1 Mineralization and hydrothermal alteration*

One of the most characteristic features of porphyry systems is its alteration pattern affecting large portions of both the host rock and porphyritic stock (Creasey, 1966; Meyer and Hemley, 1967), (Figure 1.1) and the zoning of metals linked to this alteration pattern. An inner zone containing  $\text{Cu} \pm \text{Mo} \pm \text{Au}$  characterizes the potassic and phyllic cores of the system (Sillitoe, 2010). This center is encircled by kilometer-scale halos of  $\text{Zn-Pb-Ag} \pm \text{Mn}$  anomalies. Finally, a zone containing  $\text{Au-As} \pm \text{Sb}$ , which usually is found within the lithocap, follows. This zoning is a result of spatial and temporal differences in metal precipitation from the fluid resulting from changes in fluid temperature.

The two types of alteration with the largest dimensions are propylitic at deeper and phyllic alteration at shallow levels. The different alteration types are from the bottom to the top (i.e. from the oldest to the youngest) potassic, phyllic, propylitic, and advanced argillic (Figure 1.1). Each zone exhibits a specific mineral assemblage due to the characteristic features of the magmatic-hydrothermal fluids causing alteration (Sillitoe, 2010 and references therein): Potassic alteration is indicated by secondary biotite and K-feldspar and a chalcopyrite  $\pm$  bornite assemblage. Phyllic alteration partly overprints older potassic alteration. Within these characteristic pale-green rocks almost all mafic minerals have been transformed to chlorite, plagioclase to sericite, and magnetite to hematite. Additionally, pyrite and chalcopyrite were deposited. Propylitic alteration is characterized by hydration reactions and  $\text{CO}_2$  metasomatism forming chlorite, epidote, and carbonate (e.g. Sillitoe, 2010). Advanced argillic alteration forms the lithocap (Sillitoe, 1995) and is the uppermost, often eroded sequence indicated by clay minerals and alunite. Lithocaps extend to several  $>10 \text{ km}^2$ , partly even  $100 \text{ km}^2$  (Sillitoe, 1995) thus being much larger than the actual deposit below. Where carbonate rocks host porphyry deposits, exoskarns are generated at the contact to the porphyry intrusion.

### 1.1.3 Porphyry Cu deposits

Copper is a pinkish metal that has been of major economic importance for thousands of years. Presently it is mainly used as building material, constituent of various alloys, and as electrical and heat conductor. Copper is found as native Cu or more common, as constituent of minerals like covellite, (CuS), chalcocite (Cu<sub>2</sub>S), chalcopyrite (CuFeS<sub>2</sub>), bornite (Cu<sub>5</sub>FeS<sub>4</sub>), malachite (Cu<sub>2</sub>CO<sub>3</sub>(OH)<sub>2</sub>), azurite (Cu<sub>3</sub>(CO<sub>3</sub>)<sub>2</sub>(OH)<sub>2</sub>), and cuprite (Cu<sub>2</sub>O). Almost 75% of the world's demand for Cu is supplied by porphyry Cu deposits which can be found all over the world, always connected to subduction zones at convergent plate margins, mostly of Mesozoic and Cenozoic age. These collisional regimes comprise both cordilleran and island arc settings, indicated by the large porphyry Cu provinces of western North/South America and Indonesia, respectively (Figure 1.2).



**Figure 1.2**

Sketch map showing the worldwide distribution of porphyry Cu systems (after Sillitoe, 2010). Notice the clear correlation with Mesozoic and Cenozoic orogenic belts in western North and South America, the western Pacific margin, and the Tethyan orogenic belt in eastern Europe and southern Asia.

Well known examples of porphyry Cu deposits are for example the Bingham Canyon deposits in Utah/USA (containing 27.5 megatonnes (Mt) Cu, 0.78 Mt Mo, 1600 t Au, and 17700 t Ag; Krahulec, 1997) and El Teniente/Chile (containing 100 Mt Cu, 1.4 Mt Mo; Skewes et al., 2002). The actual largest known exploitable concentrations of Cu were found in the porphyry deposit at Los Bronces-Río Blanco/Chile containing 203 Mt Cu (Sillitoe,

2010 and references therein). Considering the average concentration of Cu in the Earth's upper crust (28 ppm; Rudnick and Gao, 2003), the mechanism of metal enrichment must have been very efficient.

Porphyry Cu systems are associated with multiphase, I-type granite intrusions (Ishihara, 1981) which are typically metaluminous and medium K calc-alkaline (Seedorff et al., 2005). These intrusions form large mid to upper-crustal magma chambers (Takada, 1994) due to crustal compression and thickening. Extensional settings with typical bimodal basalt-rhyolite magmatism, on the other hand, lack significant porphyry Cu deposits (Sillitoe, 1999; Tosdal and Richards, 2001) but are the ideal tectonic setting for porphyry Mo deposits (see below). Host rocks of porphyry Cu deposits could be any rock type from sedimentary to igneous (e.g. Titley, 1993) indicating that its composition does not influence the mineralization *sensu stricto* at all. However, impermeable, poorly fractured rocks like shales and carbonates could serve as a sealing layer around the porphyritic stock leading to increasing ore grade (e.g. Sillitoe, 1997).

Porphyry Cu systems can consist of several mineralized zones and areas (Sillitoe, 2010): the porphyry Cu  $\pm$  Mo  $\pm$  Au ore body in the center, subepithermal Zn-Cu- Pb  $\pm$  Ag  $\pm$  Au veins, various skarns containing Cu, Au, Zn, and Pb mineralizations, areas of carbonate replacement hosting Zn-Pb-Ag  $\pm$  Au (or Cu), and sediment hosted distal-disseminated Au-As  $\pm$  Sb  $\pm$  Hg mineralization. The shape of the central stockwork mineralization is controlled by the geometry of the intrusion, whereas the development of all other possible orebodies mentioned above depends on the wall-rocks. The uppermost part of a porphyry Cu system comprises the lithocap with its characteristic high sulfidation lodes containing Cu-Au  $\pm$  Ag mineralization.

#### **1.1.4 Granite-related (porphyry) Mo deposits**

Molybdenum is a silver-white metal that is mainly used as additive to steel. The main ore mineral is molybdenite (MoS<sub>2</sub>). Molybdenum deposits can be found all over the world (Figure 1.3), but most of the present Mo production is recovered as a by-product of porphyry Cu deposits. Pure porphyry Mo deposits (i.e. without any recoverable amounts of Cu; Mo/Cu >1; Carten et al., 1993) are rare and limited to the western part of North

America. There, the world's second largest (after porphyry Cu deposits) amounts of Mo were found in just a few deposits hosting 100-1000 Mt Mo with an ore grade of 0.1-0.3 % Mo (Ludington and Plumlee, 2009) with the average Mo concentration of the upper crust being in the range of 1.1 ppm (Rudnick and Gao, 2003).



**Figure 1.3**

Sketch map showing locations of granite-related Mo deposits. Obvious is the relationship of Mo deposits with settings of subduction and intraplate rifting at the west coast of both North and South America (after Carten et al., 1993).

Molybdenum deposits are classified based on the chemistry of the cogenetic igneous phases and detailed structural, crustal, magmatic, and hydrothermal characteristics (Westra and Keith, 1981; Carten et al. 1993) resulting in two major classes, the “*differentiated monzogranite*” and the ‘*high-silica rhyolite-alkalic suite*’. The first comprise deposits that usually occur in continental arcs, which formed from late-stage differentiates of granodiorite-monzogranite or monzonite-monzogranite intrusions. Deposits belonging to this group tend to be closer related to porphyry Cu deposits than to granite Mo deposits (Lowell and Guilbert, 1970) and will not be discussed in detail.

Characteristic features of deposits of the *high-silica rhyolite-alkalic suite* are their location in post-subduction, extensional settings usually within continental rift zones associated with multiphase alkaline magmatism, as well as the special chemical pattern of the associated igneous rocks which are enriched in F, Rb, Nb, as well as Be, Cs, Sn, Li, Th, W indicating a highly fractionated nature (Mutschler et al., 1981; Westra and Keith, 1981).

The *high-silica rhyolite-alkalic suite* can further be subdivided into ‘*Climax-type*’, ‘*transitional*’, and ‘*alkalic*’ deposits whereas the whole supergroup can be considered as a magmatic-hydrothermal continuum (Carten et al., 1993).

*Climax-type* deposits sensu stricto are just the two at Climax and Henderson (Colorado) but due to their unique richness of more than 1 Mt of total Mo and an average ore grade of more than 0.2% Mo, these two deposits are used as a general measure for the classification of porphyry Mo deposits. Climax-type deposits consist of multiple intrusions overlapping each other, like at Henderson where at least eleven events can be distinguished that formed three ore shells (Carten et al., 1988). The shapes of these single igneous bodies resemble large inverted cups, which measure up to 1000 m in diameter (White et al., 1981), with surrounding alteration halos. Another feature characteristic for these large deposits is the depth of magma emplacement being in the order of 2-4 km (e.g. Wallace et al., 1978; Westra and Keith, 1981; Klemm et al., 2008) and the long residence time of the magma in the crust that lead to optimal fractionation and enrichment of Mo in residual fluids. These metal-rich fluids then were concentrated in long cylindrical magma apices (Shinohara et al., 1995) leading to the formation of distinct ore shells. *Transitional deposits* (Carten et al., 1993) are just smaller or show lower grades in ore than the Climax-type deposits, probably due to less fractionation of high-silica rhyolite. They are more related to volcanic complexes with intrusions being partly emplaced after caldera formation. For most transitional deposits there is evidence for faulting, which might have disturbed the ‘calm’ crystallization and fractionation of a huge magma chamber within the crust. The largest difference between Climax-type and transitional deposits is the higher abundance of chalcopyrite ( $\text{CuFeS}_2$ ) in the latter ones. As the ratio of incompatible elements (such as Mo) to compatible elements (like Cu) increases with fractionation (e.g. Audétat, 2010) this might also be an indicator for less evolved fluids in transitional deposits. Climax-type and transitional deposits exclusively formed during a period of intense magmatism (~30-20 Ma; e.g. Bookstrom et al., 1988) in the southwestern USA due to extension towards the end of the Laramide orogeny (~70-35 Ma; e.g. Chapin, 2012), (Figure 1.3).

High-silica rhyolite with significant concentrations of Mo also occurs in co-magmatic association with *alkaline* volcanic and subvolcanic complexes (Carten et al., 1993). Such

deposits can be found all over the world (USA, Greenland, Norway) but their similarities to the textural, compositional, and hydrothermal characteristics of Climax-type deposits are still striking. Alkalic deposits usually formed after caldera formation and involved much smaller amounts of high-silica rhyolite than the transitional ones. Besides these distinctions, alkalic deposits are associated with the same magmatic and hydrothermal features typical of Climax-type deposits; the total of ore tonnage is just smaller (Carten et al., 1993).

### 1.1.5 The role of sulfur

The presence of sulfur in magmatic systems is evident from the occurrence of sulfide minerals in many magma-related ore deposits. This implies that sulfur plays a key role in processes that lead to the enrichment of metals such as Cu and Mo, first in the magma and in hydrothermal fluids and then within a small rock volume forming high-grade ore deposits.

In geologic environments, sulfur occurs in the liquid, solid, and gaseous state. Common oxidation states in near surface reservoirs include  $S^0$ ,  $S^{2-}$ ,  $S^{4+}$ , and  $S^{6+}$ . Most important S-complexes include  $SO_2$  and  $H_2S$ . Sulfur as sulfide and sulfate can coexist in silicate melt and in magmatic-hydrothermal fluids, whereas the sulfide/sulfate-ratio is related to the oxidation state of the reservoir, thus controlling the stability of ore-metal-bearing sulfide minerals (Simon and Ripley, 2011).

The sulfur content of reduced silicate melts may be in the order of a few tens to a few hundred ppm S dissolved as sulfide, whereas oxidized, water rich melts may contain up to 1.5 wt% S in the form of sulfate (Jugo et al., 2005a, b; Jugo 2009). These particularly high concentrations of sulfur have a major influence on the ore-forming potential of a magmatic system. Cooling and compositional changes of a silicate melt lead to the crystallization of a large number of sulfide minerals including bornite ( $Cu_5FeS_4$ ), intermediate solid solution (i.e. the high-temperature, Fe-rich modification of bornite,  $\sim Cu_2Fe_3S_5$ ), and pyrrhotite ( $-FeS$ ), (Simon and Ripley, 2011). The partitioning of metals like Cu and Au between the melt and these sulfide phases strongly depends on  $fO_2$  and  $fS_2$  according to experimental studies (Lynton et al., 1993; Jugo et al., 1999; Simon et al., 2006; Bell et al., 2009). It was

shown that the partitioning of Cu from silicate melt into pyrrhotite for example increases with increasing  $f_{S_2}$  at 100-150 MPa, 800-850°C implying that it is very likely that large amounts of Cu could precipitate as sulfide phases from the magma, possibly being excluded from further transport and deposition at the porphyry level. On the other hand, such a crystallization of metal-rich sulfide phases during the early stages of a magmatic system may lead to a first concentration of ore metals, provided that they re-dissolve and S and metals are still available at a later stage to partition into magmatic-hydrothermal fluids. Such a resorption of sulfides may happen due to auto-oxidation during magma degassing which would change the stable S-species in the melt from reduced to more oxidized (Mathez, 1984; Bell and Simon, 2011).

As was already mentioned above, the concentration of sulfur is much higher in oxidized silicate melts than under reduced conditions with maximum sulfur (as SO<sub>2</sub>) contents at a  $f_{O_2}$  of QFM+2 to QFM+3 (Jugo et al., 2005a; Binder and Keppler, 2011) which is exactly the oxidation state of most porphyry-type ore deposits (e.g. Streck and Dilles, 1998; Audétat and Pettke, 2006; Stern et al., 2007; Chambefort et al., 2008).

The most critical process for the formation of porphyry-type sulfide deposits is the partitioning of sulfur from the melt into magmatic-hydrothermal fluids. Sulfur partition coefficients  $D_{S}^{fluid/melt}$  range between 30 and 500 (Webster and Botcharnikov, 2011 and references therein). Furthermore, experimental results on the partitioning of sulfur between melt and fluid are in line with the striking presence of sulfur in volcanic eruptions (Westrich and Gerlach, 1992; Symonds et al., 1994; Wallace and Gerlach, 1994) and demonstrate that aqueous fluids exsolved from silicate melts (Keppler, 2010). Evidence for the ability of magmatic-hydrothermal fluids to transport large amounts of sulfur comes also from volcanic fumaroles and their S-rich sublimates. In arc environments volcanic gases contain ~90 mol% H<sub>2</sub>O, up to 10 mol% CO<sub>2</sub>, up to 6 mol% SO<sub>2</sub>, and up to 6 mol% HCl (Williams-Jones and Heinrich, 2005; Webster and Mandeville, 2007; Métrich and Wallace, 2008; Oppenheimer et al., 2011). The study of fluid inclusions from prominent porphyry Cu deposits provides further insight into the origin of magmatic-hydrothermal fluids and their S-content: Inclusions with chalcopyrite (CuFeS<sub>2</sub>) daughter crystals were found in the high temperature cores of porphyry Cu deposits suggesting the direct exsolution of the

metalliferous fluid from the melt (Roedder, 1971).

Phase separation of the supercritical fluid into a vapor and liquid phase (brine) due to fluid boiling leads to the enrichment of metals and S in smaller fluid volumes. Successive microanalyses of individual co-existing vapor and brine fluid inclusions from porphyry Cu deposits showed that Cu, As, and Au tend to be enriched in vapor inclusions suggesting that these metals were transported to the site of deposition by the sulfur-rich vapor phase (e.g. Lowenstern et al., 1991; Heinrich et al., 1992; Heinrich et al., 1999; Ulrich et al., 1999; Williams-Jones and Heinrich, 2005). Experimental studies then showed that Cu does indeed form stable complexes with hydro-sulfide (e.g. Helz et al., 1993; Heinrich et al., 1999; Mountain and Seward, 1999, 2003; Etschmann et al., 2010; Zajacz et al., 2011) and that sulfur in general is enriched in the vapor phase (Drummond and Ohmoto, 1985; Suleimenov and Krupp, 1994), which was also observed in natural fluid inclusions (Seo et al. 2009). The partitioning of Au into the vapor phase is connected to the formation of complexes with reduced sulfur as well (e.g., Hayashi and Ohmoto, 1991; Benning and Seward, 1996; Gibert et al., 1998; Loucks and Mavrogenes, 1999; Tagirov et al., 2005; Pokrovski et al., 2008; Zajacz et al., 2010). Sulfur-free systems, on the other hand, showed preferential partitioning of Cu and Au into the brine (Williams et al, 1995; Pokrovski et al., 2005; Simon et al., 2005; Etschmann et al., 2010) at various P-T conditions (800°C / 140 MPa, Simon et al., 2005; 25-592°C / 18-60 MPa, Etschmann et al., 2010). This is in line with the observation that an increasing activity of sulfur in a low-salinity vapor, in the absence of brine, correlates with an increase in the solubility of gold in the vapor phase (Zajacz et al., 2010). However, recent investigations showed that even if large amounts of sulfur were present in the system, both Cu and Au partitioned into the brine relative to the vapor (at 800°C and 100 MPa, Frank et al., 2011).

### 1.1.6 The source magma

The host magmatic systems are of felsic to intermediate calc-alkaline composition and are thought to be derivatives of more mafic, mantle-derived primitive magma sources (e.g. Richards, 2005). A distinction can be made between more mafic host rocks, which prevail in island arc settings and preferentially form porphyry Cu deposits, and more alkaline host

rocks that intrude in back-arc settings leading to the formation of Mo-dominated porphyry stocks within extensional regimes.

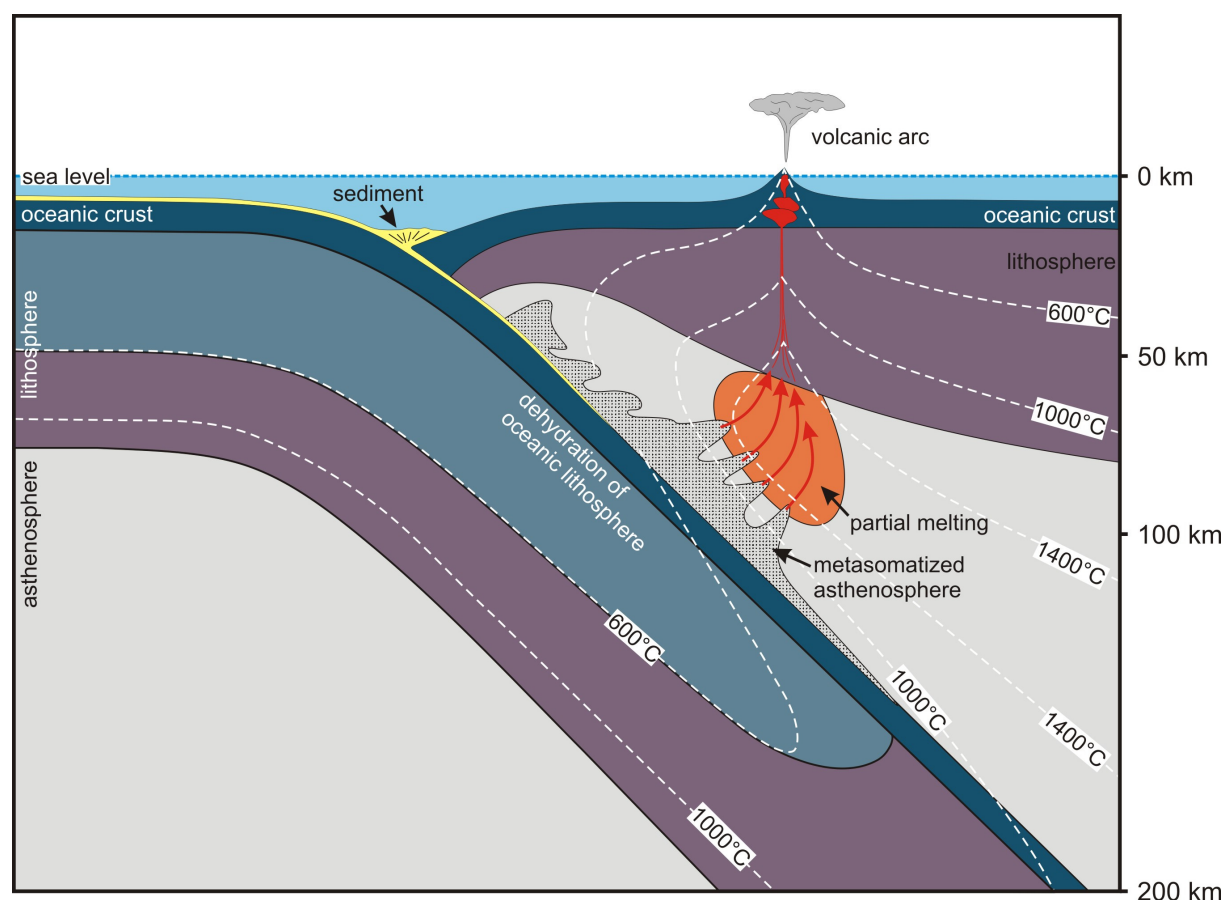


**Figure 1.4**

Schematic section illustrating the relationships between the subduction zone, metasomatism of oceanic lithosphere and the formation of primary, hydrous arc magmas within an oceanic island arc (modified from Richards, 2011).

Primary arc magmas are enriched in  $H_2O$  and sulfur, contain high concentrations of Rb, K, Ba, Sr, Cs (large-ion lithophile elements), Li, B, As, and Sb and are generated in the asthenospheric mantle wedge above a subduction zone (Tatsumi et al., 1986; Peacock, 1993; Arculus, 1994), (Figure 1.4): High pressure ( $\sim 3$  GPa), low temperature ( $700\text{--}800^\circ\text{C}$ ) metamorphism affects the subducted oceanic crust and its sediments at depths of ca. 100 km leading to the breakdown of hydrous minerals such as serpentine, amphibole, zoisite, and lawsonite (Tatsumi, 1986; Schmidt and Poli, 1998; Winter, 2001; Forneris and Holloway, 2003) and the release of a fluid phase enriched in water-soluble elements such as S, halogens, and large-ion lithophile elements. These fluids infiltrate, hydrate, and finally

metasomatize the overlying mantle wedge (e.g. Davidson, 1996; Noll et al., 1996; de Hoog et al., 2001). The fluid flux lowers the solidus temperature of the mantle and leads to partial melting and the formation of primary arc magmas which are rich in halogens, sulfur and metals, or in other words are “fertile” and capable of forming economic porphyry ore deposits (Richards, 2005). Arc magmas are relatively oxidized with values in the range of  $\sim$ QFM $<1$  to QFM $+3$  (Brandon and Draper, 1996; Parkinson and Arculus 1999; Rowins, 2000; Einaudi et al. 2003; Chambefort et al., 2008) which causes destabilization of sulfides and increasing sulfur solubility (as sulfate) in the melt (Carroll and Rutherford, 1985). Under such conditions, chalcophile elements like Cu and Au are incompatible and dissolve into the melt, hence still being available for later ore-forming processes. If the magma were more reduced, on the other hand, these elements would be sequestered by sulfide phases and thus precluded from successive processes.

In the next step, the primitive arc magmas rise until they reach the base of the crust where they pool in sill complexes (Figure 1.5) due to their higher density relative to the overlying crustal material (Hildreth and Moorbath, 1988). Crystallization of the magma is related to heat conduction into the overlying crust, leading to partial melting of felsic crustal rocks and magma mixing, the so-called MASH process (crustal **m**elting, **a**ssimilation, magma **s**torage and magma **h**omogenization; Hildreth and Moorbath, 1988). This MASH process has a major impact on the metallogenetic potential of the magma as volatiles and incompatible elements are further concentrated (Richards, 2005). Furthermore, fractionation of sulfide melt or minerals could have an effect on chalcophile metal ratios due to the different partition coefficients of Au and Cu in sulfides (Campbell and Naldrett, 1979): sulfides would sequester more Au than Cu from the magma leading to low Au/Cu ratios. This explains why Au-rich porphyries are related to more mafic, more oxidized magmas in which sulfide saturation and fractionation has not taken place (e.g. Hamlyn et al., 1985; Bornhorst and Rose, 1986; Richards et al., 1991; Spooner, 1993; Wyborn and Sun, 1994; Richards, 1995; Sillitoe, 1997, 2000).

Repeated MASH processes lead to the formation of large-volume magma chambers which guarantee a continuous flux of magma into the upper crust where large porphyry ore districts might form (Richards, 2005). The style of magma ascent depends on the rheology

of the surrounding crust material: it happens in form of diapirs in the ductile lower crust and dikes and sills in the more brittle upper crust (Richards, 2005). Large scale fracture zones which typically form at the end of orogenic episodes due to relaxation of compressional stress (e.g. McNulty et al., 1998; Simakin and Talbot, 2001) enhance and focus the ascent of the melt (Richards, 2000). The latter effect explains why the subduction-related porphyry ore deposits typically form towards the end of such tectono-magmatic processes (e.g. Richards, 2003 a, b).

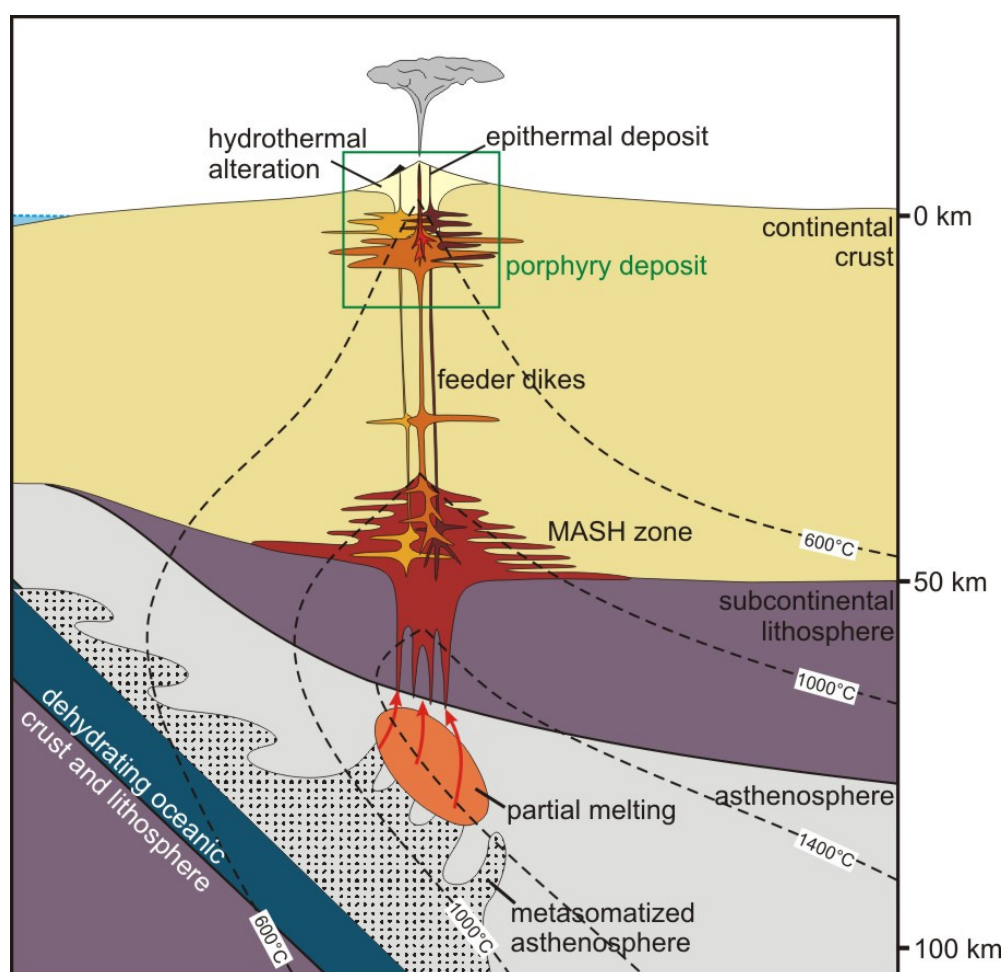


**Figure 1.5**

Schematic section through a continental arc showing the formation of the MASH zone and overlying porphyry systems (modified from Richards, 2011).

Magma ascent continues to the level of neutral buoyancy which usually lies close to the contact of the basement with supracrustal sequences where rock density decreases (e.g. Glazner and Ussler, 1988; Walker, 1989; Lister and Kerr, 1991), (Figure 1.5). Unless a

connection exists between the magma and the surface, resulting in major volcanic eruptions, large batholithic plutons form within the mid-upper crust by lateral propagation and infiltration of sills (Cruden, 1998; de Saint-Blanquat et al., 2001). As long as the supply of fresh hot magma from the underlying lower crustal magmatic system persists, the pluton remains molten and will expand, usually to the subvolcanic level forming long, cylindrical apices (Norton, 1982), (Figure 1.1).

With the onset of crystallization of anhydrous solid phases, mainly quartz and feldspar from the water-rich granitic melt, an aqueous fluid phase starts to evolve as water behaves as an incompatible element (Candela and Holland, 1986). At some point, depending on the depth/pressure of crystallization and the initial water content, the melt becomes saturated with respect to the aqueous phase and all dissolved elements partition between melt, crystals, and fluid. The initial water contents of andesitic and dacitic magmas are estimated based on the presence of hornblende and biotite and add up to 4 wt% H<sub>2</sub>O (e.g. Burnham, 1979, 1997; Naney, 1983; Hedenquist et al., 1998) implying that large amounts of fluid could be exsolved.

### *1.1.6.1 The partitioning of Cu and Mo between melt and fluid*

Molybdenum and Cu exhibit a completely different behavior with reference to the partitioning between melt, solids, and the exsolving fluid phase resulting in the enrichment of these metals in different melt types. Due to its incompatibility in major rock-forming minerals, Mo is enriched in residual melt and fluid phases regardless of the initial magma composition (Clark, 1972; Krauskopf, 1979), and increasing  $fO_2$ . Another critical factor might be the presence of Ti-, Fe-, and Mg-rich phases like titanite, mainly in less differentiated magmas, which tend to sequester Mo (Wedepohl 1978; Candela and Holland, 1986) making it unavailable for ore-forming processes. Hence, high concentrations of Mo are associated with leucocratic, highly fractionated magmas (Westra and Keith, 1981; Audétat, 2010) implying that late-stage magma may exsolve the most Mo-rich fluids. The fractionation behavior of Mo between the melt and a fluid phase is independent of halogens such as Cl and F (Candela and Holland, 1984; Keppler and Wyllie, 1981) and considered to be constant at given chemical composition and P-T conditions (Candela and Holland, 1986).

Copper, on the other hand is a compatible element which is enriched in solids and aqueous fluid phases relative to the melt. If fluid saturation is not yet attained, Cu is incorporated mainly in sulfides (Rajamani and Naldrett, 1978; Burnham, 1979) which might lead to a net depletion of Cu in the melt fraction (Candela and Holland, 1986). Depending on the redox-state of the melt, these Cu-rich sulfides are either re-dissolved and re-incorporated into the ore-forming system (Bell and Simon, 2011) or are excluded from any further processes including fluid exsolution (cf. section 1.1.5 “The role of sulfur”). In case of fluid saturation, Cu preferentially partitions into the Cl-rich aqueous fluid, and the fluid/melt partition coefficient of Cu correlates positively with the concentration of Cl in the aqueous phase (Holland, 1972; Candela and Holland, 1986) being highest at pressures around 100 MPa (Williams et al., 1995). The latter is consistent with observations that many porphyry Cu deposits formed at paleodepths of 3-4 km (e.g. Singer et al., 2008; Sillitoe, 2010). This behavior implies that the fluid phase gets enriched in Cu already in early stages of porphyry formation and that late, highly fractionated magmas are Cu-depleted.

The distinct Mo/Cu ratios within porphyry deposits can thus be explained by the evolution of the hydrothermal fluid that exsolved from the magmatic source (Candela and Holland, 1984): Low Mo/Cu ratios are ascribed to fluids generated from a H<sub>2</sub>O- and Cl-rich magma at shallow depths. These factors lead to early fluid formation, hence to the partitioning of large amounts of Cu into the aqueous phase. High Mo/Cu ratios are typical for fluids exsolved from magmas with low initial H<sub>2</sub>O- and Cl-concentrations at deeper levels. Thus, large parts of the magmatic body crystallize before water saturation is initiated resulting in Mo-rich highly fractionated melts and fluids. These residua are concentrated near the top of the magma chamber (Hildreth, 1981) due to the inward crystallization of the pluton as a result of heat loss to the country rock (e.g. Whitney, 1975; Brandeis and Jaupart, 1987; Candela, 1991; Averkin and Candela, 1994). Periodic injections of such highly fractionated fluid-saturated magma form the small stocks that are typical for porphyry Mo deposits.

### **1.1.7 The magmatic-hydrothermal fluid**

Volatiles exsolve from the magma as small bubbles (Candela, 1991). They are less dense

than the magma, but cannot escape due to the viscosity of the melt and the presence of crystals (Cloos 2001). Thus the bubble-rich magma rises convectively to the top of the chamber as a buoyant plume (Shinohara et al., 1995). Due to the pressure loss during ascent, the bubbles expand, coalesce and form a volatile-rich domain in the top parts of the intrusion body (Whitney, 1975). The degassed magma sinks again due to its higher density and gives way for fresh, hot, bubble-rich magma. Due to this process of magma convection (Shinohara et al., 1995; Cloos, 2001), large volumes of metal- and S-rich fluid can be focused in the apical portions of the magma chamber at magmatic temperatures.

The exsolved fluid phase consist mainly of H<sub>2</sub>O, S (mainly as SO<sub>2</sub> in oxidized systems, partly also reduced species), CO<sub>2</sub>, NaCl, KCl, and HCl. Due to the high concentration of Cl, elements which tend to form chloride-complexes are concentrated in the fluid phase as well. Experimental studies showed that this is the case for metals enriched in porphyry ore deposits (e.g. Holland, 1972; Ryabchikov et al., 1980, 1981; Khitarov et al., 1982; Candela and Holland, 1984; Urabe, 1985; Keppler and Wyllie, 1991). The subsequent evolution of the metalliferous hydrothermal fluid strongly depends on P-T-X conditions and can be modeled using the simple NaCl-H<sub>2</sub>O system (e.g. Bodnar et al., 1985).

At high pressure (>120 MPa, 700°C), a single-phase, supercritical fluid is exsolved from the silicate melt (Burnham, 1967, 1979) with an average salinity of 2-13 wt% NaCl<sub>equiv</sub> (e.g. Sourirajan and Kennedy, 1962; Pitzer and Pabalan, 1986; Cline and Bodnar, 1991; Cline, 1995). At lower pressures, the NaCl-H<sub>2</sub>O system is characterized by a large miscibility gap resulting in the separation of the fluid into a low salinity, low density vapor and a high salinity liquid phase, the brine (Figure 1.6). All components that were dissolved in the previously single-phase fluid fractionate between these two fluid phases. The composition of the vapor phase and brine then strongly depends on the salinity of the primary fluid, pressure and temperature. As can be seen in the NaCl-H<sub>2</sub>O phase diagram (Figure 1.6), the bell-shape of the solvus leads to decreasing salinity of the vapor and increasing salinity of the brine with decreasing pressure. This fluid evolution from single phase to boiling was also confirmed by the finding of inclusions of supercritical fluids at depth and vapor and brine inclusions in shallower regions of the Bingham Canyon deposit (Landtwing et al., 2005).

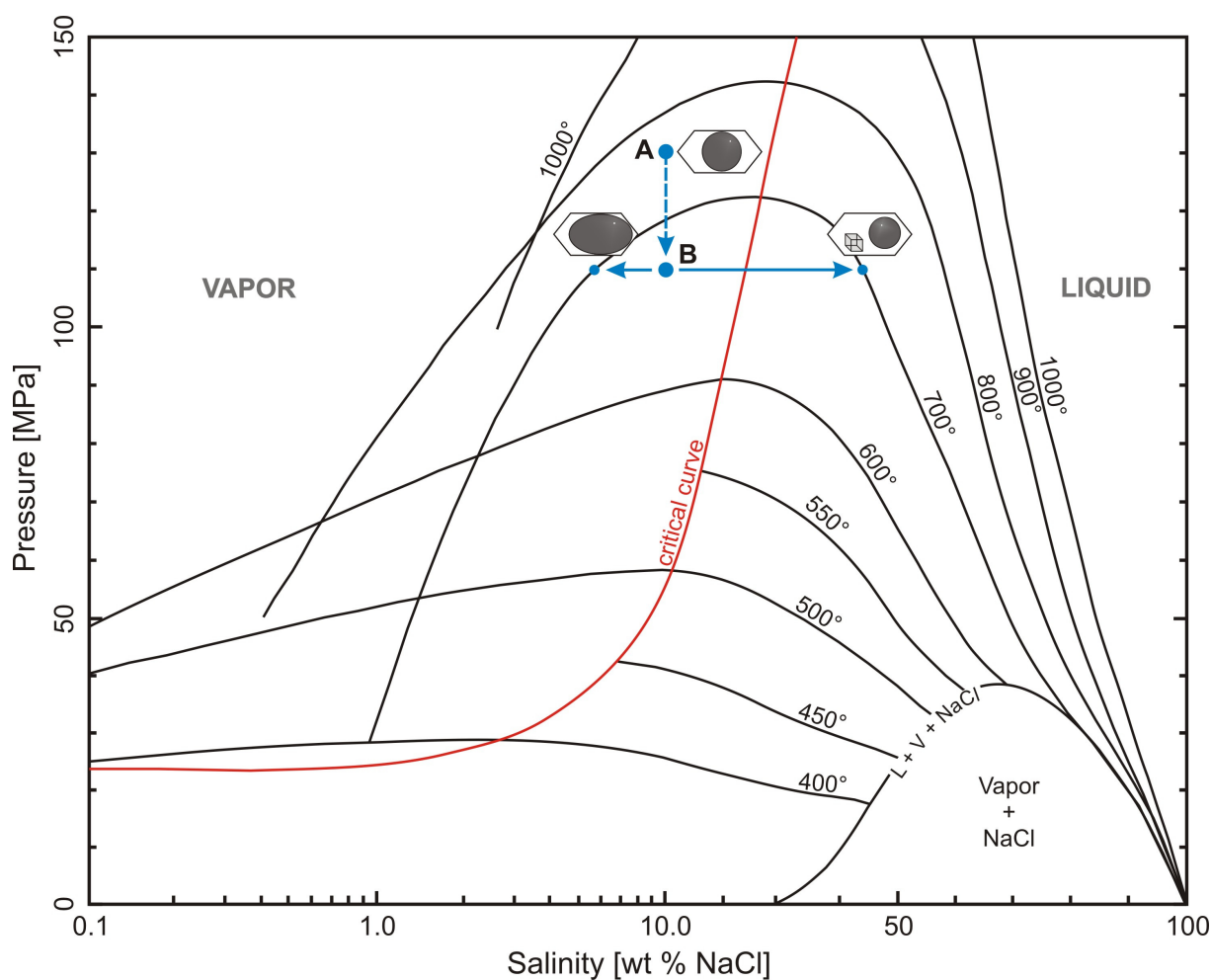


**Figure 1.6**

Phase diagram for the system NaCl-H<sub>2</sub>O. Isotherms represent phase boundaries along which a homogeneous single-phase fluid separates into a vapor and liquid phase (i.e. “fluid boiling”). A single-phase fluid of e.g. 700°C and composed of H<sub>2</sub>O and 10 wt% NaCl decompresses from 130 MPa (point A) to 110 MPa (point B). It intersects the solvus and separates into a vapor and liquid phase of ~5.7 wt% NaCl and ~43 wt% NaCl, respectively, the latter forming a halite daughter crystal upon cooling (modified from Bodnar et al., 1985).

The fluid phase is not just the carrier of metals and S, it also causes hydrothermal alteration of the host rock at the porphyry level. Fluid evolution from hot neutral to cold acidic fluid conditions causes the typical zoning with potassic alteration in the center, advanced argillic alteration close to the surface and phyllic alteration surrounding the whole porphyry stock (Figure 1.1). Early high temperature potassic alteration (700-350°C; Einaudi et al., 2003) produces an assemblage of quartz - K-feldspar - biotite ± magnetite, which is similar to the assemblage present in the igneous source rocks because the fluid is still in equilibrium with

the near-solidus magma. As soon as the fluid cools below 350°C, SO<sub>2</sub> disproportionates according to



to generate H<sub>2</sub>S and a sulfate species (depending on acidity, H<sub>2</sub>SO<sub>4</sub>, HSO<sub>4</sub><sup>-</sup>, or SO<sub>4</sub><sup>2-</sup>), (Holland, 1965; Burnham, 1967, 1979; Giggenbach, 1997). This formation of H<sub>2</sub>S leads to the precipitation of sulfide minerals (see section 1.1.8), the formation of sulfuric acid (H<sub>2</sub>SO<sub>4</sub>; together with the increasing reactivity of species such as HCl and HF; Hedenquist, 1995) to hydrolytic alteration resulting in intense phyllic alteration. At this stage, meteoric water already influences and partly overprints the hydrothermal fluid system as it was indicated by oxygen and hydrogen isotope ratios measured in sericite (Stein and Hannah, 1985). Phyllic alteration is typified by partial to complete transformation of mafic minerals to chlorite, plagioclase to sericite and/or illite, and magnetite to hematite along with deposition of pyrite and chalcopyrite (Sillitoe, 2010). Propylitic alteration is in course caused solely by circulating groundwater that was heated by the magmatic intrusion. It thus can affect huge volumes of country rock extending many kilometers around the porphyry stock (Taylor, 1974; Norton, 1982), partly overprinting earlier high temperature assemblages. Meteoric water also might redistribute ore constituents on a minor scale (Burnham and Ohmoto, 1980) or for example, concentrates them in high-grade veins.

Advanced argillic alteration occurs at temperatures <200°C close to the surface, forming the lithocap and is ascribed to the high acidic vapor plume (Stoffregen, 1987; Hedenquist et al., 1994, Arribas, 1995) that rises farthest compared to the denser brine leading to the conversion of feldspar to clay minerals.

Many of the above mentioned facts like the one that ore metals and S already have been present in the parental magma system, were transported by magmatic-hydrothermal fluids and not leached out of the country rock have been deduced from stable isotopic studies:

Common lead isotopic compositions measured in both altered and unaltered rocks from different stocks of the porphyry Mo deposit at Henderson (Colorado) fall all within a very restricted range implying that the Henderson rocks were not isotopically influenced or

contaminated with Pb from the country rocks and that a thoroughly homogeneous Pb source must exist at depth (Stein and Hannah, 1985). Moreover, the Pb isotope ratios decrease close to the contact of the stock indicating that ore solutions which produced stockwork Mo mineralization moved outward from the stock. Also, for the Bingham Canyon porphyry Cu-Mo deposit (Utah), Pb isotope ratios measured in fluid inclusions of both the Cu and Mo stages suggest a single magmatic source of Mo- and Cu mineralizing fluids (Pettke et al., 2010). Hydrogen isotope signatures were used as well to demonstrate that the influence of meteoric water to primary ore formation is limited or absent, respectively (Candela and Holland, 1986) and that the metals stem from hydrothermal fluids of magmatic origin: H-isotope signatures found in the potassic alteration zone of many porphyry deposits do not match with signatures from typical meteoric waters. Furthermore, the comparison of H-isotope ratios of fluids from porphyry systems with other crustal fluids of known origin showed that the primary ore-forming fluids are of clear magmatic origin (Hedenquist and Lowenstern, 1994). Using the relative abundances of the stable isotopes of S, the source reservoir of S in porphyry systems could be identified (Ohmoto and Rye, 1979; Seal, 2006). The ratios of S isotopes measured in sulfides from various porphyry ore deposits within the Colorado Mineral Belt are all similar and lie in the area of typical ratios of magmatic sulfur indicating that S was not leached out of the surrounding host rocks but originated from the underlying magmatic source (Stein and Hannah, 1985; Hattori and Keith, 2001). The same principle was applied to constrain the origin of Cu: The isotopic analysis of primary Cu-sulfide minerals from porphyry Cu deposits (including Chuquicamata/Chile and Butte/Montana) yielded values indicating a clear magmatic origin (Maréchal et al., 1999; Zhu et al., 2000; Larson et al., 2003; Albarède, 2004; Ehrlich, 2004; Markl et al., 2006; Asael et al., 2007; Marthur et al., 2009).

#### **1.1.8 Metal transport and deposition of Cu and Mo**

Phase separation of the previously supercritical fluid is important for the formation of porphyry ore deposits, as it appears that significant sulfide mineralization commonly appears just after the first evidence for immiscibility in the fluid inclusion record (e.g.

Gustafson and Quiroga, 1995; Arancibia and Clark, 1996). After fluid boiling, the vapor phase and brine are diversely enriched in elements and undergo an independent physical evolution due to their differences in density (Henley and McNabb, 1978): The low density vapor plume ascends to shallower, up to epithermal levels, whereas the brine stays behind at the porphyry level (Figure 1.1; see also chapter 1.2 'Genetic model').

The partitioning of ore metals between vapor and brine strongly depends on the affinity of the respective element either to form chloride complexes (in the brine) or to complex with sulfur (in the vapor). Experimental studies in the model system H<sub>2</sub>O-NaCl-KCl-HCl at temperatures of 350-450°C showed that Fe, Zn, As, Sb, and Ag partition into the high-salinity brine relative to the vapor even at reducing conditions and high concentrations of S. Gold, on the other hand is preferentially enriched in the vapor phase in the presence of ~1 wt% S with H<sub>2</sub>S being the dominant S species, whereas under these conditions, Cu equally partitions between the vapor phase and brine (Pokrovski et al., 2005).

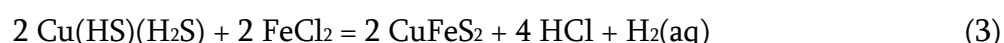
The transport of Cu is still under debate, because the analysis of natural fluid inclusions showed that vapor inclusions are highly enriched in Cu (e.g. Heinrich et al., 1999; Seo et al., 2012), but experimental studies failed to reproduce this observation (e.g. Simon et al., 2006; Pokrovski et al., 2008; Frank et al., 2011). However, it seems that the hypersaline brine is the main carrier of metals, because base metal solubilities generally increase with increasing fluid salinity which is caused by the separation of the vapor phase from the liquid (e.g. Crerar and Barnes, 1976; Holland, 1972). In this case, Cu<sup>(I)</sup> complexes with Cl to form CuCl<sup>0</sup> (Crerar and Barnes, 1976; Candela and Holland, 1984), which is the dominant complex of Cu in the temperature range of 250-350°C in aqueous chloride solutions in equilibrium with common sulfide assemblages (Crerar and Barnes, 1976). Complexes of Cu<sup>(I)</sup> and sulfur would be Cu(HS)<sub>2</sub><sup>-</sup> and Cu(HS)(H<sub>2</sub>S), (Pokrovski et al., 2008; Seo et al., 2009; Etschmann et al., 2010).

The concentration of Mo in the fluid is independent of Cl-concentrations (Candela and Holland, 1984; Wood et al., 1987) and correlates negatively with S abundance (Tingle and Fenn 1984; Candela and Holland, 1986). It is assumed that Mo<sup>(VI)</sup> is present as oxo-hydroxo species like MoO<sub>3</sub> (Candela and Holland, 1984).

Metal precipitation is mainly driven by a combination of hydrolysis of SO<sub>2</sub> in the fluid (e.g.

Holland, 1965; Burnham, 1967, 1979, Giggenbach, 1997) and rapid pressure-changes (i.e. in course of hydraulic fracturing) that lead to fluid unmixing. During its ascent, the fluid cools below  $\sim 350^{\circ}\text{C}$  and  $\text{SO}_2$  disproportionates to form  $\text{H}_2\text{S}$  and  $\text{H}_2\text{SO}_4$  (equation 1). This increase in  $\text{H}_2\text{S}$  with continued disproportionation causes metal-sulfide precipitation.

Depending on the type of Cu complexes, Cu precipitation follows the reactions (Seo et al., 2012):



or/and



Precipitation of Mo from oxy, hydroxyl, or oxy-chloride complexes of Mo always requires  $\text{H}_2\text{S}$  and  $\text{H}_2$ . Thus high  $\text{H}_2\text{S}$  activities and net reduction will favor Mo precipitation (Einaudi et al., 2003; Seedorff and Einaudi, 2004b) as Mo-sulfide according to



The separate occurrences of Cu- and Mo-rich stages in some porphyry deposits (e.g. at Bingham Canyon/Utah; Seo et al., 2012) can thus be explained by the changing redox potential and acidity of the fluid. Early Cu-stage fluids were slightly oxidized, allowing efficient precipitation of Cu-Fe sulfides, whereas late Mo-stage fluids were more reduced and acidic, leading to Mo-saturation and precipitation of molybdenite ( $\text{MoS}_2$ ). Small variations in redox conditions and acidity within the magmatic fluid source thus can cause large-scale metal separation by selective sulfide precipitation.

The site of metal precipitation is mainly dictated by the nature of the surrounding host rocks (Guillou-Frottier and Burov, 2003): Small rheological contrasts between the magma and the host rocks result in the formation of a fracture network around and near the flanks of the porphyry stock, the so-called stockwork. In case of larger rheological contrasts, breccia pipes are formed in which the fluid is focused. The latter is not favorable as the

breccia pipe might be connected to the surface leading to the loss of metals and/or brecciation would affect large volumes of host rock leading to more disseminated metal deposition. Usually, ore formation happens close to the ductile-brittle transition (Figure 1.1), (Fournier, 1999).

## *1.2 Genetic model*

The complex evolution of porphyry ore systems from the original magma over the enrichment of metals to the formation of the ore shell is summarized in a genetic model (after Richards, 2005, 2011 and references therein) highlighting the single, critical steps:

*The subduction* of oceanic lithosphere leads to subsequent metasomatism/dehydration of the oceanic crust, resulting in the discharge of large amounts of fluid. This fluid lowers the solidus and triggers *partial melting* of the lower continental crust within the accretion wedge. The resulting calc-alkaline arc magma is oxidized and rich in water, S, and halogens, hence having a high potential to form porphyry ore deposits although the metal contents are not abnormally high. This magma intrudes the overlying denser mantle lithosphere until it reaches the base of the crust (Hildreth and Moorbath, 1988) where it starts to pool in sill complexes due to its higher density in reference to the overlying crust. At this level, the magma body will start to crystallize and conduct heat into the overlying crustal portions, which results in partial melting of felsic crustal rocks at depths of 40-50 km and mixing with the more primitive arc magma. This *MASH process* (Hildreth and Moorbath, 1988) forms intermediate magmas of high buoyancy, which start to ascend after compressional tectonic forces ceased at the end of the subduction event. The *magma-upstream* is further enhanced and focused by preexisting, reactivated large scale crustal fracture zones (Richards, 2000). Ascent rates are fast, in the order of  $10^{-2}$ - $10^{-3}$  ms<sup>-1</sup> (Clemens and Mawer, 1992; Petford, 1996), implying that the mineralizing potential of the magma is unlikely to be lost on ascent through the crust and that the magma will not start to freeze in dikes (Clemens and Mawer, 1992). The whole process stops at the level of neutral buoyancy where an *upper crustal magma chamber* starts to form due to the density contrast between

the unvesiculated magma and the upper crustal lithologies (e.g. Glazner and Ussler, 1988; Walker, 1989; Lister and Kerr, 1991) at depths of ~5 km. This upper crustal magma chamber remains molten and expands as long as the flux of melt from depth sustains. Hence, the most critical factor at this stage is the continuous supply of hot, volatile-rich magma from the underlying MASH zone. The large volume magma chamber at the base of the continental crust and rapidly rising melts can thus be regarded as two of the cornerstones of porphyry-deposit-formation.

Expansion of the upper-crustal pluton leads to the *formation of elongated apices* due to the formation of localized zones of crustal extension (Guillou-Frottier and Burov, 2003). These apices measure 1-2 km in diameter and partly reach relatively shallow levels of <2 km depth (Norton, 1982). Cooling and subsequent crystallization of anhydrous minerals from the water-rich andesitic arc magmas triggers fluid exsolution and consequently the partitioning of all ore-constituents into the resulting hydrothermal, Cl-rich fluids. Again, the volume of magma available plays an important role as the hydrothermal fluids need to interact with large portions of magma because for example, Cu concentrations in intermediate composition magmas are quite low (10-150 ppm Cu; Gill, 1981). Hence, the volume of magma that is needed to form moderate sized porphyry Cu deposits ranges between 30-50 km<sup>3</sup> (Cline and Bodnar, 1991; Cline 1995), for large deposits a magma volume of >100 km<sup>3</sup> would be required.

To finally form an economic deposit, large volumes of the magmatic-hydrothermal fluid must be channeled and react with small volumes of rock in order to focus mineral deposition. Such *focusing of the metalliferous fluid* happens in the upper parts of the magmatic apices due to magma convection based on the density contrast between the melt and the fluid (Shinohara et al., 1995). Upon ascent, the hydrothermal fluid experiences major depressurization, starts to boil, and separates into two phases of contrasting density, the *low salinity vapor phase and high salinity brine*. All elements dissolved in the previously supercritical fluid fractionate between these two phases, whereas the majority of metals, including Cu, is enriched in the brine as Cl-complexes. More or less simultaneously, *metal precipitation* is initiated due to this phase separation, cooling, and reaction of the fluid with the wall rocks. These relations explain the limitation of the porphyry Cu-Mo

deposit to the sphere of the brine as it is indicated in Figure 1.1. The less dense vapor expands to shallower levels transporting significant amounts of S and Au which are deposited in epithermal regions. Metal precipitation takes place in fractures and faults that formed around the shallow intrusions during hydraulic fracturing and is attended by intensive *hydrothermal alteration* of the host rocks.

If just one of these processes is changed or absent, porphyry ore formation is disturbed or even inhibited. For example, changes in the large tectonic regime would alter subduction and would stop everything right at the beginning. A major impact affecting late stages of porphyry ore deposit formation would be surface venting of the magmatic-hydrothermal fluid, i.e. a large volcanic eruption resulting in the loss of volatiles and metals.

### ***1.3 Open questions and scope of this thesis***

#### **1.3.1 Porphyry Cu deposits**

The most uncertain parameter during the evolution of magmatic-hydrothermal fluids in porphyry Cu systems is the transport of Cu itself.

The analysis of single quartz-hosted vapor and brine fluid inclusions coexisting in trails from porphyry Cu deposits all around the world (e.g. Heinrich et al., 1999; Seo et al. 2009) showed that the vapor phase is clearly enriched in Cu and S in contrast to the brine. Hence it was inferred that the vapor phase is the main transporting agent of Cu in porphyry Cu systems. However, although numerous studies have been carried out within the last 10 years (e.g. Mountain and Seward 1999, 2003; Simon et al., 2006; Pokrovski et al., 2008; Zajacz et al., 2008; Rempel et al., 2010; Frank et al., 2011), it was not possible to experimentally reproduce the partitioning of Cu into the vapor phase, with the exception of one questionable study by Nagaseki and Hayashi (2008). Experiments confirmed the existence of Cu-hydrosulfide complexes (Mountain and Seward 2003; Etschmann et al., 2010) and showed the effect of S on the fractionation behavior of Cu: Systems containing high concentrations of reduced S resulted in higher concentrations of Cu in the vapor phase as compared to S-free systems. Other investigations of natural quartz-hosted fluid

inclusions, on the other hand, showed that vapor and brine inclusions are not completely closed systems with respect to their elemental budget due to the possibility of diffusion of  $H^+$ ,  $Cu^+$ , and  $Na^+$  through quartz into and out of the inclusion (Mavrogenes and Bodnar, 1994; Zajacz et al., 2009; Li et al., 2009-this thesis, chapter 6.4). This process might have modified the contents of natural quartz-hosted fluid inclusions possibly resulting in misleading Cu-concentrations that do not resemble the original fluid any more.

Accordingly, in this thesis the vapor/brine partitioning of Cu was studied in a series of hydrothermal experiments in aqueous Cu- and S-rich systems with a wide range of parameters (salinity, P-T,  $fO_2$ ,  $fS_2$ , pH). Additionally, it was investigated whether the diffusion of Cu through quartz may affect Cu concentrations in vapor and brine inclusions (manuscript 2, 'High Cu concentrations in vapor-type fluid inclusions: an artifact?').

### 1.3.2 Granite-related Mo deposits

Although very few high-grade porphyry Mo deposits are known and many studies have been carried out on their tectonic setting, petrography, and geologic environment, almost no data exists on the nature and bulk composition of primary magmatic fluids, which were responsible for the transport of Mo in first place. Only two studies have been carried out so far, on the Mo-deposits at Questa (New Mexico; Klemm et al., 2008) and at Cave Peak (Texas; Audétat, 2010). As already mentioned, the factor, which distinguishes between pure porphyry Mo and mixed porphyry Cu (Mo) deposits, is the Mo/Cu ratio being  $>1$  for the former implying that no recoverable amounts of Cu are present (Carten et al., 1993). However, the study of primary fluids of the Questa and Cave Peak porphyry Mo deposits yielded an ambivalent picture: Mo/Cu ratios of 0.01 and 0.20, respectively were reported suggesting different, but high concentrations of Cu dissolved in the primary fluid. Moreover, at Cave Peak sulfide phases contain 2-3 wt% Cu, which is now concentrated in exsolved chalcopyrite, whereas the high Cu concentrations in the primary fluids of the Questa deposit are contrasting with the absence of Cu-bearing minerals in the mine.

Thus, the main question that needs to be answered to obtain a better genetic model of

granite-related Mo deposits concerns the general metal content of primary mineralizing fluids and melts. Furthermore, it is unclear if the concentrations of Cu obtained from quartz hosted fluid inclusions are correct in first place, since they could have been modified post-entrapment by diffusion of Cu (cf. chapter 6.2 of this thesis).

In order to provide more data on ore-forming fluids of granite-molybdenite systems and to finally supply an answer to the problem of differing Cu concentrations in such systems, the primary fluid and melt inclusions from granite-hosted Mo deposits from Norway and Colorado have been studied (manuscript 3, 'The metal content of melts and fluids in Mo-mineralized granites').

---

## 2 EXPERIMENTAL AND ANALYTICAL METHODS

### *2.1 Hydrothermal experiments*

#### **2.1.1 Design of experiments**

Two different types of experiments have been carried out:

1) The partitioning of Cu between the vapor phase and the brine was studied under controlled pressure (50 - 130 MPa), temperature (600 - 800°C),  $fO_2$  (oxidizing - reducing), and pH (pH <0.3 - 10) conditions. As a model for natural magmatic-hydrothermal fluids, the system  $H_2O-NaCl-S (\pm HCl \pm FeCl_2 \pm KCl)$  was chosen. The fluid was trapped at run conditions as synthetic vapor and brine inclusions in quartz which were then analyzed after cooling (Stern and Bodnar, 1984; Duc-Tin et al., 2007). By analyzing 5-20 (depending on the reproducibility) inclusions of each type, a good estimate on the elemental budget of the vapor and brine phase was obtained.

2) Re-equilibration experiments of fluid inclusions in quartz were carried out to test if the Cu-contents of natural fluid inclusions may have been modified after entrapment. A piece of quartz containing synthetic fluid inclusions of known composition was loaded together with a fluid phase into a new capsule and was again heated and pressurized in the cold-seal apparatus. After the run, the re-equilibrated fluid inclusions were analyzed and the concentration of elements before and after equilibration were compared (further details are given in the second manuscript in section 6.2.4.2).

Additionally to the re-equilibration of synthetic fluid inclusions trails of natural fluid inclusions in miarolitic quartz crystals from the Erongo granite (Namibia) and the Drammen granite (Norway) were re-equilibrated at trapping conditions which were estimated from microthermometry and mineral inclusions in the quartz. A few inclusions of each trail were analyzed to obtain information about their elemental budget. The trails were then cut out of the quartz crystal and loaded together with fluid and buffer minerals into a quartz capsule.

### 2.1.2 Starting material

All synthetic fluid inclusion studies presented in this thesis were conducted using pieces of natural quartz from Brazil that have been etched in 48% hydrofluoric acid for 30-60 minutes. Using this method, artificial channels were produced along the quartz' surface which healed due to quartz growth during the experiment and thus trapped small aliquots of the fluid at run conditions (Duc-Tin et al., 2007). In order to guarantee homogeneous healing of etched channels, SiO<sub>2</sub>-glass was added which recrystallized at run conditions forming a new layer of quartz around the natural crystal. Etched quartz pieces were loaded together with the aqueous fluid (H<sub>2</sub>O + NaCl ± KCl ± HCl and traces of elements loaded as FeCl<sub>2</sub>, PbCl<sub>2</sub>, CoCl<sub>2</sub>, As<sub>2</sub>O<sub>3</sub>, LiCl, CsCl, H<sub>3</sub>BO<sub>3</sub>, RbCl), solid starting material, and powdered SiO<sub>2</sub>-glass into metal capsules (see next section) which were sealed by arc welding. Solids were used as a source of elements like chalcocite for Cu, chalcopyrite for Cu and Fe, molybdenite for Mo, silver foil for Ag, elemental sulfur, and as buffer assemblages. For example, the assemblage albite-biotite-orthoclase-bornite-chalcopyrite-magnetite-anhydrite was used to effectively buffer *f*O<sub>2</sub>, *f*S<sub>2</sub>, and pH.

All minerals were crushed and sieved to a size of 160-250 μm in order to assure a large surface area and to still be able to recognize the minerals after the run under the optical microscope. In some experiments, sodium sulfide (Na<sub>2</sub>S) and S and Ti were used to produce H<sub>2</sub>S, for instance, according to the reactions



and



since H<sub>2</sub>S is a gas that is only partly soluble in water and therefore cannot be easily loaded into metal capsules.

### 2.1.3 Preparation of sample capsules

The samples were loaded into metal capsules of 5 mm OD, 4.6 mm ID, and ~45 mm length which subsequently were closed by arc welding. Mostly, gold capsules were used as these

are inert against sulfur. Partly also capsules made of platinum and a gold-copper ( $\text{Au}_{95}\text{Cu}_{05}$ ) alloy were used, as well as gold capsules with inner walls coated by Cu. In most experiments, inside the metal capsule, an inner capsule made of synthetic  $\text{SiO}_2$  was used to avoid reactions of the sample with the capsule material. The new assembly consists of a quartz container which holds the sample and is placed into the gold capsule. The container which is made of synthetic quartz is closed by a plug of  $\text{SiO}_2$ -glass and a rounded lid made of the same material as the container (Figure 2.1). As soon as run temperature and pressure are reached the plug recrystallizes and grows together with the container and the lid. Due to this tight sealing any interaction between charge and noble metal capsule are reduced to a minimum. Further details and a full description of the usability of this new method are given in the first manuscript (section 6.1 ‘The ‘quartz capsule’ – a new method to avoid alloying problems with noble metal capsules in hydrothermal experiments’).

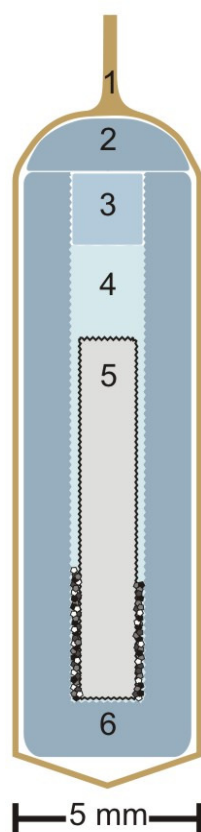


**Figure 2.1**

Setup of the quartz capsule: 1= Au capsule, 2= cap made of synthetic quartz, 3= plug made of  $\text{SiO}_2$  glass, 4= fluid (plus  $\text{SiO}_2$  glass and buffer minerals, illustrated as small dots), 5= etched piece of natural quartz, 6= container made of synthetic quartz.

### 2.1.4 Cold-seal pressure vessels

The apparatus which was used to apply hydrothermal pressures of 70-150 MPa and temperatures of 600-800°C is the so-called cold-seal pressure vessel (e.g. Matthews et al., 2003). The Bayerisches Geoinstitut has 14 such devices available of two different designs: with horizontally and vertically positioned bombs (Figure 2.2). For this study only pressure vessels of the vertical design were used because they are easier to handle and allow rapid quenching of the sample.



**Figure 2.2**

Hydrothermal lab at the Bayerisches Geoinstitut. At the left side there are horizontal pressure vessels with their typical box-shaped isolation-covers, in the center of the room there are the vertical rapid quench autoclaves with their blue furnaces at the top. The panel to control pressures and temperatures follows to the right.

The term “cold-seal” reflects the fact that the closure of the bomb is outside the furnace and is thus relatively cool compared to the part within the furnace. The autoclaves are made of a nickel-alloy (IN 713 LC) and the pressure medium is water which is supplied through the cone seal at the cold end of the bomb. Temperature is measured by an external thermocouple and controlled from a central panel. The autoclave is the only portion of the system that is placed inside the furnace and is separated from an extension tube by a

coupling and a double cone (Matthews et al., 2003), (Figure 2.3). Cooling water circulates outside of the double cone. Rapid quenching can be induced by dropping the sample capsule from the hot furnace to the cold end of the bomb. This is accomplished by lowering the outer magnet which keeps the sample holder in place inside the furnace.

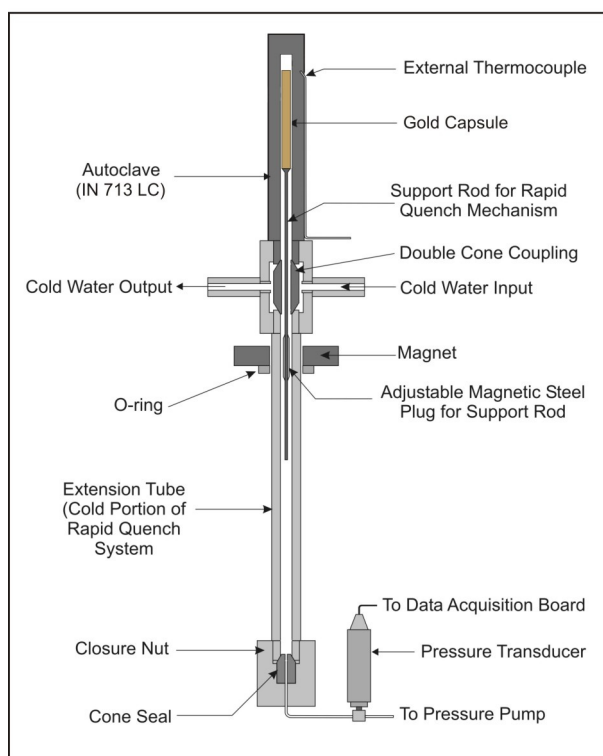


**Figure 2.3**

Schematic diagram of the rapid quench, cold-seal autoclave (modified from Matthews et al., 2003).

This experimental setup is similar to previous designs by Phil Ihinger from the California Institute of Technology (cf. Matthews et al., 2003). Usually, the redox state cannot be controlled in most experiments using cold-seal vessels but since water was used as pressure medium the intrinsic oxygen fugacity of the autoclaves was typically close to that of the Ni-NiO buffer due to the Ni-alloy (IN 713 LC) the bombs are made of. In cases where more oxidizing conditions were needed,  $f_{O_2}$  was internally buffered and, if possible, the run-time was set to be as short as possible. Capsules were put into rapid quench autoclaves and heated isobarically at run-pressure. Experiments using quartz-capsules were heated along an isochoric path to ensure constant density and volume of the fluid inside the capsule in order

to prevent rupture of the quartz container (details are described in the first manuscript in section 6.1.3). At the end of the run cooling of the sample was done isobarically and along the same isochoric path, respectively. After the autoclave has cooled to room temperature, the capsule was recovered, weighted to check for leakage, and subsequently was opened with a razor blade. The pH of the quench fluid inside the capsule was measured using indicator paper. Remaining solids and buffer minerals were recovered and stored for further analyses. The quartz pieces were cleaned for subsequent analysis of the contained fluid inclusions (see next section). Partly, some fluid inclusions got trapped along the inner walls of the quartz capsule itself. In this case, the capsule was cut along its c-axis and the respective pieces hosting fluid inclusions were polished and prepared just like the piece of natural quartz.

## ***2.2 Analytical methods***

Any fluid inclusion analysis started with cutting of the sample into thin slices and polishing of both sides of these thick sections. If necessary, the sample was then cut into smaller pieces which would fit into the sample holders of the heating-cooling stage and the ablation cell of the LA-ICP-MS.

### **2.2.1 Optical microscopy**

Optical microscopy was used to identify fluid inclusions and daughter crystals. For further analyses high-resolution pictures (Figure 2.4) of the sample were printed out and inclusions of interest were marked.

Fluid inclusions are mainly selected for analysis according to their size, shape, and position within the quartz. For good Raman- and LA-ICP-MS analyses the inclusions should be as close to the surface as possible. On the other hand, fluid inclusions decrepitate easily upon heating during microthermometry-analysis if the overlying quartz layer is too thin and cannot stand the increasing pressure of the trapped fluid. As a good compromise, those inclusions which lie in depths equal to their maximum size were selected.

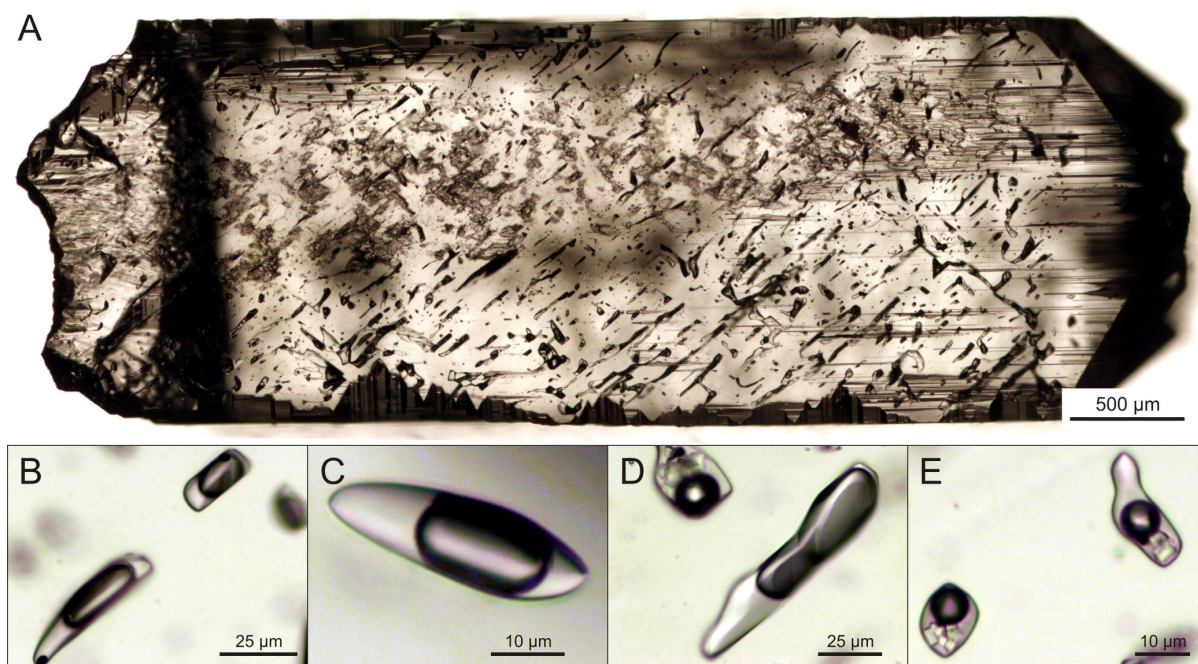


**Figure 2.4**

Synthetic fluid inclusions in quartz. **A** Photograph of a polished quartz-column containing synthetic fluid inclusions after a 4-day run at 800°C, 130 MPa in a NaCl-S-H<sub>2</sub>O dominated fluid. Fluid inclusions formed along channels that previously had been etched into the quartz-surface by HF-treatment. During the run the quartz crystal grew in all directions, indicated not just by the closed channels but also by newly grown quartz at the right and left side. **B-E** Microphotographs of vapor (B, C, D) and brine (D, E) inclusions from the same sample.

### 2.2.2 Microthermometry

After a first selection of fluid inclusions based on optical parameters, microthermometric analyses were carried out using a heating-cooling stage. Microthermometry is based on the observation of phase changes within fluid inclusions which take place during freezing of the fluid and heating of ice, clathrates, and salts like NaCl. From the temperatures at which these changes take place, one can, with reference to simple fluid systems such as NaCl-H<sub>2</sub>O, derive estimates of the PVTX state of the fluids at the time of trapping. Upon cooling, the fluid shrinks much more than the host crystal which may lead to the formation of a vapor bubble in the formerly homogeneous fluid inclusion (Sorby, 1858). Daughter crystals develop as soon as the fluid intersects the saturation curve of any dissolved solid (e.g. halite/NaCl).

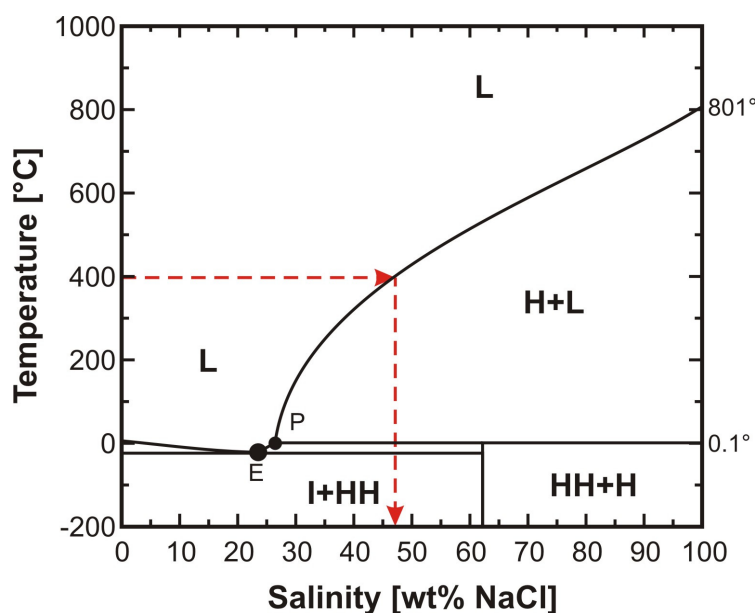


**Figure 2.5**

Vapor-saturated phase relations in the system NaCl-H<sub>2</sub>O. With the known melting temperature of halite one can directly estimate the salinity of the trapped fluid (red dashed lines). Thus a halite melting temperature of e.g. 400°C equals with a salinity of 47 wt% NaCl. The halite solubility curve extends from the peritectic to the NaCl triple point at 801°C. I = ice; L = liquid; HH = hydrohalite; H = halite; P = peritectic (0.1°C, 26.3 wt% NaCl); E = eutectic (-1.2°C, 23.2 wt% NaCl), (modified after Bodnar and Vityk, 1994).

*Heating* of multiphase inclusions results in the dissolution of daughter minerals, particularly the more soluble ones, and in the homogenization of the vapor and liquid phases. The temperature at which daughter minerals dissolve is related to their solubility in the fluid phase. For a saturated NaCl-H<sub>2</sub>O system (i.e. a brine inclusion) the final melting temperature for halite is directly proportional to the wt% NaCl in solution (Figure 2.5).

Bodnar and Vityk (1994) described the salinity as a function of halite dissolution temperature according to

$$\begin{aligned} \text{Salinity (wt\%)} = & 26.242 + 0.4928 \Psi + 1.42 \Psi^2 - 0.223 \Psi^3 + 0.04129 \Psi^4 + \\ & 6.295 \cdot 10^{-3} \Psi^5 - 1.967 \cdot 10^{-3} \Psi^6 + 1.1112 \cdot 10^{-4} \Psi^7 \end{aligned} \quad (9)$$

where  $\Psi = T(^{\circ}\text{C})/100$ . Equation (3) represents the solubility of NaCl in water from the peritectic temperature (0.1°C) to the NaCl triple point (801°C).

Homogenization of a fluid inclusion may happen by disappearance of the vapor bubble (i.e. homogenization into the liquid state), expansion of the vapor bubble (i.e. homogenization into the vapor state), or by fading of the liquid-vapor meniscus (i.e. critical homogenization into a supercritical fluid). The temperature of homogenization is in a boiling fluid (i.e. if two phases, vapor and brine, are coexisting), equal to the trapping temperature. This is not the case for supercritical fluids trapped above the boiling curve (Figure 1.6; Bodnar et al., 1985) as the development of a vapor bubble forms at temperatures far lower than trapping. Thus the homogenization temperature is just an estimation of the minimum temperature of formation.

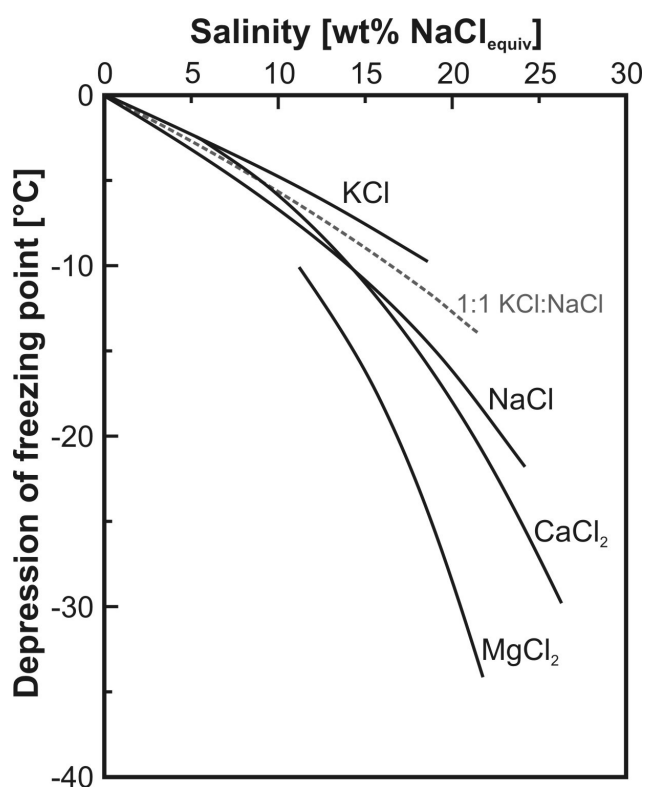


**Figure 2.6**

Diagram showing the depression of the freezing point of pure water as a function of the amount (wt%) and type of salt in solution (modified from Shepherd et al., 1985).

*Freezing* of a fluid inclusion below room temperature results in solidification of the fluid: it freezes to a solid (ice) and a vapor phase. The reversed course of this process (i.e. melting) is direct proportional to the composition of the fluid, which means that the depression of the ice melting point of an aqueous fluid inclusion provides a measure of the total solute

concentration (Roedder, 1984; Hall et al., 1988), (Figure 2.6). Since NaCl is the major solute in most inclusions, the depression of the melting point of ice is expressed as an equivalent of wt% NaCl. The relationship of melting temperature and salinity was identified by Bodnar (1993), based on experimental data from Hall et al. (1988):

$$\text{Salinity (wt\%)} = 1.78 \theta - 0.0442 \theta^2 + 0.000557 \theta^3 \quad (10)$$

where  $\theta$  is the depression of the melting point in °C. Equation (4) yields an accuracy of  $\pm 0.05$  wt% NaCl at all temperatures from 0.0°C to -21.2°C, the eutectic temperature for H<sub>2</sub>O-NaCl.

In more complex systems with components such as CO<sub>2</sub>, H<sub>2</sub>S, and SO<sub>4</sub>, additional phase changes can be observed upon freezing. Gas hydrates (clathrates) form, which incorporate large amounts of H<sub>2</sub>O leading to an increase of the relative concentration of salt in the remaining liquid phase. Thus the calculation of the salinity based on ice melting points yields values that are far too high. If large quantities of CO<sub>2</sub> are in the system, the difference to true salinity may exceed 100%. Therefore ice melting points need to be corrected for the amount of CO<sub>2</sub> which is a function of clathrate melting (e.g. Collins, 1979; Diamond, 1992, 2001). Moreover, natural aqueous systems usually contain also CH<sub>4</sub>, N<sub>2</sub>, and sulfur compounds which form mixed hydrates with CO<sub>2</sub> (e.g. Shepherd et al., 1985) making the calculation of salinities even more difficult. For such cases special programs have been developed (Bakker, 1997) which were also applied in this thesis to calculate NaCl- and CO<sub>2</sub> concentrations of natural fluid inclusions (see section 6.3.5)

Further details, including the apparatus, are given in the methods sections of the manuscripts (6.1.3, 6.2.3, and 6.3.5).

### **2.2.3 Raman Spectroscopy**

Raman spectroscopy was applied to detect CO<sub>2</sub> and sulfur-species within fluid inclusions as well as to identify solid mineral inclusions in natural quartz crystals and precipitates on the gold capsule walls.

Raman spectroscopy is based on the interaction of monochromatic light (in this case from a

laser source) with molecular vibrations of the sample which results in scattering of the incident light (Figure 2.7). The spectrum of scattered light consists of a dominant frequency that equals the incident frequency, the so called Rayleigh scattering which is filtered out. Raman scattering, on the other hand, is a shift in energy of the incident light due to the interaction of the photons of the incident light with the molecules of the sample. Thereby this molecule gets excited from its ground state ( $m$ ) to a virtual state of higher energy. As soon as the molecule relaxes, it emits a photon of lower energy than the incident photon and ends up in a higher vibrational stage. Thus, energy gets absorbed by the molecule resulting in the so-called Stokes scattering. However, due to thermal energy, some molecules may be present in an excited state ( $n$ ) right from the beginning. Scattering from this state to the ground state  $m$  is called anti-Stokes scattering which implies that energy is transferred from the sample to the scattered photon (i.e. to the light). Since at room temperature the number of molecules in an excited vibrational state ( $n$ ) is rather small, anti-Stokes scattering is weak.

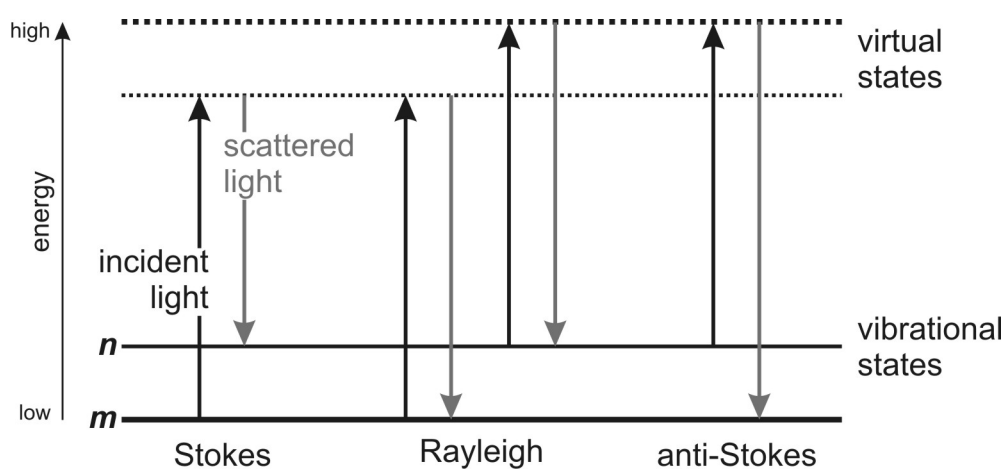


**Figure 2.7**

Schematic sketch of the Rayleigh and Raman scattering process.  $m$  = ground vibrational state, lowest energy;  $n$  = excited vibrational state, higher energy (after Smith and Dent, 2005).

Vibrational information and thus Raman shift is specific to chemical bonds and the symmetry of molecules, thus it is used to identify phases. The Raman shift is expressed as wavenumber  $w$  [ $\text{cm}^{-1}$ ] according to

$$\Delta w = \left( \frac{1}{\lambda_0} - \frac{1}{\lambda_1} \right) \quad (11)$$

where  $\lambda_0$  is the wavelength of the incident light and  $\lambda_1$  the wavelength of the Raman spectrum.

For Raman analyses conducted in this work, no special sample preparation was necessary. The polished thick sections were directly irradiated by the green laser beam generated by a Coherent Innova 90C argon ion laser and resulting scattered light was detected by a Horiba LabRAM HR 800 spectrometer. The resulting spectra of bands of Stokes-scattering of analyzed fluid phases were checked for  $\text{SO}_4^{2-}$ ,  $\text{HSO}_4^-$ ,  $\text{SO}_2$ ,  $\text{CO}_2$ ,  $\text{H}_2\text{S}$ ,  $\text{H}_2\text{O}$ , and  $\text{H}_2$  peaks (Burke, 2001). To identify solid inclusions, spectra of the unknown phases were compared with Raman spectra from reference materials and/or spectra from databases like the RRUFF-Project (<http://rruff.info/>).

For details concerning parameters of the measurements refer also to the methods sections in the manuscripts (6.1.3, 6.2.3, and 6.3.3)

#### 2.2.4 LA-ICP-MS

After application of all methods discussed above, fluid inclusions were finally analyzed by Laser Ablation (LA) – Inductively Coupled Plasma (ICP) – Mass Spectrometry (MS) which resulted in complete destruction of the inclusion. Nevertheless, LA-ICP-MS is the method of choice for fast measurements of element concentrations in fluid inclusions.

The setup of the apparatus is as follows: The sample is stored in an air-tight chamber where it is hit by the 193 nm laser-beam. The aerosol produced by ablation of the sample is carried in a gas flow of helium mixed with a small amount of hydrogen to the ICP. In the ICP, argon is electrically heated by an inductive coil to very high temperatures forming a plasma. The sample aerosol is first dried, atomized, and finally ionized. This ion beam leaves the ICP through a set of lenses which focus the beam before it enters the mass spectrometer. In the quadrupole mass spectrometer, which operates in high vacuum, ions are separated according to their mass to charge ratio. This is done by applying an electrical field of alternating and direct current potentials to an array of four rods. The ions pass the array of

rods with the applied potentials allowing only those ions of the selected mass to pass. By alternation of the applied current the wanted masses (elements) are detected one by one in very short times resulting in a quasi-simultaneous measurement of as many elements as required. For details concerning functional parameters of the measurements refer also to the methods sections in the manuscripts (6.1.3, 6.2.3, and 6.3.3).

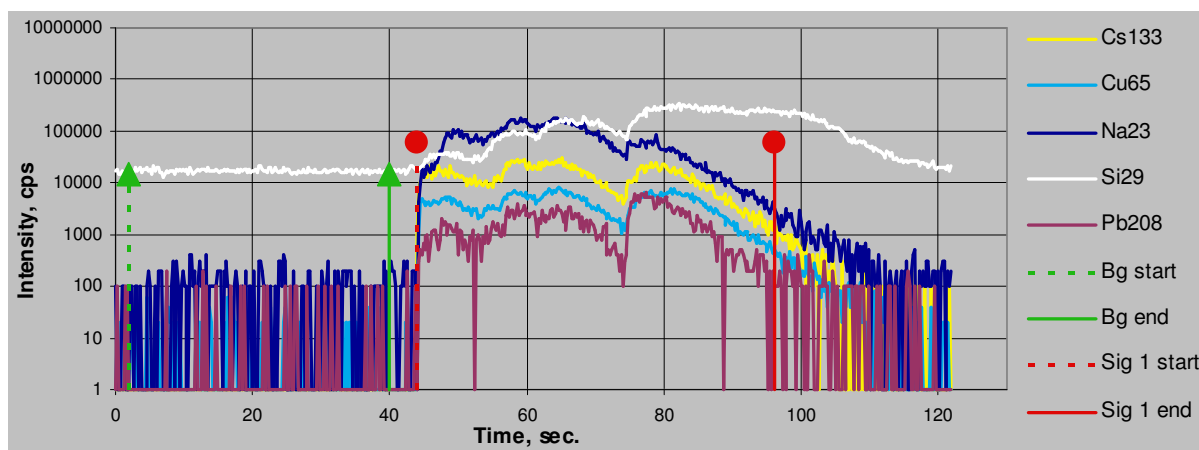


**Figure 2.8**

Typical counts per second versus time signal of an ablated brine inclusion measuring 15  $\mu\text{m}$ . Note the stepwise opening of the inclusion indicated by single plateaus of the Si-signal (white line). Vertical green lines define the background interval, red lines the selected interval of sample-ablation.

For fluid inclusion analysis using laser ablation, a special aperture is placed between the laser beam and the sample, which allows stepwise enlargement of the laser beam and stepwise opening of the inclusion. Thus quartz breakout and explosion of the inclusion is minimized. To obtain good statistical data correction, sets of up to 20 analyses were compiled with four measurements of NIST 610-glass as external standard bracketing up to 16 inclusion analyses (Spandler et al., 2011). Although the NIST 610 glass was standardized for almost 70 elements, it is not suitable for Cl- and S-analyses. To obtain useful values for these two elements, measurements of a well characterized piece of afghanite  $((\text{Na,Ca,K})_8[\text{Al}_6\text{Si}_6\text{O}_{24}](\text{SO}_4,\text{Cl}_2,\text{CO}_3)_3 \cdot 0.5\text{H}_2\text{O})$ , a Cl-, and S-rich silicate, were added as another external standard before and after effective fluid inclusion analyses (Seo et al., 2011). The resulting signals with their typical plateaus reflecting single laser beam-sizes

(Figure 2.8) was then processed in an Excel worksheet created by Dr. Bodo Hattendorf from the Laboratory of inorganic chemistry, ETH Zürich. Each analysis involved a 40 second gas blank interval at the beginning to correct for the background. Signals of every element were corrected for spikes and searched for specific characteristics like a sudden peak of Cu correlating with S in the middle of the signal which would indicate ablation of a Cu-sulfide daughter crystal.

Finally just that part of the signal where the inclusion was ablated (Figure 2.8) was integrated and used for the calculation of mass ratios based on external standardization which in turn were converted into absolute elemental concentrations using a known value as internal standard. Internal standards for both synthetic and natural vapor and brine inclusions, as well as for natural single-phase inclusions were concentrations of Na obtained from microthermometry. For synthetic single phase fluid inclusions the known concentrations of Rb or Cs in the fluid was taken as these elements tend to be not very reactive due to their large ionic radii. In case of melt inclusions the concentration of Al, estimated from similar melts as described in the literature, was taken as internal standard (details are given in the third manuscript in chapter 6.3.5).

### 3 RESULTS AND DISCUSSION

At this point a detailed summary will be given of the results presented in the manuscripts following in chapter 6. The manuscripts which all have been submitted, partly are already published or in press, provide an answer to many of the questions outlined at the beginning of this thesis.

#### *3.1 Cu partitioning between vapor and brine*

Vapor–brine partitioning experiments were carried out covering a wide range in temperature (600–800°C), pressure (70–130 MPa), fluid compositions (NaCl ± KCl ± FeCl<sub>2</sub>; S concentrations ranging from ~0.5 to ~6.6 wt%),  $f_{O_2}$  conditions (H<sub>2</sub>S-dominated to SO<sub>2</sub>-dominated), and fluid acidities (quench fluid pH ≤0.3 to 10).

First, the runs 04C and B021 from Nagaseki and Hayashi (2008) were reproduced under identical conditions at 600–650°C, 50–97 MPa, using an aqueous NaCl–HCl–CuCl–S-rich fluid and anthracene (C<sub>14</sub>H<sub>10</sub>) as reducing agent, but yielded completely different results: In contrast to their findings that Cu highly partitions into the vapor phase (with partition coefficients  $D_{Cu^{vap/brine}}$  of  $8.41 ± 4.83$  and  $13.18 ± 9.59$ ), very low  $D_{Cu^{vap/brine}}$ -values of  $0.32 ± 0.14$  and  $0.22 ± 0.11$  were obtained. However, since the small data volume in the study of Nagaseki and Hayashi (2008) of just one vapor measurement and their obviously wrong mass balance cast doubt on the high  $D_{Cu^{vap/brine}}$ -values, it is more likely that the numbers obtained in this study are correct and that the partition coefficient of Cu between the vapor and the brine at these conditions is in the order of 0.2–0.3.

Subsequent experiments were carried out using a natural mineral assemblage consisting of chalcopyrite–bornite–magnetite–biotite–orthoclase–albite–muscovite–quartz (± anhydrite) to internally buffer pH,  $f_{O_2}$ ,  $f_{S_2}$ , and the activity of Cu at similar values as they prevail in natural porphyry Cu deposits.  $D_{Cu^{vap/brine}}$  values obtained in these three experiments are low and well reproducible ( $0.11 ± 0.04$  to  $0.15 ± 0.04$ ), although different amounts of HCl and S were used in the starting mixture. This reproducibility and the oxidized state of S in the fluid inclusions imply that the buffer assemblages were effective throughout the runs.

The other experiments were conducted in compositionally simpler systems of just a few

components. (i) Two experiments with an aqueous fluid containing CuCl and elemental S were performed at 600°C, 70 MPa and 700°C, 100 MPa resulting in  $D_{\text{Cu}^{\text{vap/brine}}}$  values of  $0.17 \pm 0.04$  and  $0.16 \pm 0.09$ , respectively. (ii) A similar experiment was run with chalcocite as Cu-source and elemental S at 800°C, 130 MPa, resulting in a  $D_{\text{Cu}^{\text{vap/brine}}}$  value of  $0.31 \pm 0.03$  and intermediate sulfur valences ( $\text{H}_2\text{S} + \text{SO}_4^{2-}$ ). (iii)  $\text{H}_2\text{S}$ -dominated fluids were produced by the reaction of S with Ti metal and of  $\text{Na}_2\text{S}$  with HCl-bearing solutions. The resulting  $D_{\text{Cu}^{\text{vap/brine}}}$ -values are all  $\leq 0.20$ , independent of temperature (600-800°C), fluid acidity (quench fluid pH  $\leq 1$  to 10), or the concentration of S (0.5 - 6.6 wt%) in the fluid. (iv) One run with oxidized S-species in the fluid yielded a similarly low  $D_{\text{Cu}^{\text{vap/brine}}}$  value of  $0.22 \pm 0.07$ , as well as (v) one run containing a S-rich fluid and a buffer assemblage of chalcocite-albite-muscovite-orthoclase-topaz resembling the fluid that was trapped in vapor and brine inclusions in the Erongo granite (Namibia) yielding  $D_{\text{Cu}^{\text{vap/brine}}}$  value of  $0.08 \pm 0.04$  at 650°C, 80 MPa.

To summarize, none of these experiments resulted in  $D_{\text{Cu}^{\text{vap/brine}}}$  values greater than 0.31 although a large range of geologically relevant conditions has been covered. This result simply implies that Cu does not partition into the vapor phase at any plausible condition and that another explanation is suggested for the high concentrations of Cu measured in natural, quartz-hosted vapor inclusions (e.g. Heinrich et al., 1999; Seo et al., 2009).

### ***3.2 Re-equilibration of synthetic fluid inclusions***

Experiments have been carried out, which demonstrate that the Cu content of quartz-hosted fluid inclusions can be modified via cation exchange after their formation (Li et al., 2009; details are given in the fourth manuscript, section 6.4 ‘Rapid Na, Cu exchange between synthetic fluid inclusions and external aqueous solutions: Evidence from LA-ICP-MS analysis’): In these experiments, NaCl-Cu-rich fluid inclusions (synthesized in quartz at 700°C, 140-200 MPa) were re-equilibrated at 600-800°C, 70-140 MPa in a KCl-Cu-rich fluid, resulting in the loss of up to 83 % of the original concentration of Na and the gain of ~6000 ppm Cu in the inclusion. Other elements with larger ionic radii (i.e., K, Fe, Ba, Sr) were not exchanged, demonstrating that the inclusions remained physically intact and that

Na and Cu were transported through quartz by diffusion. However, whereas the diffusion of Na was triggered by a concentration gradient of Na between the inner and outer fluid, Cu diffused 'uphill' resulting in up to 10 times higher Cu concentrations in re-equilibrated fluid inclusions as compared to the outer fluid. These results show that the diffusion of Cu (and Na) in fact can modify the elemental budget of quartz hosted fluid inclusions, although the main process may not be the interdiffusion of Na and Cu.

In view of these findings, more re-equilibration experiments were carried out. Coexisting vapor and brine inclusions were first synthesized from H<sub>2</sub>O-NaCl-Cu-S-rich fluids at 800°C, 130 MPa and then re-equilibrated in a second step at 800°C, 70 MPa in fluids of slightly different compositions: i) In a first set, vapor and brine inclusions were re-equilibrated in a compositionally similar, but less acidic fluid (the quench fluid pH was 3 in contrast to a pH  $\leq 0.3$  in the primary run) resulting in a remarkable gain in Cu within the vapor inclusions, which changed the Cu partition coefficient  $D_{\text{Cu}^{\text{vap/brine}}}$  from  $0.31 \pm 0.05$  before re-equilibration to  $8.3 \pm 4.9$  after re-equilibration, whereas the concentrations of most other elements remained stable within analytical errors. New vapor and brine inclusions that were trapped during the re-equilibration run in a separate piece of quartz contained similar amounts of Cu as the fluid analyzed after the first step, implying that the outer fluid was not anomalously enriched in Cu and that diffusion of Cu was not caused by a gradient in Cu concentration. ii) The second pair of experiments did not contain S in the starting fluid resulting in just a small increase in  $D_{\text{Cu}^{\text{vap/brine}}}$  from  $0.37 \pm 0.06$  before re-equilibration to  $0.53 \pm 0.07$  after re-equilibration. iii) The third set of experiments was run with S in the starting fluid but without any pH change between the first and second step. It resulted in the decrease of  $D_{\text{Cu}^{\text{vap/brine}}}$  values from  $0.48 \pm 0.14$  to  $0.09 \pm 0.05$ . iv) A fourth pair of experiments run at H<sub>2</sub>S-dominated conditions resulted in a change of  $D_{\text{Cu}^{\text{vap/brine}}}$  from  $0.09 \pm 0.03$  to  $8.3 \pm 7.0$  whereas v) experiments run at oxidizing conditions yielded just a small increase of  $D_{\text{Cu}^{\text{vap/brine}}}$  from  $0.22 \pm 0.07$  to  $0.98 \pm 0.49$ . These results suggest that large increases in  $D_{\text{Cu}^{\text{vap/brine}}}$  values are produced only if (a) an originally acidic fluid is replaced by a less acidic one, and (b) the original fluid contains significant amounts of S. Additionally, the oxidation state of S also matters, as a more reduced fluid in the first step enhances the

increase of Cu in the vapor phase as compared to SO<sub>2</sub>-dominated fluids.

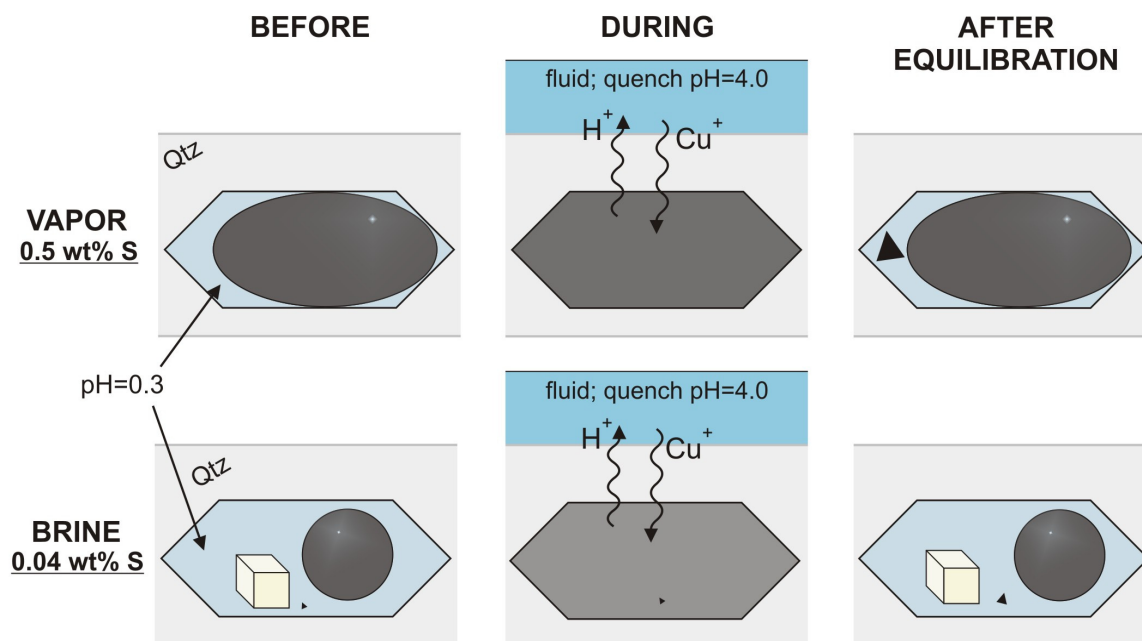


**Figure 3.1**

Sketch to illustrate the mechanism of Cu diffusion. A gradient in fluid acidity causes protons to diffuse out of the fluid inclusions, which in turn causes Cu (+ Na, Ag) to diffuse inward to maintain charge balance. The incoming Cu combines with S to precipitate as sulfides (black triangles). Because the amount of Cu that can be gained by this process is limited by the amount of sulfur present in the fluid inclusion, sulfur-rich vapor inclusions can take up more Cu than sulfur-poor brine inclusions.

Based on all these findings, a new model was developed, which explains the high concentrations of Cu found in the vapor phase of natural samples and after re-equilibration experiments (Figure 3.1): A gradient in fluid acidity causes H<sup>+</sup> to diffuse out of the fluid inclusions which in turn causes Cu<sup>+</sup> (and Na<sup>+</sup>, Ag<sup>+</sup>) to diffuse into the fluid inclusion to maintain charge balance. The incoming Cu combines with S to precipitate as sulfides which explains the large daughter crystals that are often found within natural vapor inclusions. Because the amount of Cu that can be gained by this process is limited by the amount of S present in the inclusion, S-rich vapor inclusions can take up more Cu than Cl-rich, S-poor brine inclusions resulting in artificially high  $D_{\text{Cu}}^{\text{vap/brine}}$ -values. Such a process is supported by findings in nature, where rock-buffered cooling and/or the dilution of magmatic-hydrothermal fluids by meteoric waters leads to an increase in fluid pH with time

(Burnham, 1979). Also the analysis of vapor inclusions of porphyry Cu deposits showed that they are really enriched in S (Seo et al., 2009).

All re-equilibration experiments mentioned above have been carried out at 800°C in order to speed up the diffusion process due to time constraints. To get an idea about the diffusion of Cu at lower, geologically more relevant temperatures, a minimum diffusion coefficient of Cu was calculated for a temperature of 800°C, being  $2.9 \times 10^{-10} \text{ m}^2\text{s}^{-1}$  and extrapolated it down to 400°C resulting in  $\sim 1.5 \times 10^{-12} \text{ m}^2\text{s}^{-1}$ . Based on this value it would take a maximum of 80 years for a 20  $\mu\text{m}$  sized fluid inclusion covered by 5 mm quartz to gain 5 wt% Cu at 400°C. Compared to the typical life span of a magmatic-hydrothermal fluid system this is negligibly small, suggesting that many natural, quartz-hosted fluid inclusions have been modified post entrapment and that true vapor-brine partition coefficients of Cu are in the range of 0.2-0.3, as it can be inferred from above mentioned partitioning experiments using natural mineral buffers.

### ***3.3 Re-equilibration of natural fluid inclusions***

In order to check whether the above mentioned modification of fluid inclusions in quartz could be reversed, a re-equilibration experiment was performed on a natural quartz sample containing coexisting trails of vapor and brine inclusions from a miarolitic cavity within the Erongo granite (Namibia). The analysis of these inclusions showed that the vapor phase contained high concentrations of Cu. The original fluid was reconstructed based on: i) the analysis of main- and trace elements by LA-ICP-MS yielding  $D_{\text{Cu}^{\text{vap/brine}}}$ -values of 10-66 and further suggesting that the vapor phase contained significant amounts of S; ii) microthermometry measurements yielding fluid salinities of  $\sim 4 \text{ wt}\% \text{ NaCl}_{\text{equiv}}$  in the vapor inclusions and 46-55 wt%  $\text{NaCl}_{\text{equiv}}$  in the brine inclusions and homogenization temperatures of  $\sim 600\text{-}650^\circ\text{C}$  suggesting entrapment pressures of  $\sim 60\text{-}80 \text{ MPa}$ ; iii) the presence of solid inclusions of K-feldspar, albite, and muscovite within the quartz crystal indicating that the fluid was acidic.

The trail of vapor and brine inclusions was then re-equilibrated for 22 days in a fluid composed of 15 wt% NaCl, 5 wt% KCl, 2 wt% S, and 1000-3000 ppm Pb, Rb, and Cs, which

corresponds to a 75 : 25 mixture of the analyzed vapor and brine inclusions at its original P-T conditions which were estimated to be 650°C and 80 MPa. The sample was equilibrated in the presence of a mineral assemblage of albite-muscovite-orthoclase-topaz, which buffered the fluid pH at a very low value and an excess amount of chalcocite ( $\text{Cu}_2\text{S}$ ) as Cu-source.

The analysis of the inclusion after the run showed that most of the Cu (and smaller amounts of Na) was lost from vapor inclusions, changing the  $D_{\text{Cu}}^{\text{vap/brine}}$  from  $11 \pm 9.3$  to  $0.06 \pm 0.04$ , which is exactly the contrary of what was observed in the re-equilibration experiments on synthetic fluid inclusions.

Another re-equilibration experiment was carried out using a sample from the Mo-mineralized Drammen granite (Norway) in order to find out if the unexpectedly high concentrations of Cu measured in intermediate density, single-phase fluid inclusions are true or may also have been modified post entrapment by the diffusional uptake of Cu. The procedure was similar to the one described above: a trail of inclusions was re-equilibrated in a fluid of similar composition than the trapped one. In this case the fluid was composed of 6.35 wt% NaCl, 3.2 wt% KCl, 0.5 wt% S, 350-650 ppm Cs and Rb, and 0.4 mol/kg<sub>solution</sub> HCl. Copper and Mo were added in excess amounts as chalcopyrite ( $\text{CuFeS}_2$ ) and molybdenite ( $\text{MoS}_2$ ) and the albite-muscovite-orthoclase-topaz mineral assemblage again was used to buffer the pH at a low value.

The analysis of the inclusions after the run revealed that within analytical uncertainty, only the concentrations of Na, Rb, and Cs changed significantly. Sodium decreased by a factor of three, whereas Rb and Cs increased by a factor of two. The concentration of Cu did not change within analytical uncertainty, however, it became much more reproducible changing from a Cu-value of  $1220 \pm 560$  to  $770 \pm 190$  ppm. This suggests that the high Cu-concentrations of some fluid inclusions in fact have been modified and during re-equilibration were brought more in line with the lower concentrations of Cu observed in other inclusions. However, the change was relatively small compared to the high degree of Cu diffusion observed in the re-equilibration studies of synthetic fluid inclusions and inclusions from the Erongo granite described above. This is probably related to the fact that the fluid inclusions on this trail from the Drammen granite contained much less sulfur

(~0.3 wt% S) than the synthetic vapor inclusions (~2.5 wt% S) and vapor inclusions from the Erongo granite (~2 wt% S). As was discussed in section 3.2, the amount of S inside an inclusion is the critical factor for the post-entrapment modification of Cu concentrations, implying that the elemental budget of fluid inclusions containing just small amounts of S is not altered much. Copper concentrations measured in such S-poor, quartz hosted natural fluid inclusions are thus much more reliable.

### ***3.4 Composition of melts and fluids in Mo-mineralized granites***

The analysis of melt-, fluid-, and solid inclusions in miarolitic quartz from three Mo-mineralized granites from Colorado and Norway provides new data on the composition of melts and primary magmatic-hydrothermal fluids forming porphyry Mo deposits.

Samples come from the Treasure Mountain Dome which is situated in the intensely mineralized Colorado Mineral Belt (USA). Although in close vicinity to the largest porphyry Mo deposits Climax, and Urad-Henderson, this granite is just of minor economic importance. Two relatively fractionated lithologies ('granular facies' and an outer 'leucocratic border phase') have been sampled, the latter hosting miarolitic cavities lined with euhedral crystals of quartz. The analysis of melt inclusions in quartz phenocrysts and miarolitic quartz showed that with increasing degree of crystallization and fractionation, incompatible elements like Cs, Rb, W, and Mo get enriched in the residual melt, whereas compatible elements like Mg, Fe, Ti, Ca, and Sr get depleted. Titanium concentrations decrease from melt inclusions analyzed in the leucocratic border phase, throughout the granular facies, to those in miarolitic quartz, whereas the concentrations of Rb, Mo, and W follow the opposite trend. In a closed system, the observed increase from ~5 ppm to ~90 ppm Cs in the residual melt requires a degree of crystallization of at least 90%. Thus, the melt inclusions analyzed in miarolitic quartz represent the very last melt fractions in almost completely crystallized granite. Molybdenite inclusions within the quartz phenocrysts of the border phase, together with the incompatible behavior of Mo suggest that the intruding magma originally was molybdenite-saturated.

The evolution of the mineralizing fluid from an originally single-phase, magmatic fluid

which enters the two-phase field upon decompression and cooling, to a fluid that finally becomes diluted by meteoric water is traced by different generations of fluid inclusions: intermediate-density fluid inclusions of relatively low salinities (5-10 wt% NaCl<sub>equiv</sub>), coexisting vapor and brine inclusions with increasingly disparate salinities, and low-salinity aqueous fluid with densities  $\geq 0.8-0.9$  g/cm<sup>3</sup>. The concentration of Mo within supercritical, intermediate density fluid inclusions shows a large variation between the different miarolitic quartz crystals from 2-5 ppm to 50-150 ppm, suggesting that most Mo precipitated at a certain moment from the magmatic-hydrothermal fluid at near-magmatic conditions. The concentrations of most other elements remained constant within a factor of ~2-3, apart from Cu, which varies by a factor of 6 to 60 in all samples. CO<sub>2</sub> concentrations vary from 2.5 to 7.9 mol%, S concentrations from <0.13 to 1.3 wt%, whereas Raman spectra reveal that sulfur occurs mostly as SO<sub>4</sub><sup>2-</sup> in the liquid portion of the fluid inclusions at ambient conditions. Homogenization temperatures were not determined to avoid decrepitation of the few high-temperature, magmatic fluid inclusions. A maximum pressure estimate of ~100 MPa may be inferred from solid inclusions of andalusite within the contact zone of the border phase and the host rocks.

Coexisting intermediate density fluid and melt inclusions provide an insight into the fluid-melt partitioning behavior of dissolved elements: The highest values are observed for Pb, Zn, and possibly Cu, while Ce and Al display the least preference for the fluid phase. The partition coefficient  $D_{\text{Mo}}^{\text{fluid/melt}}$  of Mo is  $2.4 \pm 1.8$  which is significantly below the threshold value of 25 which marks the passage from fractionation into the melt to fractionation into the fluid phase (at an estimated entrapment pressure of ~100 MPa, and a water solubility of ~4 wt% H<sub>2</sub>O), implying that the Mo concentration in the residual melt increased with increasing degree of crystallization. Copper, on the other hand, shows quite high  $D_{\text{Cu}}^{\text{fluid/melt}}$  of  $37.4 \pm 60.3$ .

Further samples have been studied from the Drammen ('medium- to fine-grained granite') and Glitrevann ('aplitic granite') granites, situated in the Oslo Rift (Norway), a region well-known for its rift-related Mo-mineralization.

Twenty melt inclusions of the Drammen granite were analyzed, of which 14 were situated along a 2 cm long transect through the border of a miarolitic cavity, extending from fine-

grained aplite over a pegmatitic contact zone into a euhedral quartz crystal, clearly indicating that W concentrations increase with increasing degree of melt fractionation. Molybdenum concentrations first increase from 11 to 32 ppm and then dramatically decrease to values around 6 ppm in the most evolved melts within the euhedral quartz crystal suggesting that at the very last stages of magma solidification changes in P, T,  $fS_2$ , and/or  $fO_2$  led to the precipitation of molybdenite.

Fluid evolution within the Drammen granite is similar to the one in the Treasure Mountain Dome, starting with intermediate-density, partly CO<sub>2</sub>-bearing fluid inclusions with salinities of 4.4-6.3 wt% NaCl<sub>equiv</sub>, passing through a stage of two-phase fluid, and finally reaching a state where aqueous, high-density fluid inclusions were trapped. However, P-T conditions (~680°C / 140 MPa) of the magmatic-hydrothermal fluid at Drammen, reconstructed from the intersection of intermediate-density fluid inclusion isochors with the granite solidus, differ from the ones in Colorado, especially regarding the much higher pressure. Molybdenum concentrations in intermediate-density fluid inclusions range from 3 to 270 ppm, with the majority of values clustering around 30-40 ppm Mo. Copper concentrations show a large scatter, ranging from 8 ppm to 3500 ppm without any apparent relationship to other elements. Although roughly contemporaneous, none of the analyzed fluid and melt inclusions were unambiguously coexisting. Accordingly, no fluid–melt partition coefficients were calculated.

Useful miarolitic quartz samples from the Glitrevann granite were limited and thus only a few results can be presented. Analyses of melt inclusion in quartz crystals within the aplitic granite shows that these melts are just slightly more fractionated than the average whole-rock composition reported in the literature (Jensen, 1985). Molybdenum concentrations add up to  $12 \pm 1$  ppm.

Within the quartz crystals from miarolitic cavities, no melt inclusions were found. Intermediate-density fluid inclusions are rare and restricted to the base of the crystals, but coexisting vapor and brine inclusions are more abundant, with late-stage brine inclusions reaching salinities of up to 80 wt% NaCl<sub>equiv</sub>. Intermediate-density fluid inclusions have salinities of 6.7-8.1 wt% NaCl<sub>equiv</sub>, contain 2.1-3.5 mol% CO<sub>2</sub>, 5-180 ppm Cu with the majority of values clustering around 20 ppm, and rather low Mo concentrations in the order

of ~5 ppm. The fact that none of these inclusions contains more than 1100 ppm Al suggests that they probably do not represent magmatic fluids, but were trapped at subsolidus conditions, being comparable to the Mo-poor intermediate-density fluid inclusions measured in some Treasure Mountain samples.

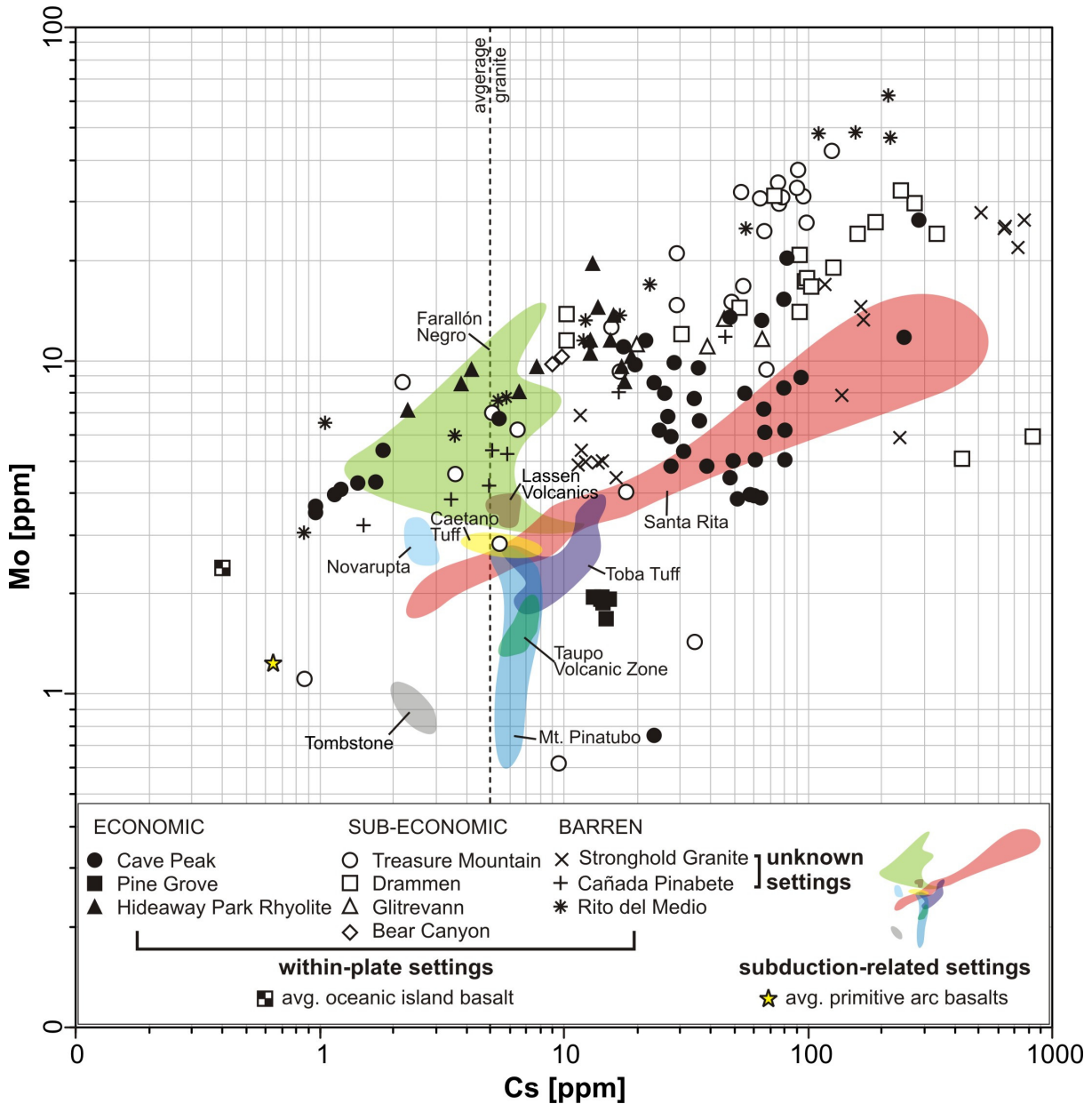


**Figure 3.2**

Molybdenum versus Cs-concentrations of melt inclusions from Mo- and Cu mineralized granites and porphyries, sorted according to their economic relevance and tectonic setting. Note the generally lower Mo/Cs-ratios of subduction-related melts compared to melts from within-plate settings. Sources of data: see section 6.3.6.

The comparison of this data from subeconomic deposits with data from economic porphyry Mo deposits and barren granites in intra-plate settings worldwide shows that with regard to the metal content of input melts there is no systematic difference between economically Mo-mineralized and barren granites. Melts from subduction-related porphyry Cu (Mo ± Au) deposits, on the other hand, exhibit lower Mo-contents than similarly evolved melts from within-plate settings. The same applies for Mo-concentrations in the input fluids: Maximum Mo concentrations in porphyry Mo-related fluids are similar to those observed in fluids from sub-economically mineralized and barren intrusions in within-plate settings. Furthermore, fluids from Mo-mineralized granites have higher Cs and Mo contents than those from porphyry Cu (Mo) deposits which reflects the higher degree of fractionation of melts in the former occurrences (Figure 3.2). This is in line with the higher concentrations of compatible Cu in porphyry Cu (Mo)-related fluids. However, absolute Cu concentrations are always at least five times higher than Mo concentrations, even in those fluids that produced pure Mo mineralization, leading to the question where all this Cu went, since no recoverable Cu-ore was found in most porphyry Mo deposits. A possible explanation is the selective precipitation of Mo at near-magmatic levels in contrast to Cu and Fe, which were possibly deposited at higher levels and thus might have already been eroded.

In summary, the range of Mo concentrations measured in single-phase, pre-mineralization fluids from barren and productive intrusions is relatively small (~1.6 orders of magnitude), suggesting that the Mo-mineralization potential was to a larger extent controlled by other factors. These factors are very likely the size and shape of the underlying batholithic system, the depth of magma emplacement, and the episodic intrusion of magmas ensuring a constant flux of metals and sulfur to the porphyry level resulting in high-grade ore shells within a small rock volume.

## 4 REFERENCES

- Albarède, F., (2004) The stable isotope geochemistry of copper and zinc. *Reviews in Mineralogy and Geochemistry* **55**, 409-427.
- Arancibia, O. N. and Clark, A. H., (1996) Early magnetite-amphibole-plagioclase alteration-mineralization in the Island Cooper porphyry copper-gold-molybdenum deposit, British Columbia. *Economic Geology* **91**, 402-438.
- Arculus, R. J., (1994) Aspects of magma genesis in arcs. *Lithos* **33**, 189-208.
- Arribas, A. J., (1995) Characteristics of high-sulfidation epithermal deposits, and their relation to magmatic fluid. In: Thompson, J. F. H. (Ed.), *Magmas, fluids, and ore deposits*. Mineralogical Association of Canada Short Course Series. 419-454.
- Asael, D., Matthews, A., Bar-Matthews, M., and Halicz, L., (2007) Copper isotope fractionation in sedimentary copper mineralization (Timna Valley, Israel). *Chemical Geology* **243**, 238-254.
- Audétat, A., (2010) Source and evolution of molybdenum in the porphyry Mo(-Nb) deposit at Cave Peak, Texas. *Journal of Petrology* **51**, 1739-1760.
- Audétat, A. and Pettke, T., (2006) Evolution of a porphyry-Cu mineralized magma system at Santa Rita, New Mexico (USA). *Journal of Petrology* **47**, 2021-2046.
- Audétat, A., Pettke, T., Heinrich, C. A., and Bodnar, R. J., (2008) The composition of magmatic-hydrothermal fluids in barren versus mineralized intrusions. *Economic Geology Special Paper* **103**, 877-908.
- Averkin, Y. A. and Candela, P. A., (1994) Thermo- and fluid dynamic effects of expansion in the model granitic system Ab-Q-H<sub>2</sub>O during crystallization and volatile separation. *Eos, Transactions, American Geophysical Union* **75**, S363.
- Bakker, R. J., (1997) Clathrates: Computer programs to calculate fluid inclusion V-X properties using clathrate melting temperatures. *Computers & Geosciences* **23**, 1-18.
- Bell, A. and Simon, A. C., (2011) Evidence for the alteration of the Fe<sup>3+</sup>/ΣFe of silicate melt caused by the degassing of chlorine-bearing aqueous volatiles. *Geology* **39**, 499-502.
- Bell, A., Simon, A. C., and Guillong, M., (2009) Experimental constraints on Pt, Pd, and Au partitioning in silicate melt-sulfide-oxide-aqueous fluid systems at 800°C, 150 MPa, and variable sulfur fugacity. *Geochimica et Cosmochimica Acta* **73**, 5778-5792.
- Benning, L. G. and Seward, T. M., (1996) Hydrosulfide complexing of gold(I) in hydrothermal solutions from 150-500°C and 500 to 1500 bars. *Geochimica et Cosmochimica Acta* **60**, 1849-1872.
- Binder, B. and Keppler, H., (2011) The oxidation state of sulfur in magmatic fluids. *Earth and Planetary Science Letters* **301**, 190-198.
- Bodnar, R. J., (1993) Revised equation and table for determining the freezing point depression of H<sub>2</sub>O-NaCl solutions. *Geochimica et Cosmochimica Acta* **57**, 683-684.

- Bodnar, R. J. and Vityk, M. O., (1994) Interpretation of microthermometric data for H<sub>2</sub>O-NaCl fluid inclusions. In: Vivo, B. D. and Frezzotti, M. L. (Eds.), *Fluid Inclusions in Minerals, Methods and Applications*. Virginia Tech, Blacksburg/VA. 117-130 p.
- Bodnar, R. J., Burnham, C. W., and Sterner, S. M., (1985) Synthetic fluid inclusions in natural quartz. III. Determination of phase equilibrium properties in the system H<sub>2</sub>O-NaCl to 1000°C and 1500 bars. *Geochimica et Cosmochimica Acta* **49**, 1861-1873.
- Bookstrom, A. A., (1989) The Climax-Alma granite batholith of Oligocene age and the porphyry molybdenum deposits of Climax, Colorado, U.S.A. *Engineering Geology* **27**, 543-568.
- Bookstrom, A. A., Carten, R. B., Shannon, R. D., and Smith, R. P., (1988) Origins of bimodal leucogranite-lamprophyre suites, Climax and Red Mountain porphyry molybdenum systems, Colorado: Petrologic and strontium isotopic evidence. *Colorado School of Mines Quarterly* **83**, 1-65.
- Bornhorst, T. J. and Rose, W. I., (1986) Partitioning of gold in young calc-alkaline volcanic rocks from Guatemala. *Journal of Geology* **94**, 412-418.
- Brandeis, G. and Jaupert, C., (1987) The kinetics of nucleation and crystal growth and scaling laws for magmatic crystallization. *Contributions to Mineralogy and Petrology* **96**, 24-34.
- Brandon, A. D. and Draper, D. S., (1996) Constraints on the origin of the oxidation state of mantle overlying subduction zones: An example from Simcoe, Washington, USA1. *Geochimica et Cosmochimica Acta* **60**, 1739-1749.
- Burnham, C. W., (1967) Hydrothermal fluids at the magmatic stage. In: Barnes, H. L. (Ed.), *Geochemistry of hydrothermal ore deposits*. Holt, Rinehart and Wilson, New York. 34-76.
- Burnham, C. W., (1979) Magmas and hydrothermal fluids. In: Barnes, H. L. (Ed.), *Geochemistry of hydrothermal ore deposits, 2<sup>nd</sup> edition*. John Wiley & Sons. 71-136.
- Burnham, C. W., (1997) Magmas and hydrothermal fluids. In: Barnes, H. L. (Ed.), *Geochemistry of hydrothermal ore deposits, 3<sup>rd</sup> edition*. Wiley & Sons, New York. 63-124.
- Burnham, C. W. and Ohmoto, H., (1980) Late-stage processes of felsic magmatism. *Mining Geology Special Issue* **8**, 1-11.
- Chambefort, I., Dilles, J. H., and Kent, A. J. R., (2008) Anhydrite-bearing andesite and dacite as a source for sulfur in magmatic-hydrothermal mineral deposits. *Geology* **36**, 719-722.
- Campbell, I. H. and Naldrett, A. J., (1979) The influence of silicate:sulfide ratios in the geochemistry of magmatic sulfides. *Economic Geology* **74**, 1503-1506.
- Campbell, T. H., Ballard, J. R., Palin, J. M., Allen, C., and Faunes, A., (2006) U-Pb zircon geochronology of granitic rocks from the Chuquicamata-El Abra porphyry copper belt of northern Chile: Excimer laser ablation ICP-MS analysis. *Economic Geology* **101**, 1327-1344.
- Candela, P. A., (1991) Physics of aqueous phase evolution in plutonic environments. *American Mineralogist* **76**, 1081-1091.

- Candela, P. A. and Holland, H. D., (1984) The partitioning of copper and molybdenum between silicate melts and aqueous fluids. *Geochimica et Cosmochimica Acta* **48**, 373-380.
- Candela, P. A. and Holland, H. D., (1986) A mass transfer model for copper and molybdenum in magmatic hydrothermal systems: the origin of porphyry-type ore deposits. *Economic Geology* **81**, 1-19.
- Chapin, C. E., (2012) Origin of the Colorado Mineral Belt. *Geosphere* **8**, 28-43.
- Carroll, M. R. and Rutherford, M. J., (1985) Sulfide and sulfate saturation in hydrous silicate melts. *Journal of Geophysical Research* **90**, **Supplement**, C601-C612.
- Carten, R. B., Geraghty, E. P., and Walker, B. M., (1988) Cyclic development of igneous features and their relationship to high-temperature hydrothermal features in the Henderson porphyry molybdenum deposit, Colorado. *Economic Geology* **83**, 266-296.
- Carten, R. B., White, W. H., and Stein, H. J., (1993) High-grade granite-related molybdenum systems: Classification and origin. In: Kirkham, R. V., Sinclair, W. D., Thorpe, R. I., and Duke, J. M. (Eds.), *Mineral Deposit Modeling*. Geological Association of Canada, Special Paper 40. 521-554.
- Chambefort, I., Dilles, J. H., and Kent, A. J. R., (2008) Anhydrite-bearing andesite and dacite as a source for sulfur in magmatic-hydrothermal mineral deposits. *Geology* **36**, 719-722.
- Chapin, C. E., (2012) Origin of the Colorado Mineral Belt. *Geosphere* **8**, 28-43.
- Clark, K. F., (1972) Stockwork molybdenum deposits in the Western Cordillera of North America. *Economic Geology* **67**, 731-758.
- Clark, A. H., (1993) Are outsized porphyry copper deposits either anatomically or environmentally distinctive. In: Whiting, B. H., Hodgson, C. J., and Mason, R. (Eds.), *Giant Ore Deposits*. SEG Special Publication Queen's University,
- Clemens, J. D. and Mawer, C. K., (1992) Granitic magma transport by fracture propagation. *Tectonophysics* **204**, 339-360.
- Cline, J. S., (1995) Genesis of porphyry copper deposits: The behavior of water, chloride, and copper in crystallizing melts. *Arizona Geological Society Digest* **20**, 69-82.
- Cline, J. S. and Bodnar, R. J., (1991) Can economic porphyry copper mineralization be generated by a typical calc-alkaline melt? *Journal of Geophysical Research* **96**, 8113-8126.
- Cloos, M., (2001) Bubbling magma chambers, cupolas, and porphyry copper deposits. *International Geology Review* **43**, 285-311.
- Collins, P. L. F., (1979) Gas hydrates in CO<sub>2</sub>-bearing fluid inclusions and the use of freezing data for estimation of salinity. *Economic Geology* **74**, 1435-1444.
- Creasey, S. C., (1966) Hydrothermal alteration. In: Titley, S. and Hicks, C. L. (Eds.), *Geology of the porphyry copper deposits, southwestern United States*. University of Arizona Press, Tucson. 51-74.
- Crerar, D. A. and Barnes, H. L., (1976) Ore solution Chemistry V. Solubilities of chalcopyrite and chalcocite assemblages in hydrothermal solution at 200 °C to 350 °C.

*Economic Geology* **71**, 772-794.

Cruden, A. R., (1998) On the emplacement of tabular granites. *Journal of the Geological Society, London* **155**, 853-862.

Cunningham, C. G., (1978) Pressure gradients and boiling as mechanisms for localizing ore in porphyry systems. *U. S. Geological Survey Journal of Research* **6**, 745-754.

Davidson, J. P., (1996) Deciphering mantle and crustal signatures in subduction zone magmatism. In: Bebout, G. E., Scholl, D. W., Kirby, S. H., and Platt, J. P. (Eds.), *Subduction: Top to bottom*. American Geophysical Union, Geophysical Monograph 251-262.

Deckart, K., Clark, A. H., Aguilar, C., Vargas, R., Bertens, A., Mortensen, J. K., and Fanning, M., (2005) Magmatic and hydrothermal chronology of the giant Rio Blanco porphyry copper deposit, central Chile: Implications of an integrated U-Pb and <sup>40</sup>Ar/<sup>39</sup>Ar database. *Economic Geology* **100**, 905-934.

de Hoog, J. C. M., Mason, P. R. D., and van Bergen, M. J., (2001) Sulfur and chalcophile elements in subduction zones: constraints from a laser ablation ICP-MS study of melt inclusions from Galunggung Volcano, Indonesia. *Geochimica et Cosmochimica Acta* **65**, 3147-3164.

de Saint-Blanquat, M., Law, R. D., Bouchez, J.-L., and Morgan, S. S., (2001) Internal structure and emplacement of the Papoose Flat pluton: An integrated structural, petrographic, and magnetic susceptibility study. *Geological Society of America Bulletin* **113**, 976-995.

Diamond, L. W., (1992) Stability of CO<sub>2</sub> clathrate hydrate + CO<sub>2</sub> liquid + CO<sub>2</sub> vapour + aqueous KCl-NaCl solutions: Experimental determination and application to salinity estimates of fluid inclusions. *Geochimica et Cosmochimica Acta* **56**, 273-280.

Diamond, L. W., (2001) Review of the systematics of CO<sub>2</sub>-H<sub>2</sub>O fluid inclusions. *Lithos* **55**, 69-99.

Dilles, J. H. and Wright, J. E., (1988) The chronology of early Mesozoic arc magmatism in the Yerington district, Nevada, and its regional implications. *Geological Society of America Bulletin* **100**, 644-652.

Dilles, J. H., Tomlinson, A. J., Martin, M. W., and Blanco, N., (1997) El Abra and Fortuna complexes: A porphyry copper batholith sinistrally displaced by the Falla Oeste. *Congreso Geológico Chileno, 8<sup>th</sup>, Antofagasta, 1997, Actas* **3**, 1883-1887.

Drummond, S. E. and Ohmoto, H., (1985) Chemical evolution and mineral deposition in boiling hydrothermal systems. *Economic Geology* **80**, 126-147.

Duc-Tin, Q., Audétat, A., and Keppler, H., (2007) Solubility of tin in (Cl, F)-bearing aqueous fluids at 700°C, 140 MPa: A LA-ICP-MS study on synthetic fluid inclusions. *Geochimica et Cosmochimica Acta* **71**, 3323-3335.

Ehrlich, S., Butler, I., Halicz, L., Rickard, D., Oldroyd, A., and Matthews, A., (2004) Experimental study of the copper isotope fractionation between aqueous Cu(II) and covellite, CuS. *Chemical Geology* **209**, 259-269.

- Einaudi, M. T., Hedenquist, J. W., and Inan, E. E., (2003) Sulfidation state of fluids in active and extinct hydrothermal systems: Transitions from porphyry to epithermal environments. *Society of Economic Geologists. Special Publication* **10**, 285-313.
- Etschmann, B. E., Liu, W., Testemale, D., Müller, H., Rae, N. A., Proux, O., Hazemann, J. L., and Brugger, J., (2010) An *in situ* XAS study of copper(I) transport as hydrosulfide complexes in hydrothermal solutions (25-592 °C, 180-600 bar): Speciation and solubility in vapor and liquid phases. *Geochimica et Cosmochimica Acta* **74**, 4723-4739.
- Forneris, J. F. and Holloway, J. R., (2003) Phase equilibria in subducting basaltic crust: implications for H<sub>2</sub>O release from the slab. *Earth and Planetary Science Letters* **214**, 187-201.
- Fournier, R. O., (1968) Depths of intrusion and conditions of hydrothermal alteration in porphyry copper deposits. *Geological Society of America, Abstracts with Programs, Annual Meeting New Mexico*, 101.
- Fournier, R. O., (1999) Hydrothermal processes related to movement of fluid from plastic into brittle rock in the magmatic-epithermal environment. *Economic Geology* **94**, 1193-1211.
- Frank, M. R., Simon, A. C., Pettke, T., Candela, P. A., and Piccoli, P. M., (2011) Gold and copper partitioning in magmatic-hydrothermal systems at 800°C and 100 MPa. *Geochimica et Cosmochimica Acta* **75**, 2470-2482.
- Gibert, F., Pascal, M. L., and Pichavant, M., (1998) Gold solubility and speciation in hydrothermal solutions: experimental study of the stability of hydrosulphide complex of gold (AuHS) at 350 to 450°C and 500 bars. *Geochimica et Cosmochimica Acta* **62**, 2931-2947.
- Giggenbach, W. F., (1997) The origin and evolution of fluids in magmatic-hydrothermal systems. In: Barnes, H. L. (Ed.), *Geochemistry of hydrothermal ore deposits, 3<sup>rd</sup> edition*. John Wiley, New York. 737-796.
- Gill, J. B., (1981) *Orogenetic andesites and plate tectonics*. Springer-Verlag, New York. 390 p.
- Glazner, A. F. and Ussler, W., (1988) Trapping of magma at midcrustal density discontinuities. *Geophysical Research Letters* **15**, 673-675.
- Guillou-Frottier, L. and Burov, E., (2003) The development and fracturing of plutonic apices: implications for porphyry ore deposits. *Earth and Planetary Science Letters* **214**, 341-356.
- Gustafson, L. B. and Quiroga, G., (1995) Patterns of mineralization and alteration below the porphyry copper body at El Salvador, Chile. *Economic Geology* **90**, 2-16.
- Hall, D. L., Sterner, S. M., and Bodnar, R. J., (1988) Freezing point depression of NaCl-KCl-H<sub>2</sub>O solutions. *Economic Geology* **83**, 197-202.
- Hamlyn, P. R., Keays, R. R., Cameron, W. E., Crawford, A. J., and Waldron, H. M., (1985) Precious metals in magnesian low-Ti lavas: implications for metallogenesis and sulfur saturation in primary magmas. *Geochimica et Cosmochimica Acta* **49**, 1797-1811.

- Hattori, K. H. and Keith, J. D., (2001) Contribution of mafic melt to porphyry copper mineralization: evidence from Mount Pinatubo, Philippines, and Bingham Canyon, Utah, USA. *Mineralium Deposita* **36**, 799-806.
- Hayashi, K. I. and Ohmoto, H., (1991) Solubility of gold in NaCl- and H<sub>2</sub>S-bearing aqueous solutions at 250-350°C. *Geochimica et Cosmochimica Acta* **55**, 2111-2126.
- Hedenquist, J. W., (1995) The ascent of magmatic fluid: discharge versus mineralization. In: Thompson, J. F. H. (Ed.), *Magmas, Fluids, and Ore Deposits*. Mineralogical Society of Canada, Short Course Series 23. 263-289.
- Hedenquist, J. W. and Lowenstern, J. B., (1994) The role of magmas in the formation of hydrothermal ore deposits. *Nature* **370**, 519-527.
- Hedenquist, J. W., Matsuhisa, Y., Izawa, E., White, N. C., Giggenbach, W. F., and Aoki, M., (1994) Geology, geochemistry, and origin of high sulfidation Cu-Au mineralization in the Nansatsu district, Japan. *Economic Geology* **89**, 1-30.
- Hedenquist, J. W., Arribas, A. J., and Reynolds, J. R., (1998) Evolution of an intrusion-centered hydrothermal system: Far Southeast-Lepanto porphyry and epithermal Cu-Au deposits, Philippines. *Economic Geology* **93**, 373-404.
- Heinrich, C. A., Ryan, C. G., Mernagh, T. P., and Eadington, P. J., (1992) Segregation of ore metals between magmatic brine and vapor - A fluid inclusion study using PIXE microanalysis. *Economic Geology* **87**, 1566-1583.
- Heinrich, C. A., Günther, D., Audétat, A., Ulrich, T., and Frischknecht, R., (1999) Metal fractionation between magmatic brine and vapor, determined by microanalysis of fluid inclusions. *Geology* **27**, 755-758.
- Helz, G. R., Charnock, J. M., Vaughan, D. J., and Garner, C. D., (1993) Multinuclearity of aqueous copper and zinc bisulfide complexes: an EXAFS investigation. *Geochimica et Cosmochimica Acta* **57**, 15-25.
- Henley, R. W. and McNabb, A., (1978) Magmatic vapor plumes and ground-water interaction in porphyry copper emplacement. *Economic Geology* **73**, 1-20.
- Hildreth, W., (1981) Gradients in silicic magma chambers: Implications for lithospheric magmatism. *Journal of Geophysical Research* **86**, 10153-10192.
- Hildreth, W. and Moorbath, S., (1988) Crustal contributions to arc magmatism in the Andes of central Chile. *Contributions to Mineralogy and Petrology* **98**, 455-489.
- Holland, H. D., (1965) Some applications of thermochemical data to problems of ore deposits II. Mineral assemblages and the composition of ore forming fluids *Economic Geology* **60**, 1101-1166.
- Holland, H. D., (1972) Granite, solutions and base metal deposits. *Economic Geology* **67**, 281-301.
- Ishihara, S., (1981) The granitoid series and mineralization. *Economic Geology* **75<sup>th</sup>** Anniversary Volume, 458-484.
- Jensen, I. S., (1985) Geochemistry of the central granitic stock in the Glitrevann cauldron

within the Oslo rift, Norway. *Norsk Geologisk Tidsskrift* **65**, 201-216.

Jugo, P. J., (2009) Sulfur content at sulfide saturation in oxidized magmas. *Geology* **37**, 415-418.

Jugo, P. J., Candela, P. A., and Piccoli, P. M., (1999) Magmatic sulfides and Au: Cu ratios in porphyry deposits: an experimental study of copper and gold partitioning at 850°C, 100 MPa in a haplogranitic melt-pyrrhotite-intermediate solid solution-gold metal assemblage, at gas saturation. *Lithos* **46**, 573-589.

Jugo, P. J., Luth, R. W., and Richards, J. P., (2005a) An experimental study of the sulfur content in basaltic melts saturated with immiscible sulfide or sulfate liquids at 1300°C and 1.0 GPa. *Journal of Petrology* **46**, 783-798.

Jugo, P. J., Luth, R. W., and Richards, J. P., (2005b) Experimental data on the speciation of sulfur as a function of oxygen fugacity in basaltic melts. *Geochimica et Cosmochimica Acta* **69**, 497-503.

Kamenetsky, V. S. and Danyushevsky, L. V., (2005) Metals in quartz-hosted melt inclusions: Natural facts and experimental artifacts. *American Mineralogist* **90**, 1674-1678.

Keppler, H., (2010) The distribution of sulfur between haplogranitic melts and aqueous fluids *Geochimica et Cosmochimica Acta* **74**, 645-660.

Keppler, H. and Wyllie, P. J., (1991) Partitioning of Cu, Sn, Mo, W, U, and Th between melt and aqueous fluid in the systems haplogranite-H<sub>2</sub>O HCl and haplogranite-H<sub>2</sub>O HF. *Contributions to Mineralogy and Petrology* **109**, 139-150.

Khitarov, N. I., Malinin, S. P., Lebedev, Y. B., and Shibayeva, N. P., (1982) The distribution of Zn, Cu, Pb, and Mo between a fluid phase and a silicate melt of granitic composition at high temperatures and pressures. *Geochemistry International* **19**, 123-136.

Klemm, L. M., Pettke, T., and Heinrich, C. A., (2008) Fluid and source magma evolution of the Questa porphyry Mo deposit, New Mexico, USA. *Mineralium Deposita* **43**, 533-552.

Krahulec, K. A., (1997) History and production of the West Mountain (Bingham) mining district, Utah. In: John, D. A. and Ballantyne, G. H. (Eds.), *Geology and ore deposits of the Oquirrh and Wasatch Mountains, Utah*. Guidebook Series of the Society of Economic Geologists. 189-217.

Krauskopf, K. B., (1979) *Introduction to geochemistry*. McGraw-Hill Book Co., New York. 617 p.

Landtwing, M. R., Pettke, T., Halter, W. E., Heinrich, C. A., Redmond, P. B., Einaudi, M. T., and Kunze, K., (2005) Copper deposition during quartz dissolution by cooling magmatic-hydrothermal fluids: The Bingham porphyry. *Earth and Planetary Science Letters* **235**, 229-243.

Larson, P. B., Maher, K., Ramos, F. C., Chang, Z., Gaspar, M., and Meinert, L. D., (2003) Copper isotope ratios in magmatic and hydrothermal ore-forming environments. *Chemical Geology* **201**, 337-350.

Li, Y., Audétat, A., Lerchbaumer, L., and Xiong, X. L., (2009) Rapid Na, Cu exchange between synthetic fluid inclusions and external aqueous solutions: evidence from LA-ICP-

- MS analysis. *Geofluids* **9**, 321-329.
- Lister, J. R. and Kerr, R. C., (1991) Fluid-mechanical models of crack propagation and their application to magma transport in dykes. *Journal of Geophysical Research* **96**, 10049-10077.
- Loucks, R. R. and Mavrogenes, J. A., (1999) Gold solubility in supercritical hydrothermal brines measured in synthetic fluid inclusions. *Science* **284**.
- Lowell, J. D. and Guilbert, J. M., (1970) Lateral and vertical alteration-mineralization zoning in porphyry copper ore deposits. *Economic Geology* **65**, 373-408.
- Lowenstern, J. B., Mahood, G. A., Rivers, M. L., and Sutton, S. R., (1991) Evidence for extreme partitioning of copper into a magmatic vapor phase. *Science* **252**, 1345-1460.
- Ludington, S. and Plumlee, G. S., (2009) Climax-type porphyry molybdenum deposits. *USGS open-file report 2009 1215*, 16 pages.
- Lynton, S. J., Candela, P. A., and Piccoli, P. M., (1993) An experimental study of the partitioning of copper between pyrrhotite and a high silicate rhyolitic melt. *Economic Geology* **88**, 901-915.
- Maréchal, C., Télouk, P., and Albarède, F., (1999) Precise analysis of copper and zinc isotopic compositions by plasma-source mass spectrometry. *Chemical Geology* **156**, 251-273.
- Markl, G., Lahaye, Y., and Schwinn, G., (2006) Copper isotopes as monitors of redox processes in hydrothermal mineralization. *Geochimica et Cosmochimica Acta* **70**, 4215-4228.
- Marthur, R., Titley, S., Barra, F., Brantley, S., Wilson, M., Phillips, A., Munizaga, F., Maksaev, V., Vervoort, J., and Hart, G., (2009) Exploration potential of Cu isotope fractionation in porphyry copper deposits. *Journal of Geochemical Exploration* **102**, 1-6.
- Mathez, E. A., (1984) Influence of degassing on oxidation states of basaltic magmas. *Nature* **310**, 371-375.
- Matthews, W., Linnen, R. L., and Guo, Q., (2003) A filler-rod technique for controlling redox conditions in cold-seal pressure vessels. *American Mineralogist* **88**, 701-707.
- Mavrogenes, J. A. and Bodnar, R. J., (1994) Hydrogen movement into and out of fluid inclusions in quartz: Experimental evidence and geologic implications. *Geochimica et Cosmochimica Acta* **58**, 141-149.
- McNulty, B. A., Farber, D. L., Wallace, G. S., Lopez, R., and Palacois, O., (1998) Role of plate kinematics and plate-slip-vector partitioning in continental magmatic arcs: Evidence from the Cordillera Blanca, Peru. *Geology* **26**, 827-830.
- Métrich, N. and Wallace, P. J., (2008) Volatile abundances in basaltic magmas and their degassing paths tracked by melt inclusions. *Reviews in Mineralogy and Geochemistry* **69**, 363-402.
- Meyer, C. and Hemley, J. J., (1967) Wall rock alteration. In: Barnes, H. L. (Ed.), *Geochemistry of hydrothermal ore deposits*. Holt, Rinehart and Winston, New York. 166-235.

- Mortensen, G. L., Ghosh, D. K., and Ferri, F., (1995) U-Pb geochronology of intrusive rocks associated with copper-gold porphyry deposits in the Canadian Cordillera. *Canadian Institute of Mining, Metallurgy and Petroleum. Special Volume* **46**, 142-158.
- Mountain, B. W. and Seward, T. M., (1999) The hydrosulphide/sulphide complexes of copper(I): Experimental determination of stoichiometry and stability at 22°C and reassessment of high temperature data. *Geochimica et Cosmochimica Acta* **63**, 11-29.
- Mountain, B. W. and Seward, T. M., (2003) Hydrosulfide/sulfide complexes of copper(I): Experimental confirmation of the stoichiometry and stability of  $\text{Cu}(\text{HS})_2^-$  to elevated temperatures. *Geochimica et Cosmochimica Acta* **67**, 3005-3014.
- Mutschler, F. E., Wright, E. G., Ludington, S., and Abbott, J. T., (1981) Granite molybdenum systems. *Economic Geology* **76**, 874-897.
- Nagaseki, H. and Hayashi, K., (2008) Experimental study of the behavior of copper and zinc in a boiling hydrothermal system. *Geology* **36**, 27-30.
- Naney, M. T., (1983) Phase equilibria of rock-forming ferromagnesian silicates in granitic systems. *American Journal of Science* **283**, 993-1033.
- Noll, P. D., Newsom, H. E., and Ryan, J. G., (1996) The role of hydrothermal fluids in the production of subduction zone magmas: Evidence from siderophile and chalcophile trace elements and boron. *Geochimica et Cosmochimica Acta* **60**, 587-611.
- Norton, D. L., (1982) Fluid and heat transport phenomena typical of copper-bearing pluton environments. In: Titley, S. R. (Ed.), *Advances in geology of porphyry copper deposits of southwestern North America*. University of Arizona Press, Tucson. 59-72.
- Ohmoto, H. and Rye, R. O., (1979) Isotopes of sulfur and carbon. In: Barnes, H. L. (Ed.), *Geochemistry of hydrothermal ore deposits, 2<sup>nd</sup> edition*. John Wiley, New York. 509-567.
- Oppenheimer, C., Scaillet, B., and Martin, R. S., (2011) Sulfur degassing from volcanoes: source conditions, surveillance, plume chemistry and earth system impacts. *Reviews in Mineralogy and Geochemistry* **73**, 363-421.
- Parkinson, I. J. and Arculus, R. J., (1999) The redox-state of subduction zones: insights from arc-peridotites. *Chemical Geology* **160**, 409-423.
- Pasteris, J. D., (1996) Mount Pinatubo volcano and "negative" porphyry copper deposits. *Geology* **24**, 1075-1078.
- Peacock, S. M., (1993) Large-scale hydration of the lithosphere above subducting slabs. *Chemical Geology* **108**, 49-59.
- Petford, N., (1996) Dykes or diapirs? *Geological Society of America, Special Paper* **315**, 105-114.
- Pettke, T., Oberli, F., and Heinrich, C. A., (2010) The magma and metal source of giant porphyry-type ore deposits, based in lead isotope microanalysis of individual fluid inclusions. *Earth and Planetary Science Letters* **296**, 267-277.
- Pitzer, K. S. and Pabalan, R. T., (1986) Thermodynamics of NaCl in steam. *Geochimica et Cosmochimica Acta* **50**, 1445-1454.

- Pokrovski, G. S., Roux, J., and Harrichoury, J.-C., (2005) Fluid density control on vapor-liquid partitioning of metals in hydrothermal systems. *Geology* **33**, 657-660.
- Pokrovski, G. S., Borisova, A. Y., and Harrichoury, J.-C., (2008) The effect of sulfur on vapor-liquid fractionation of metals in hydrothermal systems. *Earth and Planetary Science Letters* **266**, 345-362.
- Rajamani, V. and Naldrett, A. J., (1978) Partition of Fe, Co, Ni, and Cu between sulfide liquid and basaltic melts and the composition of Ni-Cu sulfide deposits. *Economic Geology* **73**, 82-93.
- Rempel, K. U., Liebscher, A., Schettler, G., and Heinrich, W., (2010) The fractionation of Fe and Cu between brine and CO<sub>2</sub> at up to 130 °C and 8.4 MPa, with implications for metal mobilization in CO<sub>2</sub> storage reservoirs. *Geophysical Research Abstracts* **12**.
- Richards, J. P., (1995) Alkalic-type epithermal gold deposits - a review In: Thompson, J. F. H. (Ed.), *Magmas, fluids, and ore deposits*. Mineralogical Association of Canada, Short Course Series. 367-400.
- Richards, J. P., (2000) Lineaments revisited. *Society of Economic Geologists. Newsletter* **42**, 14-20.
- Richards, J. P., (2003a) Tectono-magmatic precursors for porphyry Cu-(mo-Au) deposit formation. *Economic Geology* **96**, 1515-1533.
- Richards, J. P., (2003b) Metallogeny of the Neo-Tethyan arc in central Iran. In: al., E.-e. (Ed.), *Mineral exploration and sustainable development (7th Biennial SGA Meeting, Athens)*. Millpress, Rotterdam. 1237-1239.
- Richards, J. P., (2005) Cumulative factors in the generation of giant calc-alkaline porphyry Cu deposits. In: Porter, T. M. (Ed.), *Super porphyry copper and gold deposits: A global perspective*. PCG Publishing, Adelaide. 7-25.
- Richards, J. P., (2011) Magmatic to hydrothermal metal fluxes in convergent and collided margins. *Ore Geology Reviews* **40**, 1-26.
- Richards, J. P., McCulloch, M. T., Chappell, B. W., and Kerrich, R., (1991) Sources of metals in the Porgera gold deposit, Papua New Guinea: evidence from alteration, isotope, and noble metal geochemistry. *Geochimica et Cosmochimica Acta* **55**, 565-580.
- Roedder, E., (1971) Fluid inclusion studies on the porphyry-type ore deposits at Bingham, Utah, Butte, Montana, and Climax, Colorado. *Economic Geology* **66**, 98-120.
- Roedder, E., (1984) *Fluid inclusions: Reviews in Mineralogy*. Mineralogical Society of America, Blacksburg. 644 p.
- Rowins, S. M., (2000) Reduced porphyry copper-gold deposits: A new variation on an old theme. *Geology* **28**, 491-494.
- Rudnick, R. L. and Gao, S., (2003) Composition of the continental crust. In: Rudnick, R. L. (Ed.), *Treatise on Geochemistry*. Elsevier. 1-64.
- Ryabchikov, I. D., Orlova, G. P., Yefimov, A. S., and Kalenchuk, G. Y., (1980) Copper in a granite-fluid system. *Geochemistry International* **17**, 29-34.

- Ryabchikov, I. D., Rekharskiy, V. I., and Kudrin, A. V., (1981) Mobilization of molybdenum by fluids during crystallization of granite melts. *Geochemistry International* **18**, 183-186.
- Schmidt, M. W. and Poli, S., (1998) Experimentally based water budgets for dehydrating slabs and consequences for arc magma generation. *Earth and Planetary Science Letters* **163**, 361-379.
- Seal, R. R., (2006) Sulfur isotope geochemistry of sulfide minerals. *Reviews in Mineralogy and Geochemistry* **61**, 633-677.
- Seedorff, E. and Einaudi, M. T., (2004) Henderson porphyry molybdenum system, Colorado. II. Decoupling of introduction and deposition of metals during geochemical evolution of hydrothermal fluids. *Economic Geology* **99**, 39-72.
- Seedorff, E., Dilles, J. H., Proffett, J. M., Einaudi, M. T., Zurcher, L., Stavast, W. J. A., Johnson, D. A., and Barton, M. D., (2005) Porphyry deposits: Characteristics and origin of hypogene features. *Economic Geology 100<sup>th</sup> Anniversary Volume* **100**, 251-298.
- Seo, J. H., Guillong, M., and Heinrich, C. A., (2009) The role of sulfur in the formation of magmatic-hydrothermal copper-gold deposits. *Earth and Planetary Science Letters* **282**, 323-328.
- Seo, J. H., Guillong, M., Aerts, M., Zajacz, Z., and Heinrich, C. A., (2011) Microanalysis of S, Cl, and Br in fluid inclusions by LA-ICP-MS. *Chemical Geology* **284**, 35-44.
- Seo, J. H., Guillong, M., and Heinrich, C. A., (2012) Separation of molybdenum and copper in porphyry deposits: The roles of sulfur, redox, and pH in ore mineral deposition at Bingham Canyon. *Economic Geology* **107**, 333-356.
- Shepherd, T. J., Rankin, A. H., and Alderton, D. H. M., (1985) *A practical guide to fluid inclusion studies*. Blackie and Son, Glasgow and London. 250 p.
- Shinohara, H., Kasahaya, K., and Lowenstern, J. B., (1995) Volatile transport in a convecting magma column: Implications for porphyry Mo mineralization. *Geology* **23**, 1091-1094.
- Sillitoe, R. H., (1973) The tops and bottoms of porphyry copper deposits. *Economic Geology* **68**, 799-815.
- Sillitoe, R. H., (1980a) Cauldron subsidence as a possible inhibitor of porphyry copper formation. *Mining Geology Special Issue* **8**, 85-93.
- Sillitoe, R. H., (1985) Ore-related breccias in volcanoplutonic arcs. *Economic Geology* **80**, 1467-1514.
- Sillitoe, R. H., (1995) Exploration of porphyry copper lithocaps. In: Mauk, J. L. and St. George, J. D. (Eds.), *Proceedings Pan American Conference on Research on Fluid Inclusions Congress 1995*. Australasian Institute of Mining and Metallurgy, Publication Series 9/95. 527-532.
- Sillitoe, R. H., (1997) Characteristics and controls of the largest porphyry copper-gold and epithermal gold deposits in the circum-Pacific region. *Australian Journal of Earth Sciences* **44**, 373-388.
- Sillitoe, R. H., (1999) VMS and porphyry copper deposits: products of discrete tectono-

- magmatic settings. In: al., S. e. (Ed.), *Mineral deposits: Processes to processing*. Proceedings of the Fifth biennial SGA meeting and the Tenth quadrennial IAGOD symposium, London. 7-10.
- Sillitoe, R. H., (2000) Gold-rich porphyry deposits: Descriptive and genetic models and their role in exploration and discovery. *Reviews in Economic Geology* **13**, 315-345.
- Sillitoe, R. H., (2010) Porphyry copper systems. *Economic Geology* **105**, 3-41.
- Simakin, A. and Talbot, C., (2001) Tectonic pumping of pervasive granitic melts. *Tectonophysics* **332**, 387-402.
- Simon, A. C. and Ripley, E. M., (2011) The role of magmatic sulfur in the formation of ore deposits. *Reviews in Mineralogy and Geochemistry* **73**, 513-578.
- Simon, A. C., Pettke, T., Candela, P. A., Piccoli, P. M., and Heinrich, C. A., (2005) Gold partitioning in melt-vapor-brine systems. *Geochimica et Cosmochimica Acta* **69**.
- Simon, A. C., Pettke, T., Candela, P. A., Piccoli, P. M., and Heinrich, C. A., (2006) Copper partitioning in a melt-vapor-brine-magnetite-pyrrhotite assemblage. *Geochimica et Cosmochimica Acta* **70**, 5583-5600.
- Singer, D. A., Berger, V. I., and Moring, B. C., (2008) Porphyry copper deposits of the world: Database and grade and tonnage models. *U. S. Geological Survey Open-File Report 2008-1155*, <http://pubs.usgs.gov/of/2008/1155>.
- Skewes, M. A., Arévalo, A., Floody, R., Zuniga, P. H., and Stern, C. R., (2002) The giant El-Teniente breccia deposit: Hypogene copper distribution and emplacement. In: Goldfarb, R. J. and Nielsen, R. L. (Eds.), *Integrated Methods for Discovery: Global Exploration in the 21st Century*. Society of Economic Geologists Special Publication. 299-332.
- Skinner, B. J., (1997) Hydrothermal mineral deposits: What we do and don't know. In: Barnes, H. L. (Ed.), *Geochemistry of hydrothermal ore deposits, 3<sup>rd</sup> edition*. John Wiley & Sons, New York. 1-30.
- Smith, E. and Dent, G., (2005) *Modern Raman Spectroscopy. A practical approach*. John Wiley & Sons, Chinchester 210 p.
- Sorby, H. C., (1858) On the microscopical structure of crystals indicating the origin of rocks and minerals. *Quarterly Journal of the Geological Society of London* **14**, 453-500.
- Sourirajan, S. and Kennedy, G. C., (1962) The system H<sub>2</sub>O-NaCl at elevated temperatures and pressures. *American Journal of Science* **260**, 115-141.
- Spandler, C., Pettke, T., and Rubatto, D., (2011) Internal and external fluid sources for eclogite-facies veins in the Monviso Meta-ophiolite, Western Alps; implications for fluid flow in subduction zones. *Journal of Petrology* **52**, 1207-1236.
- Spooner, E. T. C., (1993) Magmatic sulphide/volatile interaction as a mechanism for producing chalcophile element enriched, Archean Au-quartz, epithermal Au-Ag and Au skarn hydrothermal ore fluids. *Ore Geology Reviews* **7**, 359-379.
- Stein, H. J. and Hannah, J. L., (1985) Movement and origin of ore fluids in Climax-type systems. *Geology* **13**, 469-474.

- Stern, C. R., Funk, J. A., Skewes, M. A., and Arévalo, A., (2007) Magmatic anhydrite in plutonic rocks at the El Teniente Cu-Mo deposit, Chile, and the role of sulfur- and copper-rich magmas in its formation. *Economic Geology* **102**, 1335-1344.
- Sterner, S. M. and Bodnar, R. J., (1984) Synthetic fluid inclusions in natural quartz I. Compositional types synthesized and applications to experimental geochemistry. *Geochimica et Cosmochimica Acta* **48**, 2659-2668.
- Stoffregen, R., (1987) Genesis of acid-sulfate alteration and Au-Cu-Ag mineralization at Summitville, Colorado. *Economic Geology* **82**, 1575-1591.
- Streck, M. J. and Dilles, J. H., (1998) Sulfur evolution of oxidized arc magmas Walker, G. P. L., (1989) Gravitational (density) controls on volcanism, magma chambers and intrusions. *Australian Journal of Earth Sciences* **36**, 149-165. as recorded in apatite from a porphyry copper batholith. *Geology* **26**, 523-526.
- Suleimenov, O. M. and Krupp, R. E., (1994) Solubility of hydrogen sulfide in pure water and in NaCl solutions, from 20 to 320°C and at saturation pressures. *Geochimica et Cosmochimica Acta* **58**, 2433-2444.
- Symonds, R. B., Rose, W. I., Bluth, G. J., and Gerlach, T. M., (1994) Volcanic-gas studies: Methods, results, and implications. *Reviews in Mineralogy* **30**, 1-66.
- Takada, R. M., (1994) The influence of regional stress and magmatic input on styles of monogenetic and polygenetic volcanism. *Journal of Geophysical Research* **99**, 13563-13573.
- Tagirov, B. R., Salvi, S., Schott, J., and Baranova, N. N., (2005) Experimental study of gold-hydrosulphide complexing in aqueous solutions at 350-500°C, 500 and 1000 bars using mineral buffers. *Geochimica et Cosmochimica Acta* **69**, 2119-2132.
- Tatsumi, Y., Hamilton, D. L., and Nesbitt, R. W., (1986) Chemical characteristics of fluid phase released from a subducted lithosphere and the origin of arc magmas: Evidence from high pressure experiments and natural rocks. *Journal of Volcanology and Geothermal Research* **29**, 293-309.
- Taylor, H. P., (1974) The application of oxygen and hydrogen isotope studies to problems of hydrothermal alteration and ore deposition. *Economic Geology* **69**, 843-883.
- Tingle, T. and Fenn, P., (1984) Transport and concentration of molybdenum in granite molybdenite systems: Effects of fluorine and sulfur. *Geology* **12**, 156-158.
- Titley, S. R., (1993) Characteristics of porphyry copper occurrence in the American Southwest. *Geological Association of Canada. Special Paper* **40**, 433-464.
- Tosdal, R. M. and Richards, J. P., (2001) Magmatic and structural controls on the development of porphyry Cu ± Mo ± Au deposits. *Reviews in Economic Geology* **14**, 157-181.
- Wyborn, D. and Sun, S., (1994) Sulphur-undersaturated magmatism - a key factor for generating magma-related copper-gold deposits. *AGSO Research Newsletter* **21**, 7-8. *Geology* **14**, 157-181.
- Tweto, O. and Sims, P. K., (1963) Precambrian ancestry of the Colorado mineral belt. *Geological Society of America Bulletin* **74**, 991-1014.
- Ulrich, T., Günther, D., and Heinrich, C. A., (1999) Gold concentrations of magmatic brines and the metal budget of porphyry copper deposits. *Nature* **399**, 676-679.

- Urabe, T., (1985) Aluminous granite as a source magma of hydrothermal ore deposits: an experimental study. *Economic Geology* **80**, 148-157.
- Waite, K. A., Keith, J. D., Christiansen, E. H., Whitney, J. A., Hattori, K. H., Tingey, D. G., and Hook, C. J., (1997) Petrogenesis of the volcanic and intrusive rocks associated with the Bingham Canyon porphyry Cu-Au-Mo deposit, Utah. *Society of Economic Geologists. Guidebook Series* **29**, 69-90.
- Walker, G. P. L., (1989) Gravitational (density) controls on volcanism, magma chambers and intrusions. *Australian Journal of Earth Sciences* **36**, 149-165.
- Wallace, P. J. and Gerlach, T. M., (1994) Magmatic vapor source for sulfur dioxide released during volcanic eruptions: evidence from Mount Pinatubo. *Science* **265**, 497-499.
- Wallace, S. R., MacKenzie, W. B., Blair, R. G., and Muncaster, N. K., (1978) Geology of the Urad and Henderson molybdenite deposits, Clear Creek County, Colorado, with a section on a comparison of these deposits with those at Climax/Colorado. *Economic Geology* **73**, 325-368.
- Webster, J. D. and Mandeville, C., (2007) Fluid immiscibility in volcanic environment. *Reviews in Mineralogy and Geochemistry* **65**, 313-362.
- Webster, J. D. and Botcharnikov, R. E., (2011) Distribution of sulfur between melt and fluid in S-O-H-C-Cl-bearing magmatic systems at shallow crustal pressures and temperatures. *Reviews in Mineralogy and Geochemistry* **73**, 247-283.
- Wedepohl, K. H., (1978) *Handbook of geochemistry*. Springer-Verlag, Berlin, 4202-4204.
- Westra, G., (1979) Porphyry copper genesis at Ely, Nevada. In: Ridge, J. D. (Ed.), *Papers on mineral deposits of western North America*. Nevada Bureau of Mines and Geology, Report. 127-140.
- Westra, G. and Keith, S. B., (1981) Classification and genesis of stockwork molybdenum deposits. *Economic Geology* **76**, 844-873.
- Westrich, H. R. and Gerlach, T. M., (1992) Magmatic gas source for the stratospheric SO<sub>2</sub> cloud from the June 15, 1991 eruption of Mount Pinatubo. *Geology* **20**, 687-870.
- White, W. H., Bookstrom, A. A., Kamilli, R. J., Ganster, M. W., Smith, R. P., Ranta, D. E., and Steininger, R. C., (1981) Character and origin of Climax-type molybdenum deposits. *Economic Geology* **75th Anniversary Volume**, 270-316.
- Whitney, J. A., (1975) Vapor generation in a quartz monzonite magma: A synthetic model with application to porphyry copper deposits. *Economic Geology* **70**, 346-358.
- Williams, T. J., Candela, P. A., and Piccoli, P. M., (1995) The partitioning of copper between silicate melts and two-phase aqueous fluids: An experimental investigation at 1 kbar, 800°C and 0.5 kbar, 580°C. *Contributions to Mineralogy and Petrology* **121**, 388-399.
- Williams-Jones, A. E. and Heinrich, C. A., (2005) Vapor transport of metals and the formation of magmatic-hydrothermal ore deposits. *Economic Geology* **100**, 1287-1312.
- Winter, J. D., (2001) An introduction to igneous and metamorphic petrology. 697 p.
- Wood, S. A., Crerar, D. A., and Borcsik, M. P., (1987) Solubility of the assemblage pyrite-

- pyrrhotite-magnetite-sphalerite-galena-gold-stibnite-bismuthinite-argenitite-molybdenite in H<sub>2</sub>O-NaCl-CO<sub>2</sub> solutions from 200 to 350°C. *Economic Geology* **82**, 1864-1887.
- Wyborn, D. and Sun, S., (1994) Sulphur-undersaturated magmatism - a key factor for generating magma-related copper-gold deposits. *AGSO Research Newsletter* **21**, 7-8.
- Zajacz, Z., Halter, W. E., Pettke, T., and Guillong, M., (2008) Determination of fluid/melt partition coefficients by LA-ICP-MS analysis of co-existing fluid and silicate melt inclusions: controls on element partitioning. *Geochimica et Cosmochimica Acta* **72**, 2169-2197.
- Zajacz, Z., Hanley, J. J., Heinrich, C. A., Halter, W. E., and Guillong, M., (2009) Diffusive reequilibration of quartz-hosted silicate melt and fluid inclusions: Are all metal concentrations unmodified? *Geochimica et Cosmochimica Acta* **73**, 3013-3027.
- Zajacz, Z., Seo, J. H., Candela, P. A., Piccoli, P. M., Heinrich, C. A., and Guillong, M., (2010) Alkali metals control the release of gold from volatile-rich magmas. *Earth and Planetary Science Letters* **297**, 50-56.
- Zajacz, Z., Seo, J. H., Candela, P. A., Piccoli, P. M., and Tossell, J. A., (2011) The solubility of copper in high-temperature magmatic vapors: A quest for the significance of various chloride and sulfide complexes. *Geochimica et Cosmochimica Acta* **75**, 2811-2827.
- Zhu, X. X., O'Nions, R. K., Guo, Y., Belshaw, N. S., and Rickard, D., (2000) Determination of natural copper isotope variation by plasma-source mass spectrometry; implications for use as geochemical tracers. *Chemical Geology* **163**, 139-149.

Online references: <http://rruff.info/>

---

## 5 LIST OF MANUSCRIPTS AND STATEMENT OF THE AUTHOR'S CONTRIBUTION

1 Lerchbaumer L. and Audétat A. (2012) The 'quartz capsule' – a new method to avoid alloying problems with noble metal capsules in hydrothermal experiments. *European Journal of Mineralogy* 24/3 (2012), *in press*; doi: 10.1127/0935-1221/2012/0024-2216.

In course of the partitioning-studies I designed this new capsule together with my supervisor Andreas Audétat (AA). I carried out all experiments and subsequent analyses. Final conclusions were drawn by me together with AA and I finally wrote the manuscript.

2 Lerchbaumer L. and Audétat A. (2012) High Cu contents in vapor-type fluid inclusions: an artifact? *Geochimica et Cosmochimica Acta* (2012), *in press*; doi: 10.1016/j.gca.2012.04.033.

I did all partitioning and re-equilibration experiments and subsequent analyses. Interpretation of the data was done together with AA and I wrote the manuscript.

3 Lerchbaumer L. and Audétat A. (2012) The metal content of silicate melts and aqueous fluids in sub-economically Mo-mineralized granites: implications for porphyry Mo genesis. *Economic Geology* (2012), *submitted*.

I studied and analyzed the natural samples (previously collected by AA) and I conducted the experiments and subsequent analyses. Data interpretation was done by me together with AA and I finally wrote the manuscript.

4 Li Y., Audétat A., Lerchbaumer L., and Xiong X. L. (2009) Rapid Na, Cu exchange between synthetic fluid inclusions and external aqueous solutions: Evidence from LA-ICP-MS analysis. *Geofluids* (2009) 9, 321-329.

This study was mainly done by Li Yuan. I contributed data from microthermometry-analyses and carried out similar experiments. The latter ones do not appear in the final version of the paper but contributed to the general understanding of the study.

## 6 MANUSCRIPTS

### ***6.1 The 'quartz capsule' – a new method to avoid alloying problems with noble metal capsules in hydrothermal experiments***

L. LERCHBAUMER AND A. AUDÉTAT

Bayerisches Geoinstitut, Universität Bayreuth, 95440 Bayreuth, Germany

*European Journal of Mineralogy* 24/3 (2012), in press; doi: 10.1127/0935-1221/2012/0024-2216.

#### **6.1.1 Abstract**

A specially designed quartz liner effectively prevents alloying problems with noble metal capsules during hydrothermal experiments at elevated pressures and temperatures. The liner consists of three pieces: a cylindrical container made of a single quartz crystal, a SiO<sub>2</sub> glass plug, and a rounded closure lid made of a single quartz crystal. Soon after the final pressure and temperature have been reached, recrystallisation of the SiO<sub>2</sub> glass plug causes the quartz cap to be tightly sealed onto the quartz container, thus producing a quartz capsule that fully isolates the charge from the surrounding noble metal capsule. The efficiency of the method is demonstrated on experiments with Cu and S ( $\pm$  Fe, Ag)-bearing, NaCl-H<sub>2</sub>O dominated fluids, which are complicated by the fact that all commonly used noble metals (and -alloys) react with either of these elements. Even small amounts of added Ag are still present after the run, showing that interaction with outer gold capsules was minimal. The new method makes it also possible to study chemical systems involving compounds with low melting points, such as Sn, Bi, Te, Tl, and Hg, and it allows the surrounding noble metal capsules to be replaced by capsules made of non-noble materials if necessary. A disadvantage of the method is that it cannot be used in conjunction with external  $fO_2$  buffers, as the fluid inclusions form before equilibrium with respect to an external  $fO_2$  buffer is reached.

### 6.1.2 Introduction

In experiments conducted at elevated  $P$ - $T$  conditions the sample is usually contained in noble metal capsules in order to prevent its chemical reaction with the surroundings. The choice of the capsule material depends on many factors such as temperature stability, permeability to hydrogen, malleability, metal price, and its reactivity with the charge or the pressure medium (*e.g.*, Huebner, 1971). Commonly used metals and alloys are Au, Pt, Ag, AuPd, and AgPd. Although called "noble", none of these materials is completely inert, with the degree of reactivity increasing with increasing temperature. At temperatures above  $\sim 600$  °C, (i) Au significantly alloys with Cu, (ii) Pt (at high  $T$  also AuPd) alloys with Fe, (iii) AgPd alloys with Ni, and (iv) Pt, Ag and Pd-bearing alloys react with S to form sulphides (*e.g.*, Barton & Toulmin, 1964; Pan & Wood, 1994). Furthermore, all of these materials alloy with Sn, Bi, Te, Tl, and Hg to form intermediate compounds with low melting points, causing the capsules to fail if the abundance of the latter elements is high. A major problem in studies related to ore formation is posed by experiments containing Cu and S ( $\pm$  Fe) simultaneously because none of the capsule materials listed above is inert with respect to both of these elements. At the same time, it is desirable to perform experiments at known  $f_{O_2}$  conditions.

Several methods have been developed to overcome this problem. One option is to design the experiments such that the activities of Cu,  $S_2$ , and  $O_2$  are all buffered. This can be done by either buffering  $f_{O_2}$  externally and using internal mineral assemblages that constrain  $f_{S_2}$  and Cu activity (*e.g.*, Simon *et al.*, 2006, 2008; Frank *et al.*, 2011), or by using mineral assemblages that fix all three variables (*e.g.*, pyrite-pyrrhotite-magnetite-chalcopyrite; Seyfried & Ding, 1993). Although these approaches work well, the number of applications is rather limited because only few Cu-, Fe-, and S-containing mineral assemblages are available that are able to buffer  $f_{S_2}$  ( $\pm f_{O_2}$ ), and because efficient  $f_{O_2}$  buffering through Au capsules (which are needed in Fe- and S-bearing experiments) requires temperatures of  $\geq 700$  °C (Chou, 1986).

To retain a higher experimental flexibility it would be desirable to find a way to circumvent the alloying problems. At temperatures up to 500 °C, flexible titanium cells (*e.g.*, Seyfried & Ding, 1993; Pokrovski *et al.*, 2008) or rigid titanium autoclaves (*e.g.*,

Rempel *et al.*, 2010) have been used, which inner surfaces were previously passivated by acid treatment. However, we found that in hydrothermal experiments above  $\sim 500$  °C passivation is no longer possible because the reaction of Ti to  $\text{TiO}_2$  does not stop, leading to complete transformation of Ti sheets of 0.02 mm thickness into rutile after 6 days at 700 °C. A method allowing S- and Cu-bearing fluids to be studied *in situ* by Synchrotron-XAS at temperatures up to 600 °C has been developed by Testemale *et al.* (2005). In this method the sample is contained in a rigid cylinder made of glassy carbon and pressure is applied by two glassy carbon pistons. Most recently, Zajacz *et al.* (2011) used  $\text{Au}_{97}\text{Cu}_{03}$  alloy capsules to investigate Cu-solubility in sulphide-bearing fluids at 1000 °C and 150 MPa. In these experiments no significant interaction between the charge and the capsule material was observed. In contrast, our experiences with  $\text{Au}_{95}\text{Cu}_{05}$  tubing at 600-700 °C and 70-100 MPa were less promising, as fluids containing 1-2 mol/kg<sub>solution</sub>  $\text{H}_2\text{S}$  reacted with the alloy to form an irregular layer of CuS of 0-15  $\mu\text{m}$  thickness within 5 days. Thus, a substantial amount of S was lost during these runs. The formation of CuS could potentially have been prevented by using an alloy containing less Cu, but then the Cu content of the fluid inclusions may have become too low to be analysed reliably. Furthermore, this approach does not allow determination of the actual *solubilities* of Cu-bearing minerals because the alloy fixes the Cu activity likely at some different value.

Even more challenging are experiments involving elements with low melting points such as Sn, Bi, Te, Tl, and Hg. Native Bi, for example, has a melting point of only 271 °C and can dissolve up to 20 wt% Au at 300 °C. Due to this behaviour it has been proposed that Bi melts may efficiently scavenge Au from hydrothermal fluids (Douglas *et al.* 2000; Tooth *et al.* 2008). However, the same behaviour renders it virtually impossible to conduct Bi-rich experiments in noble metal capsules because the capsules either melt or transform into brittle crystalline phases, resulting in capsule leakage.

The aim of this study was to develop a hydrothermal experimental technique that reduces the interaction between charge and noble metal container to a minimum and allows aliquots of the fluid to be trapped as synthetic fluid inclusions in quartz. Although the data presented here deal only with Cu-, S-, ( $\pm$  Fe) and Bi-bearing systems the method can equally be used with other compounds and thus is able to prevent any kind of alloying

problems. Notice also that our target  $P$ - $T$  conditions ( $\sim 700$ - $800$  °C and 100-150 MPa) are fundamentally different from those of piston-cylinder experiments in which capsules made of quartz (Ballhaus *et al.*, 1994) or olivine (*e.g.*, Ballhaus *et al.*, 1991; Holzheid & Grove, 2002; Berry *et al.*, 2005) have been previously used. In these latter experiments, pressures and temperatures are so high that the liners deform, which strongly facilitates their sealing and the transmittance of confining pressure.

### 6.1.3 Methods

The setup of our experiments is shown in Figure 6.1.1. The quartz capsule itself consists of a beaker made of single crystal synthetic quartz, a closure cap made of the same material, and a neatly fitting plug of SiO<sub>2</sub> glass inserted into the uppermost part of the beaker. The beaker measures 16 mm in length, 4.4 mm in outer diameter and 2 mm in inner diameter, and is drilled out of synthetic quartz in such a way that the c-axis of the crystal is parallel to the length of the container. The bottom edge of the beaker is rounded to avoid any damage to the surrounding metal capsule. The rounded closure cap measures 2 mm in thickness and is cut such that the c-axis is oriented perpendicular to the flat base. The rounding of the closure cap is important, as it causes the cap to be pressed onto the beaker during the pressurisation at the beginning of the experiment. The base of the cap and the top of the beaker are polished flat to ensure quick sealing. The plug is made of SiO<sub>2</sub> glass, which dissolves and re-precipitates on the crystalline quartz, thus producing a seal between the container and the capsule lid.

In our experiments the cylindrical space within the quartz beaker was filled with a piece of natural quartz from Brazil,  $\sim 25$   $\mu$ l aqueous solution (H<sub>2</sub>O, NaCl  $\pm$  FeCl<sub>2</sub>  $\pm$  HCl with minor amounts of dissolved Co, Cu, Cs, Pb, and Rb),  $\sim 1.5$ - $7$  mg SiO<sub>2</sub> glass, and in some cases other solid starting materials such as AgCl, As<sub>2</sub>O<sub>3</sub>, H<sub>3</sub>BO<sub>3</sub>, elemental S, and/or small grains (160-250  $\mu$ m diameter) of arsenopyrite, cassiterite, chalcocite, magnetite, molybdenite, pyrrhotite, and pyrite. It is essential that more solution is loaded than is necessary to fill the sample volume at run conditions, otherwise the surrounding pressure cannot be transmitted (see below). In one run (LL175) native Bi was filled into the quartz beaker. In all cases the

inserted piece of quartz measured ca. 1.0 x 1.8 x 10 mm and was cut such that its longest dimension was parallel to the c-axis of the quartz crystal. The surface was etched in 48 % hydrofluoric acid for 30 minutes to obtain small channels that favour the formation of fluid inclusions during overgrowth of new quartz (*e.g.*, Duc-Tin *et al.*, 2007; Li & Audétat, 2008). The inner walls of the beaker were etched as well to obtain additional surface for fluid inclusion formation. The filled quartz capsule was then inserted into a gold capsule of 40 mm length and a wall thickness of 0.2 mm that subsequently was sealed by arc welding. Finally, the finished capsule was loaded into a water-filled cold-seal pressure vessel, pressurised to ~40 MPa and then taken out again, to check whether the gold capsule was squeezed correctly onto the quartz capsule.

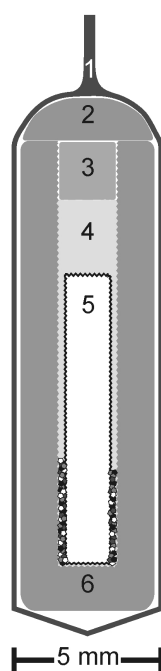


**Figure 6.1.1**

Setup of the quartz capsule. 1 = Au capsule, 2 = cap made of synthetic quartz, 3 = plug made of SiO<sub>2</sub> glass, 4 = fluid (plus SiO<sub>2</sub> glass and buffer minerals, illustrated as small dots), 5 = etched piece of natural quartz, 6 = container made of synthetic quartz.

Finished capsules were put into cold-seal rapid-quench autoclaves of the design described in Matthews *et al.* (2003). After pressurizing to ~40 MPa, the capsules were heated nearly isobarically to 400 °C. During this procedure the NaCl-H<sub>2</sub>O solution expanded and part of it escaped from the quartz capsule into the surrounding gold capsule.

Above 400 °C pressure and temperature were raised simultaneously in a manner that the fluid density stayed approximately constant at  $\sim 0.6 (\pm 0.1) \text{ g/cm}^3$ . This ensured that the fluid remained in the one-phase field during heating. Once the run temperature was reached, pressure was lowered to the final conditions within a few minutes. Subsequent recrystallisation of the  $\text{SiO}_2$  glass plug and growth of new quartz between the quartz cap and the beaker resulted in the formation of a tight seal and thus isolated the inner fluid from the gold capsule. Control experiments without quartz capsules were conducted in a similar way but contained a larger piece of etched quartz ( $\sim 5 \text{ mm} \times 5 \text{ mm} \times 8 \text{ mm}$ ) and more fluid ( $\sim 50\text{-}110 \mu\text{l}$ ), which were loaded directly into Au, copper-coated Au, or  $\text{Au}_{95}\text{Cu}_{05}$ -alloy capsules. In runs LL135 and LL136, in which  $\text{H}_2\text{S}$  was generated by the reaction of  $\text{Na}_2\text{S}$  with HCl-rich solution, the two components were loaded separately to avoid any chemical reaction before the capsule was completely closed. This was done as follows: First, the solution was inserted into the base of the gold capsule by means of a pipette, then the capsule was crimped shut a few millimetre above the solution, then the piece of etched quartz was put loaded together with  $\text{Na}_2\text{S}$  into the upper part, and finally the capsule was sealed by arc welding. Subsequent heating to  $\sim 100 \text{ }^\circ\text{C}$  caused the fluid in the lower part of the capsule to expand and to join the upper part.

After the experiments the capsules were weighted to check for leakage and then opened with a razor blade. The pieces of etched quartz containing the synthetic fluid inclusions were polished and adequate fluid inclusions were marked for further analyses.

Major and trace element concentrations in individual fluid inclusions were analysed by laser ablation ICP-MS (LA-ICP-MS). Measurements were performed using a 193 nm ArF Excimer laser (Geolas M system; Coherent) attached to a quadrupole mass spectrometer (Elan DRC-e; Perkin Elmer). The sample chamber was flushed with helium gas at a rate of 0.4 l/min and hydrogen gas at a rate of 5 ml/min (Guillong & Heinrich, 2007). The ICP-MS system was tuned to a thorium oxide rate of  $\sim 0.05 \%$  and a rate of doubly charged Ca ions of  $\sim 0.1 \%$  during ablation of NIST SRM 610 glass. Dwell times were 10-20 ms per isotope, except for Cu ( $\pm$  Au) which were measured for 40-50 ms. Additional information about the instrumentation can be found in *e.g.*, Pettke *et al.* (2004) and Pettke (2008). External standardisation was based on NIST SRM 610 glass, using the preferred values listed in the

GeoReM database (<http://georem.mpch-mainz.gwdg.de/>). Chlorine was not measured because the signals in low salinity fluid inclusions were generally too small to be quantified reliably.

Elemental concentration ratios measured by LA-ICP-MS were converted to absolute values using an internal standard, i.e., a known concentration of one element in the fluid. In experiments performed in the single-phase fluid field we used the concentration of Rb in the starting solution for this purpose because Rb is insoluble in all solid phases present in our runs. In experiments performed in the two-phase fluid region we used Na concentrations deduced from microthermometrically determined  $\text{NaCl}_{\text{equiv}}$  values as internal standard. Microthermometry was done on a Linkam heating-cooling stage (THSMG 600) with an operation range of -198 to +600 °C, whereas  $\text{NaCl}_{\text{equiv}}$  values were calculated from the melting curves of ice and halite reported in Bodnar & Vityk (1994). For vapour inclusions the fluid salinity was determined for every inclusion that subsequently was analysed by LA-ICP-MS in order to be able to quantify small amounts of co-trapped brine, which is very common in vapour inclusions (*e.g.*, Bodnar *et al.*, 1985). This was done by defining the least saline vapour inclusion as vapour endmember and calculating the proportion of vapour and brine in mixed inclusions by mass balance. That way corrected vapour salinities were up to three times lower than uncorrected ones. For brine inclusions we used average salinities highly reproducible within one experiment.

Combined analytical uncertainties are estimated at 10-20 % (*e.g.*, Heinrich *et al.*, 2003). Most of this reflects systematic errors arising from the internal and external standardisation and thus does not influence the data reproducibility, except for elements close to the detection limits where analytical errors increase due to counting statistics.

In most of the sulphur-bearing runs the trapped fluid was additionally analysed by Raman spectroscopy in order to determine sulphur speciation in the quenched liquid. This was done with a Horiba LabRAM HR 800 spectrometer connected to a Coherent Innova 90C argon ion laser, using an exposure time of 20 seconds and an accumulation time of 2 seconds.

#### 6.1.4 Results

Within this study the quartz capsule method was tested in 12 experiments at temperatures

of 600-800 °C and pressures of 70-150 MPa (Tables 6.1.1 and 6.1.2). In 50 % of the cases the quartz cap was tightly attached to the quartz beaker after the experiment and could be removed only with force using a razor blade, or even had to be cut off with a diamond blade. In the remaining 50 % of cases the cap did not fully seal with the quartz beaker but still prevented significant interaction of the fluid with the surrounding noble metal capsule. No clear relationship between the duration of the experiments and the tightness of the sealing could be observed, but a minimum runtime of one day appears to be necessary.

**Table 6.1.1** Overview of performed experiments

fluid	excess solids	quartz capsule	runs
1-phase	no	yes	LL075
1-phase	yes	yes	LL082, LL107, LL156
2-phase	yes	no	LL117
2-phase	no	yes	LL089, LL093
2-phase	yes	yes	LL091, LL126, LL133, LL154, LL167, LL175
2-phase	no	no	LL108, LL135, LL136, LL173, LL174

The size of the synthesised fluid inclusions is independent of the presence/absence of a quartz capsule, but strongly depends on temperature and fluid composition. At 800 °C, fluid inclusions greater than 20 µm in diameter were obtained in fluids of any composition (Figure 6.1.2), whereas at 600 and 700 °C, inclusions of this size were only obtained in runs to which HCl was added. In general, the speciation of sulphur analysed by Raman spectroscopy in the liquid portion of the fluid inclusions is in agreement with the oxidation state of the starting materials (i.e., Na<sub>2</sub>S gave H<sub>2</sub>S; Na<sub>2</sub>SO<sub>4</sub> gave SO<sub>4</sub><sup>2-</sup>; and elemental sulphur gave both), suggesting that only little hydrogen was exchanged with the external fluid as long as fluid inclusions formed. In experiments containing no or only little (< 1 wt%) sulphur, measured fluid salinities and reconstructed fluid isochores agree well with P-V-T-X properties in the model H<sub>2</sub>O-NaCl system and the given run conditions. For example, the salinities of vapour and brine inclusions in S-free run LL175 (15 and 37 wt% NaCl, respectively) agree well with the limits of the two-phase field at 700 °C / 120 MPa (~12 and 35 wt% NaCl; Bodnar et al., 1985), and the isochore constructed for the single-phase fluids trapped in run LL082 (7.1 wt% NaCl; T<sub>hom</sub> = 305 °C into the liquid) passes within 10 MPa

through the run conditions of 600 °C / 150 MPa. In experiments with significant amounts of sulphur, however, significant mismatches are observed with regard to the phase relations and isochores in the model H<sub>2</sub>O-NaCl system. The two-phase fluid field appears to be significantly widened, and calculated isochores suggest entrapment pressures that are up to 50 MPa too low. Importantly, exactly the same mismatches are observed also in runs performed without quartz capsules, showing that the problem is caused by the presence of sulphur rather than by a failure of pressure transmission in the quartz capsules.

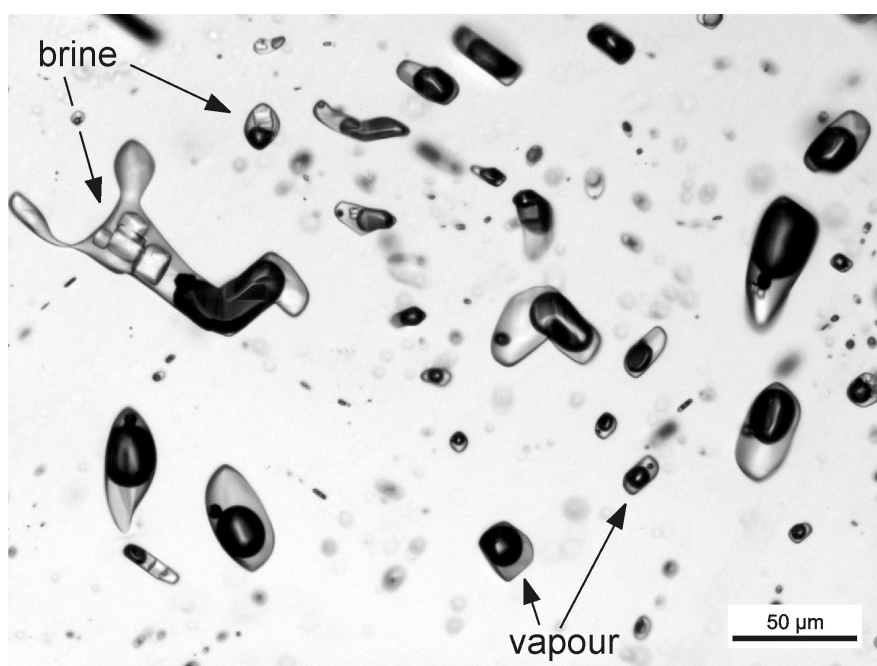


**Figure 6.1.2**

Synthetic fluid inclusions in quartz, produced at 800 °C and 130 MPa in a quartz capsule experiment (Run LL154).

The results of LA-ICP-MS analyses are summarised in Table 6.1.2 and are discussed below. Experiments performed in the one-phase fluid field allow the composition of the synthetic fluid inclusions to be easily compared with the starting concentrations (Figure 6.1.3). In one experiment (LL075), which was performed at 700 °C and 150 MPa in a quartz capsule, a solution containing 7.18 wt% NaCl, 5100 ppm Cu (added as CuCl), 520 ppm Co, 570 ppm Rb, 530 ppm Cs, 510 ppm Pb, and 0.25 mol/kg<sub>solution</sub> HCl was loaded together with 6.44 wt% elemental S and 1200 ppm Ag (as AgCl) into the quartz capsule. Because the 6.44 wt% S dissolved completely into the fluid the concentrations of all elements present in the

starting solution need to be reduced by 6.0 %. Such corrected values are listed as "starting concentrations" in Table 6.1.2. Elemental concentrations measured in the synthetic fluid inclusions agree within 12 % with the starting concentrations of elements added in solution (Na, Cu, Cs, Pb, and Co), but are slightly higher for the two elements that were added as solids (+ 15 % in the case of S; + 25 % in the case of Ag). The latter can be explained by the fact that part of the loaded fluid was expelled from the quartz capsule during heating to 400 °C, thus the mass of elements loaded as solids increased relative to the mass of fluid remaining in the capsule. The presence of small amounts of Au in the synthesised fluid inclusions (Table 6.1.1) shows that some interaction with the Au capsule did occur before the fluid became fully isolated. However, the above results suggest that only little Cu and Ag were lost from the charge and therefore, that interaction of the inner fluid with the gold capsule was very limited. Quantification of Cu and Ag concentrations in the gold capsule would not contribute much to or against this conclusion, as there is always fluid expelled from the quartz capsule during heating, which will lose dissolved metals to the gold capsule also after the quartz capsule had sealed.

Other experiments involving single-phase fluids in quartz capsules were conducted with excess amounts of added solids (LL082 with pyrite, pyrrhotite, chalcopyrite, magnetite; LL107 with chalcocite; LL156 with cassiterite). In these runs it cannot be quantified how much metal was lost through alloying because major elements (e.g., Cu in case of excess chalcopyrite) were buffered at their solubility limit, and minor elements may have been taken up by these excess solids (e.g., Mo and Ag may be taken up by excess chalcopyrite). On the other hand, they provide important insights regarding the question whether equilibrium between fluid and solids has been reached before fluid entrapment. In the etched plate technique (Duc-Tin *et al.*, 2007) fluid inclusion formation occurs during the overgrowth of new quartz over the etched quartz substrate, with the SiO<sub>2</sub> being derived mainly from SiO<sub>2</sub> glass. This process is relatively slow compared to the healing of cracks in pre-cracked quartz pieces, and thus results in fluid entrapment over a considerable amount of time. If the added solids dissolve too slowly, then the corresponding element concentrations in the fluid inclusions will not be constant. The fact that the measured concentrations of Cu and Sn in these experiments are reproducible suggests that

equilibrium between fluid and solids was reached faster than the onset of fluid inclusion formation.

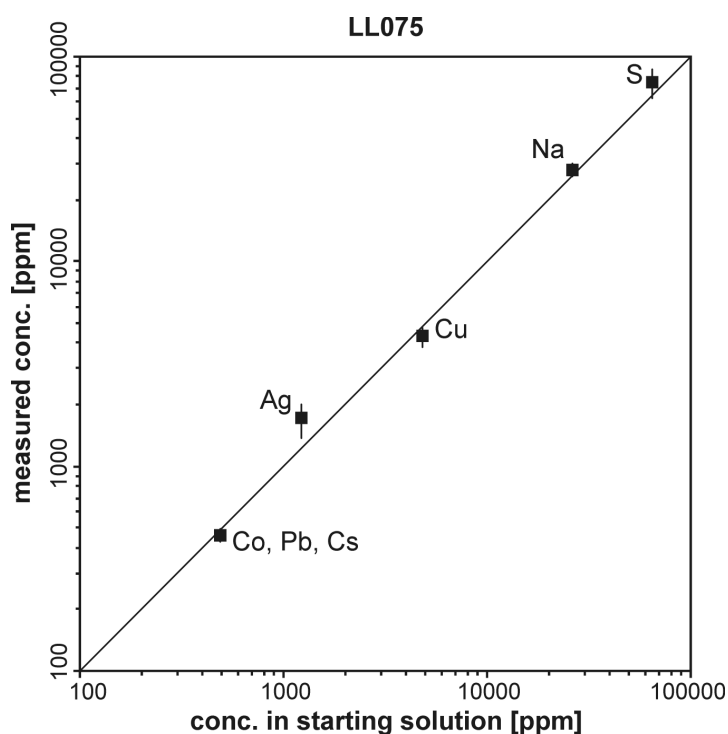


**Figure 6.1.3**

Comparison of starting concentrations in the experimental charge with elemental concentrations measured in synthetic fluid inclusions (Run LL075; 700 °C / 150 MPa). The slightly higher concentration of Ag and S in the synthetic fluid inclusions is due to fact that these elements have been added as solids and thus became enriched relative to the other compounds when part of the fluid escaped from the quartz capsule during heating. Error bars denote 1 sigma standard deviations.

**Figure 6.1.4 →**

Results from three sets of compositionally similar experiments conducted with and without quartz capsule in the two-phase fluid field. (a) Run LL093 (700 °C / 105 MPa, *with* quartz capsule) versus (b) run LL136 (700°C / 100 MPa, *without* quartz capsule in a Au<sub>95</sub>Cu<sub>05</sub>-capsule); and (c) run LL089 (800 °C / 130 MPa, *with* quartz capsule) versus (d) run LL174 (800 °C / 130 MPa, *without* quartz capsule in a pure gold capsule); (e) run LL167 (800 °C / 140 MPa, *with* quartz capsule) versus (f) run LL117 (800 °C / 130 MPa, *without* quartz capsule in a Au<sub>95</sub>Cu<sub>05</sub>-capsule). Notice the much larger error bars of Cu (but not of Pb and other trace elements) in the runs performed without quartz capsule. Error bars denote 1 sigma standard deviations.

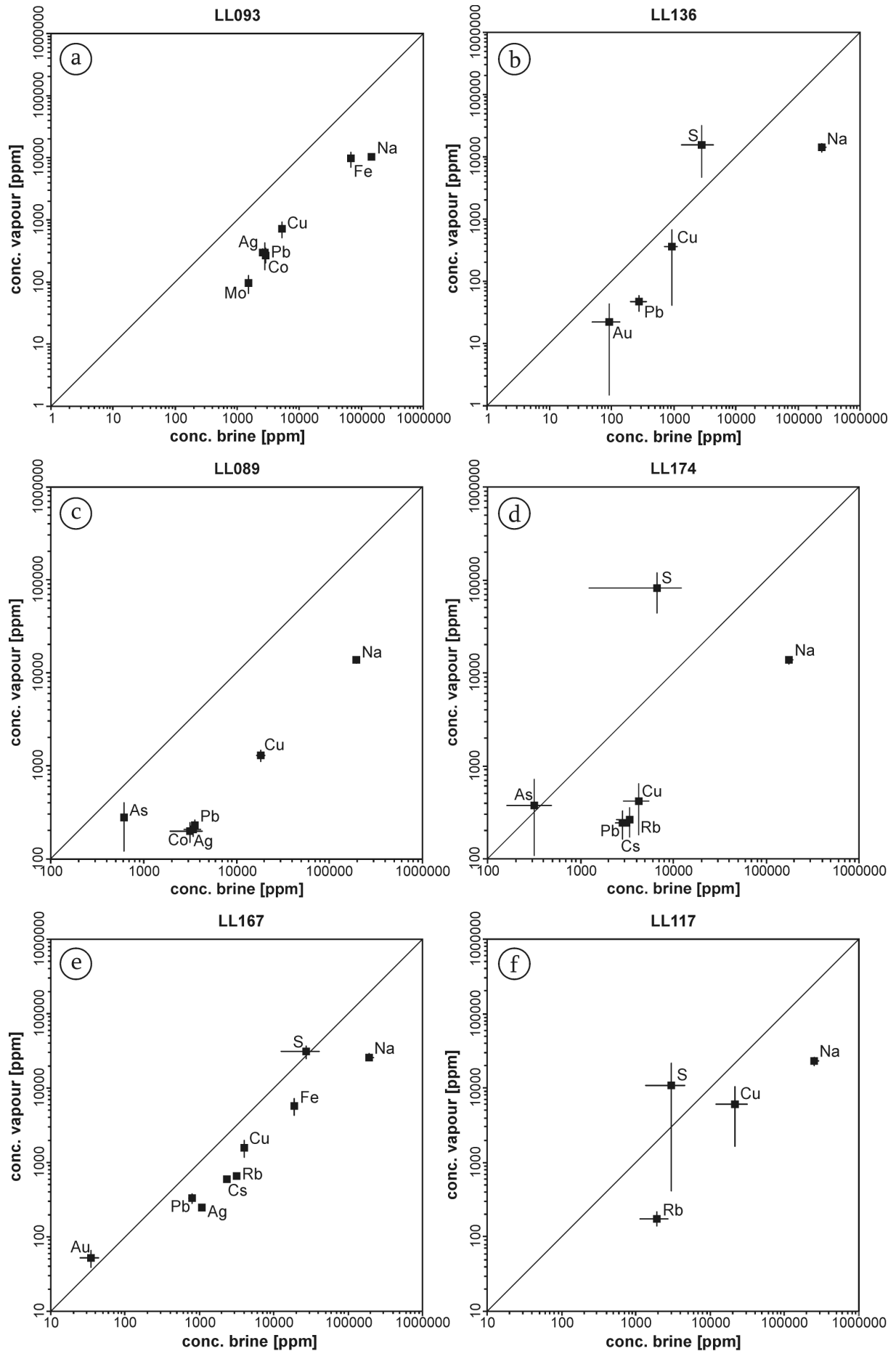


**Table 6.1.2 LA-ICP-MS analyses of runs with and without the quartz-capsule technique**

# run	LL075	LL082	LL089	LL091	LL093
<b>T [°C]</b>	700	600	800	700	700
<b>P [MPa]</b>	150	150	130	115	105
<b>capsule</b>	Au + Qtz	Au + Qtz	Au + Qtz	Au + Qtz	Au + Qtz
<b>t [days]</b>	5	6	6	4	5
<b>pH*</b>	≤ 1	≤ 1	≤ 1	≤ 1	≤ 1
<b>fluid composition</b>	NaCl, CuCl, HCl, H <sub>2</sub> O Pb, Co, Rb, Cs	NaCl, H <sub>2</sub> O Pb, Co, Rb, Cs	NaCl, CuCl, HCl, H <sub>2</sub> O Pb, Co, Rb, Cs, As	NaCl, HCl, H <sub>2</sub> O	NaCl, FeCl <sub>2</sub> , CuCl, HCl, H <sub>2</sub> O Pb, Co
<b>solids</b>	S, AgCl	Py, Po, Ccp, Mag Mo, AgCl	S, Mo, AgCl, Ti	Py, Po, Ccp, Mo, AgCl, Ti	Na <sub>2</sub> S, Mo, AgCl
	<b>starting conc. (n=22)</b>	<b>starting measured conc. (n=10)</b>	<b>starting conc. (n=5)</b>	<b>starting conc. (n=4)</b>	<b>starting conc. (n=8)</b>
<b>Na [wt%]</b>	2.64	2.75	2.39	2.69	2.59
<b>S [wt%]</b>	≤ 6.44	≤ 10.91	≤ 5.44	≤ 13.79	≤ 0.50
<b>Fe [wt%]</b>	-	≤ 20.02	-	≤ 14.56	1.68
<b>Sn [wt%]</b>	-	-	-	-	-
<b>B [ppm]</b>	-	-	-	-	-
<b>Co [ppm]</b>	490	500	430	-	480
<b>Cu [ppm]</b>	4800	≤ 3.03	4300	≤ 2.86	4700
<b>As [ppm]</b>	-	-	250	-	-
<b>Rb [ppm]</b>	540	510	430	-	-
<b>Mo [ppm]</b>	-	≤ 220	≤ 240	≤ 270	≤ 260
<b>Ag [ppm]</b>	≤ 1200	≤ 550	≤ 300	≤ 340	≤ 330
<b>Cs [ppm]</b>	490	570	430	-	-
<b>Au [ppm]</b>	-	< 30	< 7	< 7	< 7
<b>Pb [ppm]</b>	470	470	420	-	660
<b>Bi [ppm]</b>	-	-	-	-	-
	<b>vapour (n=4)</b>	<b>brine (n=9)</b>	<b>vapour (n=5)</b>	<b>vapour (n=4)</b>	<b>vapour (n=4)</b>
	1.04	19.48	1.38	2.21 ± 0.85	1.04
	< 15.98	< 10.74	3.12 ± 1.54	n.a.	< 15.98
	0.97 ± 0.26	7.96 ± 0.51	-	1.97 ± 0.39	0.97 ± 0.26
	-	-	-	-	-
	-	-	-	-	-
	260 ± 50	3100 ± 1200	200 ± 50	-	260 ± 50
	690 ± 210	1300 ± 170	1300 ± 170	420 ± 70	690 ± 210
	-	620	260 ± 140	-	-
	-	3700 ± 600	240 ± 20	-	-
	80 ± 20	< 360	< 30	40	80 ± 20
	300 ± 50	3400 ± 660	210 ± 30	260	300 ± 50
	-	3600 ± 690	230 ± 30	-	-
	< 40	< 51	< 7	< 7	< 40
	280 ± 130	3500 ± 230	230 ± 30	-	280 ± 130
	2700 ± 70	-	410 ± 50	-	2700 ± 70

*Italic numbers* mark elements that were used as internal standard; n.a. = not analysed; n.k. = not known because it is the capsule material; \* quench pH measured after the run; ≤ (S, Fe, Cu, Ag, Mo) = gives the maximum amount of these elements if the entire solid would have been dissolved; Cc = chalcocite, Ccp = chalcopyrite, Cst = cassiterite, Hem = hematite, Mag = magnetite, Mo = molybdenite, Po = pyrrhotite, Py = pyrite, Cu<sub>el</sub> = elementary copper

Table 6.1.2 Part 2

# run	LL107	LL108	LL117	LL126
<i>T</i> [°C]	700	700	800	800
<i>P</i> [MPa]	150	100	130	130
capsule	Pt + Qtz	Au with Cu coating	Au <sub>95</sub> Cu <sub>05</sub>	Au + Qtz
<i>t</i> [days]	4	4	5	4
pH*	≤ 1	n.a.	2	2
fluid composition	NaCl, HCl, H <sub>2</sub> O Pb, Co, Rb, Cs	HCl, H <sub>2</sub> O, Pb, Co	NaCl, H <sub>2</sub> O, Rb	NaCl, H <sub>2</sub> O, Rb
solids	Cc, S, Mo, AgCl	Na <sub>2</sub> S	S, Cc	Cc
	starting conc. (n=6)	starting conc. (n=4)	starting conc. (n=12)	starting conc. (n=7)
	measured conc. (n=6)	vapour (n=4)	vapour (n=12)	vapour (n=7)
		brine (n=6)	brine (n=8)	brine (n=6)
Na [wt%]	2.74	4.54	6.69	6.68
S [wt%]	≤ 6.52	≤ 3.16	≤ 1.91	≤ 0.14
Fe [wt%]	-	-	-	-
Sn [wt%]	-	-	-	-
B [ppm]	-	-	-	-
Co [ppm]	500	300	-	-
Cu [ppm]	≤ 10500	5400 ± 330	n.k.	≤ 5700
As [ppm]	-	-	-	-
Rb [ppm]	500	500	510	500
Mo [ppm]	≤ 260	≤ 80	-	-
Ag [ppm]	≤ 330	≤ 150	-	-
Cs [ppm]	520	490 ± 50	-	-
Au [ppm]	-	n.k.	n.k.	-
Pb [ppm]	490	480 ± 80	-	-
Bi [ppm]	-	-	-	-
		24.27	25.00	22.66
		n.a.	n.a.	< 0.4
		2.31	2.31	2.05 ± 0.14
		6.68	6.68	6.68
		2.05 ± 0.14	2.05 ± 0.14	2.05 ± 0.14
		1000 ± 200	1000 ± 200	1000 ± 200
		6500 ± 710	6500 ± 710	6500 ± 710
		1700 ± 280	1700 ± 280	1700 ± 280
		< 8	< 8	< 8

*Italic numbers* mark elements that were used as internal standard; n.a. = not analysed; n.k. = not known because it is the capsule material; \* quench pH measured after the run; ≤ (S, Fe, Cu, Ag, Mo) = gives the maximum amount of these elements if the entire solid would have been dissolved; Cc = chalcocite, Ccp = chalcopyrite, Cst = cassiterite, Hem = hematite, Mag = magnetite, Mo = molybdenite, Po = pyrrhotite, Py = pyrite, Cuel = elementary copper

Table 6.1.2 Part 3

# run	LL133	LL135	LL136	LL154
T [°C]	800	700	700	800
P [MPa]	130	100	100	130
capsule	Au + Qtz	Au <sub>95</sub> Cu <sub>05</sub>	Au <sub>95</sub> Cu <sub>05</sub>	Au + Qtz
t [days]	4	5	5	4
pH*	5	10	10	7
fluid composition	NaCl, H <sub>2</sub> O, Rb	HCl, H <sub>2</sub> O, Pb, Co	HCl, H <sub>2</sub> O, Pb, Co	NaCl, H <sub>2</sub> O, Rb, Pb
solids	Cu <sub>el</sub>	Na <sub>2</sub> S	Na <sub>2</sub> S	S, Cc, As <sub>2</sub> O <sub>3</sub> , H <sub>3</sub> BO <sub>3</sub> , Ag
Na [wt%]	6.68	2.12 ± 0.07	23.39	-
S [wt%]	-	-	-	-
Fe [wt%]	-	-	-	-
Sn [wt%]	-	-	-	-
B [ppm]	-	-	-	-
Co [ppm]	-	280	n.a.	-
Cu [ppm]	≤ 2100	10 ± 2	50 ± 10	-
As [ppm]	-	-	-	-
Rb [ppm]	500	170 ± 5	1800 ± 160	-
Mo [ppm]	-	-	-	-
Ag [ppm]	-	-	-	-
Cs [ppm]	-	-	-	-
Au [ppm]	-	< 30	< 40	-
Pb [ppm]	-	-	-	-
Bi [ppm]	-	-	-	-
starting conc.	6.65	9.48	9.37	6.65
vapour (n=5)	2.76 ± 0.13	1.42	1.42	2.76 ± 0.13
brine (n=7)	24.06	25.35	24.18	24.06
starting conc.	≤ 2.04	≤ 6.61	≤ 6.53	≤ 2.04
vapour (n=5)	6.20 ± 1.85	2.38 ± 1.09	1.55 ± 1.67	6.20 ± 1.85
brine (n=7)	1.59 ± 0.15	1.14 ± 0.34	0.29 ± 0.15	1.59 ± 0.15
starting conc.	-	-	-	-
vapour (n=5)	-	-	-	-
brine (n=7)	-	-	-	-
starting conc.	910	-	-	910
vapour (n=5)	5700 ± 420	-	-	5700 ± 420
brine (n=7)	1900 ± 190	-	-	1900 ± 190
starting conc.	-	280	n.k.	-
vapour (n=5)	-	n.a.	n.k.	-
brine (n=7)	-	n.a.	n.k.	-
starting conc.	≤ 5200	n.k.	n.k.	≤ 5200
vapour (n=5)	2000 ± 220	290 ± 270	360 ± 320	2000 ± 220
brine (n=7)	9000 ± 320	1700 ± 310	940 ± 230	9000 ± 320
starting conc.	1200	-	-	1200
vapour (n=5)	12300 ± 420	-	-	12300 ± 420
brine (n=7)	7600 ± 700	-	-	7600 ± 700
starting conc.	480	-	-	480
vapour (n=5)	220 ± 20	-	-	220 ± 20
brine (n=7)	1800 ± 80	-	-	1800 ± 80
starting conc.	≤ 430	-	-	≤ 430
vapour (n=5)	600 ± 80	-	-	600 ± 80
brine (n=7)	5700 ± 150	-	-	5700 ± 150
starting conc.	-	n.k.	n.k.	-
vapour (n=5)	-	40 ± 30	20 ± 20	-
brine (n=7)	-	190 ± 110	90 ± 40	-
starting conc.	480	280	279	480
vapour (n=5)	190 ± 20	80 ± 60	50 ± 10	190 ± 20
brine (n=7)	1200 ± 50	100 ± 40	280 ± 80	1200 ± 50

*Italic numbers* mark elements that were used as internal standard; n.a. = not analysed; n.k. = not known because it is the capsule material; \* quench pH measured after the run; ≤ (S, Fe, Cu, Ag, Mo) = gives the maximum amount of these elements if the entire solid would have been dissolved; Cc = chalcocite, Ccp = chalcopyrite, Cst = cassiterite, Hem = hematite, Mag = magnetite, Mo = molybdenite, Po = pyrrhoite, Py = pyrite, Cu<sub>el</sub> = elementary copper



Fourteen experiments were conducted at  $P$ - $T$ - $X$  conditions under which the starting solutions split into two different fluids (a low-density vapour phase and a high-density brine). One half of these experiments was performed without excess solids, the other half with excess solids (Table 6.1.1). From both types of experiments we performed runs *with* quartz capsules and runs *without* quartz capsules in order to see how much the quartz capsule helps to improve the reproducibility of the fluid inclusion compositions. In the following we first discuss the results obtained from runs *without* excess solids.

Runs LL093 and LL136 (Figure 6.1.4a, b) both contained  $H_2S$  (which was proven by Raman spectroscopy) that was produced by adding sulphur as  $Na_2S$  and chlorine as  $HCl$ , which react to  $NaCl$  and  $H_2S$  according to the reaction  $Na_2S + 2HCl \leftrightarrow H_2S + 2NaCl$ . The runtime for both experiments was 5 days. Run LL093 was conducted in a quartz capsule and contained Fe and Cu added in the form of chlorides ( $\Sigma_{Cl} = 6.1$  wt%), whereas run LL136 was conducted in a  $Au_{95}Cu_{05}$  capsule and contained no Fe ( $\Sigma_{Cl} = 15.5$  wt%) with the capsule serving as Cu source. While the reproducibility of Na and Pb are comparable, copper concentrations in fluid inclusions from the latter experiment show a much larger spread (Figure 6.1.4a, b). This is unlikely a consequence of slow Cu diffusion out of the  $Au_{95}Cu_{05}$  capsule because Cu in fact accumulated as crystalline  $CuS$  along the capsule wall. Rather, the formation of  $CuS$  lead to a continuous decrease in  $fS_2$  in the fluid and thus to a decrease in Cu solubility over time (*e.g.*, Simon *et al.*, 2006; Frank *et al.*, 2011).

Another pair of experiments (LL089 + LL174; Figure 6.1.4c, d) was performed with a bulk fluid containing ~6 wt%  $NaCl$ , ~4300 ppm Cu added as  $CuCl$ , and ~6 wt% S added as elemental sulphur. In these two runs S reacted to  $H_2S$  by means of metallic Ti that was added as fine powder. The runtime was 6 days. Again the reproducibility of Cu concentrations in the run conducted *with* quartz capsule (LL089) is much better than the ones in the run conducted *without* quartz capsule (LL174), while the reproducibility of all other elements is about the same. Mass balance calculations based on a reconstructed vapour/brine mass ratio of 9/1 suggest that less than 48 % of the Cu and Ag were lost during run LL089, whereas 87 % of the Cu and more than 95 % of the Ag were lost during run LL174. Runs LL108, LL135, LL136, and LL173 were all performed *without* excess solids and *without* quartz capsule. Runs LL108, LL135, and LL136 resulted in highly non-reproducible

Cu concentrations ( $1\sigma$  relative standard deviation in vapour and brine are 55-96 % and 18-24 %, respectively), whereas run LL173 resulted in a standard deviation of 30 % (Table 6.1.2).

An improvement in the reproducibility of Cu concentrations is evident also in experiments in which two-phase fluids were trapped in the presence of excess solids. Run LL167 was performed with excess chalcocite in a quartz capsule and resulted in relative standard deviations of 4 % in the brine and 25 % in the vapour, whereas a similar run performed in a  $\text{Au}_{95}\text{CuO}_5$  capsule (LL117) resulted in standard deviations of 45 % and 73 %, respectively (Figure 6.1.4e, f). Other runs with excess solids performed in quartz capsules resulted in  $\leq 20$  % standard deviation in the Cu concentrations of both vapour and brine (LL091, LL126, LL133, LL154; Table 6.1.2). In summary, the evidence presented above suggests that Cu concentrations in fluid inclusions are highly reproducible in runs performed *with* quartz capsules, but typically are poorly reproducible in runs performed *without* quartz capsules that do not contain excess Cu-bearing solids. An influence of oxidation state on the magnitude of Cu–Au alloying is not apparent.

The usefulness of the quartz capsule was proven also in a run saturated with molten bismuth (LL175). In this experiment, 20 wt% NaCl, 9.87 wt% Bi, and 1.04 wt% Au were filled into the quartz beaker and run at 700 °C and 120 MPa. After 4 days the surrounding Au capsule was still intact, and the loaded Bi formed a droplet at the bottom of the quartz beaker. A similar experiment conducted without quartz liner resulted in failure of the Au capsule due to alloying of Au and Bi. There the Au capsule attained a bronze colour and became so brittle that it dismembered into several grains upon slight squeezing. In the run with quartz capsule the 1.04 wt% of loaded Au loaded completely dissolved in the bismuth melt, causing the Au concentration in the fluid to be low ( $< 27$  ppm in vapour;  $< 8$  ppm in the brine). The solubility of Bi in the fluid was in the order of 20 ppm. However, the data show a relatively large spread because the inclusions were very small and the measurements thus near the detection limit.

### 6.1.5 Concluding Remarks

The results presented above demonstrate that the quartz capsule is an effective way to avoid alloying problems with noble metal capsules. The main focus of our study was to avoid loss of Cu to Au capsules, but also loss of Ag and Bi was prevented efficiently. The latter implies that the quartz capsule method is useful in any hydrothermal study involving elements that either react with Au and Pt to form crystalline phases or produce alloys with low melting points such as Sn, Te, Tl, Ge, or Hg. Furthermore, the method allows the noble metal capsules to be replaced by capsules made of non-noble metals if necessary, for example due to reasons of cost, temperature stability, or higher/lower permeability to hydrogen.

Of course the quartz capsule also bears some disadvantages: (1) it is not possible to initiate the formation of fluid inclusions after a given time of equilibration by in-situ cracking because this would destroy the quartz capsule, (2) part of the fluid is expelled from the quartz capsule at the beginning of the experiment, and (3) the method is limited to quartz-bearing systems if *e.g.*, applied to silicate melts.

In-situ cracking is a necessary prerequisite if one wants to buffer  $fO_2$  externally because diffusional equilibration of hydrogen through noble metal capsules can be slower than the formation of fluid inclusions. In experiments with internal buffers, on the other hand, equilibration of the fluid with the solids is usually faster than the formation of fluid inclusions (*e.g.*, Simon *et al.*, 2007). Several possibilities exist to control  $fO_2$  in quartz capsule experiments: (1) it can be buffered internally by mineral assemblages such as quartz-fayalite-magnetite or ilmenite-magnetite-rutile if these minerals do not disturb the remaining charge; (2) in experiments with single-phase fluids it may be controlled by using variable amounts of oxidised/reduced starting materials and calculating  $fO_2$  based on thermodynamic principles; and (3) rather than being controlled actively,  $fO_2$  may be monitored by sensors, such as the composition of pyrrhotite in equilibrium with magnetite (*e.g.*, Whitney, 1984), the hydrogen content of rutile (Colasanti *et al.*, 2011), or via  $fO_2$ -dependent solubilities of trace elements (*e.g.*, Sn, U; Wilson & Eugster, 1990; Bali *et al.*, 2011).

To ensure that the fluid within the rigid quartz capsule is at the same pressure as the fluid within the autoclave it is necessary to load more solution into the quartz capsule than

is necessary to fill the sample volume at run conditions. In this case, overpressure generated within the quartz capsule during heating at the beginning of the experiment can be continuously released by expulsion of fluid into the space between quartz capsule and the surrounding noble metal capsule, and the pressure within the quartz capsule will always be the same as in the autoclave. If the amount of added solution is too little, then the pressure within the quartz capsule is lower than the confining pressure and nothing can be moved in to compensate the pressure deficit. In this case, the final pressure within the quartz capsule will be considerably lower than the confining pressure, except if the quartz capsule breaks. For this reason some fluid should be expelled from the quartz capsule at the beginning of the experiment. By calculating the final fluid volume and comparing it with the remaining space within the quartz capsule the amount of expelled fluid can be minimized, but to be sure that the final pressure is reached there should always be an excess of fluid.

#### 6.1.6 Acknowledgements

We sincerely thank Hubert Schulze for the manufacturing of the quartz capsules, Uwe Dittmann for his assistance during sample preparation, and Zoltan Zajacz, Adam Simon, Christian Ballhaus, Craig Manning, and Robert Linnen for their critical reviews which improved this paper a lot. This work was funded by the Deutsche Forschungsgemeinschaft under project number: AU 314/1-1.

#### 6.1.7 References

- Bali, E., Audétat, A., Keppler, H. (2011) The mobility of U and Th in subduction zone fluids: an indicator of oxygen fugacity and fluid salinity. *Contrib. Min. Pet.*, **161**, 597-613.
- Ballhaus, C., Berry, R.F., Green, D.H. (1991) High pressure experimental calibration of the olivine-orthopyroxene-spinel oxygen geobarometer: implications for the oxidation state of the upper mantle. *Contrib. Min. Pet.*, **107**, 27-40.
- Ballhaus, C., Ryan, C.G., Mernagh, T.P., Green, D.H. (1994) The partitioning of Fe, Ni, Cu, Pt, and Au between sulfide, metal, and fluid phases: a pilot study. *Geochim. Cosmochim. Acta*, **58**, 811-826.
- Barton, P.B.J., & Toulmin, P.I. (1964) The electrom-tarnish method for the determination of the fugacity of sulfur in laboratory sulfide systems. *Geochim. Cosmochim. Acta*, **28**, 619-640.

- Berry, A.J., Hermann, J., O'Neill, H.C., Foran, G. (2005) Fingerprinting the water site in mantle olivine. *Geology*, **33**, 869-872.
- Bodnar, R.J., Burnham, C.W., Sterner, S.M. (1985) Synthetic fluid inclusions in natural quartz. III. Determination of phase equilibrium properties in the system H<sub>2</sub>O-NaCl to 1000°C and 1500 bars. *Geochim. Cosmochim. Acta*, **49**, 1861-1873.
- Bodnar, R.J., & Vityk, M.O. (1994) Interpretation of microthermometric data for H<sub>2</sub>O-NaCl fluid inclusions. in "Fluid Inclusions in Minerals, Methods and Applications", B.D. Vivo & M.L. Frezzotti, eds., Virginia Tech, Blacksburg/VA, 117-130.
- Chou, I.-M. (1986) Permeability of precious metals to hydrogen at 2 kb total pressure and elevated temperatures. *Am. J. Sci.*, **286**, 638-658.
- Colasanti, C.V., Johnson, E.A., Manning, C.E. (2011) An experimental study of OH solubility in rutile at 500-900 °C, 0.5-2 GPa, and a range of oxygen fugacities. *American Mineralogist*, **96**, 1291-1299.
- Douglas, N., Mavrogenes, J.A., Hack, A., England, R. (2000) The liquid bismuth collector model: an alternative gold deposition mechanism. *15th Australian Geological Convention, Geological Society of Australia*, abstract 135.
- Duc-Tin, Q., Audétat, A., Keppler, H. (2007) Solubility of tin in (Cl, F)-bearing aqueous fluids at 700°C, 140 MPa: A LA-ICP-MS study on synthetic fluid inclusions. *Geochim. Cosmochim. Acta* **71**, 3323-3335.
- Frank, M.R., Simon, A.C., Pettke, T., Candela, P.A., Piccoli, P.M. (2011) Gold and copper partitioning in magmatic-hydrothermal systems at 800°C and 100 MPa. *Geochim. Cosmochim. Acta*, **75**, 2470-2482.
- Guillong, M., & Heinrich, C.A. (2007) Sensitivity enhancement in laser ablation ICP-MS using small amounts of hydrogen in the carrier gas. *J. Anal. Atomic Spec.*, **22**, 1488-1494.
- Heinrich, C.A., Pettke, T., Halter, W.E., Aigner-Torres, M., Audétat, A., Günther, D., Hattendorf, B., Bleiner, D., Guillong, M., Horn, I. (2003) Quantitative multi-element analysis of minerals, fluid and melt inclusions by laser-ablation inductively-coupled-plasma mass-spectrometry. *Geochim. Cosmochim. Acta*, **67**, 3473-3496.
- Holzheid, A., & Grove, T.L. (2002) Sulfur saturation limits in silicate melts and their implications for core formation scenarios for terrestrial planets. *Am. Mineral.*, **87**, 227-237.
- Huebner, J.S. (1971) Buffering techniques for hydrostatic systems at elevated pressures. in "Research techniques for high pressure and high temperature", G.C. Ulmer, ed., Springer, New York, 123-177.
- Li, Y., & Audétat, A. (2008) A method to synthesize large fluid inclusions in quartz at controlled times and under unfavorable growth conditions. *Am. Mineral.*, **94**, 367-371.
- Matthews, W., Linnen, R.L., Guo, Q. (2003) A filler-rod technique for controlling redox conditions in cold-seal pressure vessels. *Am. Mineral.*, **88**, 701-707.
- Pan, P., & Wood, S.A. (1994) Solubility of Pt and Pd sulfides and Au metal in aqueous

- bisulfide solutions. *Mineral. Depos.*, **29**, 373-390.
- Pettke, T., Halter, W., Webster, J.D., Aigner-Torres, M., Heinrich, C.A. (2004) Accurate quantification of melt inclusions chemistry by LA-ICP-MS: a comparison with EMP and SIMS and advantages and possible limitations of these methods. *Lithos*, **78**, 333-361.
- Pettke, T. (2008) Analytical protocols for element concentration and isotope ratio measurements in fluid inclusions by LA-(MC-)ICP-MS. *in* "Laser ablation ICP-MS in the earth sciences: current practices and outstanding issues", P. Sylvester, ed., Mineralogical Association of Canada, Quebec, 189-217.
- Pokrovski, G.S., Borisova, A.Y., Harrichoury, J.-C. (2008) The effect of sulfur on vapor-liquid fractionation of metals in hydrothermal systems. *Earth Planet. Sci. Lett.*, **266**, 345-362.
- Rempel, K.U., Liebscher, A., Schettler, G., Heinrich, W. (2010) Vapor-liquid equilibrium in the systems CuCl-NaCl-H<sub>2</sub>O, CuCl-NaHS-NaCl-H<sub>2</sub>O and CuCl<sub>2</sub>-NaCl-CO<sub>2</sub>-H<sub>2</sub>O to 450 °C and 40 MPa. *EMPG XIII, Toulouse*, abstract.
- Seyfried, W.E.J., & Ding, K. (1993) The effect of redox on the relative solubilities of copper and iron in Cl-bearing aqueous fluids at elevated temperatures and pressures: An experimental study with application to seafloor hydrothermal systems. *Geochim. Cosmochim. Acta*, **57**, 1905-1917.
- Simon, A.C., Pettke, T., Candela, P.A., Piccoli, P.M., Heinrich, C.A. (2006) Copper partitioning in a melt-vapor-brine-magnetite-pyrrhotite assemblage. *Geochim. Cosmochim. Acta*, **70**, 5583-5600.
- Simon, A.C., Frank, M.R., Pettke, T., Candela, P.A., Piccoli, P.M., Heinrich, C.A., Glascock, M. (2007) An evaluation of synthetic fluid inclusions for the purpose of trapping equilibrated, coexisting, immiscible fluid phases at magmatic conditions. *Am. Mineral.*, **92**, 124-138.
- Simon, A.C., Pettke, T., Candela, P.A., Piccoli, P.M. (2008) The partitioning behavior of silver in vapor-brine-rhyolite melt assemblage. *Geochim. Cosmochim. Acta*, **72**, 1638-1659.
- Testemale D., Argoud R., Geaymond O., Hazemann J. L. (2005) High pressure/high temperature cell for x-ray absorption and scattering techniques. *Rev. Sci. Inst.*, **76**, 043905-043909.
- Tooth, B., Brugger, J., Ciobanu, C., Liu, W. (2008) Modelling of gold scavenging by bismuth melts coexisting with hydrothermal fluids. *Geology*, **36**, 815-818.
- Whitney, J.A. (1984) Fugacities of sulfurous gases in pyrrhotite-bearing silicic magmas. *Am. Mineral.*, **69**, 69-78.
- Wilson, G.A., & Eugster, H.P. (1990) Cassiterite solubility and tin speciation in supercritical chloride solutions. *in* "Fluid-mineral interactions", R.J. Spencer & I.M. Chou, eds., Geochemical Society, St. Louis, 179-195.
- Zajacz, Z., Seo, J.H., Candela, P.A., Piccoli, P.M., Tossell, J.A. (2011) The solubility of copper in high-temperature magmatic vapors: a quest for the significance of various

chloride and sulfide complexes. *Geochim. Cosmochim. Acta*, **75**, 2811-2827.

## 6.2 *High Cu concentrations in vapor-type fluid inclusions: an artifact?*

L. LERCHBAUMER AND A. AUDÉTAT

Bayerisches Geoinstitut, Universität Bayreuth, 95440 Bayreuth, Germany

*Geochimica et Cosmochimica Acta* (2012), doi: 10.1016/j.gca.2012.04.033

### 6.2.1 **Abstract**

Studies of natural fluid inclusions have shown that Cu commonly occurs at higher concentrations in vapor-type inclusions than in coexisting brine inclusions, a phenomenon which has been interpreted to arise from copper partitioning into the vapor phase. In the first part of this study, we attempted to experimentally reproduce this behavior in hydrothermal experiments covering a range of P-T conditions (600-800 °C, 70-130 MPa), fluid compositions (NaCl ± KCl ± FeCl<sub>2</sub>; 0.5-6.6 wt% S), fluid acidities (quench fluid pH ≤ 0.3 to 10), and sulfur speciation (H<sub>2</sub>S-dominated to SO<sub>2</sub>-dominated). However, as in several other studies we did not succeed in reproducing conditions under which Cu partitions into the vapor phase. In view of recent observations that quartz-hosted fluid inclusions can diffusively lose or gain Cu after entrapment, we set out to determine if the evidence from natural fluid inclusions could be compromised. For this purpose we synthesized vapor and brine inclusions from Cu-H<sub>2</sub>O-NaCl-S fluids at 800 °C/130 MPa and re-equilibrated them in slightly different fluids at 800 °C/70 MPa, measuring some inclusions by LA-ICP-MS after each step. Vapor inclusions indeed experienced a dramatic increase in Cu from 0.3 ± 0.03 to 5.7 ± 3.3 wt%, while brine inclusions remained largely unmodified, leading to a change in the partition coefficient  $D_{Cu}^{vap/brine}$  from a true value (i.e. before re-equilibration) of 0.4 ± 0.05 to an apparent value of 8.3 ± 4.9. The requirements for substantial diffusional gain of Cu in fluid inclusions are a change in the pH of the surrounding fluid from ≤ 1 to more neutral and the presence of S in the pre-existing fluid inclusions. These requirements are also fulfilled in nature: Cooling magmatic-hydrothermal fluids experience a change from acidic to more neutral pH due to buffering along the feldspar-mica join, and natural vapor inclusions

typically contain significant amounts of sulfur. A reversal experiment performed on natural, quartz-hosted fluid inclusions from the Erongo granite, Namibia, showed that this process can be reversed with the measured  $D_{Cu}^{vap/brine}$  value of  $11 \pm 9.3$  being modified to  $0.06 \pm 0.04$ . Thus,  $D_{Cu}^{vap/brine}$  values  $>1$  measured on natural fluid inclusions in quartz are likely a secondary feature caused by post-entrapment copper diffusion. Realistic  $D_{Cu}^{vap/brine}$  values in porphyry Cu environments are between 0.11 and 0.15, and reconstructed vapor/brine mass ratios are in the order of 4 to 9. This suggests that the main transporting agent of Cu at the porphyry level are brines and that models based on copper partitioning into the vapor phase are incorrect.

### 6.2.2 Introduction

For more than a century fluid inclusions have provided important information concerning the role of fluids in the formation of magmatic-hydrothermal ore deposits (Hedenquist and Richards, 1998). Two contrasting types of fluid inclusions are commonly found in this environment, documenting entrapment from a two-phase fluid: (i) dense, salt-rich inclusions (brines), and low-density, salt-poor inclusions (vapors). The brine phase was long thought to be the main carrier of ore metals in these systems because base metal solubilities generally increase with increasing fluid salinity (e.g., Crerar and Barnes, 1976; Holland, 1972), and because saline fluid inclusions in many deposits contain metal sulfide daughter minerals (e.g. Roedder, 1971; Nash, 1976; Bodnar, 1995). However, this view has been challenged recently by several findings. First, microanalyses of natural fluid inclusions have shown that Cu, As, and Au concentrations in vapor inclusions are commonly higher than in coexisting brine inclusions, or at least at levels implying a distinctly higher affinity to the vapor phase than typical Cl-complexed elements such as Na, K, Pb, and Zn. (e.g., Sawkins and Scherckenbach, 1981, Heinrich et al., 1992; Heinrich et al., 1999; Williams-Jones and Heinrich, 2005; Audétat et al., 2008; Seo et al. 2009). Second, experimental studies have shown that Au forms stable complexes with reduced sulfur (e.g., Hayashi and Ohmoto, 1991; Benning and Seward, 1996; Gibert et al., 1998; Loucks and Mavrogenes, 1999; Tagirov et al., 2005; Zajacz et al., 2010), which, together with the volatile nature of sulfur (Drummond and Ohmoto, 1985; Suleimenov and Krupp, 1994), provides a plausible

explanation for the observed partitioning of Au into the vapor phase (e.g., Pokrovski et al., 2008). Third, fluid inclusions trapped at deep levels and/or during early stages in the evolution of magmatic-hydrothermal systems revealed that the bulk fluids were of relatively low salinity (typically 4-10 wt% NaCl<sub>equiv</sub>) and thus split into a large proportion of vapor relative to brine upon decompression and cooling below 500 °C (e.g., Henley and McNabb, 1978; Shinohara and Hedenquist, 1997; Williams-Jones and Heinrich, 2005; Audétat et al., 2008). Taken together, these observations suggested that most of the Cu and Au in magmatic-hydrothermal systems is transported by vapor-type fluids.

Several experimental studies were conducted to investigate the solubility of Cu in two-phase fluids and to identify the conditions under which this metal preferentially partitions into the vapor phase. It was expected that Cu would form stable complexes with reduced sulfur, similar to the hydrosulfide complexes of Au. Indeed, sulfur-bearing Cu complexes were found to exist (e.g., Romberger and Barnes, 1970; Helz et al., 1993; Mountain and Seward, 2003; Etschmann et al., 2010; Zajacz et al., 2011) and it was noted that the vapor/brine partition coefficient of copper,  $D_{Cu}^{vap/brine}$ , increases when sulfur is added to the fluid (Simon et al., 2006; Nagaseki and Hayashi, 2008; Pokrovski et al., 2008; Frank et al., 2011). However, none of these studies succeeded in reproducing  $D_{Cu}^{vap/brine}$  values >1. An exception is the study of Nagaseki and Hayashi (2008), who measured  $D_{Cu}^{vap/brine}$  values up to 30. Mass balance constraints and results of our experiments performed under identical conditions (discussed below) are in disagreement with these results and suggest that the partition coefficients are in fact below unity. We have performed 19 additional vapor–brine partitioning experiments over a significant range of P-T conditions (600-800 °C, 70-130 MPa), fluid compositions (NaCl ± KCl ± FeCl<sub>2</sub>; 0.5-6.6 wt% S), fluid acidities (quench fluid pH ≤0.3 to 10) and sulfur speciation (H<sub>2</sub>S-dominated to SO<sub>2</sub>-dominated). However, as in previous studies, none of our experiments resulted in a preferential partitioning of Cu into the vapor phase.

In view of the fact that  $D_{Cu}^{vap/brine}$  values >1 in natural samples have been determined exclusively on fluid inclusions hosted by quartz and that Cu can rapidly diffuse through this mineral (Mortley, 1969; Kats, 1962) we wanted to test whether the vapor–brine partition coefficients measured in natural fluid inclusions could have been modified post entrapment.

Rapid post-entrapment modification of Cu, Ag, Li, and Na concentrations both in silicate melt inclusions and fluid inclusions via cation exchange has been shown before by Kamenetsky and Danyushevsky (2005), Zajacz et al. (2009), and Li et al. (2009). We thus performed re-equilibration experiments with synthetic fluid inclusions during which the compositional evolution of natural, magmatic-hydrothermal fluids was simulated. Additionally we performed a "reversal" experiment on natural fluid inclusions in which the compositional changes likely experienced by these inclusions were reversed. These re-equilibration experiments are the main subject presented here.

### **6.2.3 Methods**

#### *6.2.3.1 Experimental procedure*

Fluid inclusions were synthesized with the etched quartz plate technique described in Ductin et al. (2007), using etched pieces of natural quartz from Brazil that were loaded together with fluid ( $\text{H}_2\text{O}$ ,  $\text{NaCl} \pm \text{KCl} \pm \text{HCl} \pm \text{FeCl}_2 \pm \text{CuCl}$ ; doped with 200-500 ppm Rb, Cs, Co, and/or Pb), solid starting materials (e.g., elemental sulfur,  $\text{Na}_2\text{S}$ , anhydrite, AgCl,  $\text{As}_2\text{O}_3$ ,  $\text{H}_3\text{BO}_3$ , arsenopyrite, chalcocite, molybdenite), some  $\text{SiO}_2$  glass plus buffer minerals (e.g., albite, orthoclase, biotite, muscovite, topaz, bornite, chalcopyrite, magnetite, pyrite) into Au capsules of 5.0 mm O.D., 4.6 mm I.D. and 40 mm length. This method results in numerous, large (at  $\geq 700$  °C) fluid inclusions distributed over a narrow depth interval (6.2.1), which greatly facilitates subsequent microanalysis. Details regarding the experimental setup, fluid composition and solid starting materials used in individual experiments are listed in Tables 6.2.1 to 6.2.3. Typical fluid : solid ratios were  $\sim 10 : 1$ . In most cases (except for runs LL022-LL023, LL053-LL055, LL120, and LL135) we additionally used a quartz liner to reduce interactions between fluid and the surrounding noble metal capsule (Lerchbaumer and Audétat, 2012, in press). In this method the charge is placed in a cylindrical beaker made of single-crystal quartz and then closed with a  $\text{SiO}_2$  glass plug and a single-crystal quartz closure lid. Soon after the beginning of the experiment the  $\text{SiO}_2$  glass plug recrystallizes and thereby produces a tight seal between the beaker and the closure lid, thus efficiently preventing loss of Cu and S through alloying with the surrounding Au capsule. Two runs (LL120 and LL135) were conducted in  $\text{Au}_{95}\text{Cu}_5$ -alloy capsules. In runs

starting with Na<sub>2</sub>S plus HCl-bearing solutions (LL93, LL95, LL120, LL135), early reaction of these two components and corresponding loss of S before capsule welding was prevented as follows: First, the solution was inserted into the gold capsule using a pipette, then the capsule was crimped shut a few millimeters above the solution, then the piece of etched quartz was loaded together with Na<sub>2</sub>S into the upper part, and finally the capsule was sealed by arc welding. Subsequent heating to ~100 °C caused the fluid in the lower part of the capsule to expand and join the upper part of the capsule, in which it reacted with the solids.

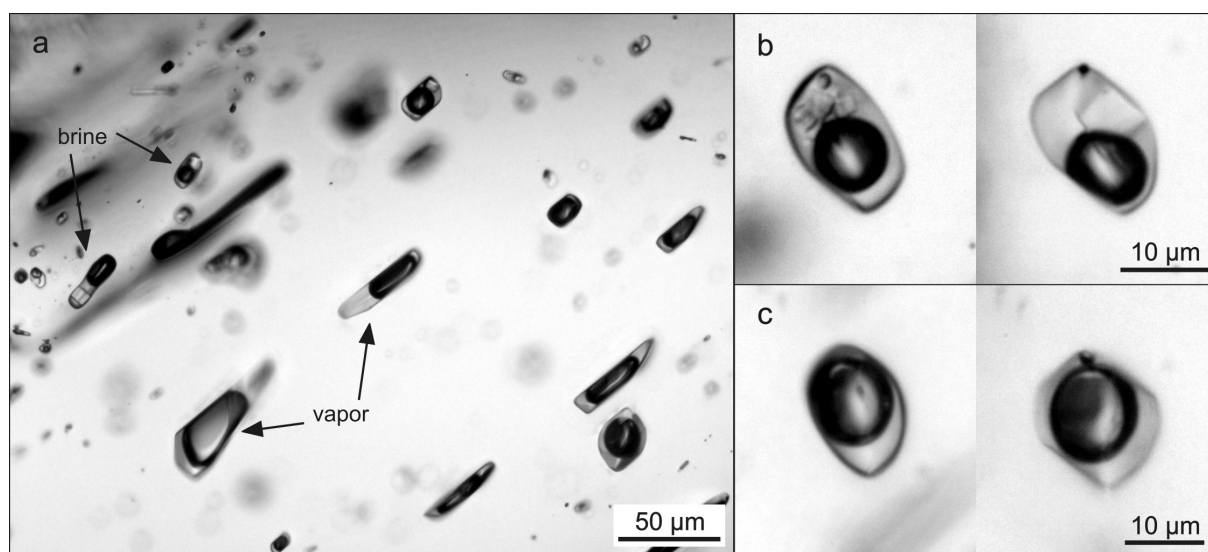


**Fig. 6.2.1**

(a) Photomicrograph of vapor and brine inclusions synthesized at 800 °C / 130 MPa (run LL141). Appearance of a brine inclusion (b) and a vapor inclusion (c) before (left) and after (right) re-equilibration at 800 °C / 70 MPa (runs LL147+LL149).

Because the rate of fluid inclusion formation in the etched quartz plate technique is relatively slow there is enough time for the fluid to equilibrate with the loaded solids before it gets trapped (Lerchbaumer and Audétat, 2012, in press). Evidence for attainment of equilibrium between fluids and solids before fluid entrapment is found in the good reproducibility of metal concentrations measured in fluid inclusions which, based on their variable levels within new quartz overgrowth, must have formed over a considerable amount of time.

Loaded capsules were put into rapid-quench cold-seal autoclaves of the design described

in Matthews et al. (2003) and then heated along an approximately fluid-isochoric path to the final run conditions of 600-800 °C and 70-130 MPa, where they were held for 4-12 days (except for run LL171, which lasted only 0.3 days). Runs were terminated by taking the autoclave out of the furnace and allowing it to cool to room temperature along an isochore defined by the density of the fluid in the autoclave plus that in the pressure line. The recovered capsules were weighed to check for leakage, opened with a razor blade, and the pH of the quench fluid was immediately measured with indicator paper. The quartz bar containing the synthetic fluid inclusions was polished and inclusions were selected for analysis.

In the re-equilibration experiments, samples prepared at 800 °C and 130 MPa in the manner described above were first analyzed by microthermometry, Raman spectroscopy, and LA-ICP-MS, and then loaded with a slightly different fluid ( $\pm$  solid materials) and a fresh quartz plate into new capsules and re-equilibrated at 800 °C and 70-130 MPa for 3-4 days. After this, both re-equilibrated fluid inclusions (in the re-used sample) and new fluid inclusions (formed in a new quartz plate) were characterized by microthermometry, Raman spectroscopy, and LA-ICP-MS again. In one "reversal" re-equilibration experiment, a natural vapor-brine fluid inclusion assemblage in a quartz crystal from the Erongo granite was immersed for 22 days in the reconstructed fluid at its original trapping conditions at  $\sim$ 650 °C and 80 MPa, and the composition of re-equilibrated fluid inclusions was compared with inclusions analyzed before the experiment.

#### *6.2.3.2 Raman spectroscopy*

Raman spectra of the liquid and vapor phase of individual fluid inclusions were taken at the Bayerisches Geoinstitut with a Horiba LabRAM HR 800 spectrometer connected to a Coherent Innova 90C argon ion laser with a wavelength of 514 nm. Measurements were recorded in the spectral region between 200 and 4500  $\text{cm}^{-1}$  with an exposure time of 20 seconds and two accumulations. The resulting spectra were checked for the presence of  $\text{H}_2\text{O}$ ,  $\text{H}_2\text{S}$ ,  $\text{SO}_2$ , and  $\text{HSO}_4^-$  bands (Burke, 2001) without quantifying absolute abundances.

### 6.2.3.3 *Microthermometry*

Microthermometry was performed on a Linkam THSMG 600 heating-cooling stage that was calibrated to an uncertainty of  $\pm 0.1$  °C in the range of -56.6 °C to 0.0 °C, and  $\pm 1$  °C at 374 °C.  $\text{NaCl}_{\text{equiv}}$  salinities of vapor and brine inclusions were determined based on the melting points of ice and halite, respectively, using the formulations of Bodnar and Vityk (1994). Fluid salinity was determined for every single vapor inclusion in order to recognize small amounts of co-trapped brine, which is common in boiling assemblages (Bodnar et al., 1985). In the case of brine inclusions we used average salinities measured in five to ten inclusions because these salinities were generally highly reproducible. In vapor inclusions containing high amounts of  $\text{H}_2\text{S}$  (LL151, LL152, LL171, LL172), accurate determination of fluid salinities was hampered by the formation of clathrates. In these cases we estimated endmember salinities based on mass balance constraints and/or phase relations in the  $\text{H}_2\text{O}$ - $\text{NaCl}$  system (Bodnar et al., 1985).

### 6.2.3.4 *Laser Ablation-Inductively Coupled Plasma-Mass Spectrometry*

LA-ICP-MS analyses were performed at the Bayerisches Geoinstitut using a 193 nm ArF Excimer laser (Geolas M system; Coherent; U.S.A.) attached to a quadrupole mass spectrometer (Elan DRC-e; Perkin Elmer, Canada). The sample chamber was flushed with He gas at a rate of 0.4 l/min, and 5 ml/min  $\text{H}_2$  gas was fed into the carrier gas between the sample chamber and the ICP-MS (Guillong and Heinrich, 2007). Isotopes that were monitored during the analysis include  $^{11}\text{B}$ ,  $^{23}\text{Na}$ ,  $^{32}\text{S}$ ,  $^{39}\text{K}$ ,  $^{55}\text{Mn}$ ,  $^{57}\text{Fe}$ ,  $^{65}\text{Cu}$ ,  $^{66}\text{Zn}$ ,  $^{75}\text{As}$ ,  $^{85}\text{Rb}$ ,  $^{98}\text{Mo}$ ,  $^{107}\text{Ag}$ ,  $^{118}\text{Sn}$ ,  $^{133}\text{Cs}$ ,  $^{208}\text{Pb}$ , and  $^{209}\text{Bi}$ , using dwell times of 10 - 40 ms per isotope. The ICP-MS system was tuned to a thorium oxide rate of  $\sim 0.05\%$  and a rate of doubly charged calcium ions of  $\sim 0.1\%$  according to measurements on NIST SRM 610 glass. External standardization was based on NIST SRM 610 glass using the values given in Spandler et al. (2011), except for sulfur which was standardized on a well-characterized piece of afghanite (Seo et al., 2011). Elemental concentration ratios measured in the fluid inclusions were converted to absolute values by using either Na or Rb as the internal standard. In most cases we used Na from the microthermometrically determined  $\text{NaCl}_{\text{equiv}}$  value and applied the empirical correction procedure of Heinrich et al. (2003) if other salts were present, except

for the clathrate-bearing vapor inclusions mentioned above, and vapor inclusions analyzed after the re-equilibration experiments. In the latter case Na concentrations proved to be unreliable because significant amounts of Na were gained during the experiments. We thus used the average Rb concentration determined in vapor inclusions prior to re-equilibration as the internal standard in the re-equilibrated inclusions. To be able to verify if fluid inclusions leaked during the re-equilibration experiments we added ~500 ppm Rb to the first fluid and ~500 ppm of Cs to the second fluid. The absence of detectable Cs in the re-equilibrated fluid inclusions confirms that they were never in direct contact with the outer fluid.

Combined analytical uncertainties are estimated to be 10-20% (Heinrich et al., 2003), except for sulfur and elements close to the detection limit, for which the uncertainties may be considerably larger. Larger uncertainties are expected also for vapor inclusions that have been re-equilibrated and/or are rich in H<sub>2</sub>S (e.g., runs LL151 and LL152) due to the difficulty to constrain the internal standard. Note, however, that element ratios are not affected by the internal standardization and thus are accurate within ~10-20% also in those samples in which the internal standard was difficult to constrain.

## **6.2.4 Results and Discussion**

### *6.2.4.1 Regular vapor-brine partitioning experiments*

Sixteen vapor–brine partitioning experiments were carried out covering a wide range in temperature (600–800 °C), pressure (70–130 MPa), fluid compositions (NaCl ± KCl ± FeCl<sub>2</sub>; sulfur concentrations ranging from ~0.5 to ~6.6 wt%), *f*O<sub>2</sub> conditions (H<sub>2</sub>S-dominated to SO<sub>2</sub>-dominated), and fluid acidities (quench fluid pH ≤0.3 to 10). These experiments are summarized in Table 6.2.1 and discussed below.

#### *6.2.4.1.1 Reproduction of Nagaseki and Hayashi's (2008) experiments*

We reproduced the runs 04C and B021 of Nagaseki and Hayashi (2008) under identical conditions in our laboratory (our runs LL022 and LL023 in Table 6.2.1). The capsule material (Au) and the amounts of loaded NaCl, S, CuCl, ZnCl<sub>2</sub>, and C<sub>14</sub>H<sub>10</sub> were the same as in the original study, and also the concentration of HCl (which is not stated in the paper,

but was 0.46 mol/kg according to the authors) was identical. We also used a pre-fractured quartz core to trap the synthetic fluid inclusions, as in the original work, and in both cases the experiments were conducted in cold-seal pressure vessels composed of Ni-rich alloys that were pressurized by water. The only difference was the method of fluid inclusion analysis (LA-ICP-MS vs. SXRF).

While Nagaseki and Hayashi (2008) report  $D_{Cu}^{vap/brine}$  values of  $8.41 \pm 4.83$  and  $13.18 \pm 9.59$  for their runs 04C and B021, respectively, we obtained  $D_{Cu}^{vap/brine}$  values of  $0.32 \pm 0.14$  and  $0.22 \pm 0.11$ , respectively. Note that both values reported by Nagaseki and Hayashi (2008) are based on a single vapor inclusion analysis each, and that in the case of run 04C the reported Cu concentrations in vapor and brine (1.74 wt% and 0.21 wt%, respectively) are in strong disagreement with the bulk fluid Cu content of 0.15 wt%. The bulk fluid had a salinity of ~11.5 wt% NaCl and thus should have split into ~85 wt% vapor and ~15 wt% brine at 650 °C / 97 MPa. With 1.74 wt% Cu in the vapor phase and 0.21 wt% Cu in the brine phase, the bulk fluid would have contained ~1.5 wt% Cu, i.e., 10 times more than was actually loaded into the capsule. A potential explanation for the high Cu values reported by Nagaseki and Hayashi (2008) is that some of their inclusions accidentally trapped Cu sulfides that precipitated from the fluid during the reaction of C<sub>14</sub>H<sub>10</sub> with CuCl-bearing solution and elemental sulfur at the beginning of the experiment.

In our experiment, Cu concentrations measured in the vapor phase ( $0.09 \pm 0.04$  wt%) and in the brine phase ( $0.26 \pm 0.02$  wt%) correspond to a calculated bulk fluid concentration of  $0.11 \pm 0.06$  wt%, which matches well with the starting concentration of 0.15 wt% Cu.

In the reproduction of their run B021, which was conducted at 600 °C / 50 MPa, we measured  $0.19 \pm 0.06$  wt% Cu in the vapor phase and  $0.87 \pm 0.38$  wt% in the brine phase, as opposed to 0.2 wt% and  $0.015 \pm 0.011$  wt%, respectively, measured by Nagaseki and Hayashi (2008). A mass balance similar to the one above is not conclusive in this case because the experiment was saturated in solid copper sulfide, with only a fraction of the loaded Cu having been in solution.

Table 6.2.1 Results of vapor-brine experiments

# run	LL022	LL023	LL053	LL054
<i>P</i> [MPa]	97	50	70	70
<i>T</i> [°C]	650	600	600	600
<i>t</i> [days]	6.5	12	12	11
pH*	≤1	≤1	4	4
<b>fluid composition</b>	NaCl, HCl, CuCl, S, C <sub>14</sub> H <sub>10</sub> Rb, Cs	NaCl, HCl, CuCl, S, C <sub>14</sub> H <sub>10</sub> Rb, Cs	NaCl, KCl, HCl, FeCl <sub>2</sub> Pb, Co, Mo, As, Ag	NaCl, KCl, HCl, FeCl <sub>2</sub> Pb, Co, Mo, As, Ag
<b>mineral buffers</b>	-	-	Ab, Bn, Bt, Ccp, Anh, Mag, Or	Ab, Bn, Bt, Ccp, Mag, Or
<i>S</i> <sub>bulk</sub> [wt%]	5.2	4.4	n.k.	n.k.
<i>S</i> species*	H <sub>2</sub> S	H <sub>2</sub> S	n.d.	SO <sub>4</sub> <sup>2-</sup>
<i>D</i> <sub>Cu</sub> vap/brine	0.32 ± 0.14	0.17 ± 0.11	0.14 ± 0.06	0.11 ± 0.04
<b>Na</b> [wt%]	vapor (n=8) 2.8 brine (n=6) 20.9	vapor (n=10) 2.7 brine (n=5) 25.2	vapor (n=13) 0.45 brine (n=7) 7.7	vapor (n=13) 0.44 brine (n=8) 8.0
<b>S</b> [wt%]	n.a.	n.a.	n.a.	n.a.
<b>Cu</b> [wt%]	0.09 ± 0.04	0.19 ± 0.06	0.04 ± 0.02	0.04 ± 0.01
<b>Fe</b> [wt%]	n.a.	n.a.	0.63 ± 0.15	0.64 ± 0.13
<b>K</b> [wt%]	n.a.	n.a.	0.41 ± 0.07	0.38 ± 0.10
<b>Zn</b> [wt%]	0.08	1.2 ± 0.29	n.a.	n.a.
<b>B</b> [ppm]	n.a.	n.a.	n.a.	n.a.
<b>Co</b> [ppm]	n.a.	n.a.	40 ± 10	60 ± 10
<b>As</b> [ppm]	n.a.	n.a.	300 ± 110	500 ± 180
<b>Rb</b> [ppm]	n.a.	n.a.	n.a.	n.a.
<b>Mo</b> [ppm]	n.a.	n.a.	< 10	50
<b>Ag</b> [ppm]	n.a.	n.a.	< 10	< 30
<b>Cs</b> [ppm]	n.a.	n.a.	n.a.	n.a.
<b>Pb</b> [ppm]	n.a.	n.a.	120 ± 20	150 ± 50
			1700 ± 110	2000 ± 310

*Italic numbers* mark elements that were used as internal standard; n.a. = not analyzed; n.d. = not detectable; n.k. = not known; \*pH and *S*-species measured in quench fluid after the run; †vapor salinity estimated from H<sub>2</sub>O-NaCl phase diagram (Bodnar et al., 1985); # contains considerable amounts of coentrapped brine; Ab = albite; Anh = anhydrite; Bn = bornite; Bt = biotite; Cc = chalcocite; Ccp = chalcopyrite; Mag = magnetite; Ms = muscovite; Or = orthoclase; Toz = topaz

Table 6.2.1 Part 2

# run	LL055	LL080	LL083	LL089
<b>P [MPa]</b>	70 600	70 600	100 700	85 600
<b>T [°C]</b>	11 2	5 ≤1	5 ≤1	6 ≤1
<b>t [days]</b>				
<b>pH*</b>				
<b>fluid composition</b>	NaCl, KCl, FeCl <sub>2</sub> Pb, Co, Mo, As, Ag	NaCl, HCl, CuCl, S Pb, Co, Mo, Ag, Rb, Cs	NaCl, HCl, CuCl, S Pb, Co, Mo, Ag, Rb, Cs	NaCl, HCl, CuCl, S, Ti Pb, Co, Mo, As, Ag, Rb, Cs
<b>mineral buffers</b>	Ab, Bn, Bt, Ccp, Anh, Mag, Or	-	-	-
<b>S<sub>bulk</sub> [wt%]</b>	n.k.	6.3	5.7	5.4
<b>S species*</b>	SO <sub>4</sub> <sup>-2</sup>	n.d.	n.d.	H <sub>2</sub> S
<b>D<sub>cu</sub>vap/brine</b>	0.15 ± 0.04	0.17 ± 0.04	0.16 ± 0.09	0.07 ± 0.01
<b>Na [wt%]</b>	vapor (n=8) 0.47 brine (n=5) 7.5	vapor <sup>#</sup> (n=2) 9.0 ± 0.18 brine (n=8) 22	vapor (n=11) 2.3 brine (n=13) 22	vapor <sup>†</sup> (n=5) 1.4 brine (n=9) 19
<b>S [wt%]</b>	n.a.	n.a.	n.a.	3.1 ± 1.5 < 11
<b>Cu [wt%]</b>	0.05 ± 0.01	0.31 ± 0.05	0.61 ± 0.30	0.13 ± 0.02 1.8 ± 0.18
<b>Fe [wt%]</b>	0.47 ± 0.10	7.3 ± 0.81	n.a.	n.a.
<b>K [wt%]</b>	0.59 ± 0.18	5.3 ± 0.53	n.a.	n.a.
<b>Zn [wt%]</b>	n.a.	n.a.	n.a.	n.a.
<b>B [ppm]</b>	n.a.	n.a.	n.a.	n.a.
<b>Co [ppm]</b>	40 ± 30	< 1900	260	200 ± 50 3100 ± 1200
<b>As [ppm]</b>	700 ± 220	570 ± 210	n.a.	260 ± 140 620
<b>Rb [ppm]</b>	n.a.	1800 ± 210	440 ± 70	240 ± 20 3700 ± 600
<b>Mo [ppm]</b>	< 10	< 1900	< 70	< 10 < 30
<b>Ag [ppm]</b>	< 50	< 3300	< 70	210 ± 30 3400 ± 660
<b>Cs [ppm]</b>	n.a.	1300 ± 60	390 ± 50	230 ± 30 3600 ± 700
<b>Pb [ppm]</b>	130 ± 30	1900 ± 80	360 ± 80	230 ± 30 3500 ± 230

*Italic numbers* mark elements that were used as internal standard; n.a. = not analyzed; n.d. = not detectable; n.k. = not known; \*pH and S-species measured in quench fluid after the run; <sup>†</sup>vapor salinity estimated from H<sub>2</sub>O-NaCl phase diagram (Bodnar et al., 1985); <sup>#</sup> contains considerable amounts of coentrapped brine; Ab = albite; Anh = anhydrite; Bn = bornite; Bt = biotite; Cc = chalcocite; Ccp = chalcopyrite; Mag = magnetite; Ms = muscovite; Or = orthoclase; Toz = topaz

Table 6.2.1 Part 3

# run	LL090	LL093	LL095	LL120
<b>P [MPa]</b>	115	105	105	100
<b>T [°C]</b>	700	700	700	700
<b>t [days]</b>	4	5	5	5
<b>pH*</b>	≤1	≤1	1-2	1-2
<b>fluid composition</b>	NaCl, HCl, CuCl, S, Ti Pb, Co, Mo, As, Ag, Rb, Cs	NaCl, HCl, CuCl, FeCl <sub>2</sub> , Na <sub>2</sub> S, Pb, Co, Mo, Ag	NaCl, HCl, CuCl, Na <sub>2</sub> S Pb, Co, Mo, Ag	HCl, Na <sub>2</sub> S Pb, Co
<b>mineral buffers</b>	-	-	Cc	Au <sub>95</sub> Cu <sub>05</sub> -capsule
<b>S<sub>bulk</sub> [wt%]</b>	5.8	0.5	n.k.	6.0
<b>S species*</b>	H <sub>2</sub> S	n.d.	H <sub>2</sub> S	H <sub>2</sub> S
<b>D<sub>Cu</sub>vap/brine</b>	0.11 ± 0.04	0.14 ± 0.04	0.20 ± 0.03	0.07 ± 0.04
	vapor <sup>†</sup> (n=6) brine (n=6)	vapor (n=3) brine (n=8)	vapor (n=4) brine (n=5)	vapor <sup>†</sup> (n=3) brine (n=6)
<b>Na [wt%]</b>	1.4	1.0	1.9 ± 0.06	1.2
<b>S [wt%]</b>	5.9 ± 1.6	< 16	< 14	2.4
<b>Cu [wt%]</b>	0.22 ± 0.08	0.07 ± 0.02	0.14 ± 0.01	0.40 ± 0.18
<b>Fe [wt%]</b>	n.a.	0.97 ± 0.26	n.a.	n.a.
<b>K [wt%]</b>	n.a.	n.a.	n.a.	n.a.
<b>Zn [wt%]</b>	n.a.	n.a.	n.a.	n.a.
<b>B [ppm]</b>	n.a.	n.a.	n.a.	n.a.
<b>Co [ppm]</b>	160 ± 60	280 ± 80	< 90	30
<b>As [ppm]</b>	590 ± 110	< 870	n.a.	n.a.
<b>Rb [ppm]</b>	230 ± 30	n.a.	n.a.	n.a.
<b>Mo [ppm]</b>	< 40	100 ± 30	160	n.a.
<b>Ag [ppm]</b>	240 ± 70	300 ± 50	< 50	n.a.
<b>Cs [ppm]</b>	240 ± 30	n.a.	n.a.	n.a.
<b>Pb [ppm]</b>	230 ± 50	300 ± 140	250 ± 50	< 50
	3600 ± 50	2800 ± 70	2400 ± 20	780 ± 50

*Italic numbers* mark elements that were used as internal standard; n.a. = not analyzed; n.d. = not detectable; n.k. = not known; \*pH and S-species measured in quench fluid after the run; <sup>†</sup>vapor salinity estimated from H<sub>2</sub>O-NaCl phase diagram (Bodnar et al., 1985); #contains considerable amounts of coentrapped brine; Ab = albite; Anh = anhydrite; Bn = bornite; Bt = biotite; Cc = chalcocite; Ccp = chalcopyrite; Mag = magnetite; Ms = muscovite; Or = orthoclase; Toz = topaz

Table 6.2.1 Part 4

# run	LL135	LL147	LL165	LL171
<b>P [MPa]</b>	100	130	80	130
<b>T [°C]</b>	700	800	650	800
<b>t [days]</b>	5	4	4	0.3
<b>pH*</b>	10	≤1	≤0.3	≤0.3
<b>fluid composition</b>	HCl, Na <sub>2</sub> S Pb, Co	NaCl, S Pb, As, Ag, Rb, B	NaCl, KCl, S Pb, Rb, Cs	Na <sub>2</sub> SO <sub>4</sub> , HCl, CuSO <sub>4</sub> Pb, As, Ag, Rb, B
<b>mineral buffers</b>	Au <sub>95</sub> Cu <sub>05</sub> -capsule	Cc	Cc, Ab, Ms, Or, Toz	-
<b>S<sub>bulk</sub> [wt%]</b>	6.6	n.k.	n.k.	4.8
<b>S species*</b>	H <sub>2</sub> S	H <sub>2</sub> S, SO <sub>4</sub> <sup>2-</sup>	H <sub>2</sub> S, SO <sub>4</sub> <sup>2-</sup>	H <sub>2</sub> SO <sub>4</sub> <sup>+</sup> , SO <sub>4</sub> <sup>2-</sup>
<b>D<sub>Cu</sub>vap/brine</b>	0.17 ± 0.16	0.31 ± 0.03	0.08 ± 0.04	0.22 ± 0.07
<b>Na [wt%]</b>	1.4	3.1	3.7 ± 0.02	2.4
<b>S [wt%]</b>	2.4 ± 1.1	2.5 ± 0.66	< 4.0	< 10
<b>Cu [wt%]</b>	0.03 ± 0.03	0.30 ± 0.03	0.57 ± 0.21	0.26 ± 0.07
<b>Fe [wt%]</b>	n.a.	n.a.	< 0.35	n.a.
<b>K [wt%]</b>	n.a.	n.a.	< 1.01	n.a.
<b>Zn [wt%]</b>	n.a.	n.a.	n.a.	n.a.
<b>B [ppm]</b>	n.a.	1300 ± 120	< 0.03	1600 ± 940
<b>Co [ppm]</b>	n.a.	n.a.	n.a.	n.a.
<b>As [ppm]</b>	n.a.	660 ± 60	< 0.01	620 ± 410
<b>Rb [ppm]</b>	n.a.	260 ± 30	1300 ± 220	190 ± 20
<b>Mo [ppm]</b>	n.a.	n.a.	n.a.	n.a.
<b>Ag [ppm]</b>	n.a.	140 ± 30	n.a.	1400 ± 780
<b>Cs [ppm]</b>	n.a.	n.a.	2000 ± 620	n.a.
<b>Pb [ppm]</b>	80 ± 60	230 ± 30	720 ± 90	560 ± 60
		100 ± 40	3700 ± 200	3300 ± 580

*italic numbers* mark elements that were used as internal standard; n.a. = not analyzed; n.d. = not detectable; n.k. = not known; \*pH and S-species measured in quench fluid after the run; †vapor salinity estimated from H<sub>2</sub>O-NaCl phase diagram (Bodnar et al., 1985); ‡contains considerable amounts of coentrapped brine; Ab = albite; Anth = anhydrite; Bn = bornite; Cc = chalcocite; Co = chalcopyrite; Mag = magnetite; Ms = muscovite; Or = orthoclase; Toz = topaz

**Table 6.2.2** Results of re-equilibration experiments on synthetic fluid inclusions

# run	LL115				LL122		
<i>without pH change; with sulphur in the inclusions</i>							
	BEFORE equilibration		AFTER equilibration		NEW inclusions formed during equilibration		
fluid	17 wt% NaCl, 2 wt% S 0.8 wt% Cu <sub>2</sub> S; Rb		17 wt% NaCl, 2 wt% S 0.6 wt% Cu <sub>2</sub> S; Cs				
P [MPa] / T [°C]	130 / 800		70 / 800				
t [days] / pH*	4 / ≤1		4.5 / ≤1				
S species*	n.a.		H <sub>2</sub> S, SO <sub>4</sub> <sup>-2</sup>		n.a.		
	vapor (n=6)	brine (n=8)	vapor (n=5)	brine (n=8)	vapor (n=3)	brine (n=5)	
Na [wt%]	2.1 ± 0.17	24.2	2.9 ± 0.99	26 ± 0.04	4.1 ± 0.98	31	
S [wt%]	1.1 ± 0.09	0.24 ± 0.08	1.1 ± 0.09	0.25 ± 0.14	0.98 ± 0.01	0.45	
Cu [wt%]	< 0.03	0.05 ± 0.02	0.08 ± 0.04	0.88 ± 0.07	0.18 ± 0.07	1.1 ± 0.07	
B [ppm]	n.a.	n.a.	n.a.	n.a.	n.a.	n.a.	
As [ppm]	n.a.	n.a.	n.a.	n.a.	n.a.	n.a.	
Rb [ppm]	190 ± 60	1900 ± 100	190	1900	< 2	< 5	
Ag [ppm]	n.a.	n.a.	n.a.	n.a.	n.a.	n.a.	
Cs [ppm]	< 10	< 4	< 8	< 2	260 ± 30	2000 ± 150	
Pb [ppm]	60	200 ± 130	< 90	140 ± 80	< 4	< 6	
# run	LL141				LL144		
<i>with pH change; without sulphur in the inclusions</i>							
	BEFORE equilibration		AFTER equilibration		NEW inclusions formed during equilibration		
fluid	17 wt% NaCl, 4 wt% HCl 0.5 wt% Cu <sub>2</sub> S; Rb		17 wt% NaCl, 5.7 wt% KOH, 2 wt% S, 0.6 wt% Cu <sub>2</sub> S; Cs				
P [MPa] / T [°C]	130 / 800		70 / 800				
t [days] / pH*	4 / ≤0.3		4 / 10				
S species*	n.d.		n.a.		HSO <sub>4</sub> <sup>-</sup>		
	vapor (n=7)	brine (n=7)	vapor (n=4)	brine (n=4)	vapor (n=1)	brine (n=4)	
Na [wt%]	5.3 ± 0.55	23	12 ± 0.25	22 ± 3.9	3.4	28 ± 0.06	
S [wt%]	n.a.	n.a.	n.a.	n.a.	n.a.	n.a.	
Cu [wt%]	0.81 ± 0.13	2.2 ± 0.06	0.58 ± 0.05	1.1 ± 0.11	0.18	1.7 ± 0.25	
B [ppm]	n.a.	n.a.	n.a.	n.a.	n.a.	n.a.	
As [ppm]	n.a.	n.a.	n.a.	n.a.	n.a.	n.a.	
Rb [ppm]	420 ± 100	1600 ± 40	420	1600	< 4	< 14	
Ag [ppm]	n.a.	n.a.	n.a.	n.a.	n.a.	n.a.	
Cs [ppm]	< 10	< 4	< 20	< 3	160	2100 ± 160	
Pb [ppm]	< 120	< 30	< 130	< 30	< 40	< 6	

*Italic numbers mark elements that were used as internal standard; n.a. = not analyzed; n.d. = not detectable; \* pH and S species measured in quench fluid after the run; † vapor salinity estimated from H<sub>2</sub>O-NaCl phase diagram (Bodnar et al., 1985); (?) = data not reliable; § no true endmember due to co-entrapped brine.*

Table 6.2.2 Part 2

# run	LL147				LL149	
	BEFORE equilibration		AFTER equilibration		NEW inclusions formed during equilibration	
<b>fluid</b>	17 wt% NaCl, 2 wt% S 0.7 wt% Cu <sub>2</sub> S Rb, As, Pb, Ag, B				2 wt% NaCl; 0.7 wt% Cu <sub>2</sub> S Cs, As, Pb, Ag, B	
<b>P [MPa] / T [°C]</b>	<b>130 / 800</b>				<b>70 / 800</b>	
<b>t [days] / pH*</b>	<b>4 / ≤0.3</b>				<b>4 / 3</b>	
<b>S species*</b>	H <sub>2</sub> S, SO <sub>4</sub> <sup>-2</sup>		H <sub>2</sub> S, SO <sub>4</sub> <sup>-2</sup>		SO <sub>4</sub> <sup>-2</sup>	
	vapor (n=6)	brine (n=7)	vapor (n=16)	brine (n=7)	vapor (n=6)	brine (n=6)
<b>Na [wt%]</b>	3.8 ± 0.89	19	6.2 ± 1.6	19.4 ± 1.6	0.92 ± 0.08	31
<b>S [wt%]</b>	2.5 ± 0.66	1.7 ± 1.1	2.4 ± 1.1	1.1 ± 0.64	< 0.35	< 0.02
<b>Cu [wt%]</b>	0.30 ± 0.03	0.99 ± 0.04	5.7 ± 3.30	0.68 ± 0.08	0.05 ± 0.02	1.6 ± 0.14
<b>B [ppm]</b>	1300 ± 120	850 ± 100	1500 ± 220	840 ± 90	1700 ± 650	1200 ± 90
<b>As [ppm]</b>	690 ± 50	640 ± 80	1100 ± 460	660 ± 90	3600 ± 1900	9100 ± 7500
<b>Rb [ppm]</b>	310 ± 70	1400 ± 30	<i>310</i>	<i>1400</i>	< 40	10 ± 2
<b>Ag [ppm]</b>	180 ± 50	940 ± 30	1000 ± 800	1300 ± 330	70 ± 60	6400 ± 2100
<b>Cs [ppm]</b>	< 9	< 3	< 1	< 1	440 ± 240	17200 ± 600
<b>Pb [ppm]</b>	280 ± 60	1300 ± 50	360 ± 170	1200 ± 60	360 ± 170	1200 ± 60
# run	LL147				LL150	
	BEFORE equilibration		AFTER equilibration		NEW inclusions formed during equilibration	
<b>fluid</b>	17 wt% NaCl, 2 wt% S 0.7 wt% Cu <sub>2</sub> S Rb, As, Pb, Ag, B				2 wt% NaCl; 0.7 wt% Cu <sub>2</sub> S Cs, As, Pb, Ag, B	
<b>P [MPa] / T [°C]</b>	<b>130 / 800</b>				<b>130 / 800</b>	
<b>t [days] / pH*</b>	<b>4 / ≤0.3</b>				<b>4 / 4</b>	
<b>S species*</b>	H <sub>2</sub> S, SO <sub>4</sub> <sup>-2</sup>		H <sub>2</sub> S, SO <sub>4</sub> <sup>-2</sup>		n.d.	
	vapor (n=6)	brine (n=7)	vapor (n=10)	brine (n=9)	vapor <sup>§</sup> (n=9)	brine (n=7)
<b>Na [wt%]</b>	3.8 ± 0.89	19	4.2 ± 0.45	19 ± 2.1	4.5 ± 1.3	22
<b>S [wt%]</b>	2.5 ± 0.66	1.7 ± 1.1	1.3 ± 0.51	< 2.17	< 0.06	< 0.69
<b>Cu [wt%]</b>	0.30 ± 0.03	0.99 ± 0.04	2.9 ± 1.8	4.1 ± 1.7	0.20 ± 0.07	0.86 ± 0.02
<b>B [ppm]</b>	1300 ± 120	850 ± 100	780 ± 200	1000 ± 30	580 ± 130	640 ± 90
<b>As [ppm]</b>	690 ± 50	640 ± 80	510 ± 140	610 ± 250	3600 ± 1900	9100 ± 7500
<b>Rb [ppm]</b>	310 ± 70	1400 ± 30	<i>310</i>	<i>1400</i>	< 5	< 5
<b>Ag [ppm]</b>	180 ± 50	940 ± 30	280 ± 70	1100 ± 160	240 ± 100	1300 ± 60
<b>Cs [ppm]</b>	< 9	< 3	< 1	< 2	300 ± 80	1400 ± 30
<b>Pb [ppm]</b>	280 ± 60	1300 ± 50	320 ± 40	1300 ± 140	360 ± 100	1680 ± 30

*Italic numbers mark elements that were used as internal standard; n.a. = not analyzed; n.d. = not detectable; \* pH and S species measured in quench fluid after the run; † vapor salinity estimated from H<sub>2</sub>O-NaCl phase diagram (Bodnar et al., 1985); (‡) = data not reliable; § no true endmember due to co-entrapped brine.*

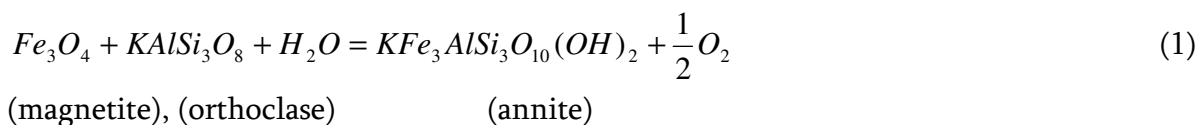
Table 6.2.2 Part 3

# run	LL151				LL152	
	BEFORE equilibration		AFTER equilibration		NEW inclusions formed during equilibration	
<b>fluid</b>	14 wt% NaCl, 16 wt% HCl 1.6 wt% S, 1.3 wt% Ti, 0.6 wt% Cu <sub>2</sub> S; Rb				2 wt% NaCl 0.6 wt% Cu <sub>2</sub> S; Cs	
<b>P [MPa] / T [°C]</b>	<b>130 / 800</b>				<b>70 / 800</b>	
<b>t [days] / pH*</b>	<b>4 / ≤0.3</b>				<b>4 / 3</b>	
<b>S species*</b>	H <sub>2</sub> S		SO <sub>4</sub> <sup>-2</sup>		SO <sub>4</sub> <sup>-2</sup>	
	vapor † (n=4)	brine (n=9)	vapor (n=10)	brine (n=15)	vapor (n=6)	brine (n=5)
<b>Na [wt%]</b>	2.5 <sup>(?)</sup>	27	26 ± 5.2 <sup>(?)</sup>	38 ± 0.06	0.90 ± 0.06	32
<b>S [wt%]</b>	0.18 ± 0.08 <sup>(?)</sup>	< 0.51	1.8 ± 2.1 <sup>(?)</sup>	< 0.37	< 0.06	< 0.13
<b>Cu [wt%]</b>	0.34 ± 0.12 <sup>(?)</sup>	3.7 ± 0.37	15 ± 8.7 <sup>(?)</sup>	1.8 ± 1.1	0.05 ± 0.01	1.6 ± 0.21
<b>B [ppm]</b>	n.a.	n.a.	n.a.	n.a.	n.a.	n.a.
<b>As [ppm]</b>	n.a.	n.a.	n.a.	n.a.	n.a.	n.a.
<b>Rb [ppm]</b>	160 ± 40 <sup>(?)</sup>	2000 ± 270	160 <sup>(?)</sup>	2000	< 4	< 10
<b>Ag [ppm]</b>	n.a.	n.a.	n.a.	n.a.	n.a.	n.a.
<b>Cs [ppm]</b>	< 7	< 10	< 1	< 5	560 ± 90	22100 ± 3200
<b>Pb [ppm]</b>	n.a.	n.a.	n.a.	n.a.	n.a.	n.a.
# run	LL171				LL172	
	BEFORE equilibration		AFTER equilibration		NEW inclusions formed during equilibration	
<b>fluid</b>	20 wt% Na <sub>2</sub> SO <sub>4</sub> 14 wt% HCl, 1.3 wt% Cu <sub>2</sub> SO <sub>4</sub> Rb, As, Pb, Ag, B				2 wt% NaCl; 0.6 wt% Cu <sub>2</sub> S Cs, As, Pb, Ag, B	
<b>P [MPa] / T [°C]</b>	<b>130 / 800</b>				<b>70 / 800</b>	
<b>t [days] / pH*</b>	<b>0.3 / ≤0.3</b>				<b>4 / 2.5</b>	
<b>S species*</b>	HSO <sub>4</sub> <sup>-</sup> , SO <sub>4</sub> <sup>-2</sup>		H <sub>2</sub> S, SO <sub>4</sub> <sup>-2</sup>		n.d.	
	vapor † (n=10)	brine (n=10)	vapor (n=13)	brine (n=7)	vapor (n=6)	brine (n=6)
<b>Na [wt%]</b>	2.4	17	5.41 ± 3.06	23 ± 2.8	1.1 ± 0.25	32
<b>S [wt%]</b>	< 10	6.8 ± 3.9	2.0 ± 1.4	12 ± 2.6	< 1.8	< 1.4
<b>Cu [wt%]</b>	0.26 ± 0.07	1.2 ± 0.20	5.7 ± 1.8	5.8 ± 2.2	0.03 ± 0.01	1.2 ± 0.11
<b>B [ppm]</b>	1600 ± 940	1200 ± 350	940 ± 600	670 ± 190	1200 ± 680	690 ± 40
<b>As [ppm]</b>	620 ± 410	410 ± 80	630 ± 310	450 ± 90	5300 ± 4000	3100 ± 2400
<b>Rb [ppm]</b>	190 ± 20	1300 ± 190	210	1420	< 10	10 ± 3
<b>Ag [ppm]</b>	1400 ± 470	12000 ± 1200	2700 ± 1000	15000 ± 4900	50 ± 60	2200 ± 300
<b>Cs [ppm]</b>	< 10	< 10	< 20	< 6	520 ± 150	18800 ± 470
<b>Pb [ppm]</b>	560 ± 60	3300 ± 580	590 ± 190	4200 ± 960	690 ± 610	9400 ± 5500

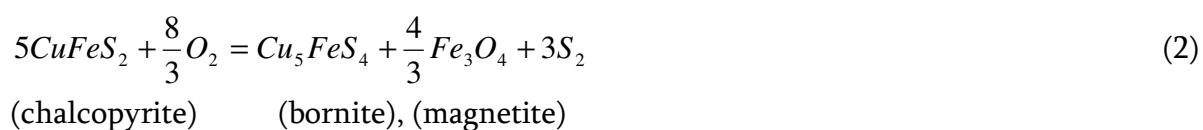
*Italic numbers mark elements that were used as internal standard; n.a. = not analyzed; n.d. = not detectable; \* pH and S species measured in quench fluid after the run; † vapor salinity estimated from H<sub>2</sub>O-NaCl phase diagram (Bodnar et al., 1985); <sup>(?)</sup> = data not reliable; <sup>§</sup> no true endmember due to co-entrapped brine.*

### 6.2.4.1.2 *New vapor-brine partitioning experiments*

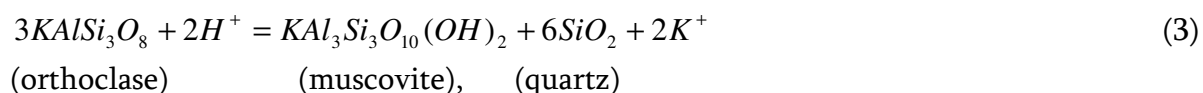
In three experiments (LL053, LL054, LL055; Table 6.2.1) we used a natural mineral assemblage consisting of chalcopyrite–bornite–magnetite–biotite–orthoclase–albite–muscovite–quartz ( $\pm$  anhydrite) to internally buffer pH,  $fO_2$ ,  $fS_2$ , and the activity of Cu. This mineral assemblage is representative of the early to intermediate mineralization stage in porphyry Cu deposits (Einaudi et al., 2003) and thus is geologically realistic. The oxygen fugacity is buffered by the reaction (Wones and Eugster, 1965):



whereby  $fO_2$  increases with decreasing annite component of the biotite. Natural, hydrothermal biotites from porphyry Cu deposits have annite components of 18-38 mol% (Burnham and Ohmoto, 1980), which fits well with the ~24 mol% annite measured in the biotites after our experiments. These experiments were conducted at 600 °C in thick-wall Au capsules (wall thickness 0.2 mm), hence  $fO_2$  should have been buffered strictly internally due to the low hydrogen diffusion rates at temperatures <700°C (Chou, 1986). With  $fO_2$  being buffered, the sulfur fugacity is constrained by the reaction (Barton and Skinner, 1979):



The fluid acidity is buffered by the coexistence of orthoclase with muscovite and quartz (Shade, 1974):



$D_{Cu}^{vap/brine}$  values obtained in these three experiments are less than unity and rather consistent ( $0.11 \pm 0.04$  to  $0.15 \pm 0.04$ ), despite variable amounts of HCl and S used in the starting mixture. This and the oxidized state of sulfur in the fluid inclusions (Table 6.2.1)

suggest that the buffer assemblages were effective.

All other experiments were conducted in compositionally simpler systems. Experiment LL147 was performed with chalcocite as Cu-source and elemental S at 800°C / 130 MPa, resulting in a  $D_{Cu}^{vap/brine}$  value of  $0.31 \pm 0.03$  and intermediate sulfur valences ( $H_2S + SO_4^{2-}$ ; Table 6.2.2). Two other experiments conducted with elemental sulfur as starting material (LL080 and LL083; run at 600°C / 70 MPa and 700°C / 100 MPa, respectively) resulted in slightly lower  $D_{Cu}^{vap/brine}$  values of  $0.17 \pm 0.04$  and  $0.16 \pm 0.09$ , respectively (Table 6.2.1).

$H_2S$ -dominated fluids were produced in experiments LL089 and LL090 by reacting elemental sulfur with Ti metal ( $2S + 2H_2O + Ti = 2H_2S + TiO_2$ ), and in experiments LL093, LL095, LL120, and LL135 by reacting solid  $Na_2S$  with HCl-bearing solutions ( $Na_2S + 2HCl = 2NaCl + 2H_2S$ ). All of these experiments yielded  $D_{Cu}^{vap/brine}$  values  $\leq 0.20$ , independent of temperature (600-800 °C), fluid acidity (quench fluid pH  $\leq 1$  to 10), or the concentrations of  $FeCl_2$  (0-4.0 wt%) and S (0.5-6.6 wt%) in the fluid.

A run with oxidized sulfur (LL171) and one intended to reproduce a natural fluid inclusion assemblage from the Erongo granite, Namibia, (LL165) resulted in similarly low  $D_{Cu}^{vap/brine}$  values ( $D_{Cu}^{vap/brine} = 0.22 \pm 0.07$  and  $0.08 \pm 0.04$ , respectively). Thus, none of our vapor–brine partitioning experiments returned a  $D_{Cu}^{vap/brine}$  value greater than 0.31, with the majority being below 0.20.

#### 6.2.4.2 Re-equilibration experiments

Re-equilibration experiments consist of an initial run analogous to the experiments described above, and a second run in which the same sample (after analyzing some of the fluid inclusions) is re-equilibrated in a slightly different fluid in a new gold capsule. To speed up diffusion the experiments were performed at 800 °C. In some experiments the second run was performed at a pressure lower than the initial run in order to simulate the progressive opening of the two-phase field commonly recorded by fluid inclusions in natural samples (e.g., Ulrich et al., 2002; Klemm et al., 2007; Audétat et al., 2008). This pressure change had little effect on the magnitude of Cu diffusion, as shown by an experiment performed at constant pressure. The fact that re-equilibrated fluid inclusions in

all runs preserved their original shapes (Figs. 6.2.1b, c) and do not contain Cs demonstrates that they did not leak. Details of each experiment and the obtained results are listed in Table 6.2.2.

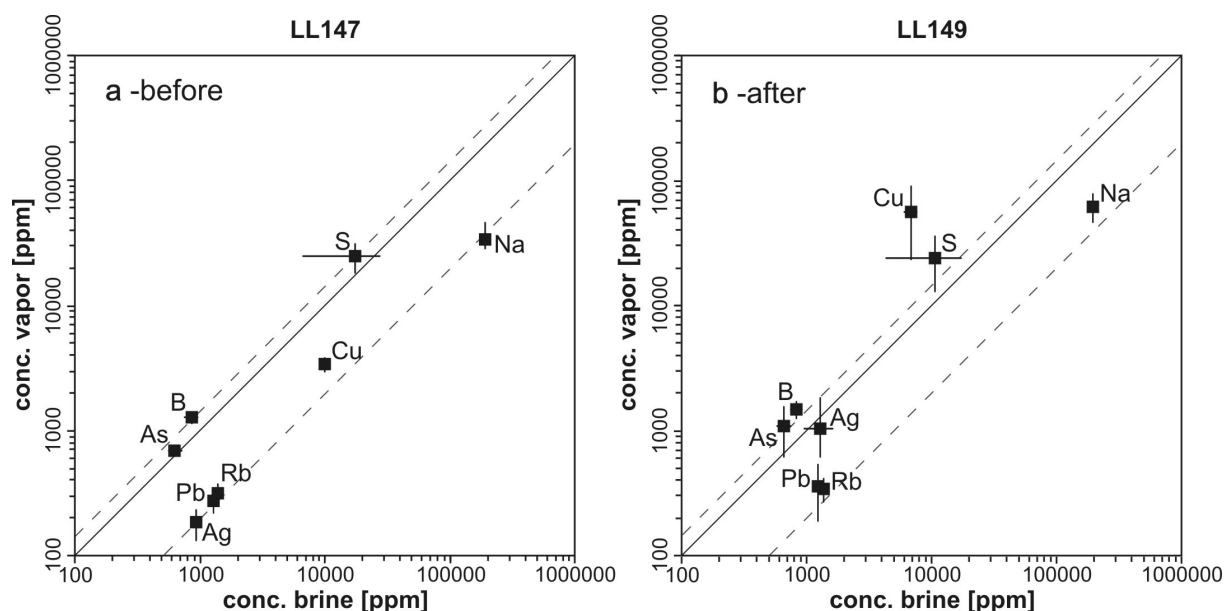


**Fig. 6.2.2**

Composition of synthetic vapor and brine inclusions before (a; run LL147) and after (b; run LL149) diffusional re-equilibration in a more neutral fluid at 800 °C and 70 MPa. Error bars express 1 $\sigma$  standard deviations.

In one experiment (runs LL147+149) vapor and brine inclusions were synthesized from an acidic, Cu- and S-bearing fluid (0.7 wt% Cu; 2 wt% S; quench fluid pH  $\leq$ 0.3) at 800 °C and 130 MPa and then re-equilibrated in a less acidic (quench fluid pH = 3) Cu- and S-bearing fluid at 800 °C and 70 MPa. Sulfur was added in elemental form, Cu was loaded as Cu<sub>2</sub>S, and  $f_{O_2}$  was externally buffered at NiNiO during both steps. Fluid inclusion compositions determined after the first step (Fig. 6.2.2a) reveal that Na, Pb, Rb, and Ag strongly partitioned into the brine phase, whereas S, B, and As partitioned into the vapor phase. Copper also partitioned into the brine phase, but slightly less strongly than Na, Pb, Rb, and Ag ( $D_{Cu}^{vapor/brine} = 0.31 \pm 0.05$ ). After re-equilibration (Fig. 6.2.2b) vapor inclusions contained ~20 times more Cu than before, whereas the Cu content of brine inclusions increased by about a factor of two. Hence, the same fluid inclusion assemblage that previously yielded a  $D_{Cu}^{vapor/brine}$  of  $0.31 \pm 0.05$  now suggests a  $D_{Cu}^{vapor/brine}$  of  $8.3 \pm 4.9$ . The

concentrations of Ag and Na increased as well, but not as dramatically as Cu. All other element concentrations remained constant within analytical uncertainty. Importantly, new fluid inclusions trapped during the second step in a separate quartz piece contained similar amounts of Cu as the fluids analyzed after the first step ( $0.30 \pm 0.03$  and  $0.99 \pm 0.04$  wt% versus  $0.20 \pm 0.07$  and  $0.86 \pm 0.02$  wt% in vapor and brine, respectively; Table 6.2.2), which implies that the Cu-gain in the re-equilibrated inclusions was not caused by a gradient in Cu concentration. Rather, Cu diffusion against a concentration gradient was possible because the chemical potential inside the re-equilibrated fluid inclusions was lower than in the outer fluid (see below).

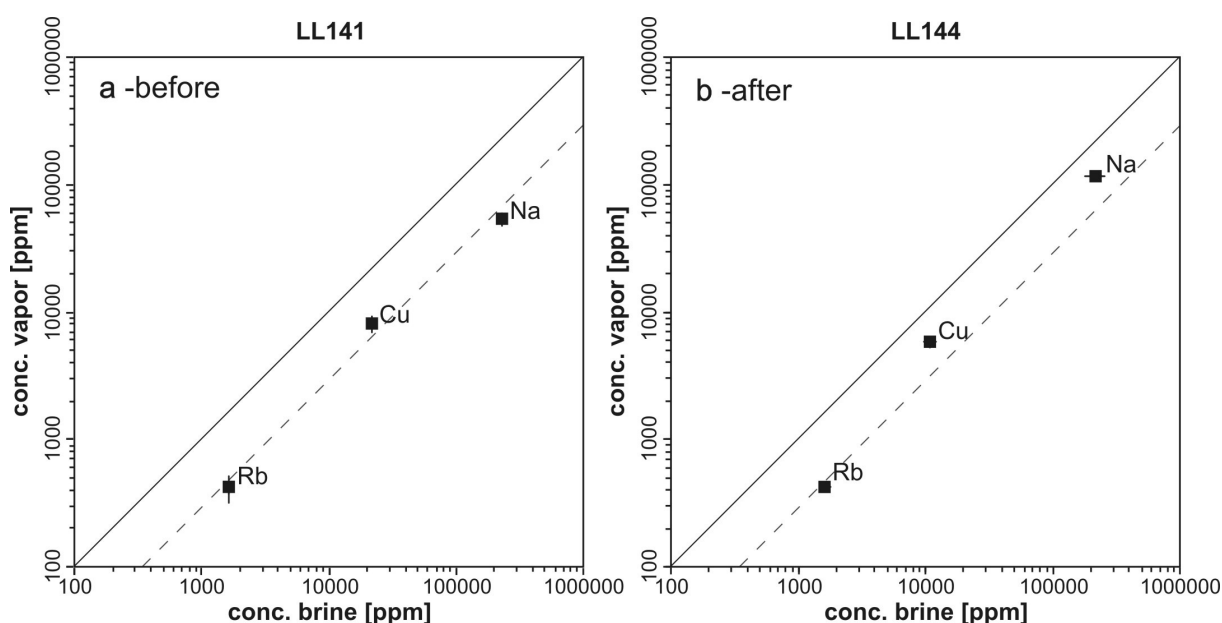


**Fig. 6.2.3**

Element concentrations in sulfur-free vapor and brine inclusions before (a; run LL141) and after (b; run LL144) diffusional re-equilibration in a more neutral fluid. Error bars express  $1\sigma$  standard deviations.

A similar experiment without sulfur in the starting fluid resulted only in a small increase in  $D_{Cu}^{vap/brine}$  from  $0.37 \pm 0.06$  to  $0.53 \pm 0.07$  (LL141+144; Fig. 6.2.3), whereas an experiment with sulfur in the starting fluid but at constant pH led to a decrease in  $D_{Cu}^{vap/brine}$  from  $0.48 \pm 0.14$  to  $0.09 \pm 0.05$  (LL115+122; Fig. 6.2.4). In contrast, an experiment analogous to the first one (LL147+149) but at constant pressure yielded a large increase in  $D_{Cu}^{vap/brine}$

from  $0.31 \pm 0.05$  to  $0.71 \pm 0.53$  (LL147+LL150; Table 6.2.2). These results suggest that large increases in  $D_{Cu}^{vap/brine}$  values are produced only if (i) an originally acidic fluid is replaced by a less acidic one, and (ii) the original fluid contains significant amounts of sulfur. The oxidation state of sulfur also matters, as H<sub>2</sub>S-dominated experiments (LL147+149 and LL151+LL152) resulted in larger increases in  $D_{Cu}^{vap/brine}$  than SO<sub>2</sub>-dominated experiments (LL171+LL172; Table 6.2.2).

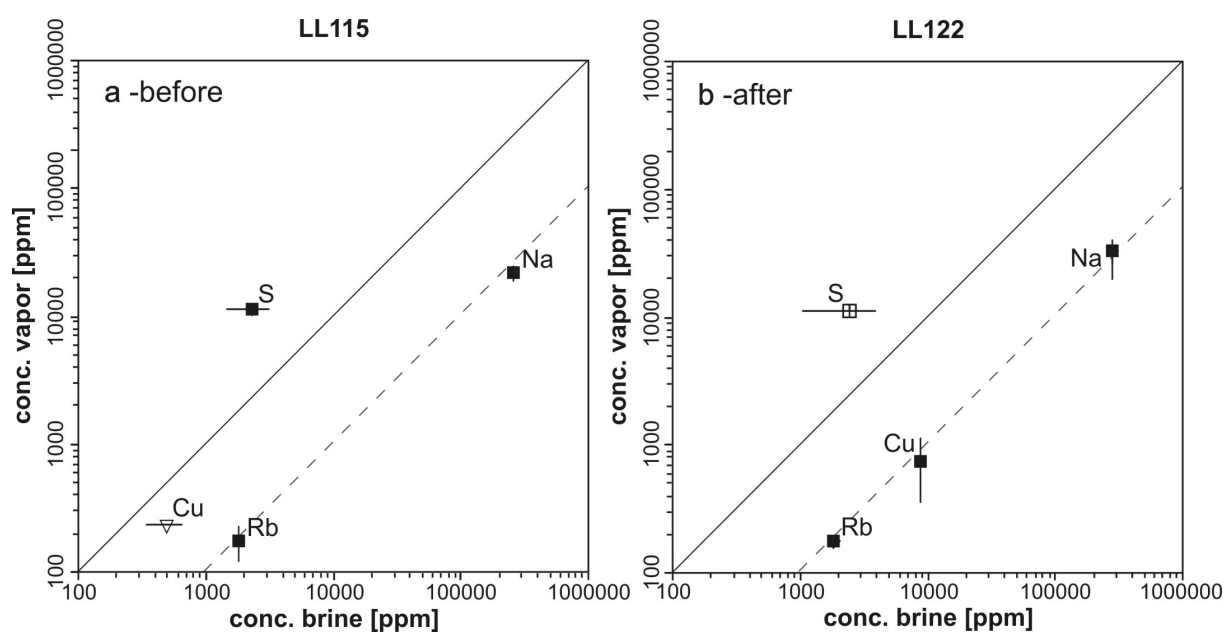


**Fig. 6.2.4**

Element concentrations in sulfur-bearing vapor and brine inclusions before (a; run LL115) and after (b; run LL122) diffusional re-equilibration in a fluid of the same acidity. Error bars express  $1\sigma$  standard deviations. The  $D_{Cu}^{vap/brine}$  before re-equilibration represents only a maximum value based on the detection limit in vapor inclusions.

The fact that major gains in Cu, Na, and Ag in our experiments occurred only when the surrounding fluid became less acidic suggests that it was ultimately caused by diffusion of H<sup>+</sup> out of the fluid inclusions, with Cu<sup>+</sup>, Na<sup>+</sup>, and Ag<sup>+</sup> diffusing back in to maintain charge balance. The fact that major gains of Cu occurred only if sulfur was present in the original fluid inclusions can be explained by the following model (Fig. 6.2.5): In contrast to Na, which stops diffusing once the Na concentration within the inclusion gets significantly higher than that in the external fluid, Cu continuously combines with sulfur in the

inclusion to precipitate as sulfide (Fig. 6.2.6), thus maintaining a low chemical potential. This allows large amounts of Cu to diffuse into the fluid inclusion despite relatively low Cu concentrations in the outer fluid. The only limiting parameter is the amount of sulfur present in the inclusion, and because sulfur typically fractionates into the vapor phase (Tables 6.2.1 and 6.2.2; see also Drummond and Ohmoto, 1985; Suleimenov and Krupp, 1994) vapor inclusions end up gaining more Cu than coexisting brine inclusions (Fig. 6.2.5). The result is an artificially high  $D_{Cu}^{vap/brine}$  value. It should be noted that absolute  $H^+$  concentrations in the fluids were very low during the experiments because HCl is almost fully associated at these P-T conditions (Frantz and Marshall, 1984).

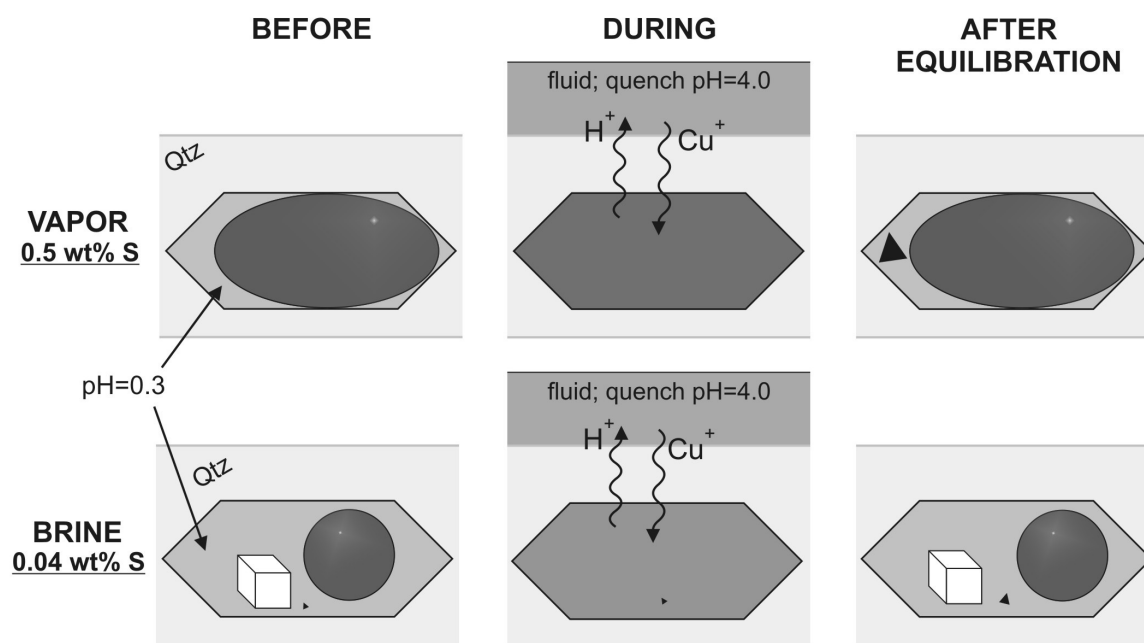
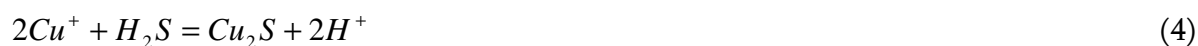


**Fig. 6.2.5**

Sketch to illustrate the mechanism of Cu diffusion. A gradient in fluid acidity causes protons to diffuse out of the fluid inclusions, which in turn causes Cu (+ Na, Ag) to diffuse inward to maintain charge balance. The incoming Cu combines with S to precipitate as sulfides (black triangles). Because the amount of Cu that can be gained by this process is limited by the amount of sulfur present in the fluid inclusion, sulfur-rich vapor inclusions can take up more Cu than sulfur-poor brine inclusions.

Thus, the driving force cannot have been a  $H^+$  concentration gradient, but apparently was a chemical potential gradient involving a reaction by which  $H^+$  was continuously generated, e.g., by the reaction of incoming Cu with sulfur:



In summary, the process can be regarded as a continuous exchange between incoming  $\text{Cu}^+$  ( $\pm \text{Na}^+$ ,  $\text{Ag}^+$ ) ions and leaving  $\text{H}^+$  ions with the goal to lower Gibbs free energy.

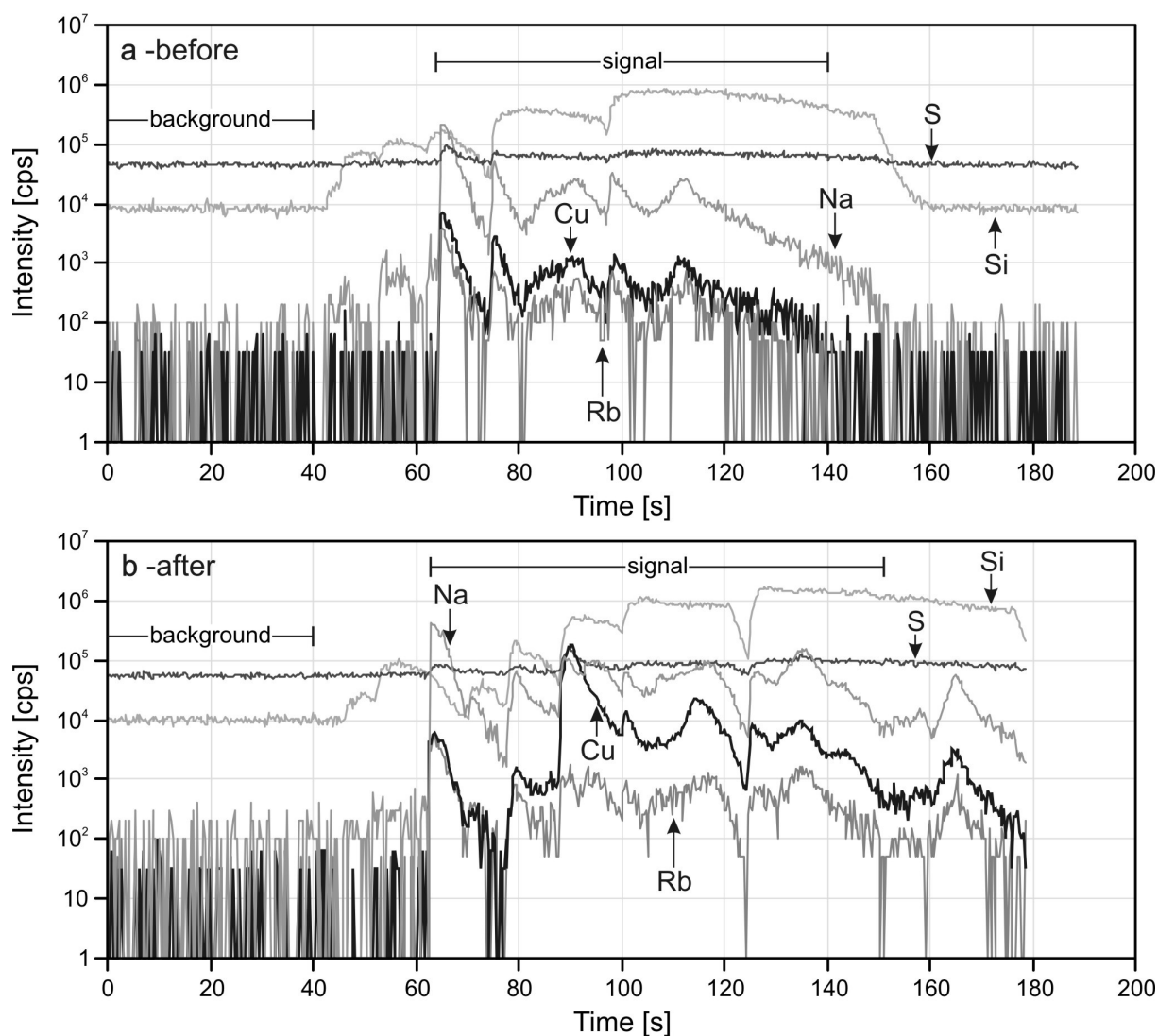


**Fig. 6.2.6**

(a) LA-ICP-MS signal of a vapor inclusion before re-equilibration; (b) LA-ICP-MS signal of another vapor inclusion of the same sample after re-equilibration (runs LL147+LL149). Inclusion sizes were 30 and 35 $\mu\text{m}$ , respectively. Before equilibration, Cu, S, Rb, and Na are mainly dissolved in the liquid phase, as indicated by their parallel signals produced during the stepwise opening of the inclusion. After re-equilibration a lot more Cu is present, with the main peak correlating with the sulfur peak at ~90 seconds. This suggests that most Cu was bonded with S in a sulfide daughter crystal.

The following evidence suggests that natural, quartz-hosted fluid inclusions from magmatic-hydrothermal environments likely experienced similar changes. Magmatic-hydrothermal fluids inevitably evolve from acidic to neutral pH as they cool in the presence of feldspar, quartz, and mica (Burnham, 1979), and most of them also contain significant amounts of sulfur (Seo et al., 2009). Copper and sulfur concentrations measured in natural fluid inclusions are well correlated and never exceed a molar Cu:S ratio of 1:2 (Seo et al., 2009). There is also a distinct correlation between measured  $D_S^{vap/brine}$  and  $D_{Cu}^{vap/brine}$ , with high values being observed in samples from tin granites (which are reduced), and low values in samples from porphyry Cu systems (which are oxidized), (Seo et al., 2009). All of these observations are consistent with the model described above.

#### *6.2.4.3 Equilibration of a natural sample from the Erongo Granite*

The Erongo granite in west-central Namibia is a Jurassic, peraluminous granite of A-type affinity (Piranjo, 1990). The granite contains abundant miarolitic cavities and locally greisen-type W-Sn-F-Be mineralization. A quartz crystal from a miarolitic cavity found at the Davib East Farm contains large, well-preserved fluid inclusions on pseudosecondary trails starting from a common growth zone (Fig. 6.2.7a). The same growth zone also hosts small inclusions of potassium feldspar, muscovite and albite (not visible in Fig. 6.2.7a). Several pseudosecondary trails contain both vapor and brine inclusions, indicating entrapment from a two-phase fluid.

Microthermometric data of the highest-temperature assemblages reveal salinities of ~4 wt% NaCl<sub>equiv</sub> in the vapor inclusions and 46-55 wt% NaCl<sub>equiv</sub> in the brine inclusions. The latter homogenize at ~600-650 °C (Table 6.2.3), which suggests entrapment pressures of ~60-80 MPa. The presence of contemporaneous potassic feldspar and muscovite implies that these fluids were acidic, which is consistent with the peraluminous nature of the granite and the development of greisens. LA-ICP-MS analyses of vapor and brine inclusions on trails A, C, and X yield  $D_{Cu}^{vapor/brine}$  values of 10-66 and further imply that the vapor phase contained 1-4 wt% of sulfur (Table 6.2.3).

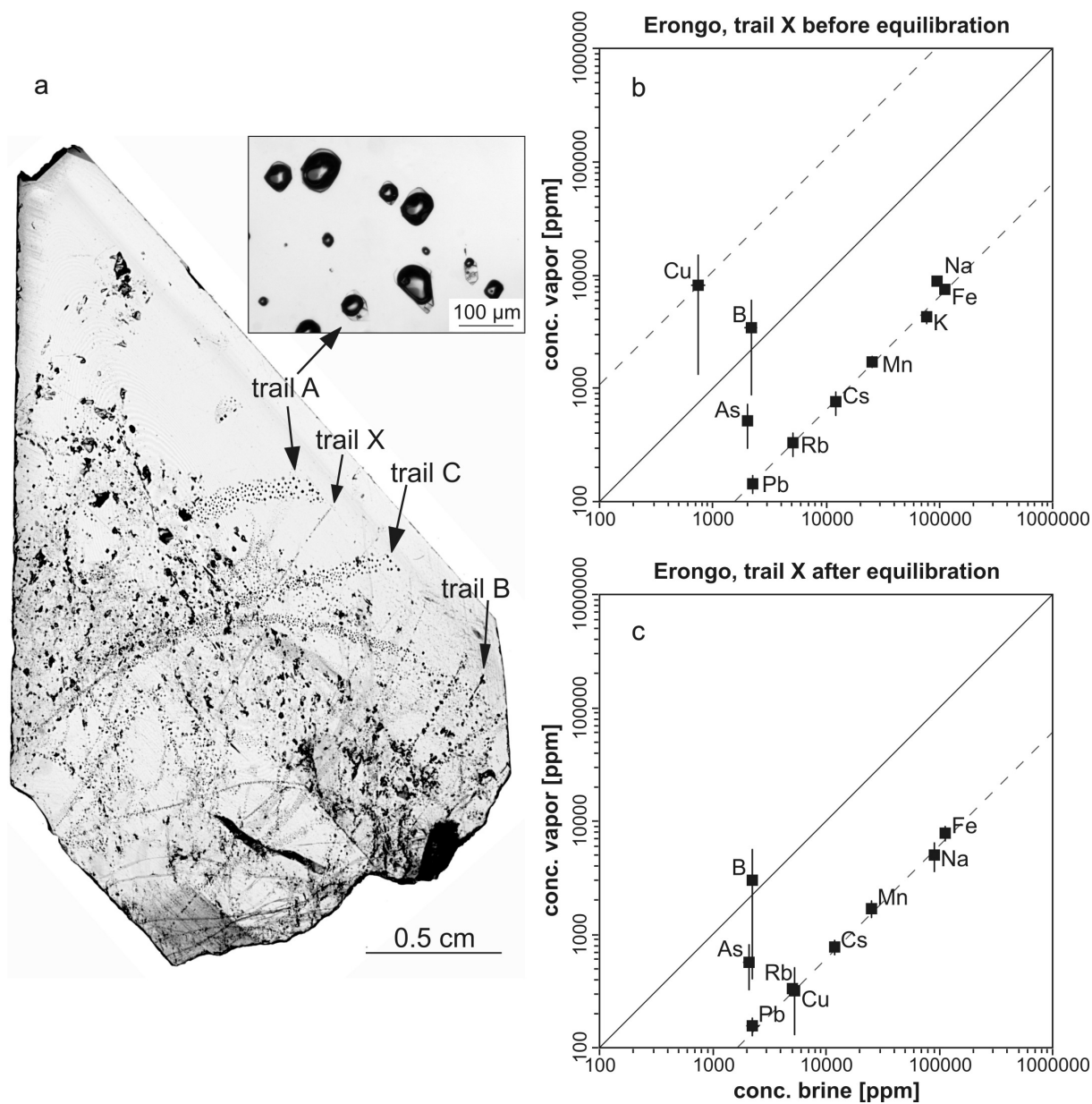


**Fig. 6.2.7**

(a) Photograph of a polished thick section through an idiomorphic quartz crystal from the Erongo granite, showing multiple generations of fluid inclusions occurring on pseudosecondary trails. Trails A, B, C, and X start from approximately the same growth zone, suggesting that they formed at a similar time. The enlargement of trail A shows several vapor inclusions (top), one brine inclusion (right), and two mixed inclusions (bottom). Composition of natural vapor and brine inclusions before (b) and after (c) diffusional re-equilibration in an acidic fluid at 650 °C / 80 MPa. Error bars express 1 $\sigma$  standard deviations.

**Table 6.2.3** Composition of untreated and re-equilibrated fluid inclusions from the Erongo granite

# run	Erongo trail A		Erongo trail B		Erongo trail C	
	boiling assemblage		vapor only		boiling assemblage	
Salinity [wt% NaCl <sub>equiv</sub> ]	3.7 ± 0.4	55 ± 4.9	4.2 ± 1.3		6.7 ± 2.1	46 ± 2.1
<i>T<sub>hom</sub></i> [°C]	> 600		<i>not visible</i>		~ 500	
	vapor (n=4)	brine (n=6)	vapor (n=13)		vapor (n=8)	brine (n=4)
Na [wt%]	1.2 ± 0.14	10 ± 1.1	1.6 ± 0.09		3.0 ± 1.3	9.0 ± 0.52
S [wt%]	4.4	< 0.52	2.1 ± 1.3		< 2.0	< 6.0
Cu [wt%]	2.0 ± 0.66	0.03 ± 0.03	3.9 ± 0.86		0.64 ± 0.24	0.06 ± 0.02
Mn [wt%]	0.11 ± 0.05	3.9 ± 0.25	0.11 ± 0.02		0.57 ± 0.25	2.7 ± 0.30
Fe [wt%]	0.57	13 ± 1.5	0.65 ± 0.27		2.2 ± 1.1	12 ± 1.1
K [wt%]	< 0.34	9.9 ± 1.9	0.54 ± 0.14		1.6 ± 0.63	6.8 ± 0.94
B [wt%]	0.82 ± 0.13	0.08 ± 0.08	1.5 ± 0.50		0.28 ± 0.14	0.17 ± 0.09
As [wt%]	1.1 ± 0.38	0.27 ± 0.11	0.82 ± 0.16		0.25 ± 0.07	0.30 ± 0.06
Cs [wt%]	0.05 ± 0.02	1.3 ± 0.07	0.06 ± 0.01		0.24 ± 0.11	1.1 ± 0.21
Rb [ppm]	260 ± 30	7300 ± 530	280 ± 70		990 ± 420	4700 ± 810
Ag [ppm]	< 70	30 ± 0	50 ± 10		< 150	< 40
Sn [ppm]	180	160 ± 10	300 ± 180		240 ± 200	750 ± 550
Pb [ppm]	110 ± 30	4100 ± 430	240 ± 180		660 ± 260	2500 ± 550
Bi [ppm]	60 ± 20	320 ± 40	50 ± 10		90 ± 60	330 ± 40
# run	Erongo trail X					
	<i>equilibration of a natural sample</i>					
	BEFORE equilibration		AFTER equilibration		NEW inclusions formed during equilibration	
Salinity [wt% NaCl <sub>equiv</sub> ]	~ 3.4 *	48 ± 2.1	fluid: 15 wt% NaCl, 5 wt% KCl 2 wt% S, 0.6 wt% Cu <sub>2</sub> S, Rb, Pb, Cs			
<i>T<sub>hom</sub></i> [°C]	> 600		<i>P</i> [Mpa] / <i>T</i> [°C]: 80 / 650			
	vapor (n=7)	brine (n=6)	vapor (n=9)	brine (n=6)	vapor (n=4)	brine (n=7)
Na [wt%]	0.88 ± 0.07	9.67 ± 0.41	0.50 ± 0.14	9.0 ± 0.69	3.7 ± 0.62	20
S [wt%]	n.a.	n.a.	n.a.	n.a.	< 4.0	2.8
Cu [wt%]	0.82 ± 0.69	0.07 ± 0.01	0.04 ± 0.03	0.52 ± 0.02	0.57 ± 0.21	3.3 ± 0.42
Mn [wt%]	0.17 ± 0.02	2.5 ± 0.11	0.17 ± 0.03	2.5 ± 0.04	< 0.03	0.04 ± 0.01
Fe [wt%]	0.75 ± 0.06	11 ± 0.55	0.79 ± 0.11	11 ± 0.23	< 0.35	< 0.28
K [wt%]	0.42 ± 0.05	7.7 ± 0.33	< 0.59	7.6 ± 0.18	< 1.01	9.4 ± 0.30
B [wt%]	0.30 ± 0.25	0.22 ± 0.03	0.30 ± 0.26	0.22 ± 0.01	< 0.03	< 0.03
As [wt%]	0.05 ± 0.02	0.20 ± 0.02	0.06 ± 0.02	0.21 ± 0.02	< 0.01	< 0.01
Cs [wt%]	0.08 ± 0.02	1.2 ± 0.05	0.08 ± 0.01	1.2 ± 0.02	0.20 ± 0.06	1.2 ± 0.07
Rb [ppm]	330 ± 80	5100 ± 260	330	5100	1300 ± 220	7200 ± 370
Ag [ppm]	n.a.	n.a.	n.a.	n.a.	n.a.	n.a.
Sn [ppm]	n.a.	n.a.	n.a.	n.a.	n.a.	n.a.
Pb [ppm]	150 ± 30	2300 ± 60	160 ± 330	2300 ± 270	720 ± 90	3700 ± 200
Bi [ppm]	n.a.	n.a.	n.a.	n.a.	n.a.	n.a.

*Italic numbers* mark elements that were used as internal standard; n.a. = not analyzed; \* estimated from H<sub>2</sub>O-NaCl phase diagram (Bodnar et al., 1985) because inclusions were too small to be measured

In order to reverse compositional changes that may have occurred in these fluid inclusions during subsequent cooling, one high-temperature trail containing small vapor and brine inclusions (trail X) was cut out and re-equilibrated at its original entrapment conditions (650 °C, 80 MPa) for 22 days (Table 6.2.3). The composition of the outer fluid was chosen such that its bulk salinity and the amounts of available S and Cu corresponded to a 75 : 25 mixture of the analyzed vapor and brine inclusions.

The result was a change in the measured  $D_{Cu}^{vap/brine}$  from  $11 \pm 9.3$  to  $0.06 \pm 0.04$ , and a change in  $D_{Na}^{vap/brine}$  from  $0.09 \pm 0.01$  to  $0.06 \pm 0.02$  (Fig. 6.2.7 b+c; Table 6.2.3), i.e., the reverse of what was observed in our re-equilibration experiments on synthetic fluid inclusions (e.g., Fig. 6.2.2). The concentrations of all other elements remained unmodified.

#### 6.2.4.4 Diffusion of $Cu^+$ at lower temperatures

Both synthetic and natural quartz crystals contain small amounts of  $Al^{3+}$  replacing  $Si^{4+}$ . The resulting charge deficit is compensated by small, single-charged cations that are located within channels parallel to the quartz c-axis. Ions that easily fit into these channels include  $H^+$ ,  $Li^+$ ,  $Na^+$ ,  $Cu^+$ , and  $Ag^+$  (Kats, 1962; Götze, 2009). It has been shown that  $H^+$  can be exchanged by any of these other ions and *vice versa* in response to a chemical potential gradient or an electric field (Verhoogen, 1952; Kats, 1962; Rybach and Laves, 1967; Mortley, 1969; Frischat, 1970; White, 1970; Kronenberg and Kirby 1987). These studies have also shown that ion diffusion along the c-axis is orders of magnitude faster than along the a or b axes, and that diffusion rates generally decrease with increasing ionic radius. Electrodiffusion ("sweeping") is used in the quartz manufacturing industry to replace  $Li^+$  and  $Na^+$  impurities by  $H^+$ , in order to improve radiation hardness and etching resistance (Martin, 1988). Published diffusion rates of  $H^+$  and  $Na^+$  parallel to the c-axis vary by orders of magnitude and depend on sample material, the type of ion exchange, and the measuring method (Kronenberg and Kirby, 1987; Mavrogenes and Bodnar, 1994). However, observed temperature dependencies are reproducible, with absolute diffusivities increasing by ~2.5 orders of magnitude between 400 °C and 800 °C (Fig. 6.2.8). It needs to be noted that the solubility of monovalent cations in synthetic quartz is very low (in the order of a few ppm; Martin, 1988; Poignon et al., 1996), hence the speed of fluid inclusion reequilibration is

governed by the diffusivity of the diffusing species rather than by their solubility in the quartz host (Qin et al., 1992).

In view of the lack of available Cu diffusion coefficients we constrained a minimum value based on the results of our re-equilibration experiments and used this value to estimate how long it would take to produce similar compositional changes at lower temperatures. This was done by estimating the flux of Cu through quartz and using Fick's first law

$$J = -D * \frac{\delta\Phi}{\delta x} \quad (5)$$

which relates the flux  $J$  (e.g., mol/m<sup>2</sup>s) to the diffusion coefficient  $D$  (m<sup>2</sup>/s) and the concentration gradient  $\delta\Phi$  (e.g., mol/m<sup>3</sup>) per distance  $\delta x$  (m) in the sample.

The flux of Cu was calculated based on a simple one-dimensional diffusion model (reflecting the fact that diffusion is mainly parallel to the c-axis), in which the fluid inclusions were approximated by cubic cavities of 20  $\mu\text{m}$  side length located 100  $\mu\text{m}$  below the quartz surface in c-axis direction. Based on a detection limit of 0.1 ppm Cu determined by LA-ICP-MS analysis of the overlying quartz we can constrain the concentration gradient within quartz at  $\leq 0.0042$  mol/m<sup>3</sup>. For a fluid inclusion of 0.2 g/cm<sup>3</sup> density gaining 5 wt% Cu within three days (Table 6.2.2) one can thus calculate a minimum diffusion coefficient of  $2.9 * 10^{-10}$  m<sup>2</sup>/s at 800 °C. This is a minimum value because the majority of Cu may have diffused earlier, and because Cu concentrations in quartz may in fact be less than 0.1 ppm. Extrapolation down to lower temperature using a slope similar to those displayed by Na<sup>+</sup>, H<sup>+</sup>, and Li<sup>+</sup> (Fig. 6.2.8) results in a minimum value of  $\sim 1.5 * 10^{-12}$  m<sup>2</sup>/s at 400 °C. Based on this value it would take a maximum of 80 years for a 20  $\mu\text{m}$  sized fluid inclusion covered by 5 mm quartz to gain 5 wt% Cu at 400 °C, a very short time compared to the typical life span of magmatic-hydrothermal systems (i.e. several thousand to tens of thousands of years; e.g., Von Quadt et al., 2011). Hence, it seems probable that the Cu content of many natural, quartz-hosted fluid inclusions (in particular that of sulfur-rich vapor inclusions) was modified since their formation.

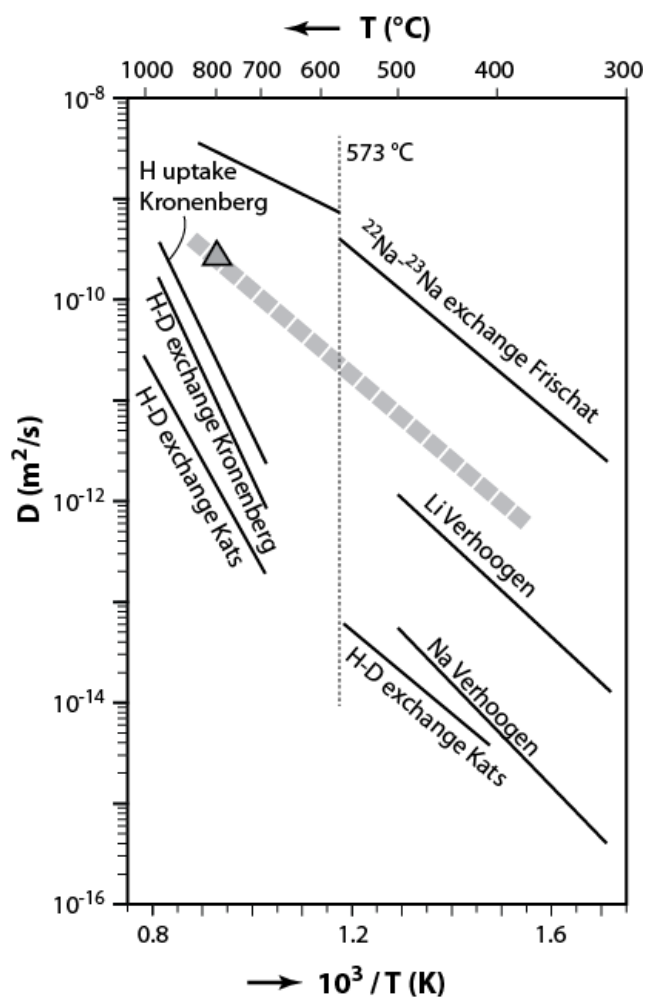


**Fig. 6.2.8**

Summary of published diffusion coefficients of Na, Li, and H in quartz for diffusion parallel to the *c*-axis. The gray triangle refers to our calculated minimum diffusion value for Cu at 800 °C, and the dashed gray line shows the expected extrapolation of this value down to 400 °C. References: Verhoogen (1952), Kats (1962), Frischat (1970), Kronenberg and Kirby (1987).

### 6.2.5 Implications for porphyry Cu ore formation

Previous experimental vapor-brine partitioning studies have been conducted mostly at  $f_{O_2}$  conditions under which  $H_2S$  is the dominant sulfur species because Cu was expected to form complexes with reduced sulfur. However, this situation is not realistic for porphyry Cu systems. Porphyry Cu systems and modern volcanoes that are considered to be present-day analogues of them (e.g., Mt. Pinatubo, El Chichón) are associated with magmas that record oxidation states of  $\log f_{O_2}$  NNO+1.0 to NNO+2.0 (Streck and Dilles, 1998; Audétat and Pettke, 2006; Stern et al., 2007; Chambefort et al., 2008; Simon and Ripley, 2011), at which

conditions the dominant sulfur species in fluids is SO<sub>2</sub> (Burnham 1997; Binder and Keppler, 2011). The experiments that most closely approximate this situation are our runs LL053-LL055 (Table 6.2.1) performed with the mineral buffer assemblage chalcopyrite-bornite-magnetite-biotite-orthoclase-albite-muscovite-quartz ( $\pm$  anhydrite), which resulted in  $D_{Cu}^{vap/brine}$  values ranging from  $0.11 \pm 0.04$  to  $0.15 \pm 0.04$ . Although SO<sub>2</sub> was dominant also in run LL171 (Table 6.2.1) the  $D_{Cu}^{vap/brine}$  value of  $0.22 \pm 0.07$  is not very informative in this case because the experiment was conducted close to the crest of the two-phase field and therefore resulted in high vapor/brine partition coefficients for all elements. The  $D_{Cu}^{vap/brine}$  values of  $0.11 \pm 0.04$  to  $0.15 \pm 0.04$  from runs LL053-LL055 are thus regarded as our most representative estimate for the partitioning behavior of copper in porphyry Cu systems.

**Table 6.2.4** Calculation of vapor/brine mass ratios in porphyry Cu systems

Deposit	Reported			Reference	Estimated salinity vapor at 500°C [NaCl <sub>equiv</sub> ]*	Calculated vapor/brine mass ratio
	bulk fluid salinity [NaCl <sub>equiv</sub> ]	pressure at 500°C [MPa]	salinity brine at 500°C [NaCl <sub>equiv</sub> ]			
Alumbrera (Argentina)	5 - 10	38	50	1	0.1	4 - 9
Bingham (USA)	7	42	43	2	0.2	5
Butte (USA)	4	60	40	3	0.8	11
El Teniente (Chile)	12	32	56	4	0.1	4
Famantina (Argentina)	6 - 18	40	45	5	0.1	2 - 7

\* salinity estimated based on the H<sub>2</sub>O-NaCl system (Bodnar et al., 1985); 1 = Ulrich et al., 2002; Heinrich et al., 2011; 2 = Landtwing et al., 2010; 3 = Rusk et al., 2008; 4 = Klemm et al., 2007; 5 = Pudack et al., 2009.

Based on the volatile content of felsic magmas and experimentally determined fluid–melt partition coefficients of Cl it has long been proposed that the fluids exsolving from magma chambers beneath porphyry Cu deposits had a relatively low bulk salinity, on the order of ~5-10 wt% NaCl<sub>equiv</sub> (e.g., Burnham, 1979; Shinohara and Hedenquist, 1997). Intermediate-density fluid inclusions recently found at deep levels of several porphyry Cu systems confirm this prediction. These fluid inclusions, which are samples of single-phase fluids before they enter the two-phase field, have salinities between 4 and 18 wt% NaCl<sub>equiv</sub>. (Table 6.2.4). Table 6.2.4 also lists reported salinities of brine inclusions trapped in the two-phase field at 500 °C (i.e., at the upper temperature limit of ore formation), plus the corresponding entrapment pressures and salinities of the vapor endmembers estimated

based on the model H<sub>2</sub>O-NaCl system. From each set of fluid salinities (single-phase input fluid plus coexisting vapor and brine at 500 °C) vapor/brine mass ratios were calculated by mass balance. The results suggest that the vapor/brine mass ratio in porphyry Cu systems was typically in the order of 4 to 9.

Combined with the  $D_{Cu}^{vap/brine}$  values of  $0.11 \pm 0.04$  to  $0.15 \pm 0.04$  estimated above, these vapor/brine mass ratios imply that the brines likely carried more Cu than the vapor-phase fluids. This is in contrast with some recent models of porphyry Cu formation in which the majority of metals and sulfur present in the deposit are considered to have precipitated from vapor-type fluids (e.g., Williams-Jones and Heinrich, 2005). On the other hand, it supports earlier models in which the majority of mineralization was linked to high salinity brines based on petrographic and microthermometric criteria (e.g. Bodnar 1995; Beane and Bodnar, 1995). The role of brines becomes even more prominent if one considers that the vapor phase ascends while the dense brine remains at depth, resulting in low vapor/brine mass ratios and a greater proportion of Cu transported by brines. In this regard, it is interesting to note that the zone of mineralization commonly corresponds to the level at which the single-phase fluids split into two-phase fluids (Redmond et al., 2004; Klemm et al., 2007; Rusk et al., 2008; Landtwing et al., 2010). Our findings thus suggest that brines generated at the base of the vapor plume dominate the transport and deposition of Cu at the porphyry level, whereas rising vapors and their cooled equivalents are responsible for the formation of epithermal Au deposits at shallower levels (Henley and McNabb, 1978; Heinrich et al., 2004).

#### 6.2.6 Acknowledgements

This work was funded by the German Science Foundation under projects number: AU 314/1-1 and AU 314/1-2. We sincerely thank Hans Keppler for scientific advice and financial support, Yuan Li for discussions, Huaiwei Ni for help with the calculation of the diffusion coefficients, and Sven Linhardt, Hubert Schulze, and Uwe Dittmann for their excellent technical support. We also like to express our gratitude to Zoltan Zajacz, Robert Bodnar, and an anonymous reviewer for their thoughtful comments.

### 6.2.7 References

- Audétat A. and Pettke T. (2006) Evolution of a porphyry-Cu mineralized magma system at Santa Rita, New Mexico (USA). *J. Petrol.* **47**, 2021-2046.
- Audétat A., Pettke T., Heinrich C. A. and Bodnar R. J. (2008) The composition of magmatic-hydrothermal fluids in barren versus mineralized intrusions. *Econ. Geol.* **103**, 877-908.
- Barton P. B. and Skinner B. J. (1979) Sulfide mineral stabilities. In *Geochemistry of hydrothermal ore deposits, 2<sup>nd</sup> edition* (ed. H. L. Barnes). John Wiley, New York. pp. 278-403.
- Beane R. E. and Bodnar R. J. (1995) Hydrothermal fluids and hydrothermal alteration in porphyry copper deposits. In *Porphyry copper deposits of the American cordillera* (eds. F. W. Pierce and J. G. Bohm). Arizona Geological Society Digest **20**, 83-93.
- Benning L. G. and Seward T. M. (1996) Hydrosulfide complexing of gold(I) in hydrothermal solutions from 150-500 °C and 500 to 1500 bars. *Geochim. Cosmochim. Acta* **60**, 1849-1872.
- Binder B. and Keppler H. (2011) The oxidation state of sulfur in magmatic fluids. *Earth Planet. Sci. Lett.* **301**, 190-198.
- Bodnar R. J. (1995) Fluid-inclusion evidence for a magmatic source for metals in porphyry copper deposits. In *Magmas, Fluids, and Ore Deposits* (ed. J. F. H. Thompson). Mineralogical Society of Canada, Short Course Series **23**, 139-152.
- Bodnar R. J. and Vityk M. O. (1994) Interpretation of microthermometric data for H<sub>2</sub>O-NaCl fluid inclusions. In *Fluid Inclusions in Minerals, Methods and Applications* (eds. B. D. Vivo and M. L. Frezzotti). Virginia Tech, Blacksburg. pp. 117-130.
- Bodnar R. J., Burnham C. W. and Sterner S. M. (1985) Synthetic fluid inclusions in natural quartz. III. Determination of phase equilibrium properties in the system H<sub>2</sub>O-NaCl to 1000 °C and 1500 bars. *Geochim. Cosmochim. Acta* **49**, 1861-1873.
- Burke W. A. J. (2001) Raman microspectrometry of fluid inclusions. *Lithos* **55**, 139-158.
- Burnham C. W. (1979) Magmas and hydrothermal fluids. In *Geochemistry of hydrothermal ore deposits* (ed. H. L. Barnes). John Wiley & Sons. pp. 71-136.
- Burnham, C. W. (1997) Magmas and hydrothermal fluids. In *Geochemistry of hydrothermal ore deposits, 3<sup>rd</sup> edition* (ed. H. L. Barnes). Wiley & Sons, New York pp. 63-124.
- Burnham C. W. and Ohmoto H. (1980) Late-stage processes of felsic magmatism. In *Granitic magmatism and related mineralization* (eds. S. Ishihara and S. Takenouchi). Mining Geology Special Issue **8**, 1-11.
- Chambefort I., Dilles J. H. and Kent A. J. R. (2008) Anhydrite-bearing andesite and dacite as a source for sulfur in magmatic-hydrothermal mineral deposits. *Geology* **36**, 719-722.
- Chou I.-M. (1986) Permeability of precious metals to hydrogen at 2 kb total pressure and elevated temperatures. *Am. J. Sci.* **286**, 638-658.
- Crerar D. and Barnes H. L. (1976) Ore solution chemistry V. Solubilities of chalcopyrite and

- chalcocite assemblages in hydrothermal solutions at 200 °C to 350 °C. *Econ. Geol.* **71**, 772-794.
- Drummond S. E. and Ohmoto H. (1985) Chemical evolution and mineral deposition in boiling hydrothermal systems. *Econ. Geol.* **80**, 126-147.
- Duc-Tin Q., Audétat A. and Keppler H. (2007) Solubility of tin in (Cl, F)-bearing aqueous fluids at 700°C, 140 MPa: A LA-ICP-MS study on synthetic fluid inclusions. *Geochim. Cosmochim. Acta* **71**, 3323-3335.
- Einaudi M. T., Hedenquist J. W. and Inan E. E. (2003) Sulfidation state of fluids in active and extinct hydrothermal systems: Transitions from porphyry to epithermal environments. *Soc. Econ. Geologists Spec. Publ.* **10**, 285-313.
- Etschmann B. E., Liu W., Testemale D., Müller H., Rae N. A., Proux O., Hazemann J. L. and Brugger J. (2010) An in situ XAS study of copper(I) transport as hydrosulfide complexes in hydrothermal solutions (25-592°C, 180-600 bar): speciation and solubility in vapor and liquid phases. *Geochim. Cosmochim. Acta* **74**, 4723-4739.
- Frank M. R., Simon A. C., Pettke T., Candela P. A. and Piccoli P. M. (2011) Gold and copper partitioning in magmatic-hydrothermal systems at 800°C and 100 MPa. *Geochim. Cosmochim. Acta* **75**, 2470-2482.
- Frantz J. D. and Marshall W. L. (1984) Electrical conductances and ionization constants of salts, acids, and bases in supercritical aqueous fluids; I, Hydrochloric acid from 100 degrees to 700 degrees C and at pressures to 4000 bars. *Am. J. Sci.* **284**, 651-667.
- Frischat G. H. (1970) Sodium diffusion in natural quartz crystals. *J. Am. Ceramic Soc.* **53**, 357-359.
- Gibert F., Pascal M. L. and Pichavant M. (1998) Gold solubility and speciation in hydrothermal solutions: experimental study of the stability of hydrosulphide complex of gold (AuHS) at 350 to 450°C and 500 bars. *Geochim. Cosmochim. Acta* **62**, 2931-2947.
- Götze J. (2009) Chemistry, textures and physical properties of quartz - geological interpretation and technical application. *Mineral. Mag.* **73**, 645-671.
- Guillong M. and Heinrich C. A. (2007) Sensitivity enhancement in laser ablation ICP-MS using small amounts of hydrogen in the carrier gas. *J. Anal. Atom. Spectrom.* **22**, 1488-1494.
- Hayashi K. I. and Ohmoto, H. (1991) Solubility of gold in NaCl- and H<sub>2</sub>S-bearing aqueous solutions at 250-350 °C. *Geochim. Cosmochim. Acta* **55**, 2111-2126.
- Hedenquist J. W. and Richards J. P. (1998) The influence of geochemical techniques on the development of genetic models for porphyry copper deposits. In *Techniques in hydrothermal ore deposits geology* (eds. J. P. Richards and P. B. Larson). *Rev. Econ. Geol.* **10**, 235-256.
- Heinrich C. A., Ryan C. G., Mernagh T. P. and Eadington P. J. (1992) Segregation of ore metals between magmatic brine and vapor: a fluid inclusion study using PIXE microanalysis. *Econ. Geol.* **87**, 1566-1583.

- Heinrich C. A., Günther D., Audétat A., Ulrich T. and Frischknecht R. (1999) Metal fractionation between magmatic brine and vapor, determined by microanalysis of fluid inclusions. *Geology* **27**, 755-758.
- Heinrich C. A., Pettke T., Halter W. E., Aigner-Torres M., Audétat A., Günther D., Hattendorf B., Bleiner D., Guillong M. and Horn I. (2003) Quantitative multi-element analysis of minerals, fluid and melt inclusions by laser-ablation inductively-coupled-plasma mass-spectrometry. *Geochim. Cosmochim. Acta* **67**, 3473-3496.
- Heinrich C. A., Driesner T., Stefánsson A. and Seward T. M. (2004) Magmatic vapour contraction and the transport of gold from the porphyry environment to epithermal deposits. *Geology* **32**, 761-764.
- Heinrich C. A., Meier D., Erni M., Von Quadt A. and Márquez-Zavalía F. (2011) Life-times and scales of Cu-Au-mineralizing magmatic-hydrothermal processes: Farallón Negro (Argentina). In *Let's talk ore deposits* (eds. F. Barra, M. Reich, E. Campos, and F. Tornos), *Proceedings of the 11th biennial SGA meeting, 26.-29. September 2011, Antafogasta, Chile*, p. 3-6.
- Helz G. R., Charnock J. M., Vaughan D. J. and Garner C. D. (1993) Multinuclearity of aqueous copper and zinc bisulfide complexes: an EXAFS investigation. *Geochim. Cosmochim. Acta* **57**, 15-25.
- Henley R. W. and McNabb A. (1978) Magmatic vapor plumes and ground-water interaction in porphyry copper emplacement. *Econ. Geol.* **73**, 1-20.
- Holland H. D. (1972) Granites, solutions and base metal deposits. *Econ. Geol.* **67**, 281-301.
- Kamenetsky V. S. and Danyushevsky L. V. (2005) Metals in quartz-hosted melt inclusions: Natural facts and experimental artifacts. *Am. Mineral.* **90**, 1674-1678.
- Kats A. (1962) Hydrogen in alpha-quartz. *Philips Res. Rep.* **17**, 133-195.
- Klemm L. M., Pettke T., Heinrich C. A. and Campos E. (2007) Hydrothermal evolution of the El Teniente Deposit, Chile: Porphyry Cu-Mo ore deposition from low-salinity magmatic fluids. *Econ. Geol.* **102**, 1021-1045.
- Kronenberg A. K. and Kirby S. H. (1987) Ionic conductivity of quartz: DC time dependence and transition in charge carriers. *Am. Mineral.* **72**, 739-747.
- Landtwing M. R., Furrer C., Redmond P. B., Pettke T., Guillong M. and Heinrich C. A. (2010) The Bingham porphyry Cu-Mo-Au deposit. III. Zoned copper-gold ore deposition by magmatic vapor expansion. *Econ. Geol.* **105**, 91-118.
- Lerchbaumer L. and Audétat A. (2012) The quartz capsule – a new method to avoid alloying problems with noble metal capsules in hydrothermal experiments. *Eur. J. Min.* **24**, in press.
- Li Y., Audétat A., Lerchbaumer L. and Xiong X. L. (2009) Rapid Na, Cu exchange between synthetic fluid inclusions and external aqueous solutions: evidence from LA-ICP-MS analysis. *Geofluids* **9**, 321-329.
- Loucks R. R. and Mavrogenes J. A. (1999) Gold solubility in supercritical hydrothermal brines measured in synthetic fluid inclusions. *Science* **284**, 2159-2163.

- Martin J. J. (1988) Electrodiffusion (sweeping) of quartz - a review. *IEEE Transactions on Ultrasonics, Ferroelectrics, and Frequency Control* **35**, 288-296.
- Matthews W., Linnen R. L. and Guo Q. (2003) A filler-rod technique for controlling redox conditions in cold-seal pressure vessels. *Am. Mineral.* **88**, 701-707.
- Mavrogenes, J. A. and Bodnar, R. J. (1994) Hydrogen movement into and out of fluid inclusions in quartz: Experimental evidence and geologic implications. *Geochimica et Cosmochimica Acta* **58**, 141-149.
- Mortley W. S. (1969) Diffusion paths in quartz. *Nature* **221**, 359-360.
- Mountain B. W. and Seward T. M. (2003) Hydrosulfide/sulfide complexes of copper (I): experimental confirmation of the stoichiometry and stability of  $\text{Cu}(\text{HS})_2^-$  to elevated temperatures. *Geochim. Cosmochim. Acta* **67**, 3005-3014.
- Nagaseki H. and Hayashi K. (2008) Experimental study of the behavior of copper and zinc in a boiling hydrothermal system. *Geology* **36**, 27-30.
- Nash J. T. (1976) Fluid-inclusion petrology - data from porphyry copper deposits and applications to exploration. *U. S. Geological Survey Professional Paper* **907-D**, 1-16.
- Piranjio F. (1990) Geology, geochemistry and mineralization of the Erongo volcanic complex, Namibia. *South African J. Geol.* **93**, 485-504.
- Poignon C., Jeandel G. and Morlot G. (1996) Study of ionic impurity mobility in quartz crystals by impedance and thermionic current measurements. *J. Appl. Phys.* **80**, 6192-6197.
- Pokrovski G. S., Borisova A. Y. and Harrichoury J.-C. (2008) The effect of sulfur on vapor-liquid fractionation of metals in hydrothermal systems. *Earth Planet. Sci. Lett.* **266**, 345-362.
- Pudack C., Halter W. E., Heinrich C. A. and Pettke T. (2009) Evolution of magmatic vapor to gold-rich epithermal liquid; the porphyry to epithermal transition at Nevados de Famatina, northwest Argentina. *Econ. Geol.* **104**, 449-477.
- Qin Z., Lu F., and Anderson A. T. (1992) Diffusive reequilibration of melt and fluid inclusions. *Am. Mineral.* **77**, 565-576.
- Redmond P. B., Einaudi M. T., Inan E. E., Landtwing M. R. and Heinrich C. A. (2004) Copper deposition by fluid cooling in intrusion-centered systems: New insights from the Bingham porphyry ore deposits, Utah. *Geology* **32**, 217-220.
- Roedder, E. (1971) Fluid inclusion studies on the porphyry-type ore deposits at Bingham, Utah, Butte, Montana, and Climax, Colorado. *Economic Geology* **66**, 98-120.
- Romberger S. B. and Barnes H. L. (1970) Ore solution chemistry III. Solubility of  $\text{CuS}$  in sulfide solutions. *Econ. Geol.* **65**, 901-919.
- Rusk B. D., Reed M. H. and Dilles J. H. (2008) Fluid inclusion evidence for magmatic-hydrothermal fluid evolution in the porphyry copper-molybdenum deposit at Butte, Montana. *Econ. Geol.* **103**, 307-334.
- Rybach L. and Laves F. (1967) Sodium diffusion experiments in quartz crystals. *Geochim.*

*Cosmochim. Acta* **31**, 539-546.

Sawkins F. J. and Scherkenbach D. A. (1981) High copper content of fluid inclusions in quartz from northern Sonora: implications for ore-genesis theory. *Geology* **9**, 37-40.

Seo J. H., Guillong M. and Heinrich C. A. (2009) The role of sulfur in the formation of magmatic-hydrothermal copper-gold deposits. *Earth Planet. Sci. Lett.* **282**, 323-328.

Seo J. H., Guillong M., Aerts M., Zajacz Z. and Heinrich C. A. (2011) Microanalysis of S, Cl and Br in fluid inclusions by LA-ICP-MS. *Chem. Geol.* **284**, 35-44.

Shade J. W. (1974) Hydrolysis reactions in the SiO<sub>2</sub>-excess portion of the system K<sub>2</sub>O-Al<sub>2</sub>O<sub>3</sub>-SiO<sub>2</sub>-H<sub>2</sub>O in chloride fluids at magmatic conditions. *Econ. Geol.* **69**, 218-228.

Shinohara H. and Hedenquist J. W. (1997) Constraints on magma degassing beneath the Far Southeast porphyry Cu-Au deposit, Philippines. *J. Petrology* **38**, 1741-1752.

Simon A. C., Pettke T., Candela P. A., Piccoli P. M. and Heinrich C. A. (2006) Copper partitioning in a melt-vapor-brine-magnetite-pyrrhotite assemblage. *Geochim. Cosmochim. Acta* **70**, 5583-5600.

Simon A. C. and Ripley E. M. (2011) The role of magmatic sulfur in the formation of ore deposits. *Rev. Mineral. Geochem.* **73**, 513-578.

Spandler C., Pettke T. and Rubatto D. (2011) Internal and external fluid sources for eclogite-facies veins in the Monviso Meta-ophiolite, Western Alps; implications for fluid flow in subduction zones. *J. Petrol.* **52**, 1207-1236.

Stern C. R., Funk J. A., Skewes M. A. and Arévalo A. (2007) Magmatic anhydrite in plutonic rocks at the El Teniente Cu-Mo deposit, Chile, and the role of sulfur- and copper-rich magmas in its formation. *Econ. Geol.* **102**, 1335-1344.

Streck M. J. and Dilles J. H. (1998) Sulfur evolution of oxidized arc magmas as recorded in apatite from a porphyry copper batholith. *Geology* **26**, 523-526.

Suleimenov O. M. and Krupp R. E. (1994) Solubility of hydrogen sulfide in pure water and in NaCl solutions, from 20 to 320°C and at saturation pressures. *Geochim. Cosmochim. Acta* **58**, 2433-2444.

Tagirov B. R., Salvi S., Schott J. and Maranova N. N. (2005) Experimental study of gold-hydrosulphide complexing in aqueous solutions at 350-500 °C, 500 and 1000 bars using mineral buffers. *Geochim. Cosmochim. Acta* **69**, 2119-2132.

Ulrich T., Günther D. and Heinrich C. A. (2002) The evolution of a porphyry Cu-Au deposit, based on LA-ICP-MS analysis of fluid inclusions: Bajo de la Alumbrera, Argentina. *Econ. Geol.* **97**, 1889-1920.

Verhoogen J. (1952) Ionic diffusion and electrical conductivity in quartz. *Am. Mineral.* **37**, 637-655.

Von Quadt A., Erni M., Martinek K., Moll M., Irena P. and Heinrich C. A. (2011) Zircon crystallization and the lifetimes of ore-forming magmatic-hydrothermal systems. *Geology* **39**, 731-734.

White S. (1970) Ionic diffusion in quartz. *Nature* **225**, 375-376.

- 
- Williams-Jones A. E. and Heinrich C. A. (2005) Vapor transport of metals and the formation of magmatic-hydrothermal ore deposits. *Econ. Geol.* **100**, 1287-1312.
- Wones D. R. and Eugster H. P. (1965) Stability of biotite: experiment, theory, and application. *Am. Mineral.* **50**, 1228-1272.
- Zajacz Z., Hanley J. J., Heinrich C. A., Halter W. E. and Guillong M. (2009) Diffusive re-equilibration of quartz-hosted silicate melt and fluid inclusions: Are all metal concentrations unmodified? *Geochim. Cosmochim. Acta* **73**, 3013-3027.
- Zajacz Z., Seo J. H., Candela P. A., Piccoli P. M., Heinrich C. A. and Guillong M. (2010) Alkali metals control the release of gold from volatile-rich magmas. *Earth Planet. Sci. Lett.* **297**, 50-56 .
- Zajacz Z., Seo J. H., Candela P. A., Piccoli P. A. and Tossell J. A. (2011) The solubility of copper in high-temperature magmatic vapors: a quest for the significance of various chloride and sulfide complexes. *Geochim. Cosmochim. Acta* **75**, 2811-2827.

### ***6.3 The metal content of silicate melts and aqueous fluids in sub-economically Mo-mineralized granites: Implications for porphyry Mo genesis***

L. LERCHBAUMER AND A. AUDÉTAT

Bayerisches Geoinstitut, Universität Bayreuth, 95440 Bayreuth, Germany

*Economic Geology (2012), submitted*

#### **6.3.1 Abstract**

To better understand the factors leading to porphyry Mo mineralization we studied melt and fluid inclusions in three sub-economically Mo-mineralized granites in well-known Mo provinces: the Treasure Mountain Dome in the Colorado Mineral Belt (USA), and the Drammen and Glitrevann granites in the Oslo Rift (Norway). Melt and fluid inclusions were investigated in samples ranging from coarsely crystallized whole rocks to euhedral quartz crystals within miarolitic cavities. The major and trace element chemistry of individual inclusions was determined by laser-ablation ICP-MS. Melt inclusions record a clear trend of increasing Mo concentrations with increasing degree of melt differentiation as monitored by Cs, extending from ~5-10 ppm Mo at 5 ppm Cs to ~17-40 ppm Mo at 100 ppm Cs. Coexisting magmatic fluids were single-phase, had a salinity of 4-6 wt% NaCl<sub>equiv</sub>, a density of 0.6-0.7 g/cm<sup>3</sup> and contained ~0.5 wt% S and up to 6 mol% CO<sub>2</sub>. Molybdenum concentrations in these fluids ranged from ~20 ppm to ~200 ppm Mo, except for some highly evolved fluids that had lower Mo contents.

Comparison of our data with published fluid and melt inclusion data from porphyry Mo deposits, porphyry Cu (Mo, Au) deposits, and barren intrusions reveals that most subduction-related magmas have lower Mo/Cs ratios than within-plate magmas, but that within these two groups there are no systematic differences between barren and productive intrusions. This suggests that the mineralization potential was not primarily controlled by the metal content of the melts and fluids, but rather by other factors such as size of the

magma chamber and the efficiency of residual melt and fluid extraction from the magma chamber and their focusing into a small apophysis at its top. Based on our data it can be calculated that at least several tens of km<sup>3</sup> of magma were necessary to form intermediate-sized Mo deposits, and at least several hundred km<sup>3</sup> to form giant ( $\geq 1$ Mt Mo) deposits. All three granites investigated in this study would have been large enough to produce at least an intermediate-sized Mo deposit, but they nevertheless are only sub-economically mineralized. Their low productivity thus appears to be the result of poor fluid focusing. Factors promoting a high degree of fluid focusing include: (i) accumulation of major volumes of fractionated, crystal-poor melts at the top of the magma chamber, (ii) formation of an apophysis, and (iii) development of convection cells that lead to an efficient circulation of these fractionated melts through the apophysis.

### **6.3.2 Introduction**

Molybdenum, a sought-after alloying metal due to its high-strength properties and very high melting point, is principally mined from porphyry-type ore deposits. About half of the production stems from porphyry Mo deposits, in which this metal is the principal commodity (i.e. Mo/Cu >1), and the other half from porphyry Cu (Mo, Au) deposits, in which Mo is recovered as a valuable byproduct (e.g., Carten et al., 1993). This study focuses on the formation of the former type of deposits, and more specifically on the subclass of Climax-type deposits, which are associated with highly evolved, rift-related rhyolites, as opposed to the subclass of low-grade, arc-related deposits that are associated with less evolved, calc-alkaline magmas (Westra and Keith, 1981; Carten et al., 1993). Up to now, by far the largest producers of the Climax type were Climax (Colorado, USA), Urad-Henderson (Colorado, USA), and Questa (New Mexico, USA), which have provided nearly 80% of the Mo mined from porphyry Mo deposits (Mutschler et al., 1999). Although many porphyry Mo occurrences have been thoroughly investigated with respect to their geologic setting, intrusion sequence, petrography, wallrock alteration, and ore distribution, only little data exists concerning the metal content of the silicate melts and the magmatic-hydrothermal fluids that were responsible for the transport and deposition of Mo. One of the main reasons for this paucity of data is the difficulty to find analyzable fluid and melt inclusions, which

appears to reflect unfavorable formation conditions combined with a high percentage of subsequent inclusion destruction in this type of ore deposits. So far, larger data sets have been available only from two occurrences: the porphyry Mo deposit at Questa/New Mexico (Klemm et al., 2008; only fluid inclusion data), and the porphyry Mo (Nb) deposit at Cave Peak/Texas (Audétat, 2010; both fluid and melt inclusion data). Additionally, limited melt inclusion data are available from Pine Grove/Utah (Lowenstern, 1994; Audétat et al., 2011), and from the Henderson-related Hideaway Park ignimbrite (USGS Denver Inclusion Analysis Laboratory, online reference 1).

The studies on Cave Peak and Questa returned rather contrasting values for metal contents in magmatic bulk fluids: At Cave Peak, intermediate-density fluid inclusions coexisting with highly fractionated melt inclusions contain ~100 ppm Mo and ~600 ppm Cu (i.e., Mo/Cu ~0.2), whereas at Questa, pre-mineralization, intermediate-density fluid inclusions trapped in quartz of a magmatic-hydrothermal breccia contain ~40 ppm Mo and ~3000 ppm Cu (i.e., Mo/Cu ~0.01). Particularly in the latter case the high Cu concentrations are unexpected, given the fact that the deposit does not contain any recoverable copper.

To get a better overview of the composition of Mo-mineralizing melts and fluids we investigated samples from three sub-economically Mo-mineralized intrusions. As was mentioned above, analyzable fluid and melt inclusions are rather rare in intrusions associated with economic Mo deposits, hence we focused on small, sub-economic occurrences that contain well-preserved inclusions, noting that the difference between economic and sub-economic occurrences does not necessarily lie in the composition of the melts and fluids, but may be due to other parameters such as the size of the magma chamber and the degree of fluid focusing. The two main questions addressed in this study are: (i) What are typical metal concentrations in Mo-mineralizing fluids and melts?, and (ii) What factors determine the Mo-mineralizing potential of granitic intrusions?

### **6.3.3 Samples**

Samples were collected from granitic intrusions in two areas that are well known for granite-related Mo mineralization: the Colorado Mineral Belt (USA), and the Oslo Rift (Norway).

### 6.3.3.1 *Treasure Mountain Dome (Colorado, USA)*

The Treasure Mountain Dome is a large, granitic intrusion in the central part of the Colorado Mineral Belt, which hosts some of the world's biggest porphyry Mo deposits including the famous Climax and Urad-Henderson ore bodies (Figure 6.3.1). The Colorado Mineral Belt is a NE-trending belt of about 400 km length and 20-60 km width. The belt hosts numerous Au, Ag, Cu, Mo, Pb, and Zn deposits. Most of these deposits are genetically associated with monzonitic to granitic intrusions of Laramide (~70-80 Ma to 35-55 Ma) age (Bookstrom, 1989; Tweto and Sims, 1963), whereas all porphyry Mo deposits are of Oligocene (23-34 Ma) to Pliocene (5.3-2.6 Ma) age (e.g., White et al., 1981; Wareham and Rice, 1998). Minor Mo mineralization occurring in pegmatitic segregations or as local disseminations within the Precambrian basement be related to igneous activity at 1.7., 1.4, and 1.0 Ga (Lehmann, 1987).

The Colorado Mineral Belt coincides with a large-scale negative Bouguer anomaly (Figure 6.3.1) that reflects primarily Laramide-age intrusions emplaced along a reactivated Precambrian shear zone. However, local negative Bouguer anomalies are spatially associated with the porphyry Mo deposits and are interpreted to reflect large leucogranite bodies that were emplaced in the Oligocene to Pliocene, i.e., more than 10 Ma after subduction-related magmatism in the Laramide period stopped, but coinciding with the initiation of the Rio Grande Rift (White et al., 1981; Bookstrom, 1989). A fundamental change in the mode of magmatism is evident also in the major and trace element chemistry of the magmas. Laramide-age magmas cover the entire suite from monzonitic to granitic compositions and show a clearly subduction-related, calcalkaline character, whereas magmas associated with porphyry Mo mineralization are strongly bimodal (high-silica rhyolites coexisting with minor lamprophyres; Bookstrom et al., 1988), distinctly potassic, and of A-type (i.e., intraplate) affinity (e.g., White et al. 1981; Carten et al., 1993; USGS Denver Inclusion Analysis Laboratory, online reference 1).

The Treasure Mountain Dome, located about 10 km SE of the town of Marble, has been dated at an age of  $12.4 \pm 0.6$  Ma (Obradovich et al., 1969). It shares many similarities with the Oligocene (23-34 Ma) Climax-Alma batholith ~90 km to the northeast, whose apophyses produced the Climax and Urad-Henderson deposits (Bookstrom, 1989). Forceful

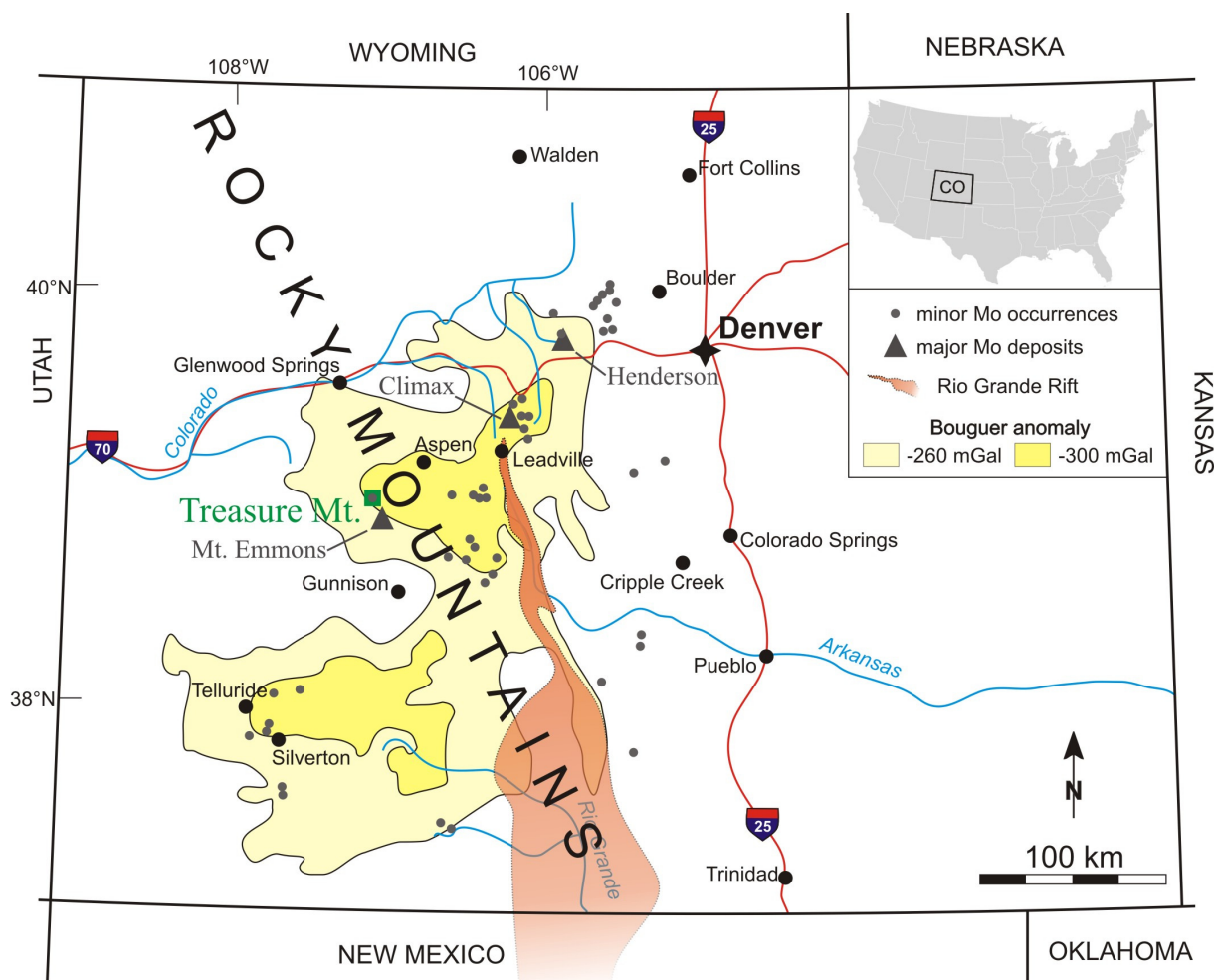


**Figure 6.3.1**

Sketch map of Colorado showing the location of major and minor Mo deposits and occurrences (Lehmann, 1987) relative to an underlying batholith indicated by Bouguer anomaly-minima (USGS-data; online reference 4) and the Rio Grande Rift (dimensions from White et al., 1981). The boundaries of the Colorado Mineral Belt more or less coincide with the outer limits of the -260 mGal anomaly.

intrusion of granitic magma into Paleozoic sedimentary rocks at Treasure Mountain formed a dome that measures 15 km in length, 12 km in width, and ~1.4 km in height (Mutschler, 1976). The crest of the intrusion is exposed at an altitude of ~3880 m close to the top of Treasure Mountain. In this area, molybdenite-bearing veins and disseminations within the granite and in the overlying Precambrian basement are common. Vein-type mineralization is represented by small, widely-spaced quartz-sericite-pyrite-fluorite veins containing minor molybdenite, whereas disseminations are represented by quartz-pyrite-sericite-orthoclase-fluorite-tourmaline-molybdenite greisens (Mutschler, 1976). Small pegmatitic

veins and miarolitic cavities filled with quartz, orthoclase, pyrite, and fluorite are also common.

Four different granite facies have been distinguished by Mutschler (1976): (i) a medium- to coarse-grained, equigranular to slightly porphyritic facies that occurs only at intermediate to low elevations ('Granular facies'), (ii) a porphyritic facies with 60-90 vol% phenocrysts of quartz and K-feldspar set in a fine-grained matrix, forming an up to 200 m thick sheet above the granular facies ('Twin Bridges porphyry facies'), (iii) a leucocratic porphyry facies containing 20-50 vol% phenocrysts of quartz, K-feldspar, and plagioclase set in a very fine-grained matrix, forming an up to 100 m thick border phase in the apical part of the intrusion ('Bear Mountain porphyry phase') and (iv) an even more leucocratic porphyry phase containing small phenocrysts of quartz, K-feldspar, and albite in an extremely fine-grained matrix, occurring as dikes intruded into Paleozoic and Mesozoic sediments along the flanks of the dome ('White Quartz porphyry phase'). Samples were taken from the granular facies at an elevation of 3580 m (sample *TM 2*; coordinates 39° 01' 45.2" N, 107° 06' 26.4" W; WGS84 datum), from the leucocratic Bear Mountain porphyry border phase (in the following simply called 'border phase') at an elevation of 3870 m (sample *TM 7*; 39° 01' 15.7" N, 107° 06' 40.2" W), and from three miarolitic cavities (samples *TM 5*, *TM 10*, *TM 12*) in the vicinity of the latter sample, all hosted by the border phase. The miarolitic cavities measured 5-15 cm in diameter and were lined with euhedral crystals of quartz, orthoclase, ± fluorite.

### *6.3.3.2 Drammen granite (Norway)*

The Drammen granite is a composite granitic body in the central part of the Oslo Rift (Figure 6.3.2), which formed during Permo-Carboniferous rifting in northern Europe. The various occurrences of Mo (and Fe, Mn, Ti, W, Mb, Zn, Pb, Cu, Bi) mineralization in the Oslo region stem from this rift-related, subalkaline magmatism (Schönwandt and Petersen, 1983). Thus, all Mo occurrences of the Oslo Rift belong to the alkalic type described by Carten et al. (1993). Although numerous, none of the Mo-mineralizations are regarded as exploitable (Ihlen, 1986).

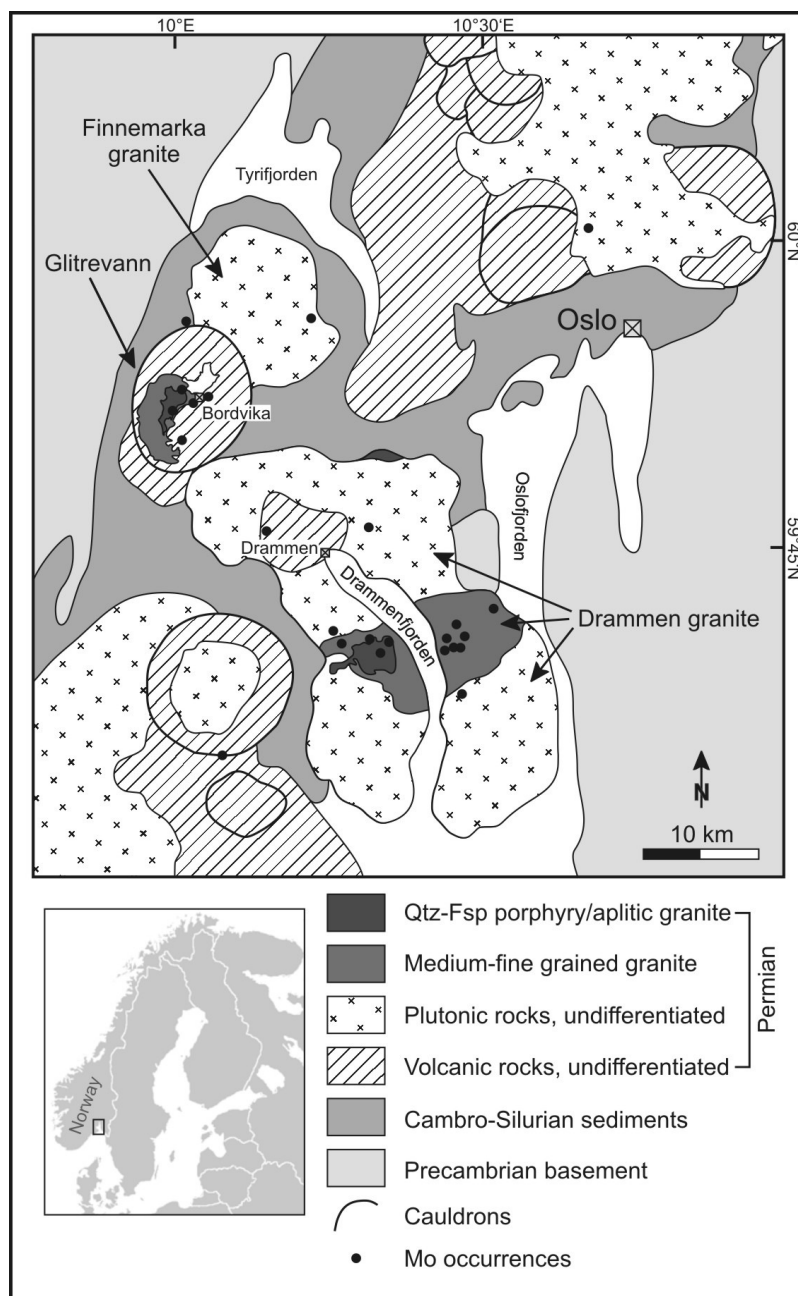


**Figure 6.3.2**

Sketch map of the Glitrevann and Drammen granites in the central Oslo Rift, showing the lithologies discussed in this work (modified after Ihlen et al., 1982; Schönwandt and Petersen 1983; Schönwandt et al., 1986). The ‘Qtz-Fsp (quartz-feldspar) porphyry/aplitic granite’ phase within the Glitrevann granite corresponds to the extent of the aplitic granite (see text for details).

The geologic history of the Oslo region goes back to the Proterozoic, when the basement rocks formed and subsequently were metamorphosed in the Sveconorwegian orogeny (1200-900 Ma), (e.g. Berthelsen, 1980; Skjernaas and Pedersen, 1982). Faulting of these gneisses, metagabbros, metasediments, and migmatites started some 970 Ma ago and

continued intermittently until post-Permian times (Starmer 1972, 1985 a, b). Today's Oslo Rift formed in the period of 305-240 Ma (e.g. Sundvoll and Larsen, 1990). The Oslo graben, which is the main rift structure exposed on land, extends N-NE with a total length of 400 km. Within this graben, Paleozoic sedimentary and magmatic rocks are preserved, whereas the areas to the east and west consist of Precambrian metamorphic rocks. Erosion stripped away parts of the volcanic rocks, exposing underlying intrusive rocks and structures (Neumann et al., 1992). The earliest magmatic activity in the rift is represented by syenitic and mafic sills dated at 304-294 Ma (Sundvoll and Larsen, 1982; Sundvoll et al., 1992). During the main phase of rifting large volumes of "rhomb porphyry" lavas interlayered with basalts were erupted (Ramberg et al., 1977). Rifting terminated with the formation of central volcanoes along preexisting fractures and faults, and the magmatic style changed from basaltic extrusions to intrusion of composite batholiths of intermediate to granitic compositions at 275-240 Ma (Neumann et al., 1992).

The largest of these granitic bodies is the Drammen granite, a complex of polyphase intrusions of biotite-granites and porphyries dated at 270-278 Ma by Rb-Sr chronology (Sundvoll and Larsen, 1990). Ihlen et al. (1982) subdivided the granitic rocks of the intrusion into eight textural facies, which all grade into each other. Because molybdenite mineralization is confined to the 'medium- to fine-grained, partly porphyritic granite' and the 'quartz-feldspar porphyries with aplitic to microcrystalline groundmass' as defined by Ihlen et al. (1982), only these two lithologies will be discussed in further detail. The first facies (herein called 'medium- to fine-grained granite') comprises an area of 60-70 km<sup>2</sup> on both sides of the Drammen fjord in the central part of the complex (Figure 6.3.2). The average grain size of this rock is 1-3 mm, with some samples displaying a porphyritic texture. High contents of quartz and plagioclase, plus the appearance of muscovite and fresh or slightly chloritized biotite are typical features. The second facies (herein called 'quartz-feldspar porphyry') occurs at the western edge of the medium- to fine-grained granite (Figure 6.3.2). This facies contains 2-4 mm sized phenocrysts of quartz, alkali-feldspar, and plagioclase embedded in a reddish, microcrystalline groundmass (Ihlen et al., 1982).

Mineralization occurs as (i) quartz-fluorite-molybdenite-veins and disseminations of molybdenite ± wolframite within the surrounding granite, and (ii) as contact-metasomatic

deposits of Fe-Cu-Zn-Pb-Bi  $\pm$  Mo within surrounding metasedimentary and metavolcanic rocks (e.g. Bugge, 1963; Ihlen and Vokes, 1978 a; Ihlen et al., 1982).

The samples described in this study were collected from the medium- to fine-grained granite on the eastern shore of the Drammenfjord, a few hundred meters east of Grimsrudbukta ( $\sim 59^{\circ} 41' 06''$  N,  $10^{\circ} 25' 58''$  E). Sample *Dra 2* is a miarolitic cavity of  $\sim 10$  cm size that was hosted by a local segregation of aplite, whereas samples *Dra 6* and *Dra 20* are similar-sized miarolitic cavities that were hosted by medium-grained granite. All cavities contained euhedral crystals of smoky quartz, orthoclase, albite, and white mica.

### 6.3.3.3 *Glitrevann granite (Norway)*

The Glitrevann caldera is the northernmost one of a prominent N-S trending array of calderas west of the Drammen granite (Figure 6.3.2), featuring porphyry-style molybdenum mineralization in subvolcanic rocks (Geyti and Schönwandt, 1979). The Glitrevann caldera cuts the Finnemarka granite and is in turn cut by the Drammen granite. Thus, the age of the Drammen granite marks the upper limit for caldera formation (Schönwandt and Petersen, 1983). The Glitrevann complex consists of a central granitic stock surrounded by a syenitic ring complex and Permian lavas (Ofte Dahl 1953). An overview of the evolution of the structure is given by Schönwandt and Petersen (1983): It started with the eruption of rhyolitic dome complexes and ignimbrites associated with basaltic volcanism. Eruption of voluminous ash flows in the southern sector then caused collapse and formation of the semi-circular Glitrevann caldera. Within this central caldera, meso- and mega breccias, as well as rhyolitic ash flows are preserved. The northern part of the caldera was flooded simultaneously by rhomb porphyry flows, basaltic lava, and ash tuffs. The final events were the eruption of the Bordvika ignimbrite, intrusion of syenitic ring dikes, and the emplacement of a central, composite granite stock which caused uplift of the caldera.

The central granitic stock can be subdivided into three types: medium-grained granite, porphyritic granite, and aplitic granite (Jensen, 1985), with the latter hosting the majority of mineralization (Schönwandt and Petersen, 1983). Based on crosscutting relationships and trace element abundances it is clear that aplitic granite is the youngest phase (Jensen, 1985). The aplitic granite occupies ca. 20% of the outcrop area and is made up of a fine-grained

intergrowth of quartz and alkali feldspar containing few feldspar-, quartz-, and biotite phenocrysts. Due to its compositional similarity with the 'quartz-feldspar porphyry' these two lithologies are not distinguished in Figure 6.3.2.

Molybdenum-mineralization within the granitic stock is manifold (Schönwandt, 1986) and occurs: (i) as disseminations in pervasively sericite-altered host rocks, (ii) in the aplite granite in open fractures together with quartz and pyrite, (iii) in quartz-alkali feldspar pegmatites, and (iv) in miarolitic cavities together with pyrite, quartz, and alkali feldspar. In the central part of the caldera, where the Bordvika ignimbrite covers the aplitic zone in the form of a massive, impermeable cap rock, the mineralization forms a stockwork of quartz-molybdenite veins enveloped by sericitic alteration (Geyti and Schönwandt, 1979).

Samples were taken from two miarolitic cavities hosted by aplitic granite on the southern shore of Lake Sandungen (59° 51' 06" N, 10° 02' 29" E). The cavities measured 5-10 cm in diameter and were lined with quartz and orthoclase.

#### 6.3.4 Methods

Doubly-polished thick sections of 0.1-1.0 mm thickness were prepared from both whole rocks and euhedral quartz crystals from miarolitic cavities. The latter were preferentially cut parallel to the c-axis of the crystal. Basic investigation of the samples was performed by optical microscopy using reflected and transmitted light, and appropriate fluid-, melt-, and solid inclusions were selected based on petrographic time relationships, inclusion size, and state of preservation. Since one of the main goals of this study was to characterize the composition of magmatic bulk fluids we focused our search on early, intermediate-density fluid inclusions rather than on later vapor and brine inclusions. Selected fluid-, melt-, and solid inclusions were analyzed by the following methods:

##### *6.3.4.1 Microthermometry*

Microthermometry was performed on a Linkam THSMG 600 heating-cooling stage that was calibrated to an uncertainty of  $\pm 0.1^\circ\text{C}$  at  $-56.6^\circ\text{C}$  and  $0.0^\circ\text{C}$  and to  $\pm 1^\circ\text{C}$  at  $374^\circ\text{C}$ . Fluid salinity and homogenization temperature were determined for each inclusion unless this was not possible due to small size. Most fluid inclusions contained enough  $\text{CO}_2$  to form

clathrates, but not enough to saturate in CO<sub>2</sub> liquid, in which case the accurate determination of fluid salinities is difficult. For these fluid inclusions we used the software “ICE” (Bakker, 1997) to calculate salinities based on the melting points of ice and clathrate, the volume fraction of liquid, and Peng and Robinson’s (1976) equation of state for the system (H<sub>2</sub>O)-CO<sub>2</sub>-CH<sub>4</sub>-N<sub>2</sub>-C<sub>2</sub>H<sub>6</sub>. This approach resulted in NaCl<sub>equiv</sub> values that were almost 50% lower than those calculated from ice melting temperatures and suggests CO<sub>2</sub> concentrations ranging from 2.0-7.9 mol% CO<sub>2</sub>. In fluid inclusions that did not form clathrates upon freezing, NaCl<sub>equiv</sub> salinities were determined based on ice melting temperatures using the equations in Bodnar and Vityk (1994). Fluid isochores were constructed based on homogenization temperatures and recalculated NaCl<sub>equiv</sub> values using the formulas in Bodnar and Vityk (1994) and neglecting any influence of CO<sub>2</sub>, as the study of Schmidt and Bodnar (2000) showed that addition of 4 mol% CO<sub>2</sub> to an aqueous fluid with a density of ~0.7 g/cm<sup>3</sup> (Th<sub>tot</sub> (→L) ~350°C) and a salinity of 6 wt% NaCl results in only a small shift of the corresponding isochore.

#### *6.3.4.2 Raman spectroscopy*

Raman spectra were taken of solid inclusions as well as of the liquid and gaseous portions of fluid inclusions with a Horiba LabRAM HR 800 spectrometer connected to a Coherent Innova 90C argon ion laser situated at the Bayerisches Geoinstitut, using an exposure time of 20 seconds and 2 accumulations. The resulting spectra obtained from fluid inclusion were checked for the presence of H<sub>2</sub>O, H<sub>2</sub>S, SO<sub>2</sub>, HSO<sub>4</sub><sup>-</sup>, and CO<sub>2</sub> bands (Burke, 2001) without quantifying absolute abundances. Spectra of solid inclusions and mineral phases were compared with spectra currently available from databases such as the RRUFF Project (online reference 2) and the online service from the Geofluids Laboratory at the University of Siena (online reference 3).

#### *6.3.4.3 Laser ablation-inductively coupled-mass spectrometry*

LA-ICP-MS measurements were performed at the Bayerisches Geoinstitut with a 193 nm ArF Excimer laser (Geolas M system; Coherent; USA) attached to a quadrupole mass spectrometer (Elan DRC-e; Perkin Elmer; Canada). The sample chamber was flushed with

He gas at a rate of 0.4 l/min, to which 5 ml/min H<sub>2</sub> gas was added on the way to the ICP-MS (Guillong and Heinrich, 2007). Elements were measured on isotopes <sup>7</sup>Li, <sup>11</sup>B, <sup>23</sup>Na, <sup>25</sup>Mg, <sup>27</sup>Al, <sup>32</sup>S, <sup>35</sup>Cl, <sup>39</sup>K, <sup>42</sup>Ca, <sup>49</sup>Ti, <sup>55</sup>Mn, <sup>57</sup>Fe, <sup>65</sup>Cu, <sup>66</sup>Zn, <sup>75</sup>As, <sup>85</sup>Rb, <sup>88</sup>Sr, <sup>89</sup>Y, <sup>90</sup>Zr, <sup>93</sup>Nb, <sup>98</sup>Mo, <sup>107</sup>Ag, <sup>118</sup>Sn, <sup>133</sup>Cs, <sup>140</sup>Ce, <sup>181</sup>Ta, <sup>184</sup>W, <sup>208</sup>Pb, <sup>209</sup>Bi, <sup>232</sup>Th and <sup>238</sup>U, using dwell times of 10-50 ms per isotope. The ICP-MS system was tuned to a thorium oxide rate of ~0.05% and a rate of doubly charged calcium ions of ~0.1% according to measurements on NIST SRM 610 glass. External standardization for Cl and S was based on the afghanite standard described in Seo et al. (2011), and for all other elements based on NIST SRM 610 glass using the values given in Spandler et al. (2011). Element concentration ratios measured in fluid and melt inclusions were then turned into absolute values by using the concentration of either Na or Al as internal standard. For fluid inclusions we used Na from the microthermometrically (or via ICE program) determined NaCl<sub>equiv</sub> value and applied the empirical correction formula of Heinrich et al. (2003) to account for the effect of other major cations. For melt inclusions we used Al concentrations of compositionally similar whole rock analyses reported in the literature. Combined analytical uncertainties are estimated at 10-20% (Heinrich et al., 2003), except for elements close to the detection limit.

#### *6.3.4.4 Re-equilibration experiments*

One fluid inclusion trail of Drammen sample *Dra 6B* was first characterized by microthermometry, Raman spectroscopy, and LA-ICP-MS and then cut out of the quartz wafer. The resulting quartz column was loaded together with fluid and buffer minerals (muscovite, orthoclase, albite, and topaz to produce an acidic pH; plus chalcopyrite to buffer the Cu content) into a quartz capsule that itself was welded into a gold capsule (Lerchbaumer and Audétat, 2012a). A small piece of etched quartz from Brazil was added as well to trap the loaded fluid, which major-element composition was similar to that of the already existing fluid inclusions in the quartz column. The experiment was run at 650°C and 140 MPa for 22 days. After cooling, the capsule was opened and the pH of the quench fluid was measured with indicator paper. Subsequently, both the re-equilibrated Drammen sample and the small quartz piece containing newly formed fluid inclusions were polished and prepared for analysis. In the re-equilibrated Drammen sample only fluid inclusions

<60  $\mu\text{m}$  in size and <~50  $\mu\text{m}$  depth below the surface were analyzed. The results were then compared with the results obtained from fluid inclusions analyzed before re-equilibration. Similar re-equilibration experiments on both natural and synthetic fluid inclusions are described in Lerchbaumer and Audétat (2012b).

### 6.3.5 Results

An overview of the information obtained from melt and fluid inclusions, including fluid salinity, sulfur content, concentrations of Mo, Cu, and Cs, and estimated formation conditions is given in Table 6.3.1. The full data set is presented in Tables 6.3.2, 6.3.3, and 6.3.4.

#### 6.3.5.1 *Treasure Mountain Dome*

A total of 25 melt inclusions were analyzed from quartz phenocrysts in the leucocratic border phase (sample *TM 7*), from quartz grains in the granular facies (sample *TM 2*), and from quartz crystals in miarolitic cavities in the border phase (samples *TM 10*, *TM 12*) (Table 6.3.2). As internal standard for the calculation of absolute element values from LA-ICP-MS element ratios we took the average Al-concentration of three similarly evolved granites at Climax, Henderson, and Urad (~12.2 wt%  $\text{Al}_2\text{O}_3$ ; Bookstrom, 1981; Mutschler et al., 1981; White et al., 1981). With increasing degree of crystallization and fractionation, incompatible elements like Cs, Rb, W, and Mo get enriched in the residual melt, whereas compatible elements like Mg, Fe, Ti, Ca, and Sr get depleted. Plots of the concentrations of Ti, Mo, W, and Rb against Cs (which is the element that behaved most incompatibly) are shown in Figure 6.3.3. Titanium concentrations decrease regularly from melt inclusions analyzed in the leucocratic border phase, over those analyzed in the granular facies, to those analyzed in miarolitic quartz, whereas the concentrations of Rb, Mo, and W follow the opposite trend. In a closed system the observed increase from ~5 ppm to ~90 ppm Cs in the residual melt requires a degree of crystallization of at least 90%. Thus, the melt inclusions analyzed in miarolitic quartz represent the very last melt fractions in an almost completely crystallized granite. The fact that the melt inclusions analyzed in the leucocratic border phase are less fractionated than those analyzed in the granular facies is somewhat

unexpected because the higher SiO<sub>2</sub> content (Mutschler, 1976) and leucocratic appearance of the former rock suggests a higher degree of fractionation. However, the melt inclusions analyzed in the granular zone were hosted by relatively small quartz grains that may have crystallized after magma intrusion, for which reason they may be younger and thus more evolved than the ones analyzed in the phenocrysts in the leucocratic border phase. In either way, the analyses provide important insight into the behavior of ore metals and other trace elements during the crystallization of this granite. Molybdenum concentrations in the residual silicate melt increased from ~5 ppm at ~5 ppm Cs to ~35 ppm at ~90 ppm Cs, and W concentrations increased from ~2 ppm to 20 ppm within the same crystallization interval, implying that both Mo and W behaved strongly incompatibly. Interestingly, the quartz phenocrysts in the border phase contain inclusions of molybdenite that were trapped at approximately the same time as the analyzed melt inclusions (Audétat et al., 2011), whereas no molybdenite inclusions were found in the three thick sections prepared from the granular facies. Together with the incompatible behavior of Mo noted above, this suggests that the intruding magma originally was molybdenite-saturated, but then became molybdenite-undersaturated with increasing degree of crystallization.

A cross-section through a euhedral quartz crystal from miarolitic cavity *TM 12* is shown in Figure 6.3.4. The crystal contains melt inclusions and intermediate-density (0.6-0.7 g/cm<sup>3</sup>) fluid inclusions in its basal zone, vapor and brine inclusions (late-trapped brines approaching the composition of salt melts) in pseudosecondary trails in the next, comparatively clear growth zone, abundant solid inclusions of K-feldspar, muscovite, albite, fluorite, anhydrite, and pyrite in the overlying dark growth zone, and high-density aqueous inclusions ( $\pm$  very low-density vapor inclusions) and solid inclusions of epidote, rutile, and chlorite in later growth zones. The intermediate-density fluid inclusions in the base of the crystal have salinities of  $5 \pm 1.3$  wt% NaCl<sub>equiv</sub>. Homogenization temperatures were not determined for these inclusions because their number was very limited and we did not want to risk their decrepitation before they could be analyzed by LA-ICP-MS. Quartz crystals from miarolitic cavity *TM 10* do not contain melt inclusions, but apart from that record a very similar fluid evolution. The succession from intermediate-density fluid inclusions with salinities of 5-10 wt% NaCl<sub>equiv</sub> and relatively low homogenization tempera-

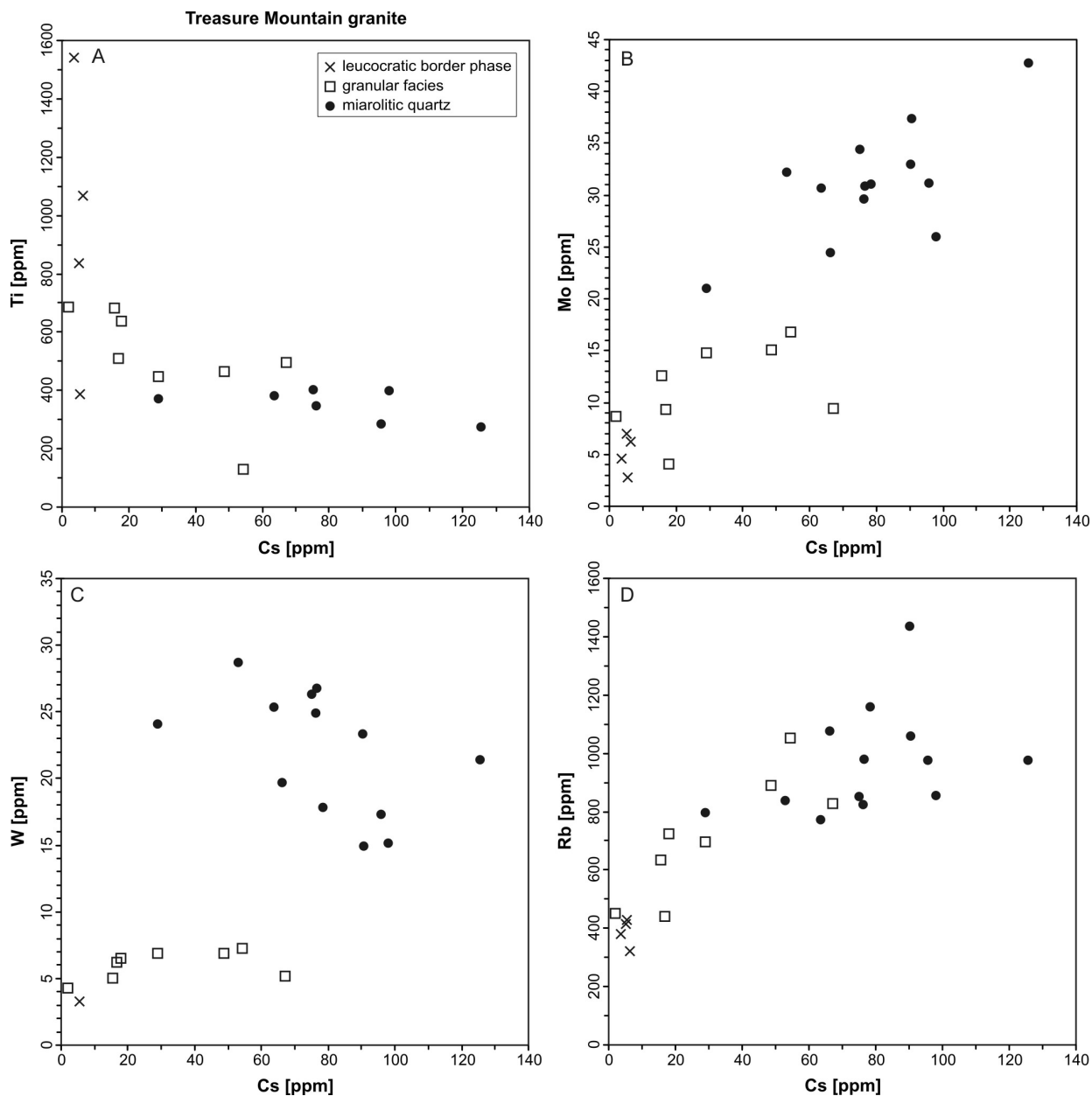


**Figure 6.3.3**

**A-D** Compositional evolution of silicate melts in the Treasure Mountain Dome, as recorded by quartz-hosted melt inclusions. Cesium is used in the abscissa because it is one of the most incompatible elements in granitic magmas and thus is an ideal indicator of melt fractionation.

tures (300-550°C), over immiscible vapor and brine inclusions with increasingly disparate salinities and higher homogenization temperatures (>550°C), to low-salinity aqueous fluid with densities  $\geq 0.8-0.9 \text{ g/cm}^3$  is typical for quartz crystals from miarolitic cavity-bearing granites in general and reflects the evolution of originally single-phase, magmatic fluids as they enter the two-phase field upon decompression and cooling, and finally get

diluted/superseded by invading meteoric water (e.g., Audétat and Pettke, 2003; Audétat et al., 2008). Since our main goal is to characterize the composition of the magmatic bulk fluid, only data from the intermediate-density fluid inclusions are presented here.

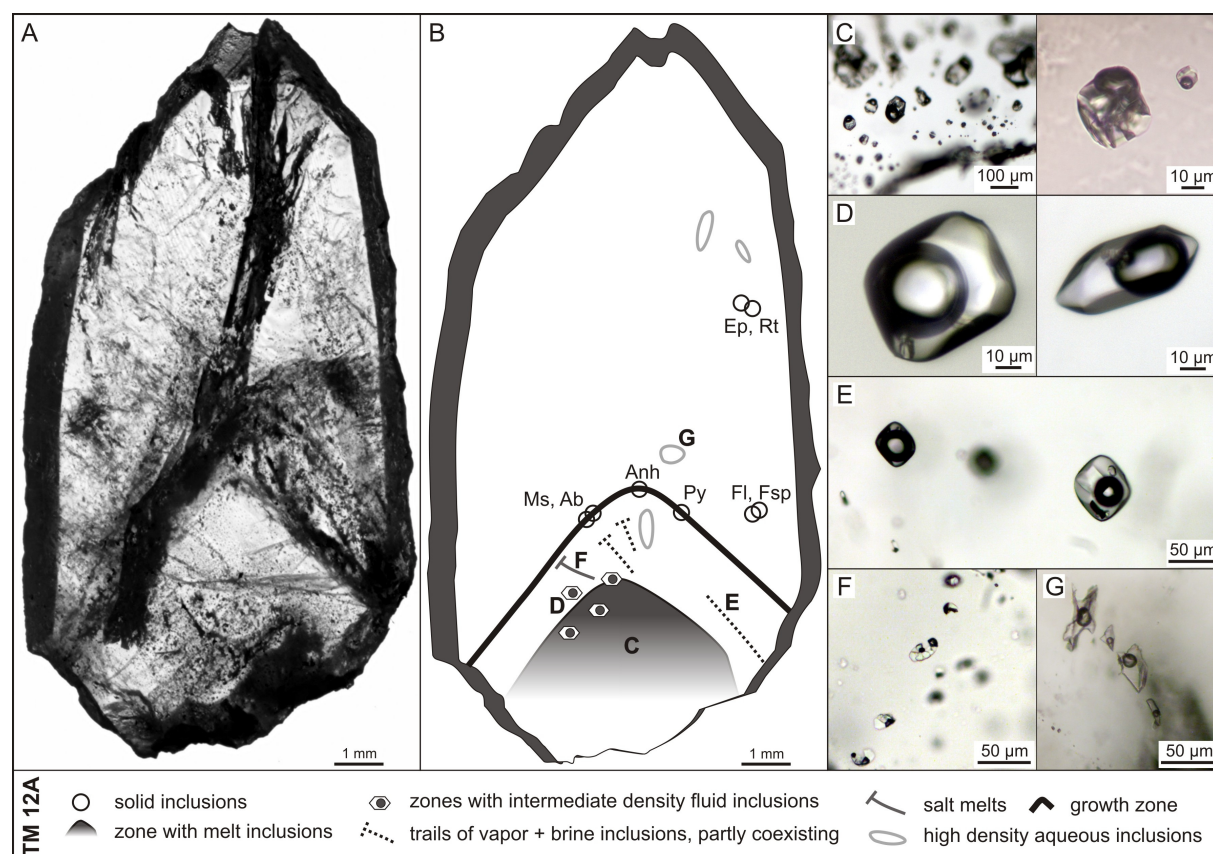


**Figure 6.3.4**

**A** Photograph of a thick-section through a quartz crystal from miarolitic cavity in the Treasure Mountain Dome (sample *TM12A*), cut parallel to the *c*-axis of the crystal. **B** Sketch of the same sample showing petrographic relationships between different types of melt, fluid, and solid inclusions (Ab = albite, Anh = anhydrite, Fl = fluorite, Fsp = feldspar (both plagioclase and K-feldspar), Ms = muscovite, Py = pyrite). **C-G** Photomicrographs of melt inclusions (C), early, intermediate-density fluid inclusions (D), coexisting vapor and brine inclusions (E), salt melts (F), and late, high-density aqueous inclusions (G), with their corresponding location indicated in the sketch map.

The compositions of 22 intermediate-density fluid inclusions analyzed in quartz from three different miarolitic cavities (*TM 5*, *TM 10*, *TM 12*) are listed in Table 6.3.3. Of those, only the inclusions from cavity *TM 12* coexist with melt inclusions and thus are certain to represent magmatic fluids, whereas the inclusions analyzed from the other two samples

may have formed at subsolidus conditions. Distinctly higher concentrations of Al in inclusions from the former sample (indicating a higher amount of dissolved silicates) support this interpretation.

Because we did not determine the homogenization temperatures of intermediate-density fluid inclusions in sample *TM 12* we are unable to reconstruct entrapment conditions based on the intersection of fluid isochores with the granite solidus (e.g., Audétat and Pettke, 2003). However, an upper pressure limit of ~100 MPa (at 700°C) is indicated by the occurrence of andalusite in metamorphosed shales at the contact of the leucocratic border phase to the overlying sediments, whereas a value of 100 MPa was estimated for contact-metamorphosed limestone at the base of the Treasure Mountain (Everett and Hoisch, 2008). Molybdenum concentrations are low (2-5 ppm) in the intermediate-density fluid inclusions analyzed from samples *TM 5* and *TM 10*, but high (50-150 ppm) in the ones from sample *TM 12*, suggesting that most Mo precipitated from the magmatic-hydrothermal fluid at near-magmatic conditions. In contrast, the concentrations of most other elements remained constant within a factor of ~2-3. A notable exception is Cu, which varies by a factor of 6 to 60 in all three samples. CO<sub>2</sub> and S concentrations vary from 2.5 to 7.9 mol% and <0.13 to 1.3 wt%, respectively, with 80% of the latter values ranging between 0.3 and 0.7 wt%. Raman spectra reveal that S occurs mostly as SO<sub>4</sub><sup>2-</sup> in the liquid portion of the fluid inclusions at ambient conditions.

Fluid/melt partition coefficients calculated from the averages of five melt inclusions and six coexisting fluid inclusions in sample *TM 12* are presented in Figure 6.3.5. Generally, the partition coefficients agree well with those determined on coexisting fluid and melt inclusions from other granites. The highest values are observed for Pb, Zn, and potentially Cu (notice the large uncertainty associated with the latter element), while Ce and Al display the least preference for the fluid phase. At the estimated entrapment pressure of ~100 MPa the solubility of H<sub>2</sub>O in the silicate melt is ~4 wt% (e.g. Holtz et al., 2001), which requires a fluid/melt partition coefficient >25 to result in depletion of the corresponding element in the residual silicate melt during open-system, fluid-saturated magma crystallization (assuming 100% incompatibility of this element with respect to the crystallizing solids). The fluid/melt partition coefficient of Mo ( $2.4 \pm 1.8$ ) is significantly below this threshold value,

implying that the Mo concentration in the residual melt should have increased with increasing degree of crystallization (unless significant amounts of Mo were incorporated into the crystallizing minerals). This prediction is in agreement with the compositional evolution shown in Figure 6.3.3B. In contrast, Cu concentrations in the melt inclusions show only a slight (if any) increase with increasing degree of fractionation (2-11 ppm in *TM 7*, 1-15 ppm in *TM 2*, and 3-30 ppm in *TM 10* and *TM 12*), which is compatible with its high fluid/melt partition coefficient ( $D_{\text{Mo}}^{\text{fluid/melt}} = 37.4 \pm 60.3$ ).

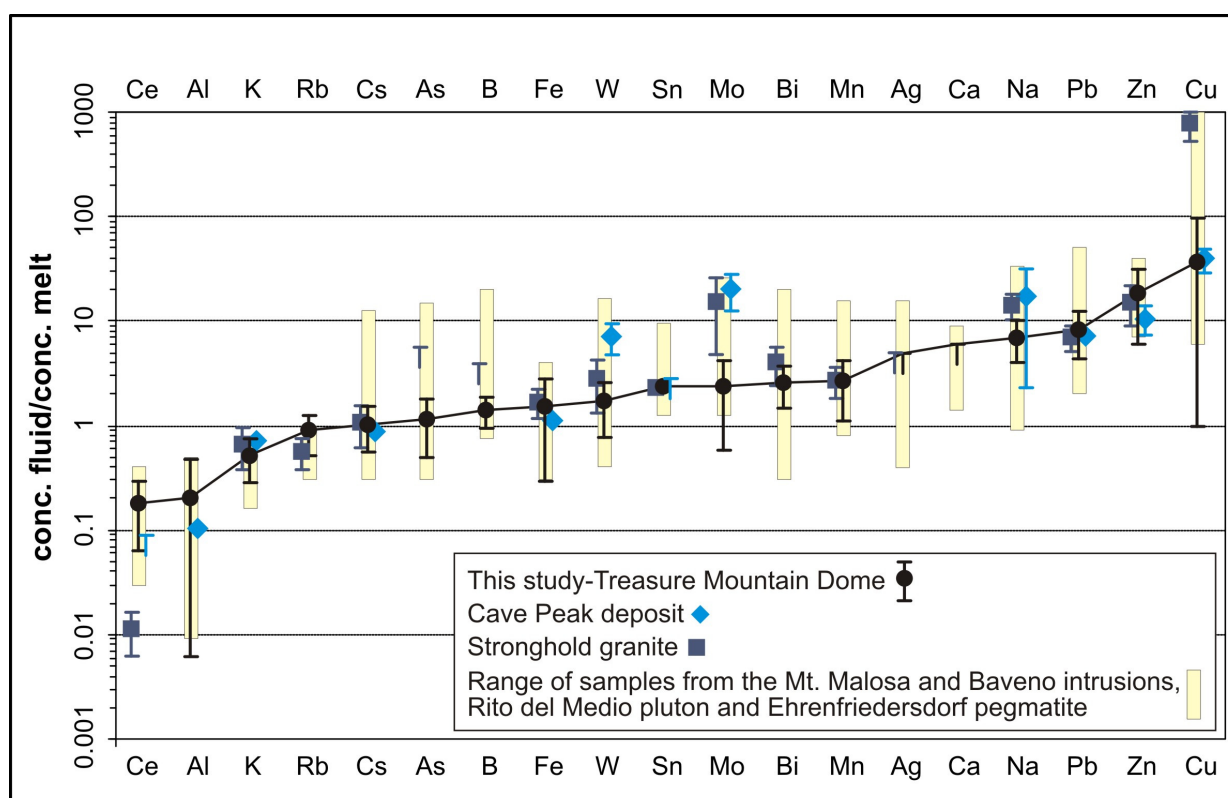


**Figure 6.3.5**

Fluid/melt partition coefficient determined on coexisting fluid and melt inclusions in the Treasure Mountain Dome compared to similar data obtained from the Mo-deposit at Cave Peak (Texas; Audétat, 2010), the Stronghold granite (Arizona; Audétat et al., 2008), and four other granites (Zajacz et al., 2008): Mount Malosa (Malawi), Baveno (Italy), Rito del Medio (New Mexico) and Ehrenfriedersdorf (Germany). In cases where element concentrations in the fluid or in the melt were below the detection limit, corresponding maximum partition coefficients are indicated by truncated error bars. Error bars express  $1\sigma$  standard deviations.

### 6.3.5.2 Drammen granite

A total of 20 melt inclusions were analyzed from the Drammen granite. Six of them were analyzed in two euhedral quartz crystals from miarolitic cavity Nr. 6 (samples *Dra 6A* and *Dra 6B*) and the remaining 14 inclusions along a 2 cm long transect through the border of another cavity (sample *Dra 2*). This transect extends from fine-grained aplite over a pegmatitic contact zone into a euhedral quartz crystal. As internal standard for LA-ICP-MS analyses we used the average  $\text{Al}_2\text{O}_3$  content of two whole-rock analyses of quartz-feldspar porphyry reported in Ihlen et al. (1982). A comparison of our melt inclusion data with whole-rock analyses reported from various textural facies of the Drammen granite is shown in Figure 6.3.6. The melt inclusion data nicely continue the trends displayed by the whole-rock data, suggesting that they are part of the same magma evolution. Although Cs clearly was less compatible than Rb also in this granite (Table 6.3.2; Cs increases by two orders of magnitude as Rb doubles), we plotted everything against Rb to be able to include the whole-rock data from the literature. Molybdenum and W concentrations generally increase with increasing degree of melt fractionation (from <10 ppm Mo and <5 ppm W at <500 ppm Rb, to ~30 ppm Mo and ~30 ppm W at ~1200 ppm Rb), except for a few extremely evolved melt inclusions analyzed in miarolitic quartz, which are strongly depleted in Mo. The three anomalously high Mo concentrations in the whole-rock data of 'medium- to fine-grained granite' and 'quartz-feldspar porphyry' (Figure 6.3.6D) probably reflect minor hydrothermal mineralization. Along the transect through the border of miarolitic cavity *Dra 2*, Rb, Cs, and W concentrations continuously increase from melt inclusions analyzed in the aplite to those analyzed in euhedral quartz crystals, whereas Mo concentrations first increase and then dramatically decrease in the most evolved melts analyzed. The latter reflects either efficient Mo-extraction by fluids, or incorporation of Mo in crystallizing solids. The presence of molybdenite inclusions in the euhedral quartz crystals points to the second explanation and suggests that at the very last stages of magma solidification perturbations in P, T,  $f_{\text{S}_2}$ , and/or  $f_{\text{O}_2}$  led to wholesale molybdenite precipitation.

The fluid evolution recorded in the miarolitic cavities of the Drammen granite is principally the same as the one in the Treasure Mountain Dome, starting with intermediate-density (0.6-0.7 g/cm<sup>3</sup>), partly CO<sub>2</sub>-bearing fluid inclusions with salinities of 4.4-6.3 wt% NaCl<sub>equiv</sub>

(corresponding to the TypeA-II inclusions described in Olsen and Griffin, 1984), then passing through a stage in which the fluid was two-phase, and finally reaching a state where aqueous, high-density fluid inclusions were trapped. However, in the samples of the Drammen Granite the proportion of intermediate-density fluid inclusions to subsequent vapor and brine inclusions is much larger, and the immiscibility gap recorded by vapor and brine inclusions is much smaller. Brines with salinities greater than ~35 wt% NaCl<sub>equiv</sub> are conspicuously absent in our samples. This suggests that the Drammen granite solidified at significantly higher pressure than the Treasure Mountain Dome, which is in accord with conditions of ~680°C / 140 MPa reconstructed from the intersection of intermediate-density fluid inclusion isochores (~5.7 wt% NaCl<sub>equiv</sub>, Th<sub>tot</sub> ~425°C) with the granite solidus, and with pressure estimates of 130-150 MPa reported by Olsen and Griffin (1984) and Larsen et al. (2009). CO<sub>2</sub> concentrations in these intermediate-density fluid inclusions were mostly too low to result in clathrate formation upon cooling (implying that CO<sub>2</sub> concentrations were below 1.6 mol%; Hedenquist and Henley, 1985), but in some inclusions of sample *Dra 6* clathrates were observed, which melting temperatures indicate CO<sub>2</sub> concentrations up to 2.4 mol%. Sulfur concentrations measured by LA-ICP-MS range from 0.2 to 0.5 wt% (Table 6.3.1).

Solid inclusions identified within quartz crystals from miarolitic cavities include topaz, muscovite, albite, K-feldspar, and molybdenite on early growth zones, and tourmaline, epidote, chlorite, hematite, and galena on later growth zones.

Molybdenum concentrations in intermediate-density fluid inclusions range from 3 to 270 ppm, with the majority of values measured in Al-rich (i.e., high-temperature) inclusions clustering around 30-40 ppm Mo (Table 6.3.3). Copper concentrations show a large scatter, ranging from 8 ppm to 3500 ppm without any apparent relationship to other elements. Although roughly contemporaneous, none of the analyzed fluid and melt inclusions were unambiguously coexisting, for which reason we did not calculate fluid/melt partition coefficients. However, average Mo concentrations in melt and fluid inclusions of sample *Dra 6* (20 ppm vs. 30-40 ppm, respectively) imply a  $D_{\text{Mo}}^{\text{fluid/melt}}$  value of about 2, which is similar to the value of  $2.4 \pm 1.8$  determined in the Treasure Mountain Dome. This  $D_{\text{Mo}}^{\text{fluid/melt}}$  value is far below the threshold value that would be required for a net depletion

of Mo in the residual silicate melt during fluid-saturated crystallization of the Drammen granite (~20; corresponding to a water solubility of ~5.0 wt% at 150 MPa / 700°C).

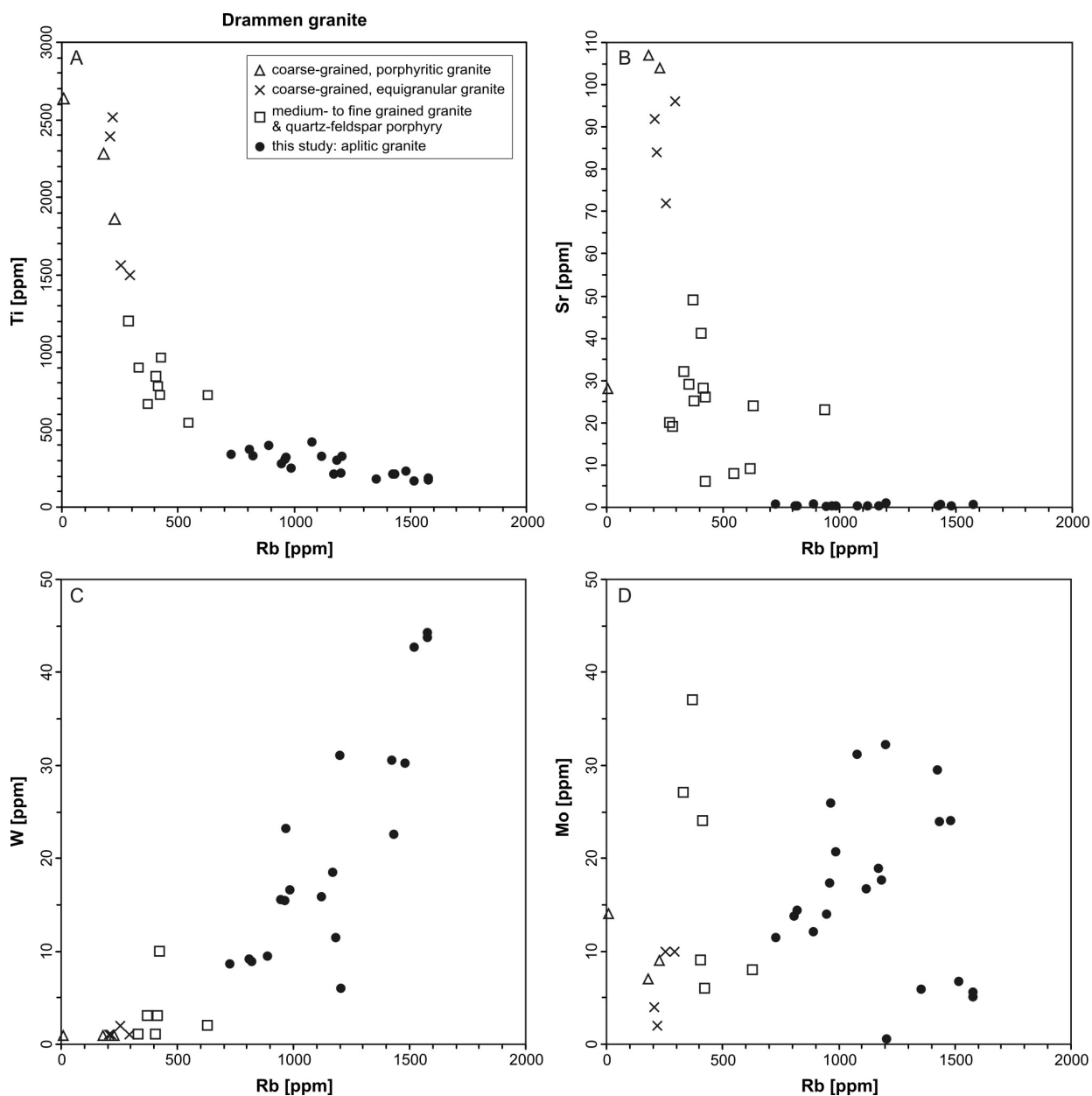


**Figure 6.3.6**

Compositional evolution of melt inclusions (black squares) and whole rocks (open symbols and crosses) of the Drammen granite. Whole rock data are from Ihlen et al. (1982) and Tronnes and Brandon (1992). In this case we use Rb as an indicator of melt fractionation because there are no Cs data available for the whole rocks. Titanium and Sr decrease with increasing degree of melt fractionation, whereas W and Mo generally increase, except for some extremely evolved melts trapped in miarolitic quartz that were strongly depleted in Mo.

Table 6.3.1 Overview of measured samples from the Treasure Mountain Dome, the Drammen and Glitrevann granites

Sample	type of inclusion	n	Salinity [wt% NaCl <sub>equiv</sub> ]	Th <sub>hot</sub> [°C]	to #	CO <sub>2</sub> * [mol%]	Temperature [°C]	Pressure [MPa]	S [wt%]	Cs [ppm]	Mo [ppm]	Cu [ppm]	Mo/Cu
TM 5A	fluid	5	6.2 ± 2.1	500	V	2.5 - 5.2	n.k.	n.k.	<0.35 - 0.52	87 - 160	1 - 3	12 - 100	0.026 ± 0.023
TM 5B	fluid	6	4.4 ± 1.9	n.a.	V	3.2 - 5.7	n.k.	n.k.	<0.13 - 1.28	45 - 160	1 - 2	2 - 120	0.028 ± 0.029
TM 10A	fluid	5	6.3 ± 1.6	430 - 530	V	2.6 - 7.9	n.k.	n.k.	0.49 - 0.61	26 - 73	5 - 7	< 20 - 120	0.069 ± 0.048
TM 12A	fluid	6	5.0 ± 1.3	-	-	3.3 - 6.0	n.k.	≤ 100 <sup>§</sup>	n.a.	60 - 170	47 - 160	33 - 1900	0.13 ± 0.18
TM 7 border phase	melt	4	-	-	-	-	-	-	-	4 - 6	3 - 7	< 2 - 11	0.68 ± 0.35
TM 2 granular facies	melt	8	-	-	-	-	-	-	-	2 - 67	4 - 17	1 - 15	1.59 ± 1.48
TM 10A+12A miar. Qtz	melt	13	-	-	-	-	-	-	-	29 - 130	21 - 43	3 - 30	2.11 ± 1.90
Dra 2 <sup>¶</sup>	melt	14	-	-	-	-	-	-	-	10 - 1100	6 - 32	< 1	> 16.27
Dra 2B	fluid	6	9.5 ± 0.5	-	-	< 1.6 <sup>†</sup>	n.k.	n.k.	0.52	520 - 970	4 - 65	8 - 3500	0.022 ± 0.044
Dra 6A	fluid	3	5.8	425	L	2.2 - 2.4	650 - 700	130 - 150	<0.67	58 - 280	26 - 48	410 - 1500	0.044 ± 0.040
Dra 6A	melt	3	-	-	-	-	-	-	-	92 - 100	14 - 18	< 2	> 8.00
Dra 6B	fluid	5	5.7 ± 0.2	420	L	2.3	650 - 700	130 - 150	0.20 - 0.30	180 - 250	20 - 46	530 - 2600	0.019 ± 0.012
Dra 6B	melt	3	-	-	-	-	-	-	-	93 - 190	21 - 26	< 3	> 7.67
Dra 20	fluid	2	11.0 ± 1.5	~ 550	M	< 1.6 <sup>†</sup>	n.k.	n.k.	< 1.09	240 - 360	150 - 270	58 - 90	2.79 ± 1.47
Git 2B	fluid	4	6.7 ± 0.7	~ 520	V	2.7 - 3.3	n.k.	n.k.	0.66	22 - 76	< 3 - 5	17 - 180	0.085 ± 0.113
Git 3A	fluid	6	8.1 ± 2.6	-	-	2.0 - 3.5	n.k.	n.k.	< 0.19 - 0.53	35 - 130	< 1 - 8	5 - 17	0.40 ± 0.43
Git granite	melt	4	-	-	-	-	-	-	-	20 - 65	11 - 13	< 4	> 2.95

<sup>¶</sup>Homogenization to liquid (L) or vapor (V) or by fading of the mensicus (M); <sup>\*</sup>calculated from clathrate melting point using the software ICE (Bakker, 1997); <sup>†</sup>minimum concentration of CO<sub>2</sub> necessary to form clathrates (in the simple H<sub>2</sub>O-CO<sub>2</sub> system; Hedenquist and Henley, 1985); <sup>‡</sup>based on the presence of solid inclusions of andalusite; <sup>§</sup>section through aplitic granite, pegmatitic zone and miarolitic quartz n.a. = not analyzed; n.k. = not known because fluid inclusions are not clearly cogenetic with melt inclusions; miar. Qtz = miarolitic quartz.

**Table 6.3.2** LA-ICP-MS data of melt inclusions with reference samples

sample	Na <sup>#</sup> [wt%]	Mg [wt%]	Al* [wt%]	K [wt%]	Ca [wt%]	Ti [wt%]	Mn [wt%]	Fe [wt%]	Cu [ppm]	Zn [ppm]	As [ppm]	Li [ppm]	B [ppm]	Rb [ppm]
<i>Climax</i> <sup>a</sup>	2.15	0.36	6.30	4.15	0.50	0.01	0.02	0.89	-	-	-	-	-	-
<i>Henderson</i> <sup>a</sup>	2.30	0.45	6.51	5.31	0.64	0.01	0.05	0.61	-	-	-	-	-	-
<i>Urad</i> <sup>b</sup>	2.37	0.07	6.51	4.23	0.54	0.11	0.03	1.10	-	-	-	-	-	-
<b>Treasure mountain granite, leucocratic border zone</b>														
TM 7B, MI 3	0.35	0.02	6.44	2.78	0.28	0.15	0.06	0.40	5	110	n.a.	n.a.	n.a.	380
TM 7A, MI 1	0.22	0.01	6.44	2.74	0.24	0.08	0.06	0.34	11	53	n.a.	n.a.	n.a.	420
TM 7C, MI 4	0.21	0.02	6.44	2.74	0.33	0.04	0.07	0.47	(2)	55	n.a.	n.a.	n.a.	430
TM 7E, MI 5	0.21	0.02	6.44	2.77	0.30	0.11	0.06	0.41	7	44	n.a.	n.a.	n.a.	320
<b>Treasure mountain, granular zone</b>														
TM 2, MI 2	0.21	0.02	6.44	3.04	(0.81)	0.07	0.05	0.42	12	30	2	47		450
TM 2, MI 7	0.22	0.01	6.44	2.76	(2.03)	0.07	0.07	0.37	(7)	23	2	59	21	630
TM 2, MI 8	3.56	0.01	6.44	2.35	(0.51)	0.05	0.06	0.31	1	32	3	(1)	23	440
TM 2, MI 1	0.25	0.01	6.44	2.83	(2.03)	0.06	0.09	0.30	2	28	4	53	24	720
TM 2, MI 5	0.26	0.01	6.44	2.68	(0.65)	0.04	0.08	0.36	(2)	38	5	37	26	700
TM 2, MI 4	0.25	0.01	6.44	2.79	(6.51)	0.05	0.09	0.26	(19)	31	5	(17)	24	890
TM 2, MI 3	0.19	0.00	6.44	2.64	(2.56)	0.01	0.07	0.11	6	20	8	25	67	1100
TM 2, MI 9	0.21	0.01	6.44	2.66	(3.64)	0.05	0.09	0.24	15	24	3	23	31	830
<b>Treasure mountain, miarolitic quartz</b>														
TM 10A1, MI 5	0.09	0.01	6.44	1.92	(3.66)	0.04	0.15	0.34	4	83	1	62	16	790
TM 10A2, MI 2	0.21	n.a.	6.44	2.83	(4.25)	n.a.	0.09	0.35	(6)	30	7	n.a.	44	840
TM 10A1, MI 2	0.16	0.01	6.44	2.18	(1.61)	0.04	0.10	0.36	(4)	36	7	80	44	770
TM 10A1, MI 7	0.27	0.01	6.44	2.44	(11.91)	(0.01)	0.09	0.25	(36)	42	(20)	(41)	(77)	1100
TM 10A1, MI e1	0.24	0.01	6.44	2.32	0.17	0.04	0.09	0.33	(5)	31	8	56	47	850
TM 10A1, MI 1	0.19	0.01	6.44	2.06	(2.83)	0.03	0.09	0.32	22	31	8	66	52	820
TM 10A2, MI 1	0.27	n.a.	6.44	2.69	(2.19)	n.a.	0.08	0.30	(4)	30	6	n.a.	39	980
TM 10A1, MI 3	0.25	n.a.	6.44	3.00	(5.15)	n.a.	0.08	0.29	(9)	30	8	n.a.	41	1400
TM 12A1, MI 1	0.21	n.a.	6.44	2.99	n.a.	n.a.	0.10	0.20	(17)	18	10	n.a.	55	1200
TM 12A1, MI 2	0.21	n.a.	6.44	3.10	n.a.	n.a.	0.10	0.13	30	(51)	10	n.a.	51	1100
TM 12A1, MI 3	0.17	0.01	6.44	2.42	(1.31)	0.03	0.12	0.28	3	48	8	33	47	980
TM 12A1, MI 4	0.15	0.01	6.44	2.18	(1.69)	0.04	0.11	0.29	(5)	30	6	26	42	860
TM 12A1, MI 5	0.16	0.01	6.44	2.33	(1.16)	0.03	0.11	0.27	(3)	33	10	36	54	980
<i>Drammen</i> 14 <sup>c</sup>	2.93	-	6.69	3.50	0.21	0.09	0.09	0.50	-	-	-	14	-	430
<i>Drammen</i> 60 <sup>c</sup>	2.66	0.04	6.54	3.64	0.26	0.11	0.11	0.63	-	-	-	2	-	330
Dra 6A, MI 1	0.17	0.01	6.62	2.25	(0.67)	0.03	0.08	0.36	(2)	29	25	130	120	950
Dra 6B, MI e1	0.20	0.01	6.62	3.20	0.05	0.03	0.07	0.31	(3)	25	46	530	190	970
Dra 6B, MI 4	0.15	0.01	6.62	2.87	(2.73)	0.03	0.10	0.37	(8)	26	30	660	130	990
Dra 6A, MI 2	0.20	0.01	6.62	2.65	(1.44)	0.03	0.09	0.44	(4)	36	29	360	140	1100
Dra 6A, MI 4	0.18	(0.02)	6.62	2.73	(16.23)	0.03	0.09	0.30	(39)	46	22	230	120	1200
Dra 6B, MI 3	0.17	0.00	6.62	3.22	(2.63)	0.02	0.02	0.09	(8)	8	42	500	200	1400
<b>section through Drammen granite, pegmatitic zone and miarolitic quartz</b>														
Dra 2 MI 1 granite	0.21	0.02	6.62	3.16	(1.07)	0.03	0.07	0.48	(2)	26	6	140	16	730
Dra 2 MI 2 granite	0.21	0.02	6.62	2.96	(3.44)	0.04	0.07	0.47	(10)	30	(5)	130	(22)	810
Dra 2 MI 3 granite	0.20	0.01	6.62	2.66	(0.95)	0.04	0.08	0.34	(3)	28	7	110	39	890
Dra 2 MI 4 granite	0.28	0.01	6.62	2.97	(1.32)	0.03	0.08	0.48	(4)	41	20	160	110	820
Dra 2 MI 5 granite	0.29	0.01	6.62	3.08	(1.07)	0.04	0.09	0.42	(3)	34	34	190	170	1100
Dra 2 MI 6 granite	0.19	0.01	6.62	2.79	(1.24)	0.02	0.08	0.14	(4)	22	60	66	320	1200
Dra 2 MI 1, pegm. z.	0.28	0.01	6.62	2.84	(1.83)	0.03	0.08	0.35	(5)	30	23	140	140	960
Dra 2 MI 2, pegm. z.	0.26	0.01	6.62	2.81	(0.79)	0.02	0.09	0.28	(2)	28	35	120	160	1200
Dra 2B, MI 2, Qtz	0.08	0.01	6.62	2.37	(1.45)	0.02	0.07	0.18	(4)	19	55	390	180	1400
Dra 2B, MI 3, Qtz	0.13	0.01	6.62	2.67	(1.90)	0.02	0.07	0.18	(5)	19	47	400	250	1500
Dra 2B, MI 1, Qtz	0.19	0.01	6.62	2.44	(4.11)	0.02	0.07	0.12	(10)	11	60	200	220	1600
Dra 2 MI 1, Qtz	0.16	0.01	6.62	2.37	(3.13)	0.02	0.07	0.14	(10)	13	62	170	210	1400
Dra 2 MI 2, Qtz	0.16	0.01	6.62	2.55	(4.05)	0.02	0.07	0.16	(12)	15	65	300	270	1500
Dra 2 MI 3, Qtz	0.13	0.01	6.62	2.57	(0.60)	0.02	0.08	0.16	0	13	72	370	260	1600
<i>Glitrevann</i> 3 <sup>d</sup>	3.34	-	6.51	3.89	0.21	0.15	0.05	0.86	-	-	-	-	-	200
<i>Glitrevann</i> 5 <sup>d</sup>	3.26	-	6.40	3.76	0.26	0.10	0.02	0.79	-	-	-	-	-	240
Git 2, MI 2	3.62	0.03	6.46	2.85	(5.76)	0.07	0.06	0.58	(19)	97	42	33	160	260
Git 2, MI 3	0.17	0.02	6.46	2.83	(2.42)	0.08	0.05	0.49	(5)	35	10	12	52	420
Git 3, MI 3	0.25	0.02	6.46	2.74	(1.59)	0.07	0.05	0.48	(4)	33	16	10	68	550
Git 3, MI 9	0.22	0.01	6.46	2.78	(4.95)	0.05	0.05	0.42	(14)	36	39	21	220	550

<sup>#</sup> Na-values can be regarded too low due to post-entrapment loss of Na by diffusion (Frischat, 1970) \* Al-values used for internal standardization are average concentrations from samples from analyses cited here: <sup>a</sup> Mutschler et al., 1981; <sup>b</sup> Bookstrom, 1981; <sup>c</sup> Ihlen et al., 1982; <sup>d</sup> Jensen, 1985. n.a. = not analyzed; values in parentheses resemble detection limits;

Table 6.3.2 Cont.

Sr	Y	Zr	Nb	Mo	Ag	Sn	Cs	Ba	Ce	Ta	W	Pb	Bi	Th	U
[ppm]															
-	-	-	-	-	-	-	-	-	-	-	-	-	-	-	-
-	-	-	-	-	-	-	-	-	-	-	-	-	-	-	-
-	-	-	-	-	-	-	-	-	-	-	-	-	-	-	-
12	21	110	37	5	n.a.	(10)	4	4	56	3	(2)	24	n.a.	28	7
1	32	78	55	7	n.a.	(11)	5	4	62	3	(3)	22	n.a.	35	10
0	120	120	110	3	n.a.	11	5	(1)	46	5	3	23	n.a.	47	19
1	26	96	41	6	n.a.	(6)	6	3	66	3	(2)	25	n.a.	34	9
5	23	100	64	9	1	4	2	13	72	5	4	27	1	63	21
2	30	90	110	13	(1)	(20)	16	2	50	6	5	14	(0)	31	17
4	24	83	100	9	(0)	5	17	15	54	8	6	26	1	41	24
2	40	65	120	4	(1)	6	18	6	27	8	6	17	1	38	33
2	28	75	120	15	(0)	8	29	2	49	8	7	30	1	35	28
3	34	85	140	15	(3)	(54)	49	(6)	46	11	7	24	1	33	35
3	3	72	20	17	(1)	(24)	54	(4)	10	2	7	20	2	17	11
3	26	71	86	9	(1)	(38)	67	23	56	7	5	15	(1)	40	21
0	44	81	140	21	(2)	(35)	29	(7)	62	17	24	23	1	28	29
n.a.	n.a.	n.a.	n.a.	32	(2)	(38)	53		69		29	28	1		
0	43	52	140	31	(1)	8	64	(3)	44	23	25	26	1	19	26
(3)	39	62	120	24	(6)	(99)	66	(20)	64	12	20	25	(2)	24	24
(0)	38	77	140	34	(1)	9	75	(3)	65	21	26	28	1	28	30
(1)	37	69	130	30	(1)	(22)	76	(5)	78	20	25	26	1	32	25
n.a.	n.a.	n.a.	n.a.	31	(1)	(24)	77	n.a.	65	n.a.	27	24	1	n.a.	n.a.
n.a.	n.a.	n.a.	n.a.	33	(2)	(53)	90	n.a.	60	n.a.	23	29	1	n.a.	n.a.
n.a.	n.a.	n.a.	n.a.	31	n.a.	(80)	79	n.a.	85	n.a.	18	24	1	n.a.	n.a.
n.a.	n.a.	n.a.	n.a.	37	n.a.	(67)	91	n.a.	20	n.a.	15	22	(1)	n.a.	n.a.
0	27	78	110	31	(1)	9	96	(3)	85	18	17	28	2	26	21
(0)	32	86	120	26	(1)	9	98	(3)	70	12	15	20	1	35	28
(0)	25	81	120	43	(0)	10	130	(2)	66	15	21	26	2	25	25
26	18	139	-	6	-	4	-	-	-	-	10	-	-	-	-
32	12	110	-	27	-	4	-	-	-	-	1	-	-	-	-
0	22	92	180	14	(0)	9	92	(1)	51	26	16	20	2	21	15
0	3	80	190	26	(1)	12	190	(2)	31	35	23	21	4	19	15
0	20	71	190	21	(2)	14	93	(5)	53	33	17	15	1	21	12
0	38	250	200	17	(1)	13	100	(2)	46	17	16	22	2	43	33
(5)	35	220	180	18	(6)	(150)	100	(19)	48	17	11	21	(7)	34	25
1	9	70	190	24	(1)	9	160	(3)	44	35	23	20	5	22	16
1	14	95	110	11	0	8	10	2	62	7	9	24	1	43	29
0	0	140	120	14	(1)	(21)	10	(4)	21	9	9	8	(1)	58	33
1	17	100	100	12	(0)	8	31	1	61	8	9	13	2	43	26
0	18	120	110	14	(1)	9	53	(2)	57	5	9	8	1	46	30
0	38	140	250	31	(1)	14	73	(2)	66	26	27	20	3	45	13
1	10	28	92	32	(1)	10	240	1	33	74	31	12	8	12	14
(0)	30	140	170	17	(1)	12	97	(2)	62	16	15	25	2	44	36
0	27	120	200	19	(0)	14	130	(1)	67	18	18	21	3	35	29
0	14	57	96	29	(1)	13	270	(2)	68	18	30	11	12	20	12
0	11	66	93	24	(1)	12	340	(3)	53	21	30	9	10	17	13
1	5	42	59	5	(2)	(35)	430	(7)	29	16	44	11	4	18	20
(1)	6	24	52	6	(2)	(26)	840	(4)	29	17	38	11	4	10	16
(1)	7	28	58	7	(2)	(33)	1000	(4)	34	20	43	12	4	13	19
(0)	6	34	60	6	0	8	1100	(1)	32	22	44	14	4	13	22
23	-	-	150	-	-	-	-	44	-	-	-	-	-	-	-
12	-	-	130	-	-	-	-	11	-	-	-	-	-	-	-
2	16	110	70	11	(3)	(44)	39	4	65	4	6	22	1	35	10
1	12	120	76	11	(1)	(19)	20	(3)	48	5	4	10	0	34	13
1	54	120	190	13	(1)	8	45	2	54	14	7	13	1	53	31
1	29	15	130	12	(2)	(41)	65	2	27	20	10	13	1	10	13

**Table 6.3.3** LA-ICP-MS data of fluid inclusions

sample	T <sub>m</sub> <sup>ICE</sup> [°C]	T <sub>m</sub> <sup>CLATH</sup> [°C]	NaCl <sub>equiv.</sub> * [wt%]	CO <sub>2</sub> <sup>#</sup> [mol%]	Na [wt%]	Al [wt%]	S [wt%]	Cl [wt%]	K [wt%]	Ca [wt%]
<i>Treasure mountain, miarolitic quartz</i>										
TM 5A, FI 1b	10	4.1	8.2	5.2	2.52	0.14	0.38	5.58	0.87	(13.1)
TM 5A, FI 4	5	-0.9	5.0	2.5	1.51	0.08	(0.60)	4.57	0.41	(12.9)
TM 5A, FI 3	6.5	5.6	5.1	5.1	1.63	0.25	0.42	3.06	0.53	(14.7)
TM 5A, FI 7	5.3	6.0	4.0	5.0	1.23	(0.03)	0.52	3.99	0.55	(19.0)
TM 5A, FI 1a	10.3	3.4	8.8	4.9	2.49	0.06	(0.35)	4.85	0.81	(8.8)
TM 5B, FI 4	3.4	2.9	2.6	3.2	0.65	0.002	(0.13)	1.73	0.32	(2.4)
TM 5B, FI 5	4.1	n.v.	3.2	4.1	1.01	0.05	1.28	2.22	0.28	(8.2)
TM 5B, FI 7	5.8	4.7	4.9	4.4	1.42	0.08	0.71	2.85	0.53	(9.7)
TM 5B, FI 2b	3.7	3.5	2.9	3.4	0.89	0.06	0.27	2.46	0.35	(18.1)
TM 5B, FI 1	6.4	n.v.	5.3	4.7	1.57	(0.02)	0.39	4.77	0.69	(5.0)
TM 5B, FI 2a	10.0	n.v.	7.6	5.7	1.86	0.08	0.23	5.60	1.03	(21.3)
TM 10A1, trail B, FI 1	9.9	5.5	7.1	6.1	1.93	0.35	(2.62)	9.28	0.89	(37.6)
TM 10A1, trail B, FI 2	10.3	4.5	8.1	5.5	2.20	(0.10)	(5.79)	7.99	1.11	(97.4)
TM 10A1, FI 2	7.8	8.0	4.9	7.9	1.38	(0.03)	0.49	4.99	0.54	(14.8)
TM 10A1, FI e1	n.v.	n.v.	7.1	5.2	1.98	0.16	0.61	4.03	1.48	(8.5)
TM 10A2, FI 1	5.5	5.2	4.5	4.6	1.07	0.19	(1.67)	(6.06)	0.64	(35.3)
TM 12A1, FI 3	4.4	3.0	3.8	3.4	0.43	5.30	n.a.	n.a.	2.27	n.a.
TM 12A1, FI 6	n.v.	n.v.	4.1	4.3	1.13	0.16	n.a.	n.a.	0.71	n.a.
TM 12A1, FI 1	8.1	0.5	8.3	3.3	1.98	0.53	n.a.	n.a.	1.52	n.a.
TM 12A1, FI 5	n.v.	5.0	4.1	4.3	0.75	2.05	n.a.	n.a.	1.61	n.a.
TM 12A1, FI 2b	4.5	n.v.	3.6	4.2	1.15	0.84	n.a.	n.a.	(0.74)	n.a.
TM 12A2, FI 7	9.6	n.v.	7.0	6.0	1.76	1.22	n.a.	n.a.	1.51	n.a.
<i>Drammen granite, miarolitic quartz</i>										
Dra 2B, trail F, FI 1	6.4	-	9.7	< 1.6 <sup>†</sup>	3.2	(0.02)	(0.89)	8.25	0.81	(15.7)
Dra 2B, FI 1	5.7	-	8.8	< 1.6 <sup>†</sup>	2.7	0.51	(1.47)	5.57	1.08	(21.7)
Dra 2B, FI 2	6.3	-	9.6	< 1.6 <sup>†</sup>	3.2	0.24	(1.49)	8.19	1.00	(25.6)
Dra 2B, trail F, FI 4	6.4	-	9.7	< 1.6 <sup>†</sup>	3.2	(0.03)	(2.50)	7.04	0.88	(34.9)
Dra 2B, FI 4	5.8	-	9.0	< 1.6 <sup>†</sup>	3.0	(0.05)	(2.59)	6.99	(0.93)	(42.3)
Dra 2B, trail F, FI 3	6.6	-	10.0	< 1.6 <sup>†</sup>	2.9	(0.03)	0.51	6.95	1.27	(36.1)
Dra 6A, trail B, FI 5	5.5	-1.8	5.8	2.4	1.4	0.23	(1.30)	7.13	1.52	(24.2)
Dra 6A, trail B, FI 3	5.5	-1.8	5.8	2.4	1.8	0.20	(0.67)	6.69	0.80	(13.8)
Dra 6A, trail B, FI 2	5.5	-1.8	5.8	2.4	1.7	0.41	(2.03)	7.57	0.98	(41.0)
Dra 6B, FI 4	6.5	-	9.9	< 1.6 <sup>†</sup>	2.5	0.50	(2.78)	13.82	2.33	(17.9)
Dra 6B, trail A, FI 5	5.4	-1.8	5.7	2.4	1.5	0.19	(0.44)	3.91	1.22	(7.3)
Dra 6B, trail A, FI 3	5.4	-1.8	5.6	2.4	1.9	0.49	(2.17)	7.65	(0.59)	(28.1)
Dra 6B, trail A, FI 6	5.4	-1.8	5.7	2.4	1.7	0.11	0.30	3.83	1.12	(3.0)
Dra 6B, trail A, FI 7	5.4	-1.8	5.7	2.4	1.6	0.15	0.20	5.36	1.38	(7.1)
Dra 20, FI 1	6.6	-	10.0	< 1.6 <sup>†</sup>	3.2	(0.02)	(1.09)	11.09	0.72	(15.9)
Dra 20, FI 2	8.3	-	12.1	< 1.6 <sup>†</sup>	2.6	0.54	(1.70)	10.37	1.57	(28.6)
<i>Glitrevann granite, miarolitic quartz</i>										
Glit 2B, FI 5	6.3	1.5	6.2	3.3	1.8	(0.07)	(1.87)	5.15	0.77	(39.2)
Glit 2B, FI 4	6.2	n.v.	6.1	3.2	2.0	(0.03)	(0.68)	6.18	0.61	(16.3)
Glit 2B, FI 2	7.1	-1.0	7.5	2.7	2.0	0.07	0.66	4.73	0.87	(16.8)
Glit 2B, FI 8	n.v.	n.v.	6.9	3.1	2.2	0.07	(1.45)	6.98	0.71	(33.1)
Glit 3A, FI 2	n.v.	n.v.	7.0	3.1	2.4	0.08	0.53	3.76	0.70	(4.9)
Glit 3A, FI 4	5.5	2.4	5.1	3.5	1.2	0.03	(0.57)	3.09	0.51	(10.7)
Glit 3A, FI 14	n.v.	n.v.	7.0	3.1	2.3	0.03	(0.23)	4.19	0.70	(4.7)
Glit 3A, FI 6	7.6	0.9	7.6	3.3	2.6	0.11	(0.25)	5.25	0.81	(6.0)
Glit 3A, FI 1	9.6	0.5	9.6	3.5	3.2	0.03	(0.58)	6.45	1.03	(14.3)
Glit 3A, FI 3	10.5	-6.4	12.5	2.1	4.4	0.02	(0.19)	8.11	1.20	(4.6)

\* Salinity was corrected for clathrates using the software "ICE" (Bakker, 1997); for inclusions, where no ice-melting and/or clathrate-melting could be observed, the average of the sample was used to calculate absolute LA-ICP-MS values. In the Drammen-samples clathrate-melting occurred before ice melting, thus no correction was necessary; <sup>#</sup>calculated from clathrate melting point using the software ICE (Bakker, 1997); <sup>†</sup>minimum concentration of CO<sub>2</sub> necessary to form clathrates (in the simple H<sub>2</sub>O-CO<sub>2</sub> system; Hedenquist and Henley, 1985); n.v. = not visible; n.a. = not analyzed; values in parentheses represent

Table 6.3.3 Cont.

Mn	Fe	B	Cu	Zn	As	Rb	Mo	Ag	Sn	Cs	Ce	W	Pb	Bi
[wt%]	[wt%]	[ppm]												
0.18	0.66	160	12	610	27	160	(4)	(4)	(110)	87	7	(13)	160	7
0.41	0.28	79	(29)	530	12	120	1	(6)	(110)	90	4	(14)	130	(4)
0.27	0.13	260	100	600	36	130	(2)	(9)	(130)	100	(5)	9	150	7
0.19	0.14	250	100	560	40	130	3	(9)	(150)	130	(4)	28	190	7
0.78	0.72	46	(18)	1100	9	240	2	(3)	(73)	160	7	8	330	9
0.29	0.26	(17)	2	380	3	87	1	(1)	(21)	45	2	6	110	3
0.13	0.15	160	76	310	22	60	1	(5)	(67)	46	2	(8)	92	4
0.30	0.36	240	120	550	26	110	1	(5)	(74)	49	1	(10)	170	5
0.19	0.08	130	43	210	15	53	2	(9)	(150)	59	5	5	78	(5)
0.26	0.28	(150)	(34)	740	13	150	(6)	(7)	(72)	87	3	(11)	210	7
0.88	0.76	(120)	6	1200	11	270	(3)	(10)	(170)	160	6	(13)	320	10
0.47	0.74	260	(87)	900	26	220	7	(17)	(340)	26	(8)	23	160	8
0.49	0.77	300	(160)	960	46	200	5	(48)	(940)	26	(15)	22	190	10
0.35	0.38	190	116	680	23	260	5	(7)	(120)	51	(2)	13	130	6
0.34	0.20	220	(20)	750	18	730	5	(5)	(82)	64	(2)	6	120	5
0.33	0.66	210	41	810	39	320	6	(17)	(340)	73	(6)	18	210	6
0.16	0.30	(36)	110	340	(24)	1100	47	n.a.	(100)	60	12	(10)	100	3
0.19	0.26	(66)	310	630	(21)	580	88	n.a.	(98)	76	6	14	210	3
0.63	0.90	45	33	1000	6	950	160	n.a.	22	80	14	45	310	5
0.17	0.35	(260)	(88)	350	(60)	1100	47	n.a.	(290)	86	20	(30)	77	(5)
0.22	0.33	(220)	1900	620	(62)	870	55	n.a.	(360)	170	(8)	(23)	200	(7)
0.39	0.56	(160)	(62)	1100	(48)	1500	150	n.a.	(240)	160	8	29	350	4
0.48	0.45	990	34	780	200	800	4	(13)	(160)	520	(4)	50	160	24
0.36	0.33	780	8	550	140	450	31	(12)	(230)	700	1	57	100	15
0.25	0.11	1300	17	820	350	340	(6)	(15)	(260)	750	(6)	(25)	230	2
0.42	0.36	1100	2300	760	200	430	3	7	(430)	900	(9)	33	150	18
0.16	0.76	870	33	1400	210	1000	65	(27)	(480)	950	4	72	280	24
0.65	0.66	1300	3500	1300	290	760	6	11	(360)	970	(9)	49	190	23
0.19	0.39	540	1500	570	76	930	28	(14)	(230)	58	(10)	43	120	10
0.18	0.26	480	410	420	77	540	26	(7)	(140)	130	(4)	48	120	9
0.09	0.28	630	390	20	220	910	48	(21)	(420)	280	(11)	130	96	12
0.41	0.77	700	2600	940	130	1600	46	(43)	(320)	250	(9)	79	240	20
0.24	0.45	450	1800	520	80	390	23	2	(80)	180	1	53	120	9
0.30	0.49	580	530	330	140	380	20	(30)	(290)	200	(8)	(29)	120	10
0.07	0.24	490	1600	530	88	430	26	1	17	210	1	10	120	8
0.07	0.18	430	910	740	98	580	26	1	9	220	1	42	130	9
0.38	0.60	1300	58	1100	260	160	150	(8)	(160)	240	(4)	61	130	21
0.68	1.29	1100	90	740	390	270	270	(12)	(250)	360	4	110	200	36
0.31	0.39	280	17	820	36	95	(8)	(21)	(320)	22	(10)	(28)	73	(8)
0.19	0.16	230	21	730	36	61	(3)	(12)	(150)	26	(3)	(17)	100	2
0.19	1.30	270	22	550	42	96	5	(5)	(130)	28	16	7	100	4
0.44	0.16	260	180	990	35	130	(11)	(18)	(300)	76	14	(36)	170	(7)
0.10	(0.04)	99	(10)	450	33	110	1	(3)	(49)	35	1	(4)	190	(1)
0.44	0.99	150	17	1300	71	46	8	(4)	(86)	36	(2)	(13)	200	(4)
0.13	0.27	290	5	1100	21	140	(1)	(2)	(37)	52	(1)	(5)	210	3
0.11	0.17	280	(14)	1300	48	89	4	1	(45)	77	(1)	(6)	230	(2)
0.45	0.08	340	(36)	1800	54	140	(4)	(7)	(110)	98	(4)	(14)	310	(3)
0.15	(0.03)	440	(9)	2400	79	150	(1)	2	(38)	130	(1)	(5)	410	(1)

### 6.3.5.3 *Glitrevann granite*

Due to the limited number of suitable samples found in this granite we can provide only preliminary data. Four melt inclusions were analyzed in quartz grains of the aplitic granite surrounding the two miarolitic cavities *Glt 2* and *Glt 3*. As internal standard for the quantification of the LA-ICP-MS measurements we used the average Al content of whole-rock analyses of this facies reported in Jensen (1985). The least evolved melt inclusion (*Glt 2*, MI2) is compositionally similar to the most evolved whole-rock composition reported by Jensen (1985), whereas the other three melt inclusions record slightly higher degrees of fractionation (Table 6.3.2). Molybdenum concentrations are reproducible at  $12 \pm 1$  ppm.

Euhedral quartz crystals from the miarolitic cavities contain a high proportion of coexisting vapor and brine inclusions, with late-stage brine inclusions reaching salinities of up to 80 wt% NaCl<sub>equiv</sub>. Intermediate-density fluid inclusions are rare and restricted to the base of the crystals, whereas aqueous, high-density fluid inclusions occur mostly in the upper portion of the crystals. Solid inclusions comprise muscovite, feldspar, gypsum, monazite, rutile, and molybdenite along early growth zones, and muscovite, feldspar, rutile, monazite, and tourmaline along later growth zones. No melt inclusions were found. Intermediate-density fluid inclusions have densities of 0.6-0.7 g/cm<sup>3</sup>, salinities of 6.7-8.1 wt% NaCl<sub>equiv</sub> and contain between 2.1 and 3.5 mol% CO<sub>2</sub> as revealed by melting temperatures of ice and clathrates. LA-ICP-MS analyses of 10 such fluid inclusions reveal S concentrations in the order of ~0.5 wt% and rather low Mo concentrations of ~5 ppm (Table 6.3.3). The fact that none of these inclusions contains more than 1100 ppm Al suggests that they probably do not represent magmatic fluids but were trapped at subsolidus conditions (most likely between 600 and 700°C). Therefore, they are comparable to the Mo-poor intermediate-density fluid inclusions measured in samples *TM 5* and *TM 10* of Treasure Mountain.

### 6.3.5.4 *Re-equilibration of fluid inclusions from the Drammen granite*

Recent experimental re-equilibration studies on both natural and synthetic fluid inclusions (e.g. Mavrogenes and Bodnar, 1994; Li et al., 2009; Zajacz et al., 2009; Lerchbaumer and Audétat, 2012b) revealed that the Cu (as well as Na, H, Ag) content of quartz-hosted fluid

inclusions can easily be modified by diffusion after fluid entrapment. This process seems to be particularly efficient when S-bearing, acidic fluid inclusions are re-equilibrated in a more neutral fluid (Lerchbaumer and Audétat, 2012b). In this case  $H^+$  diffuses out of the acidic fluid inclusions through the host quartz into the surrounding, less acidic fluid. To maintain charge balance, small, single-charged ions like  $Cu^+$ ,  $Na^+$ , and  $Ag^+$  diffuse from the outer fluid into the fluid inclusions. Whereas the diffusion of  $Na^+$  stops once its concentration within the fluid inclusion becomes significantly higher than in the outer fluid, incoming  $Cu^+$  combines with the S present within the fluid inclusion to precipitate as Cu-sulfide. Copper concentrations in fluid inclusions can increase by more than one order of magnitude in this manner (Lerchbaumer and Audétat, 2012b).

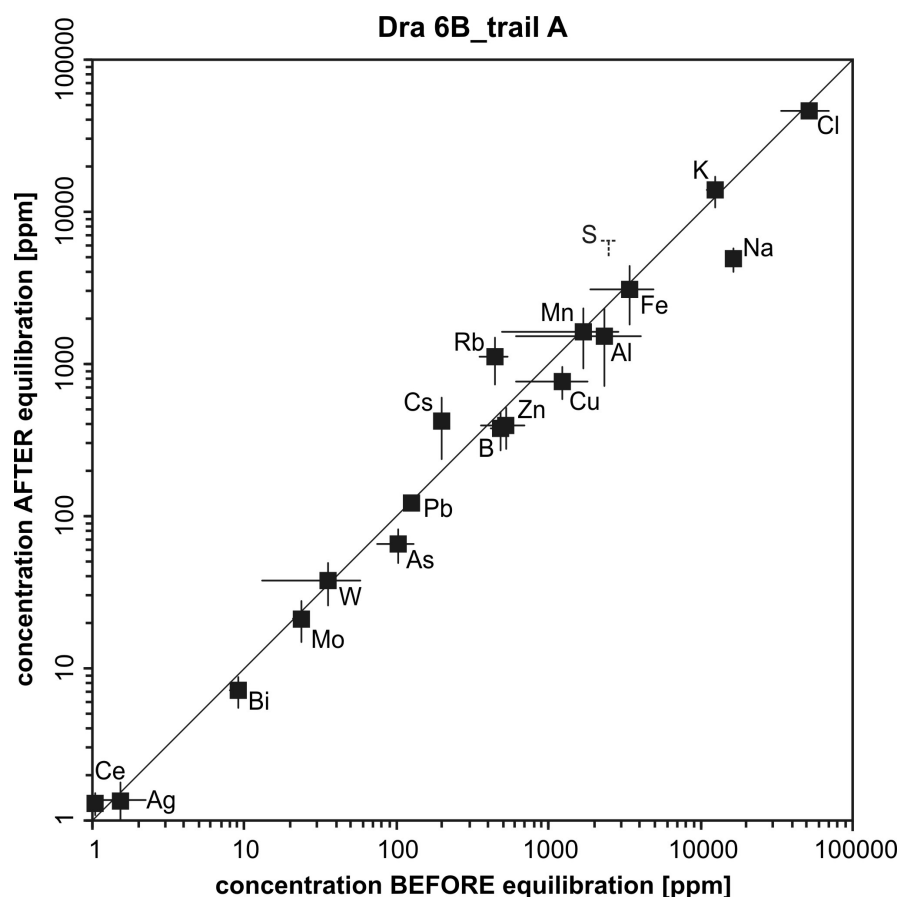


**Figure 6.3.7**

Element concentrations in fluid inclusions on trail A of sample *Dra 6B* from the Drammen granite, before and after re-equilibration at 650°C, 140 MPa. Error bars express 1 $\sigma$  standard deviations. Notice the significant changes in Na, Rb and Cs concentrations, whereas all other element concentrations stayed the same within analytical uncertainty.

**Table 6.3.4** LA-ICP-MS data of fluid inclusions before and after equilibration (sample Dra 6B, trail A)

<b>Dra 6B, trail A</b>			
	6.3 wt% NaCl, 3.2 wt% KCl, 0.6 wt% S, 0.4 mol/kg <sub>solution</sub> HCl, 620 ppm Rb, 340 ppm Cs		
<b>fluid composition</b>			
<b>mineral buffers</b>	Ccp, Mo, Ab, Ms, Or, Toz		
<b>P [MPa] / T [°C]</b>	650 / 140		
<b>t [days] / pH*</b>	22 / < 0.3		
	<b>BEFORE equilibration (n = 4)</b>	<b>AFTER equilibration (n = 5)</b>	<b>newly formed inclusions (n = 5)</b>
<b>Salinity [wt% NaCl<sub>equiv</sub>]</b>	5.7 ± 0.2	5.5 ± 0.1	12.8 ± 1.0
<b>Na [wt%]</b>	1.64 ± 0.17	0.49 ± 0.09	2.17 ± 0.14
<b>Al [wt%]</b>	0.23 ± 0.17	0.15 ± 0.08	0.36 ± 0.40
<b>S [wt%]</b>	0.25 ± 0.07	< 0.39	< 5.10
<b>Cl [wt%]</b>	5.19 ± 1.79	4.60 ± 0.44	< 25.0
<b>K [wt%]</b>	1.24 ± 0.13	1.39 ± 0.33	1.32
<b>Ca [wt%]</b>	< 2.97	< 5.90	n.a.
<b>Mn [wt%]</b>	0.17 ± 0.12	0.16 ± 0.07	0.006
<b>Fe [wt%]</b>	0.34 ± 0.15	0.31 ± 0.13	0.97 ± 0.18
<b>B [ppm]</b>	490 ± 69	380 ± 100	< 1300
<b>Cu [ppm]</b>	1200 ± 600	770 ± 190	5600 ± 410
<b>Zn [ppm]</b>	530 ± 170	400 ± 120	< 1900
<b>As [ppm]</b>	100 ± 30	70 ± 20	< 340
<b>Rb [ppm]</b>	450 ± 90	1100 ± 380	560 ± 40
<b>Mo [ppm]</b>	24 ± 3	21 ± 6	10
<b>Ag [ppm]</b>	2 ± 1	1 ± 0.4	< 46
<b>Sn [ppm]</b>	13 ± 6	< 290	< 6000
<b>Cs [ppm]</b>	200 ± 18	420 ± 190	340
<b>Ce [ppm]</b>	1.03 ± 0.08	1.3 ± 0.21	< 18
<b>W [ppm]</b>	35 ± 22	38 ± 12	< 90
<b>Pb [ppm]</b>	120 ± 4	120	< 400
<b>Bi [ppm]</b>	9 ± 1	7 ± 2	< 38

\*quench pH measured after the run; *italic numbers* mark elements that were used as internal standard; Ab = albite, Ccp = chalcopyrite, Mo = molybdenite, Ms = muscovite, Or = orthoclase, Toz = topaz; n.a. = not analyzed. Element concentrations without standard deviation are based on only one measurement. Errors are within 1σ standard deviation.

In view of these results the question arises whether the Cu contents of the natural fluid inclusions discussed above are reliable. Two lines of evidence indicate that this may not be the case: (i) in all three occurrences, acidic and S-bearing fluids were trapped at magmatic conditions and were later replaced by less acidic fluids, and (ii) Cu concentrations measured

within well-defined fluid inclusion populations are far less reproducible than the concentrations of other elements. To test whether Cu has been gained we re-equilibrated a fluid inclusion trail of sample *Dra 6B* (trailA) in an acidic surrounding fluid at its estimated entrapment conditions of  $\sim 650^\circ\text{C}$  and  $\sim 140$  MPa for 22 days. The fluid contained 6.3 wt% NaCl, 3.2 wt% KCl, 0.6 wt% S, 620 ppm Rb, 340 ppm Cs, and 0.4 mol/kg<sub>solution</sub> HCl. Copper and Mo were added in excess amounts (i.e., more than what can be dissolved during the run) in the form of chalcopyrite and molybdenite, respectively, whereas albite, muscovite, orthoclase, and topaz were added to buffer the pH at a low value. The latter was confirmed by the low pH ( $\leq 0.3$ ) measured in the quench solution after the experiment. A similar re-equilibration experiment performed on coexisting vapor and brine inclusions in a natural quartz sample from the Erongo granite (Namibia) is described in Lerchbaumer and Audétat (2012). Details regarding the composition of fluid inclusions on trail A (*Dra 6B*) before and after re-equilibration are given in Table 6.3.4, together with the composition of fluid inclusions that trapped the outer fluid during re-equilibration. Comparison of element concentrations in fluid inclusions on trail A before and after equilibration (Figure 6.3.7) reveals that within analytical uncertainty, only the concentrations of Na, Rb, and Cs changed significantly. Sodium concentrations decreased by about a factor of three, whereas Rb and Cs concentrations increased by about a factor of two. Copper concentrations decreased from  $1200 \pm 600$  to  $770 \pm 190$  ppm and became much better reproducible, suggesting that some of the fluid inclusions may have experienced postentrapmental Cu gain. However, compared to the experiments described in Lerchbaumer and Audétat (2012) the degree of Cu diffusion in the present sample was small. This is probably a consequence of the fact that the fluid inclusions on trail A contained much less sulfur ( $\sim 0.3$  wt% S) than those re-equilibrated by Lerchbaumer and Audétat (2012; 1-2 wt% S). Since other fluid inclusions analyzed from Treasure Mountain, Drammen and Glitrevann have similar S-contents as those of *Dra 6B-trailA* (Table 6.3.1) we believe that the measured Cu concentrations are more or less representative (probably within a factor of two) of the original Cu concentrations in the trapped fluids. The same applies for Bingham, whereas for Questa, Cave Peak, Butte, and El Teniente predictions are difficult to make because no S concentration data are available.

In principle, also the Cu content of the melt inclusions could have been affected by post-entrapmental diffusion (Kamenetsky and Danyushevsky, 2005; Zajacz et al., 2009). However, the values are very low (mostly <10 ppm) and fairly reproducible, for which reason we consider them to be real.

### **6.3.6 Comparison with other intrusions**

#### *6.3.6.1 Molybdenum concentrations in silicate melts*

The Mo-mineralizing potential of granitic intrusions depends on many factors, including (e.g., Keith et al., 1993): (i) the metal content of the silicate melt from which the mineralizing fluids exsolved, (ii) the metal content of these fluids (which may not simply reflect the metal content of the melt if fluid–melt partition coefficients are highly variable), (iii) the degree of fluid (and/or melt) focusing, (iv) the size and shape of the magma chamber, (v) the abundance of volatiles in the magma, and (vi) the efficiency of Mo precipitation from the magmatic-hydrothermal fluids. The following is an attempt to compare the first four of these variables among economically Mo-mineralized intrusions, sub-economically Mo-mineralized intrusions, barren intrusions, and porphyry Cu-Mo mineralized intrusions. Due to the limited amount of available data the results have to be regarded preliminary.

Molybdenum concentrations in silicate melts from various mineralized and barren intrusions are shown in Figure 6.3.8. Because whole-rocks do not reliably record original metal contents of melts and magmas (e.g., Keith et al., 1993, White et al., 1981) we exclusively rely on melt inclusion data for this purpose. As an index of the degree of melt fractionation we use Cs, which is one of the most incompatible trace elements in magmas and can easily be analyzed by LA-ICP-MS because it is a heavy, monoisotopic element free of interferences. In most magmas, Cs behaves about twice as incompatibly as Rb (e.g., Table 6.3.2 and references in Table 6.3.6). Taylor (1964) estimated the Cs and Rb contents of average granite at 5 ppm and 150 ppm, respectively.

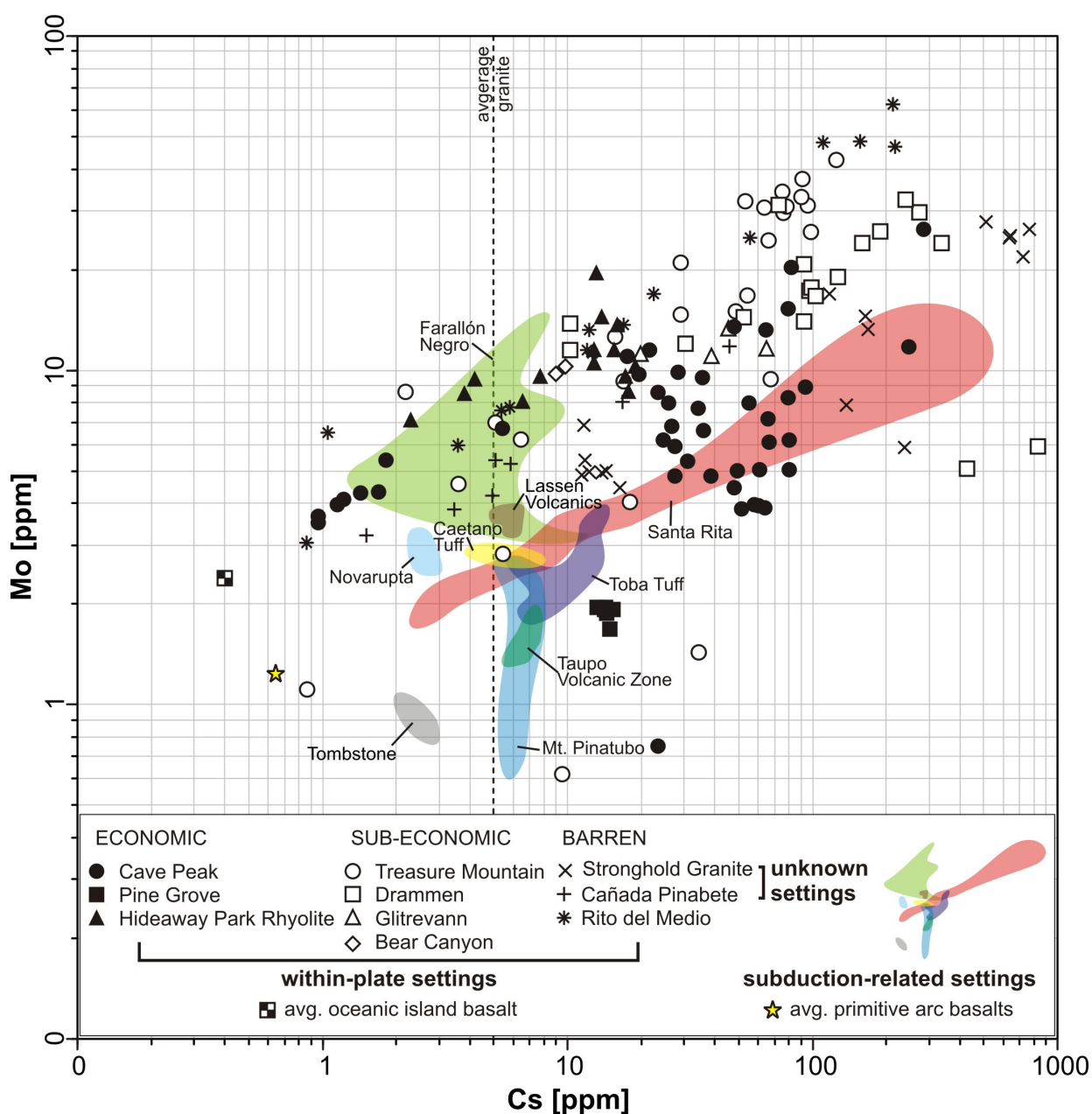
For further discussion the data is divided into subduction-related and within-plate magmas. Climax-type porphyry Mo deposits are associated with within-plate magmas, whereas porphyry Cu ( $\pm$  Mo, Au) deposits are associated with subduction-related magmas (e.g.,

Carten et al., 1993; Sillitoe, 2010; Richards, 2011). For a given Cs content, within-plate magmas (Treasure Mountain, Drammen, Glitrevann, Bear Canyon, Cave Peak, Pine Grove, Hideaway Park, Rito del Medio) generally contain more Mo than subduction-related magmas (Santa Rita, Alumbrera/Farallón Negro, Mt. Pinatubo, Taupo Volcanic Zone, Toba Tuff, Lassen Volcano, Tombstone, Novarupta, Caetano Tuff), (Figure 6.3.8). Exceptions are found in some melts analyzed from the subduction-related Farallón Negro Complex, which are similarly enriched as average within-plate magmas, some melts analyzed from Cave Peak, and those analyzed from Pine Grove, which have a distinct within-plate trace element signature (Audétat et al., 2011) but very low Mo/Cs ratios. The latter two samples, however, show evidence for magmatic molybdenite saturation (Audétat et al., 2011), which means that the Mo content of the bulk magma could have been much higher than the Mo concentrations recorded in the melt inclusions. The tectonic settings of the Stronghold granite and the Cañada Pinabete pluton are not clear. It is interesting to note that with the exception of the molybdenite-saturated melts mentioned above, the trends of the melts from within-plate settings project back to the average composition of oceanic island basalts (OIB), whereas the melts from subduction-related settings lie on or below a trend originating from the average composition of primitive arc basalts (Alumbrera/Farallón Negro being an exception).

Looking at the data from within-plate magmas only, there seems to be no systematic difference between economically Mo-mineralized granites (Cave Peak, Pine Grove, Hideaway Park rhyolite), sub-economically Mo-mineralized granites (Treasure Mountain, Drammen granite, Glitrevann granite, Bear Canyon pluton) and the barren Rito del Medio Pluton. Except for Pine Grove, all samples define trends that pass through ~10 ppm Mo at ~10 ppm Cs and have a slope of 0.5 or smaller in a corresponding log-log diagram (meaning that Mo is distinctly more compatible than Cs). This suggests that economic porphyry Mo deposits formed from melts that were not *fundamentally* different from melts occurring in other intrusions in within-plate settings. However, what appears to have varied are the size of the magma chamber and the efficiencies of residual melt extraction and fluid focusing (see below).

Melt inclusions analyzed from subduction-related intrusions have generally lower Mo

contents than similarly evolved melts analyzed from within-plate settings, except for the data from the Farallón Negro Complex. For example, at a Cs concentration of 10 ppm (~320 ppm Rb), Mo concentrations in subduction-related melts are about 2-5 ppm, whereas in within-plate melts they are about 7-16 ppm (Figure 6.3.8). In some subduction-related magmas (Alumbrera/Farallón Negro, Santa Rita) the slopes of the fractionation trends are similar to the ones observed in within-plate magmas, whereas in other subduction-related magmas (Toba Tuff, Taupo Volcanic Zone, Mt. Pinatubo) it is much steeper, suggesting that Mo behaved as incompatibly as Cs.



### ← Figure 6.3.8

Molybdenum versus Cs-concentrations of melt inclusions from Mo- and Cu mineralized granites and porphyries, sorted according to their economic relevance, and tectonic setting. Notice the generally lower Mo/Cs-ratios of subduction-related melts compared to melts from within-plate settings. Sources of data: Cave Peak: Audétat (2010); Pine Grove: Audétat et al. (2011); Hideaway Park rhyolite: pers. comm. with Celestine Mercer (2012); Treasure Mountain, Drammen, Glitrevann: this study; Bear Canyon: Audétat et al. (2011); Stronghold Granite: Audétat et al. (2008); Cañada Pinabete: Audétat et al. (2011); Rito del Medio: Audétat et al. (2008); Farallón Negro: Halter et al. (2004); Lassen Volcanics, Caetano Tuff, Novarupta, Toba Tuff, Taupo Volcanic Zone, Tombstone: Audétat et al. (2011); Santa Rita: Audétat et al. (2004, 2011); Mt. Pinatubo: Borisova et al. (2008); average oceanic island basalt: Sun and McDonough (1989); average primitive arc basalts: Bali et al. (2012, submitted); average granite: Taylor (1964).

#### 6.3.6.2 *Metal concentrations in magmatic fluids*

Molybdenum concentrations in fluid inclusions that are representative of (near-)magmatic, single-phase fluids are compiled in Figure 6.3.9. In the case of Santa Rita, where no such fluid inclusions have been identified, we used the composition of vapor inclusions trapped at ~720°C near the crest of the immiscibility field. Although the data are much more scattered than in Figure 6.3.8, the general trends appear to be the same. At any given Cs content, maximum Mo concentrations in porphyry Mo-related fluids (Cave Peak, Questa) are similar to those observed in fluids from sub-economically mineralized (Treasure Mountain, Drammen granite) and barren (Rito del Medio pluton) intrusions in within-plate settings, but are higher than porphyry Cu (Mo)-related fluids (El Teniente, Butte, Santa Rita), except for Bingham. However, most fluid inclusions analyzed from Mo-mineralized granites have higher Cs and Mo contents ( $\geq 40$  ppm Cs;  $\geq 20$  ppm Mo) than those analyzed from porphyry Cu(Mo) deposits ( $\leq 10$  ppm Cs;  $\leq 20$  ppm Mo; see also Table 6.3.5), which reflects the more evolved character of melts in the former occurrences. Exceptions are the fluids at Bingham (Landtwing et al., 2010) and the low-Cs fluid population identified at Questa (Klemm et al., 2007). A different trend is displayed by Cu: average fluids in Mo-mineralized granites contained 600-2100 ppm Cu, whereas average fluids in porphyry Cu (Mo)-mineralized intrusions contained 3500-6200 ppm Cu. Mo/Cu ratios in the fluids of

Mo-mineralized granites were thus significantly higher than in those associated with porphyry Cu (Mo) deposits (Table 6.3.5; Bingham again being an exception). A possible explanation for this phenomenon may be the higher fractionated nature of the source magma in Mo-mineralized granites, which tends to be more depleted in compatible elements like Cu. However, even in fluids from porphyry Mo deposits absolute concentrations of base metals (600-1200 ppm Cu, 300-1400 ppm Zn, 200-400 ppm Pb) were many times higher than the concentration of Mo, which raises the question where all these base metals went because ores are nearly free of base metals. A potential explanation is that Mo precipitation was highly selective, and that other metals including Cu precipitated at structurally higher levels. This interpretation is supported by the occurrence of both disseminated and vein-hosted Cu-, Pb-, and Zn mineralization above the porphyry Mo deposits at Redwell Basin and Mt. Emmons (Sharp, 1978; Thomas and Galey, 1982), a change from Mo-dominated deposits in more deeply exposed areas to Cu-Au-Pb-Ag-Zn deposits in less uplifted portions along the southern margin of the Questa Caldera (Clark and Read, 1972; Jones, 1990), and by the fact that both the Climax and Urad orebodies were already partly eroded, but it is at odds with the lack of base metal mineralization in the ~1.3 km and ~1.1 km sections preserved above the ore bodies at Henderson and Pine Grove, respectively. In their study on Questa, Klemm et al. (2008) proposed that the lack of base metal mineralization is due to a low concentration of reduced sulfur in the input fluid or in the mineralizing brine after boiling off a S-rich vapor phase. Similarly, Seo et al. (2012) concluded from a recent study on Bingham that selective precipitation of Mo vs. Cu + Fe was controlled by redox potential and fluid acidity. It needs to be noted that the pressure and temperature ranges of Mo precipitation recorded by fluid inclusions in the breccia bodies at Questa (Klemm et al., 2008; 420-360°C / ~20 MPa) and Cave Peak (Audétat, 2010; 450-550°C / ~50 MPa), and that of Mo precipitation in the stockwork at Bingham (Seo et al., 2012; 580°C / 71 MPa) are significantly lower than what has been observed in the samples examined in this study and what can be inferred from the distribution of Mo at other locations. Samples investigated in this study show a large decrease in the Mo content from the earliest, clearly magmatic fluids to slightly later, but still >600°C (based on the salinity of subsequent brines) intermediate-density fluids. Evidence for Mo precipitation at

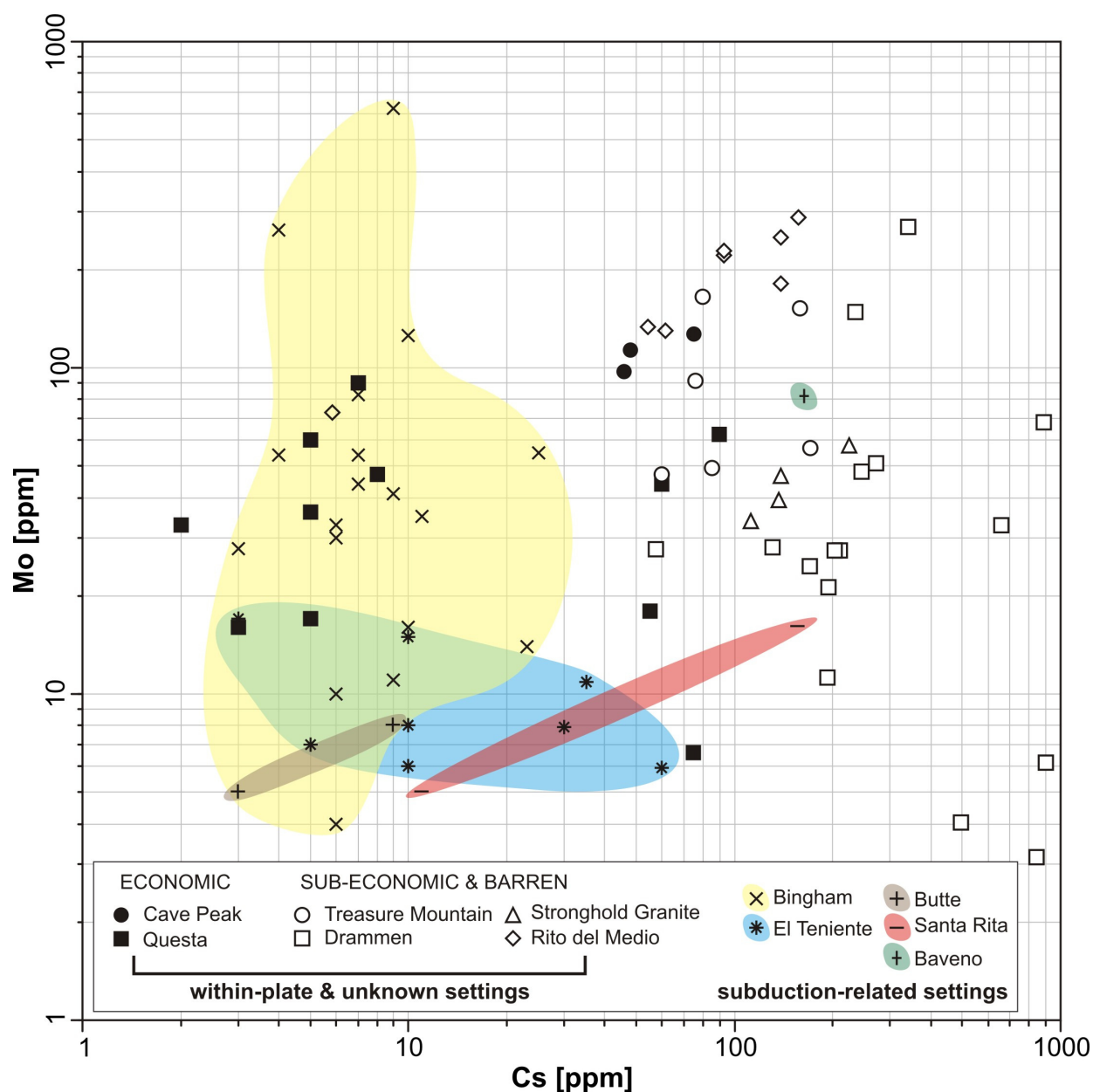


**Figure 6.3.9**

Molybdenum versus Cs-concentrations in fluid inclusions from Mo- and Cu mineralized granites and porphyries, sorted according to their economic relevance, and tectonic setting. Sources of data: Cave Peak: Audétat (2010); Questa: Klemm et al. (2008); Treasure Mountain, Drammen: this study; Stronghold Granite, Rito del Medio: Audétat et al. (2008), Zajacz et al. (2008); Bingham: Landtwing et al. (2010); El Teniente: Klemm et al. (2007); Butte: Rusk et al. (2008); Santa Rita: Audétat et al. (2004, 2011); Baveno: Zajacz et al. (2008).

near-magmatic temperatures in porphyry Mo deposits include: (i) the fact that ore shells typically straddle the parental intrusions, (ii) the presence of molybdenum-bearing vein dikes showing a continuum between magmatic and hydrothermal textures (White et al.,

1981), and (iii) the presence of primary molybdenite in unidirectional solidification textures (Carten et al., 1988; Sinclair, 2007). More work is needed to constrain the conditions of Mo precipitation and their relationship to the conditions of base metal precipitation.

Overall, the range of Mo concentrations measured in single-phase, pre-mineralization fluids from barren and productive intrusions is relatively small (~1.6 orders of magnitude; Figure 6.3.9), suggesting that the Mo-mineralization potential was to a larger extent controlled by other factors.

#### *6.3.6.3 Size, depth, and structure of magma chambers*

These parameters are difficult to quantify because porphyry Mo mineralization typically forms within and around small apophyses well above the main magma chamber, hence the latter is usually not exposed. Nevertheless, first-order estimates of the magma volumes and theoretically available amounts of Mo in the magma systems mentioned above are provided in Table 6.3.6. For each mineralized system a minimum magma volume has been calculated from the estimated Mo content of an "average melt", a minimum extraction efficiency of 50%, and the total amount of Mo present in the orebody/orebodies. The Mo content of the "average melt" was estimated as follows: first, the least fractionated melt or rock associated with mineralization was identified based on its Cs and/or Rb content, and then the corresponding Mo concentration was estimated based on the Cs-Mo trends shown in Fig. 6.3.8. Of course, this definition of the "average melt" composition is associated with considerable uncertainty, but without having access to the large intrusions underlying porphyry-type ore deposits it is all we can do. The results suggest that giant Mo deposits (here defined as  $\geq 1$  megatonne (Mt) Mo) required magma volumes of at least 100 km<sup>3</sup>, whereas medium-sized (here defined as 0.1-1.0 Mt Mo) deposits required magma volumes of at least several tens of km<sup>3</sup>. Similar results have been obtained in earlier studies: Wallace et al. (1968) calculated that 100-125 km<sup>3</sup> of magma were necessary to form the Climax orebodies, and Keith et al. (1993) argued that  $\geq 150$  km<sup>3</sup> were necessary to form the Henderson deposit.

**Table 6.3.5** Overview on S, Cs, Mo, and Cu concentrations in magmatic fluids from Mo-mineralized granites, porphyry Mo and porphyry Cu(Mo) deposits

Sample	S [wt%]	Cs [ppm]	Mo [ppm]	Cu [ppm]	Pb [ppm]	Zn [ppm]	Mo/Cu	References
<b>TM 12A</b>	0.6 ± 0.3 <sup>†</sup>	100 ± 52	79 ± 58	620 ± 720	210 ± 110	670 ± 320	0.13 ± 0.18	this study
<b>Dra 6A</b>	0.4 ± 0.1 <sup>†</sup>	230 ± 170	51 ± 18	1170 ± 320	110 ± 10	340 ± 280	0.044 ± 0.040	this study
<b>Questa</b>	?	30 ± 33	37 ± 25	2100 ± 1600	280 ± 230	730 ± 560	0.042 ± 0.066	Klemm et al. (2007)
<b>Cave Peak</b>	?	56 ± 16	112 ± 13	620 ± 120	390 ± 50	1400 ± 100	0.18 ± 0.02	Audetat (2010)
<b>Butte</b>	?	6 ± 4	7 ± 2	3500 ± 1800	20 ± 8	130 ± 40	0.004 ± 0.003	Rusk et al. (2004)
<b>Bingham</b>	0.7 ± 0.3*	9 ± 7	51 ± 36	6200 ± 3800	330 ± 90	600 ± 320	0.02 ± 0.02	Landtwing et al. (2010)
<b>El Teniente</b>	?	19 ± 18	8 ± 4	5900 ± 4000	80 ± 70	340 ± 280	0.002 ± 0.001	Klemm et al. (2007)

\*vapor data in Seo et al. (2009); <sup>†</sup>average of all fluid inclusions analyzed from this intrusion (not only TM 12A or Dra 6A)

**Table 6.3.6** Comparison of magma type, magma chamber geometry and Mo and Cs concentrations from Mo- and Cu mineralized granites

Occurrence	Geochemical signature	Depth at the top of magma chamber [km]	Ref.	Minimum size of magma chamber [km <sup>3</sup> ]	Avg. magma composition	Rb conc. [ppm]*	Ref.	Corresponding Cs conc. [ppm]	Ref.	Estimated Mo content [ppm]	Estimated total Mo in magma [Mt]	Total Mo in deposit [Mt]	Ref.	Minimum magma volume required to form deposits [km <sup>3</sup> ]
<b>Porphyry Mo deposits</b>														
Climax	within-plate	2.2 - 3.7	1, 2	40 - 50	rhyolite	500	22	15	#	15	1.8	2.2	40	110
Uradi/Henderson (Hideaway Park rhyolite)	within-plate	1.6 - 3.1	1, 2, 3	?	rhyolite	380	22	4	†	8		1.2	40	110
Mt. Emmons + Redwell Basin	within-plate	>(0.7 - 0.9)	1, 2	?	rhyolite	270	31	1 - 5	#	3 - 8		0.4	40	40-100
Questa	within-plate	3-5	4	?	rhyolite	180	32	4	†	7		0.4	40	40
Pine Grove	within-plate	ca. 4	5	100	rhyolite	250	33	6	†	2	0.5	0.2	40	75
Cave Peak	within-plate	3.0 - 5.7	6, 7	?	rhyolite	460	34	18	†	12		0.4	40	25
<b>Sub-economic Mo mineralization</b>														
Treasure Mt.	within-plate	ca. 3.7	8, 9	50	rhyolite	320 <sup>††</sup>	8	6	†	6	0.8	n.a.		
Drammen Granite	within-plate	4.8 - 5.6	8, 10	60	rhyolite	330	35	1	†	6	1.0	n.a.		
Glitrevann Granite	within-plate	>(1.2 - 1.5)	11	30	rhyolite	160	36	1	†	6	0.5	n.a.		
Bear Canyon (Log Cabin Prospect)	within-plate (?)	2 - 5	12	3	rhyolite	140	32	2	†	4	0.03	0.04	41	7
<b>No economic Mo mineralization</b>														
Rito del Medio Pluton	within-plate (?)	4.1 - 4.8	13	5	rhyolite	170	32	2	†	4	0.05	-		
Canada Pinabete Pluton	subduction (?)	3.5 - 4.8	13	5	rhyolite	145	32	3	†	4	0.05	-		
Stronghold Granite	within-plate (?)	5.6 - 6.7	6	80	dacite	150 (?)		1	†	1.5	0.32	-		
Caetano Caldera	subduction	4	14	25	rhyolite	120	14	2	14	1.5	0.10	-		
Tombstone (Schieflein granodiorite)	subduction	?		10	dacite	120	37	4.5	37	1.5	0.04	-		
<b>Porphyry Cu(-Mo, Au) deposits</b>														
Santa Rita	subduction	(4.5 - 4.8)	6	?	andesite	120	38	5	38	2.5		>0.08	40	>24
Alumbrera	subduction	(2.6 - 4.5)	15, 16	>15	andesite	80	39	1.5	39	4.5	>0.18	0.3	40	50
Bingham	subduction	(3.3 - 3.5)	17, 18	100 - 200	dacite	120	30	-		2 <sup>9</sup>	0.5 - 1.0	0.8	40	300
Butte	subduction	(5 - 9)	19	?	?			-		2 <sup>9</sup>		1.4	40	500
Yerington	subduction	4 - 5	20	65	dacite <sup>§</sup>	120	20	-		2 <sup>9</sup>	0.35	0.04	42	14

\*Minimum Rb concentration measured in melt inclusions or whole-rocks; #assuming a similar fractionation trend like the one displayed by melt inclusions from Hideaway Park rhyolite, Treasure Mountain, and the Rito del Medio Pluton; † estimated by extrapolating Rb-Cs-Mo trends of melt inclusion data; ††Lühr Hill granite, 68 wt% SiO<sub>2</sub>; †††least evolved melt inclusions which may not be representative; † estimate based on an average Rb-concentration of 120 ppm; References: 1-Mutschler et al. (1981); 2-White et al. (1981); 3-Carlen et al. (1988); 4-Möller (1989); 5-Keith et al. (1986); 6-Audétat et al. (2008); 7-Audétat et al. (2010); 8-this study; 9-Everett and Hoisch (2008); 10-Larsen et al. (2009); 11-Ofstedahl (1978); 12-Lipman, (1988); 13-Audétat and Pettke (2003); 14-John et al. (2008); 15-Ulfirch et al. (2002); 16-Proffitt (2003); 17-Redmond et al. (2004); 18-Landtwing et al. (2010); 19-Rusk et al. (2008); Diles, (1987); 21-Bookstrom (1989); 22-Bookstrom et al. (1988); 23-Mutschler (1976); 24-Tronnes and Brandon (1982); 25-Schönwandt and Petersen (1983); 26-Lipman and Reed (1989); 27-Drewes (1987); 28-Moore (1993); 29-Halter et al. (2002); 30-Maughan et al. (2004); 31-Thomas and Gale (1982); 32-Johnson et al. (1989); 33-Keith and Shanks (1988); 34-Price and Henry (1986); 35-Ihlen et al., (1982); 36-Jensen (1985); 37-Lang and Titley (1998); 38-Audétat and Pettke (2006); 39-Halter et al. (2004); 40-Mutschler (1999); 41-Keith et al. (1993); 42-Einaudi (1994).

For both mineralized and barren intrusions, an independent estimate on the amount of potentially available Mo may be obtained from the geologically constrained intrusion volume, its average composition, and the estimated Mo content of melts at this degree of melt fractionation. Three points have to be noted here: (1) as "intrusion volume" we define the maximum rock volume that could have been partially molten at the time of (potential) Mo mineralization (i.e., in large, composite batholiths like the Drammen Granite, in which several intrusive phases crosscut each other, only the latest phases associated with Mo mineralization are considered), (2) in the absence of any constraints on the intrusion thickness we assume a minimum thickness of one-fourth of the lowest exposed dimension (i.e., for a granite exposed over an area of 4 x 6 km we assume a minimum thickness of 1 km), and (3) the total amount of Mo in the magma (last but two column in Table 6.3.6) is without considering the efficiency of extraction, i.e., at an extraction efficiency of 50% the amount of Mo ending up in a hypothetical deposit would be only half of the amount listed in this column.

A comparison between the calculated minimum magma volumes for economic Mo deposits (last column in Table 6.3.6) and the minimum magma volumes associated with sub-economic and barren intrusions (fifth column in Table 6.3.6) reveals that magma volumes of the Rito del Medio pluton, the Cañada Pinabete pluton, the Bear Canyon pluton, and Schieffelin granite (Tombstone) may have been simply too small to produce economic mineralization. The magma volumes of the Stronghold granite, the Treasure Mountain Dome, the Drammen granite, and the Glitrevann granite, on the other hand, would have been large enough to produce at least a medium-sized Mo deposit. In these intrusions, factors other than magma chamber size appear to have prevented economic mineralization. An obvious candidate is the degree of fluid/melt focusing, which itself may depend on (i) the depth of intrusion, (ii) the shape of the magma chamber, (iii) the presence/absence of vent structures, and (iv) the mode of magma crystallization. The mode of magma crystallization and the presence/absence of vent structures may be controlled by the frequency and magnitude of magma chamber recharge/reactivation by ascending mafic magmas (Bachmann et al., 2007, Walker et al., 2007). For example, a granitic magma that intrudes at 2-5 km depth and evolves as an essentially closed system may never form

economic Mo mineralization because it reaches relatively quickly a mushy state, which prevents residual melts to accumulate in the upper parts of the magma chamber. In contrast, in a magma chamber that is periodically re-heated by underplating mafic magmas, residual melts are able to rise and pool under the roof to form a crystal-poor rhyolitic cap (Bachmann et al., 2007, Walker et al., 2007). From this cap, dissolved volatiles can be discharged into a confined volume of rock, particularly if an apophysis has developed near the top of the magma chamber. Possibly, this process is aided by a runaway effect: Once fractionated melts have gathered under the roof, further fractionation and spatial segregation is promoted due to their reduced viscosity. Shinohara et al. (1995) convincingly demonstrated that once fluid saturation is attained, differences in the density of bubble-bearing vs. undegassed magma can result in efficient magma convection and upward transport of fluids. Importantly, this mechanism works only if the density difference between bubble-bearing and undegassed magma is relatively large, which may be true only at relatively shallow depths. Furthermore, efficient bubble separation at the top of the magma chamber may require the presence of structures through which the volatiles can escape.

In terms of intrusion depth, the Drammen granite (4.8-5.6 km) and the Stronghold granite (5.6-6.7 km) appear to have been emplaced at deeper levels than most porphyry Mo-forming intrusions (2-5 km). In the Drammen granite the occurrence of quartz-topaz greisens in the microcrystalline quartz-feldspar porphyry near Røysjø (Ihlen et al., 1982) and the fact that this rock type is confined to topographically high levels (Tronnes and Brandon, 1992) suggest that the roof was not far. However, in the case of the Stronghold granite the top of the magma chamber could easily have been situated 1-2 km above the present level of erosion, whereas in both cases it is principally possible that economic Mo mineralization was present at structurally higher levels that have already been eroded.

Given the uncertainties outlined above it may be best to focus on the barely unroofed Treasure Mountain and Glitrevann granites, which were large enough and were emplaced at the right depth to produce economic Mo mineralization, but nevertheless are only sub-economically mineralized. Why were these intrusions not more productive? Although we don't know the ultimate answer we like to stress a few points: (i) First, the Treasure

Mountain and Glitrevann granites do not seem to have developed the apophyses that are so characteristic of porphyry Mo-forming intrusions. Also, vent structures, radial dikes, and breccia bodies, which are indicative of forceful ascent of magma and/or fluid, are conspicuously absent in these granites. Instead, miarolitic cavities are common, which testify to a low degree of fluid focusing. Based on the outcrop situation it is evident that the roofs of the Treasure Mountain and Glitrevann granites were rather flat. These characteristics are probably related, i.e., the flat roofs may have inhibited apophysis formation and venting, and thus led to poor fluid focusing. (ii) Second, the intrusion histories at Treasure Mountain and Glitrevann are comparatively simple, recording only one (or maximum two) intrusion events, whereas numerous intrusion events are characteristic for porphyry Mo deposits (at least eleven at Henderson, Carten et al., 1988; five at Climax, White et al., 1981, five at Pine Grove, Keith et al., 1986; and at least three at Cave Peak, Sharp, 1978). Age determinations on separate intrusive phases have shown that magmatic activity lasted for at least 5.5 m.y. (possibly up to 12-15 m.y.) at Climax, and for at least 5 m.y. at Urad-Henderson (White et al., 1981). Such extended life times require repeated re-activation of the magma chamber by melts ascending from depth (Bachmann et al., 2007; Walker et al., 2007) iii) Third, most magmas associated with Climax-type porphyry Mo mineralization show evidence for interaction with mafic alkaline magmas, both in the presence of lamprophyric dikes and mafic enclaves in the felsic intrusions, and in anomalously high Ni and Cr concentrations in the felsic magmas (Bookstrom et al., 1988; Wallace, 1995). Such evidence is mostly missing for the Treasure Mountain and Glitrevann granites. Interaction between mafic and felsic magmas may indirectly be linked to the degree of focusing of residual melts and associated fluids. Bachmann et al. (2007) proposed that magma chambers that are periodically re-heated by underplating mafic magmas have a higher chance to develop a cap of fractionated, crystal-poor magma than magma chambers that are not re-heated. This crystal-poor cap (see also Miller and Mittlefehldt, 1984, and Walker et al., 2007) may be essential for the formation of economic porphyry Mo mineralization because the convection model of Shinohara et al. (1995) requires relatively large volumes of crystal-poor magmas at or near aqueous fluid saturation. Magma convection may additionally be facilitated by the high fluorine content of these melts (up to

5 wt%, e.g., White et al., 1981; Wallace, 1995), which adds to the reduction in melt viscosity caused by H<sub>2</sub>O (e.g., Baker and Vaillancourt, 1995). How often and in what quantities mafic melts had to arrive in order for crystal-poor caps to develop, and how important these melts were with regard to providing metals and sulfur (e.g., Keith et al., 1986; Bookstrom et al., 1988; Carten et al., 1993; Audéat, 2010) is not clear at this stage, but helpful information may be obtained by detailed isotopic studies (Bookstrom et al., 1988; Davidson et al., 2007), trace element systematics (e.g., Cr, Ni concentrations in the felsic members; Bookstrom et al., 1988; Keith et al., 1997), and the study of melt inclusions (e.g., Saito et al., 2003, Roberge et al., 2009) and zoned phenocrysts (e.g., Wark et al., 2007).

### **6.3.7 Summary and conclusions**

Our melt and fluid inclusion study on the sub-economically Mo-mineralized granites at Treasure Mountain, Drammen, and Glitrevann has led to the following observations: (1) Molybdenum concentrations in the silicate melt generally increased with increasing degree of fractionation: in the Treasure Mountain Dome from ~5 ppm Mo at ~5 ppm Cs to ~35 ppm Mo at ~90 ppm Cs, and in the Drammen granite from ~10 ppm Mo at ~10 ppm Cs to ~30 ppm Mo at ~300 ppm Cs. (2) Magmatic fluids were single-phase, had densities between 0.6 and 0.7 g/cm<sup>3</sup> and were of relatively low salinity (~4-6 wt% NaCl<sub>equiv</sub>). At temperatures ≤600°C these fluids split into a highly saline brine and a coexisting, low-density vapor phase. The single-phase, magmatic fluids contained considerable amounts of S (~0.5 wt% S) and CO<sub>2</sub> (~3-6 mol%). (3) Molybdenum concentrations in these magmatic bulk fluids correlate with Cs concentrations, reflecting the compositional evolution of the silicate melts from which they exsolved. Molybdenum concentrations range from ~50 ppm to ~160 ppm in the Treasure Mountain Dome, and from ~30 ppm to ~270 ppm in the Drammen granite. (4) Copper concentrations are poorly reproducible and range from a few tens of ppm to several thousand ppm Cu. The large spread is probably a result of post-entrapment diffusion of Cu, but an attempt to reverse these changes resulted in only a relatively small (by a factor of two) decrease in the Cu content of re-equilibrated fluid inclusions. In any case, Mo precipitation was highly selective, as the base metal content of the fluids was up to ten times higher but there are essentially no base metals in the ore.

---

Comparison of our melt and fluid inclusion data with previous data obtained from barren intrusions, porphyry Mo-mineralized intrusions, and porphyry Cu (Mo)-mineralized intrusions reveals the following trends: (1) Melts and fluids in subduction-related intrusions were generally less fractionated and had a lower Mo content at a given Cs concentration than melts and fluids analyzed from intrusions in within-plate settings. The latter is in agreement with the lower Mo/Cs ratio of primitive arc magmas relative to oceanic island basalts and suggests that the molybdenum in both subduction-related and within-plate magmas is mantle-derived. (2) Fluids and melts in barren and sub-economically mineralized intrusions from within-plate settings lie on the same fractionation trends as those analyzed from economic porphyry Mo-deposits.

This shows that the fluids and melts that were present at high degrees of crystallinity in barren intrusions were not fundamentally different from those that formed giant porphyry Mo deposits. The difference must have been either the magma volumes or the degree of focusing of fractionated melts and thereof exsolved fluids. Based on the available data it can be calculated that at least several tens of km<sup>3</sup> magma were required to form intermediate to large deposits, and at least several hundred km<sup>3</sup> of magma to form giant deposits. Hence, some of the barren intrusions may have been simply too small to produce major Mo mineralization. However, other intrusions including the Treasure Mountain Dome, the Drammen and Glitrevann granites would have had the required size. In these intrusions the lack of economic mineralization seems to be the result of poor focusing of residual melts and fluids. Apophyses, vent structures, and breccia bodies are conspicuously absent in these intrusions. Instead, miarolitic cavities are present, testifying to a dispersed state of the fluids. There is little doubt that the presence of apophyses with overlying areas of highly fractured rocks are a critical requirement for focused fluid flow. Furthermore, the enormous amounts of Mo present in some deposits (>1 Mt Mo) associated with small (<0.5 km<sup>3</sup>) apophyses require that magma was very efficiently circulated through these apophyses (Shinohara et al., 1995). Which factors ultimately lead to the accumulation of large volumes of fractionated melts in the upper parts of magma chambers, and how these factors are related to the tectonic framework is less clear. Potential factors include the intrinsic

properties of the intruding magmas, the rate and depth of magma intrusion, and the degree of interaction with mafic magmas.

### 6.3.8 Acknowledgements

This work was funded by the German Science Foundation under project number: AU 314/1-2. We thank Ronald Bakker who provided assistance with using the 'ICE'-software, Celestine Mercer for the data from the Hideaway Park rhyolite, and Hans Keppler for additional funding and for help with the Raman spectroscopy.

### 6.3.9 References

- Cave Peak, Texas: *Journal of Petrology*, v. 51, p. 1739-1760.
- Audétat, A. and Pettke, T., 2003, The magmatic-hydrothermal evolution of two barren granites: a melt and fluid inclusion study of the Rio del Medio and Cañada Pinabete Plutons in northern New Mexico (USA): *Geochimica et Cosmochimica Acta*, v. 67, p. 91-121.
- Audétat, A. and Pettke, T., 2006, Evolution of a porphyry-Cu mineralized magma system at Santa Rita, New Mexico (USA): *Journal of Petrology*, v. 47, p. 2021-2046.
- Audétat, A., Pettke, T. and Dolejš, D., 2004, Magmatic anhydrite and calcite in the ore-forming quartz-monzodiorite magma at Santa Rita, New Mexico (USA): genetic constraints on porphyry-Cu mineralization: *Lithos*, v. 72, p. 147-161.
- Audétat, A., Pettke, T., Heinrich, C. A. and Bodnar, R. J., 2008, The composition of magmatic-hydrothermal fluids in barren versus mineralized intrusions: *Economic Geology Special Paper*, v. 103, p. 877-908.
- Audétat, A., Dolejš, D. and Lowenstern, J. B., 2011, Molybdenite saturation in silicic magmas: Occurrence and petrological implications: *Journal of Petrology*, v. 52, p. 891-904.
- Baker, D. R. and Vaillancourt, J., 1995, The low viscosities of F+H<sub>2</sub>O-bearing granitic melts and implications for melt extraction and transport: *Earth and Planetary Science Letters*, v. 132, p. 199-211.
- Bakker, R. J., 1997, Clathrates: Computer programs to calculate fluid inclusion V-X properties using clathrate melting temperatures: *Computers & Geosciences*, v. 23, p. 1-18.
- Bachmann, O., Miller, C. F. and de Silva, S. L., 2007, The volcanic-plutonic connection as a stage for understanding crustal magmatism: *Journal of Volcanology and Geothermal Research*, v. 167, p. 1-23.
- Bali, E., Keppler, H. and Audétat, A., 2012, The mobility of W and Mo in subduction zone fluids and the Mo-W-Th-U systematics of island arc magmas: *submitted* to *Earth and Planetary Science Letters*

- Berthelsen, A., 1980, Towards a palinspatic tectonic analysis of the Baltic Shield: Memoires du B.R.G.M., 26th international geological congress, Paris 1980, v. 108, p. 5-21.
- Bodnar, R. J. and Vityk, M. O., 1994, Interpretation of microthermometric data for H<sub>2</sub>O-NaCl fluid inclusions: Blacksburg/VA, Virginia Tech, Number of 117-130 p.
- Bookstrom, A. A., 1981, Tectonic setting and generation of Rocky Mountain porphyry molybdenum deposits, Arizona Geological Society Digest 14, Number of 214-226 p.
- Bookstrom, A. A., 1989, The Climax-Alma granite batholith of Oligocene age and the porphyry molybdenum deposits of Climax, Colorado, U.S.A.: Engineering Geology, v. 27, p. 543-568.
- Bookstrom, A. A., Carten, R. B., Shannon, R. D. and Smith, R. P., 1988, Origins of bimodal leucogranite-lamprophyre suites, Climax and Red Mountain porphyry molybdenum systems, Colorado: Petrologic and strontium isotopic evidence: Colorado School of Mines Quarterly, v. 83, p. 1-65.
- Borisova, A. Y., Freydier, R., Polvé, M., Salvi, S., Candaudap, F. and Aigouy, T., 2008, *In situ* multi element analysis of the Mount Pinatubo quartz-hosted melt inclusions by NIR femtosecond laser ablation-inductively coupled plasma-mass spectrometry: Geostandards and Geoanalytical Research, v. 32, p. 209-229.
- Bugge, A., 1963, Norges molybdenforekomster: Norges Geologiske Undersokelse v. 259, p. 65-84.
- Burke, W. A. J., 2001, Raman microspectrometry of fluid inclusions: Lithos, v. 55, p. 139-158.
- Carten, R. B., Geraghty, E. P. and Walker, B. M., 1988, Cyclic development of igneous features and their relationship to high-temperature hydrothermal features in the Henderson porphyry molybdenum deposit, Colorado: Economic Geology, v. 83, p. 266-296.
- Carten, R. B., White, W. H. and Stein, H. J., 1993, High-grade granite-related molybdenum systems: Classification and origin, *in* R. V. Kirkham, W. D. Sinclair, R. I. Thorpe and J. M. Duke eds., Mineral Deposit Modeling, Geological Association of Canada, Special Paper 40, p. 521-554.
- Clark, K. F. and Reed, C. B., 1972, Geology and ore deposits of the Eagle Nest area, New Mexico: New Mexico Bureau of Mines and Mineral Resources Bulletin, v. 94, 152 p.
- Davidson, J. P., Morgan, D. J., Charlier, B. L. A., Harlou, R. and Hora, J. M., 2007, Microsampling and isotopic analysis of igneous rocks: Implications for the study of magmatic systems: Annual Review of Earth and Planetary Science Letters, v. 35, p. 273-311.
- Dilles, J. H., 1987, Petrology of the Yerington Batholith, Nevada: Evidence for evolution of porphyry copper ore fluids: Economic Geology, v. 82, p. 1750-1789.
- Drewes, H., 1987, Geologic map and cross sections of the Dragoon Mountains, southeastern Arizona: U.S. Geological Survey Miscellaneous Investigations Series, Map I-1662.

- Einaudi, M. T., 1994, 6-km vertical cross section through porphyry copper deposits, Yerington District, Nevada: Multiple Intrusions, Fluids, and Metal Sources: Society of Economic Geologists. International Exchange Lecture-June 1994, v., p. <http://pangea.stanford.edu/research/ODEX/marco-yerington.html>.
- Everett, B. C. and Hoisch, T. D., 2008, Conditions of metamorphism of the Colorado Yule Marble: *Mountain Geologist*, v. 45, p. 69-76.
- Geyti, A. and Schönwandt, H. K., 1979, Bordvika-A possible porphyry molybdenum occurrence within the Oslo Rift, Norway: *Economic Geology*, v. 74, p. 1211-1220.
- Guillong, M. and Heinrich, C. A., 2007, Sensitivity enhancement in laser ablation ICP-MS using small amounts of hydrogen in the carrier gas: *Journal of Analytical Atomic Spectrometry*, v. 22, p. 1488-1494.
- Halter, W. E., Heinrich, C. A. and Pettke, T., 2004, Laser-ablation ICP-MS analysis of silicate and sulfide melt inclusions in an andesitic complex; II, Evidence for magma mixing and magma chamber evolution: *Contributions to Mineralogy and Petrology*, v. 147, p. 397-412.
- Halter, W. E., Heinrich, C. A. and Pettke, T., 2005, Magma evolution and the formation of porphyry Cu-Au ore fluids: Evidence from silicate and sulfide melt inclusions: *Mineralium Deposita*, v. 39, p. 845-863.
- Hedenquist, J. W. and Henley, R. W., 1985, The importance of CO<sub>2</sub> on freezing point measurements of fluid inclusions: evidence from active geothermal systems and implications for epithermal ore deposition: *Economic Geology*, v. 80, p. 1379-1406.
- Heinrich, C. A., Pettke, T., Halter, W. E., Aigner-Torres, M., Audétat, A., Günther, D., Hattendorf, B., Bleiner, D., Guillong, M. and Horn, I., 2003, Quantitative multi-element analysis of minerals, fluid and melt inclusions by laser-ablation inductively-coupled-plasma mass-spectrometry: *Geochimica et Cosmochimica Acta*, v. 67, p. 3473-3496.
- Holtz, F., Johannes, W., Tamic, N. and Behrens, H., 2001, Maximum and minimum water contents of granitic melts generated in the crust: a reevaluation and implications: *Lithos*, v. 56, p. 1-14.
- Ihlen, P. M., 1986, The geological evolution and metallogeny of the Oslo paleorift, *in* S. Olerud and P. M. Ihlen eds., *Metallogeny associated with the Oslo paleorift*: Uppsala, Sveriges Geologiska Undersökning, p. 6-17.
- Ihlen, P. M. and Vokes, F. M., 1978, *Metallogeny*: Bulletin - Norges Geologiske Undersökelse, v. 45, p. 75-90.
- Ihlen, P. M., Tronnes, R. G. and Vokes, F. M., 1982, Mineralization, wall rock alteration and zonation of ore deposits associated with the Drammen Granite in the Oslo Region, Norway, John Wiley & Sons Ltd, 111-136.
- Jensen, I. S., 1985, Geochemistry of the central granitic stock in the Glitrevann cauldron within the Oslo rift, Norway: *Norsk Geologisk Tidsskrift*, v. 65, p. 201-216.
- John, D. A., Henry, C. D. and Colgan, J. P., 2008, Magmatic and tectonic evolution of the Caetano Caldera, north-central Nevada; a tilted, mid-Tertiary eruptive center and source

- of the Caetano Tuff: *Geosphere*, v. 4, p. 75-106.
- Johnson, C. M., Czamanske, G. K. and Lipman, P. W., 1989, Geochemistry of intrusive rocks associated with the Latir volcanic field, New Mexico, and contrasts between evolution of plutonic and volcanic rocks: *Contributions to Mineralogy and Petrology*, v. 103, p. 90-109.
- Jones, D. M., 1990, Mid-tertiary arcuate dikes and faults of the Rio Hondo-Red River drainages, Sangre de Cristo Mountains, New Mexico: A postulated outlying ring-fracture zone to the Miocene Questa caldera: *New Mexico Geological Society - Guidebook*, 41<sup>st</sup> Field Conference, p. 365-368.
- Kamenetsky, V. S. and Danyushevsky, L. V., 2005, Metals in quartz-hosted melt inclusions: Natural facts and experimental artifacts: *American Mineralogist*, v. 90, p. 1674-1678.
- Keith, J. D., Shanks, W. C., Archibald, D. A. and Ferrar, E., 1986, Volcanic and intrusive history of the Pine Grove porphyry molybdenum system, southwestern Utah: *Economic Geology*, v. 81, p. 553-577.
- Keith, J. D. and Shanks, W. C., 1988, Chemical evolution and volatile fugacities of the Pine Grove porphyry molybdenum and ash-flow tuff system, southwest Utah, *in* R. P. Taylor and D. F. Strong eds., *Recent advances in the geology of granite-related mineral deposits*, Canadian Institute of Mining and Metallurgy Special Volume, p. 402-423.
- Keith, J. D., Christiansen, E. H. and Carten, R. B., 1993, The genesis of giant porphyry molybdenum deposits: *Society of Economic Geologists. Special Publication*, v. 2, p. 285-317.
- Klemm, L. M., Pettke, T., Heinrich, C. A. and Campos, E., 2007, Hydrothermal evolution of the El Teniente Deposit, Chile: Porphyry Cu-Mo ore deposition from low-salinity magmatic fluids: *Economic Geology*, v. 102, p. 1021-1045.
- Klemm, L. M., Pettke, T. and Heinrich, C. A., 2008, Fluid and source magma evolution of the Questa porphyry Mo deposit, New Mexico, USA: *Mineralium Deposita*, v. 43, p. 533-552.
- Landtwing, M. R., Furrer, C., Redmond, P. B., Pettke, T., Guillong, M. and Heinrich, C. A., 2010, The Bingham porphyry Cu-Mo-Au deposit. III. Zoned copper-gold ore deposition by magmatic vapor expansion: *Economic Geology*, v. 105, p. 91-118.
- Lang, J. R. and Titley, S. R., 1998, Isotopic and geochemical characteristics of Laramide magmatic systems in Arizona and implications for the genesis of porphyry copper deposits: *Economic Geology*, v. 93, p. 138-170.
- Larsen, R. B., Jacamon, F. and Kronz, A., 2009, Trace element chemistry and textures of quartz during the magmatic hydrothermal transition of Oslo Rift granites: *Mineralogical Magazine*, v. 73, p. 691-707.
- Lehmann, B., 1987, Molybdenum distribution in Precambrian rocks of the Colorado Mineral Belt: *Mineralium Deposita*, v. 22, p. 47-52.
- Lerchbaumer, L. and Audétat, A., 2012a, The 'quartz capsule' - a new method to avoid alloying problems with noble metal capsules in hydrothermal experiments: *European Journal of Mineralogy*, v. 24, in press

- Lerchbaumer, L. and Audétat, A., 2012b, High Cu concentrations in vapor-type fluid inclusions: an artifact?: *Geochimica et Cosmochimica Acta*, doi:10.1016/j.gca.2012.04.033.
- Li, Y., Audétat, A., Lerchbaumer, L. and Xiong, X. L., 2009, Rapid Na, Cu exchange between synthetic fluid inclusions and external aqueous solutions: evidence from LA-ICP-MS analysis: *Geofluids*, v. 9, p. 321-329.
- Lipman, P. W. and Brown, P. E., 1988, Evolution of silicic magma in the upper crust; the mid-Tertiary Latir volcanic field and its cogenetic granitic batholith, northern New Mexico, U.S.A.: *Transactions of the Royal Society of Edinburgh: Earth Sciences*, v. 79, p. 265-288.
- Lipman, P. W. and Reed, J. C., 1989, Geologic map of the Latir volcanic field and adjacent areas, northern New Mexico: U. S. Geological Survey Miscellaneous Investigations Series, Map I-1907.
- Lowenstern, J. B., 1994, Dissolved volatile concentrations in an ore-forming magma: *Geology*, v. 22, p. 893-896.
- Maughan, D. T., Keith, J. D., Christiansen, E. H., Pulsipher, T., Hattori, K. and Evans, N. J., 2002, Contributions from mafic alkaline magmas to the Bingham porphyry Cu-Au-Mo deposit, Utah, USA: *Mineralium Deposita*, v. 37, p. 14-37.
- Mavrogenes, J. A. and Bodnar, R. J., 1994, Hydrogen movement into and out of fluid inclusions in quartz: Experimental evidence and geologic implications: *Geochimica et Cosmochimica Acta*, v. 58, p. 141-149.
- Miller, C. F. and Mittlefehldt, D. W., 1984, Extreme fractionation in felsic magma chambers; a product of liquid-state diffusion or fractional crystallization?: *Earth and Planetary Science Letters*, v. 68, p. 151-158.
- Molling, P. A., 1989, Applications of the reaction progress variable to hydrothermal alteration associated with the deposition of the Questa molybdenite deposit, NM: Unpub. thesis, Johns Hopkins University, 249 p.
- Moore, R. B., 1993, Geologic map of the Tombstone volcanic center, Cochise County, Arizona: U. S. Geological Survey Miscellaneous Investigations Series, Map I-2420.
- Mutschler, F. E., 1976, Crystallization of a soda granite, Treasure Mountain Dome, Colorado, and the genesis of stockwork molybdenite deposits, *in* L. A. Woodward and S. A. Northrop eds., *Tectonics and Mineral Resources of Southwestern North America*, New Mexico Geological Society - Special Publication, p. 199-205.
- Mutschler, F. E., Wright, E. G., Ludington, S. and Abbott, J. T., 1981, Granite molybdenum systems: *Economic Geology*, v. 76, p. 874-897.
- Mutschler, F. E., Ludington, S. D. and Bookstrom, A. A., 1999, Giant porphyry-related metal camps of the world; a database: Open-File Report - U. S. Geological Survey 99-556, <http://pubs.usgs.gov/of/1999/of99-556/>
- Neumann, E.-R., Olsen, K. I., Baldrige, W. S. and Sundvoll, B., 1992, The Oslo Rift: a review: *Tectonophysics*, v. 208, p. 1-18.
- Obradovich, J. D., Mutschler, F. E. and Bryant, B., 1969, Potassium-argon ages bearing on

- the igneous and tectonic history of the Elk Mountains and vicinity, Colorado: A preliminary report: Geological Society of America Bulletin, v. 80, p. 1749-1756.
- Oftedahl, C., 1953, Studies on the igneous rock complex of the Oslo Region. XIII. The cauldrons: *Skrifter - Norske Videnskaps-Akademi i Oslo, I. Matematisk-Naturvidenskapelig Klasse*, v. 3, p. 108.
- Oftedahl, C., 1978, Cauldrons of the Permian Oslo Rift: *Journal of Volcanology and Geothermal Research*, v. 3, p. 343-371.
- Olsen, K. I. and Griffin, W. L., 1984, Fluid inclusion studies of the Drammen Granite, Oslo Paleorift, Norway. I. Microthermometry: *Contributions to Mineralogy and Petrology*, v. 87, p. 1-14.
- Peng, D. Y. and Robinson, D. B., 1976, A new two-constant equation of state: *Industrial and Engineering Chemistry Fundamentals*, v. 15, p. 59-64.
- Price, J. G. and Henry, C. D., 1986, *Geology of Marble Canyon: Guidebook-Bureau of Economic Geology*, University of Texas at Austin, v. 23, p. 17-26.
- Proffett, J. M., 2003, *Geology of the Bajo de la Alumbrera porphyry copper-gold deposit, Argentina: Economic Geology*, v. 98, p. 1535-1574.
- Ramberg, I. B., Gabrielsen, R. H., Larsen, B. T. and Solli, A., 1977, Analysis of fracture patterns in southern Norway: *Geologie en Mijnbouw. Netherlands Journal of Geosciences*, v. 56, p. 295-310.
- Redmond, P. B., Einaudi, M. T., Inan, E. E., Landtwing, M. R. and Heinrich, C. A., 2004, Copper deposition by fluid cooling in intrusion-centered systems: New insights from the Bingham porphyry ore deposit, Utah: *Geology*, v. 32, p. 217-220.
- Richards, J. P., 2011, Magmatic to hydrothermal metal fluxes in convergent and collided margins: *Ore Geology Reviews*, v. 40, p. 1-26.
- Roberge, J., Delgado-Granados, H. and Wallace, P. J., 2009, Mafic magma recharge supplies high CO<sub>2</sub> and SO<sub>2</sub> gas fluxes from Popocatepetl volcano, Mexico: *Geology*, v. 37, p. 107-110.
- Rusk, B. D., Reed, M. H., Dilles, J. H., Klemm, L. M. and Heinrich, C. A., 2004, Compositions of magmatic hydrothermal fluids determined by LA-ICP-MS of fluid inclusions from the porphyry copper-molybdenum deposit at Butte, MT: *Chemical Geology*, v. 210, p. 173-199.
- Rusk, B. D., Reed, M. H. and Dilles, J. H., 2008, Fluid inclusion evidence for magmatic-hydrothermal fluid evolution in the porphyry copper-molybdenum deposit at Butte, Montana: *Economic Geology*, v. 103, p. 307-334.
- Saito, G., Kazahaya, K. and Shinohara, H., 2003, Volatile evolution of Satsuma-Iwojima volcano: Degassing process and mafic-felsic magma interaction, *in* B. DeVivo and R. J. Bodnar eds., *Melt inclusions in volcanic systems*, Elsevier, p. 129-146.
- Schmidt, C. and Bodnar, R. J., 2000, Synthetic fluid inclusions: XVI. PVTX properties in the system H<sub>2</sub>O-NaCl-CO<sub>2</sub> at elevated temperatures, pressures, and salinities: *Geochimica et*

- Cosmochimica Acta, v. 64, p. 3853-3869.
- Schönwandt, H. K., 1986, The volcanic history and the molybdenite mineralization of the Glitrevann caldera: Uppsala, Sveriges Geologiska Undersökning, v. 59, p. 26-27.
- Schönwandt, H. K. and Petersen, J. S., 1983, Continental rifting and porphyry-molybdenum occurrences in the Oslo Region, Norway: Tectonophysics, v. 94, p. 609-631.
- Seo, J. H., Guillong, M. and Heinrich, C. A., 2009, The role of sulfur in the formation of magmatic-hydrothermal copper-gold deposits: Earth and Planetary Science Letters, v. 282, p. 323-328.
- Seo, J. H., Guillong, M., Aerts, M., Zajacz, Z. and Heinrich, C. A., 2011, Microanalysis of S, Cl, and Br in fluid inclusions by LA-ICP-MS: Chemical Geology, v. 284, p. 35-44.
- Seo, J. H., Guillong, M. and Heinrich, C. A., 2012, Separation of molybdenum and copper in porphyry deposits: The roles of sulfur, redox, and pH in ore mineral deposition at Bingham Canyon: Economic Geology, v. 107, p. 333-356.
- Sharp, J. E., 1978, A molybdenum mineralized breccia pipe complex, Redwell Basin, Colorado: Economic Geology, v. 73, p. 369-382.
- Shinohara, H., Kasahaya, K. and Lowenstern, J. B., 1995, Volatile transport in a convecting magma column: Implications for porphyry Mo mineralization: Geology, v. 23, p. 1091-1094.
- Sillitoe, R. H., 2010, Porphyry copper systems: Economic Geology, v. 105, p. 3-41.
- Sinclair, W. D., 2007, Porphyry deposits, *in* W. D. Goodfellow ed., Mineral deposits of Canada: A synthesis of major deposit-types, district metallogeny, the evolution of geological provinces, and exploration methods, Geological Association of Canada, Mineral Deposits Division, Special Publication, p. 223-243.
- Skjærnaa, L. and Pedersen, S., 1982, The effect of penetrative Sveconorwegian deformation on the Rb-Sr isotopic systems in the Rømskog-Aurskog-Høland area, SE Norway: Precambrian Research, v. 17, p. 215-243.
- Spandler, C., Pettke, T. and Rubatto, D., 2011, Internal and external fluid sources for eclogite-facies veins in the Monviso Meta-ophiolite, Western Alps; implications for fluid flow in subduction zones: Journal of Petrology, v. 52, p. 1207-1236.
- Starmer, I. C., 1972, The Sveconorwegian regeneration and earlier orogenic events in the Bamble series, south Norway: Norges Geologiske Undersøkelse, v. 277, p. 37-52.
- Starmer, I. C., 1985a, The evolution of the south Norwegian Proterozoic as revealed by the major and mega-tectonics of the Kongsberg and Bamble sectors, *in* A. C. Tobi and J. L. R. Touret eds., The deep Proterozoic crust in the North Atlantic provinces, NATO Advanced Study Institutes Series. Series C: Mathematical and Physical Sciences, p. 259-290.
- Starmer, I. C., 1985b, The geology of the Kongsberg district and the evolution of the entire Kongsberg sector, south Norway: Norges Geologiske Undersøkelse, v. 401, p. 35-58.
- Sun, S. S. and McDonough, W. F., 1989, Chemical and isotopic systematics of oceanic basalts: implications for mantle composition and processes, *in* A. D. Saunders and M. J.

- Norry eds., *Magmatism in the ocean basins*: London, Geological Society, Special Publications, p. 313-345.
- Sundvoll, B. and Larsen, B. T., 1982, Datings of major geological stress indicators in the development of a rift system: the Oslo paleorift: *Terra Cognita*, v. 2, p. 64.
- Sundvoll, B. and Larsen, B. T., 1990, Rb-Sr isotope systematics in the magmatic rocks of the Oslo Rift: *Norges Geologiske Undersokelse*, v. 418, p. 27-46.
- Sundvoll, B., Larsen, B. T. and Wandaas, B., 1992, Early magmatic phase in the Oslo Rift and its related stress regime: *Tectonophysics*, v. 208, p. 1-3.
- Taylor, S. R., 1964, Abundance of chemical elements in the continental crust: a new table: *Geochimica et Cosmochimica Acta*, v. 28, p. 1273-1285.
- Thomas, J. A. and Galey, J. T., 1982, Exploration and geology of the Mt. Emmons molybdenite deposits, Gunnison County, Colorado: *Economic Geology*, v. 77, p. 1085-1104.
- Tronnes, R. G. and Brandon, A. D., 1992, Mildly peraluminous high-silica granites in a continental rift: the Drammen and Finnemarka batholiths, Oslo Rift, Norway: *Contributions to Mineralogy and Petrology*, v. 109, p. 275-294.
- Tweto, O. and Sims, P. K., 1963, Precambrian ancestry of the Colorado mineral belt: *Geological Society of America Bulletin*, v. 74, p. 991-1014.
- Ulrich, T., Günther, D. and Heinrich, C. A., 2002, The evolution of a porphyry Cu-Au deposit, based on LA-ICP-MS analysis of fluid inclusions: Bajo de la Alumbrera, Argentina: *Economic Geology*, v. 97, p. 1889-1920.
- Walker, B. A., Miller, C. F., Lowery Claiborne, L., Wooden, J. L. and Miller, J. S., 2007, Geology and geochronology of the Spririt Mountain batholith, southern Nevada: Implications for timescales and physical processes of batholith construction: *Journal of Volcanology and Geothermal Research*, v. 167, p. 239-262.
- Wallace, S. R., 1995, Climax-type molybdenum deposits - What they are, where they are, and why they are: *Economic Geology*, v. 90, p. 1359-1380.
- Wallace, S. R., Muncaster, N. K., Johnson, D. C., MacKenzie, W. B., Brookstrom, A. A. and Surface, V. E., 1968, Multiple intrusion and mineralization at Climax, Colorado, A.I.M.E. Graton-Sales Volume, Number of 605-640 p.
- Wareham, C. D., Rice, C. M., Boyce, A. J. and Rogers, G., 1998, S, C, Sr, and Pb sources in the Pliocene Silver Creek Porphyry Mo System, Rice, Colorado: *Economic Geology*, v. 93, p. 32-46.
- Wark, D. A., Hildreth, W., Spear, F. S., Cherniak, D. J. and Watson, E. B., 2007, Pre-eruption recharge of the Bishop magma system: *Geology*, v. 35, p. 235-238.
- Westra, G. and Keith, S. B., 1981, Classification and genesis of stockwork molybdenum deposits: *Economic Geology*, v. 76, p. 844-873.
- White, W. H., Bookstrom, A. A., Kamilli, R. J., Ganster, M. W., Smith, R. P., Ranta, D. E. and Steininger, R. C., 1981, Character and origin of Climax-type molybdenum deposits:

Economic Geology v. 75th Anniversary Volume, p. 270-316.

Zajacz, Z., Halter, W. E., Pettke, T. and Guillong, M., 2008, Determination of fluid/melt partition coefficients by LA-ICP-MS analysis of co-existing fluid and silicate melt inclusions: controls on element partitioning: *Geochimica et Cosmochimica Acta*, v. 72, p. 2169-2197.

Zajacz, Z., Hanley, J. J., Heinrich, C. A., Halter, W. E. and Guillong, M., 2009, Diffusive reequilibration of quartz-hosted silicate melt and fluid inclusions: Are all metal concentrations unmodified?: *Geochimica et Cosmochimica Acta*, v. 73, p. 3013-3027.

Online references:

- 1 [http://minerals.cr.usgs.gov/dial/Henderson\\_Mo.html](http://minerals.cr.usgs.gov/dial/Henderson_Mo.html)
- 2 <http://rruff.geo.arizona.edu/>
- 3 <http://www.dst.unisi.it/geofluids-lab/default.html>
- 4 [http://pubs.usgs.gov/of/2000/ofr-00-0042/colo\\_boug.htm](http://pubs.usgs.gov/of/2000/ofr-00-0042/colo_boug.htm)

## ***6.4 Rapid Na, Cu exchange between synthetic fluid inclusions and external aqueous solutions: Evidence from LA-ICP-MS analysis***

Y. LI<sup>1,2,3</sup>, A. AUDÉTAT<sup>1</sup>, L. LERCHBAUMER<sup>1</sup> and X. L. XIONG<sup>2</sup>

<sup>1</sup>Bayerisches Geoinstitut, Universität Bayreuth, D-95440 Bayreuth, Germany

<sup>2</sup>Laboratory of Metallogenic Dynamics, Guangzhou Institute of Geochemistry, CAS, 510640, Guangzhou, P. R. China

<sup>3</sup>Graduate University of the Chinese Academy of Sciences, Beijing 100049, P. R. China

*Geofluids (2009) 9, 321-329.*

### **6.4.1 Abstract**

Three sets of equilibration experiments (Set 1 to Set 3) were performed in cold-seal pressure vessels to investigate the compositional modification of quartz-hosted fluid inclusions after entrapment. Each set of experiment consisted of two stages. In a pre-run, fluid inclusions containing 5-10 wt% NaCl and selected trace elements were synthesized at 700 °C / 140-200 MPa. These samples were then loaded into new capsules together with Cu-bearing solutions and some mineral buffers, and re-equilibrated at 600-800 °C and 70-140 MPa for 6-8 days. LA-ICP-MS analysis of individual fluid inclusions reveals that in re-equilibration experiments in which the outer fluid was composed of KCl ( $\pm$ FeCl<sub>2</sub>) up to 83 % of the original Na content of pre-existing fluid inclusions were lost, and up to 5660 ppm Cu were gained. Other elements with larger ionic radii (i.e., K, Fe, Ba, Sr) were not exchanged, demonstrating that the inclusions remained physically intact and that Na and Cu were transported through quartz by diffusion. The observed Na loss from pre-existing fluid inclusions correlates positively with Cu gain, with about 1 Cu atom being gained per 10 Na atoms lost. Thus, Na and Cu (plus probably H) were exchanged by interdiffusion. Remarkably, this processes resulted in up to 10 times higher Cu concentrations in re-equilibrated inclusions than were present in the outer fluid, i.e., Cu diffused "uphill". Large variations of Cu concentrations relative to the concentration of other elements are common also in natural fluid inclusion assemblages. However, no evidence for a correlation between Cu content and Na content was found so far, suggesting that Cu diffusion in natural samples

may be dominated by processes other than Na-Cu interdiffusion.

#### 6.4.2 Introduction

Fluid inclusions play an important role in understanding a large number of geological processes. Most of fluid inclusions studies are based on the assumptions that both the bulk volume and the chemical composition of the fluid inclusions remained constant since their formation. However, systematic studies on synthetic and natural fluid inclusions demonstrate that these two assumptions are not always fulfilled (e.g., Pecher, 1981; Gratier & Jenatton, 1984; Sterner & Bodnar, 1989; Hall & Bodnar, 1990; Bakker & Jansen, 1991; Hall & Sterner, 1993, 1995; Morgan et al., 1993; Mavrogenes & Bodnar, 1994; Sterner et al., 1995; Barker, 1995; Audétat & Günther, 1999; Ridley & Hagemann, 1999). Most of these studies demonstrate that water can be lost or gained from fluid inclusions due to pressure and/or water concentration gradients between the fluid inclusions and the surrounding environment. Hall & Sterner (1993) performed re-equilibration experiments during which synthetic fluid inclusions were subjected to large overpressure ( $P_{\text{int}} - P_{\text{conf}} = 150\text{-}400$  MPa), finding that preferential water loss resulted in a salinity increase by up to 22 wt% salt. Sterner et al. (1995) performed re-equilibration experiments at  $P_{\text{int}}=P_{\text{conf}}$  using external fluids that were compositionally different from the ones trapped in the fluid inclusions. Their results demonstrate that water diffuses towards the reservoir with lower  $\mu_{\text{H}_2\text{O}}$ . Diffusional loss of hydrogen has been invoked to explain the failure of chalcopyrite daughter crystals in natural brine inclusions to dissolve during heating experiments. After being equilibrated at high hydrogen pressure in a pressure vessel, the same inclusions show easy dissolution of the chalcopyrite daughter crystals during heating (Mavrogenes & Bodnar, 1994). Hydrogen diffusion has also been invoked to explain the gas composition of fluid inclusions in granulite facies rocks (e.g., Hall & Bodnar, 1990).

Similar to fluid inclusions, melt inclusions also experience postentrapmental modifications (Qin et al., 1992; Danyushevsky et al., 2000; Massare et al., 2002; Severs et al., 2007; Portnyagin et al., 2008). Recent experimental studies (Kamenetsky & Danyushevsky, 2005; Zajacz et al., 2008, 2009) revealed dramatic changes in the Na, Li, Cu and Ag content of quartz-hosted fluid and melt inclusions. Here, we confirm the findings of Zajacz et al.

(2009) regarding compositional change of quartz hosted fluid inclusions and provide further insights into the mechanisms responsible for these chemical modifications.

### 6.4.3 Experimental and analytical methods

Three sets of experiments were performed (Set 1, Set 2 and Set 3), each of which can be divided into a pre-run and a re-equilibration experiment (Table 6.4.1). In the pre-run, large, primary fluid inclusions were synthesized at 700 °C / 140 MPa (Set 1, Set 3) and 700 °C / 200 MPa (Set 2). In the re-equilibration experiment, the quartz pieces recovered from the pre-run were equilibrated in new solutions at 600 °C / 70 MPa (Set 1), 800 °C / 120 MPa (Set 2) and 700 °C / 140 MPa (Set 3).

**Table 6.4.1** Overview of run conditions and compositions of starting solutions

		Pre-run	Re-equilibration
<b>Set 1</b>	Conditions	700 °C / 140 MPa	600 °C / 70 MPa
	Starting solution	463 ppm Rb; 464 ppm Cs 5 wt% NaCl (19 670 ppm Na)	4 wt% KCl; 6 wt% FeCl <sub>2</sub> mineral buffers*
	Run time	5 days	8 days
<b>Set 2</b>	Conditions	700 °C / 200 MPa	800 °C / 120 MPa
	Starting solution	958 ppm Rb; 963 ppm Cs; 944 ppm Sr; 948 ppm Mn; 9.45 wt% NaCl (37 160 ppm Na)	20 wt% NaCl; 3 wt% S metallic Cu
	Run time	5 days	8 days
<b>Set 3</b>	Conditions	700 °C / 140 MPa	700 °C / 140 MPa
	Starting solution	501 ppm Rb; 499 ppm Cs; 5 wt% NaCl (19 670 ppm Na)	5 wt% KCl; 496 ppm S 50 ppm Cu; 410 ppm Ba
	Run time	5 days	6 days

\* see text

Primary fluid inclusions of the pre-runs were synthesized by the etched plate technique described in Duc-Tin et al. (2007) and Li & Audétat (2009). In this method, oriented quartz pieces measuring 3 x 3 x 6 mm were cut from inclusion-free, natural quartz in such a way that their longest dimension was parallel to the c-axis of the quartz crystal. By using a rough blade for the cutting and subsequently treating the quartz pieces for one hour in concentrated hydrofluoric acid, a rough surface consisting of deep, narrow etch channels was produced. Two such etched quartz pieces were loaded together with 0.05 g

silica glass and 100  $\mu\text{l}$  of an aqueous solution containing 5-10 wt% NaCl and 500-1000 ppm Rb, Cs, Sr and/or Mn (for exact concentrations, see Table 6.4.1) into platinum (Set 1) or gold (Set 2, Set 3) capsules of 4.0 cm length, 5.0 mm outer diameter and 4.6 mm inner diameter, which then were sealed by arc welding. The capsules were left in an oven at 150 °C for 24 hours to check for weight loss, which was not the case. Subsequently, the capsules were loaded into rapid quench pressure vessels of the design described in Matthews et al. (2003), using water as the pressure medium. Experimental run conditions were reached by first raising the pressure and then heating isobarically to the desired temperature. Overall uncertainties in the recorded pressures and temperatures are about 3 MPa and 10 °C, respectively. The samples were held at these P-T conditions for five days, and then the pressure vessels were removed from the furnaces and allowed to cool to room temperature within about 30 minutes. During cooling, the pressure inside the vessel followed an isochoric path defined by the volume of the vessel plus that of the pressure line. This experimental procedure resulted in a large number of fluid inclusions measuring 20-40  $\mu\text{m}$  in diameter, with some reaching sizes over 60  $\mu\text{m}$ .

In the re-equilibration experiments, the quartz pieces recovered from the pre-runs were loaded together with silica glass, sources for metals and anions (~0.001 g chalcopyrite-bornite-andalusite-orthoclase-biotite-magnetite in Set 1; 3 wt% S plus excess metallic Cu in Set 2; 100 ppm Cu in Set 3) and aqueous solutions containing 4 wt% KCl + 6 wt% FeCl<sub>2</sub> (Set 1), 20 wt% NaCl (Set 2), or 5 wt% KCl (Set 3) into gold or platinum capsules of similar size as in the pre-runs. The samples were put into the same pressure vessels as in the pre-runs and heated isobarically to 600 °C / 70 MPa (Set 1), 800 °C / 120 MPa (Set 2) or 700 °C / 140 MPa (Set 3), and kept at these conditions for 6-8 days. Whereas the re-equilibration conditions of Set 3 were the same as in the corresponding pre-run, those of the other two sets were situated along isochores of lower fluid density. As a consequence, primary fluid inclusions should have reached overpressures of 14 MPa in Set 1 and 155 MPa in Set 2 during re-equilibration. These values are calculated from the pressure difference between the imposed external pressure and the pressure along the pre-run fluid isochore at the given re-equilibration temperature.

In order to have an independent control on the composition of the external fluid during the

re-equilibration experiments we trapped some of this fluid in the form of secondary fluid inclusions. This was achieved by opening primary inclusions of the pre-run either mechanically before the start of the re-equilibration experiment (Set 1, Set 3), or during the re-equilibration experiment by in-situ cracking (Set 2; corresponding to the method described in Li & Audétat, 2009).

Quartz pieces recovered from the re-equilibration experiments were gently polished to obtain a flat sample surface. Microthermometric measurements of fluid salinities and fluid densities were performed using a Linkam THMSG 600 heating–freezing stage that was calibrated to an uncertainty of  $\sim 0.1$  °C between  $-56$  °C and  $0$  °C, and to  $\sim 0.5$  °C at  $374$  °C. Individual fluid inclusions were analyzed by Laser-ablation inductively-coupled-plasma mass-spectroscopy (LA-ICP-MS) at the Bayerisches Geoinstitut, using a Geolas M 193 nm ArF Excimer laser (Coherent / Lambda Physik) attached to an Elan DRC-e quadrupole mass spectrometer (Perkin Elmer Instruments). The laser was operated at a frequency of 10 Hz and output energy of 80 mJ, which resulted in an energy density of  $\sim 10$  J/cm<sup>2</sup> at the sample surface. The sample chamber was flushed with helium gas at a rate of 1 l/min. Measured isotopes were <sup>23</sup>Na, <sup>24</sup>Mg, <sup>27</sup>Al, <sup>29</sup>Si, <sup>39</sup>K, <sup>42</sup>Ca, <sup>49</sup>Ti, <sup>55</sup>Mn, <sup>57</sup>Fe, <sup>65</sup>Cu, <sup>85</sup>Rb, <sup>88</sup>Sr, <sup>133</sup>Cs, and <sup>197</sup>Au, using 10 ms dwell time per isotope. NIST SRM 610 glass was used as external standard and the concentrations of Cs or Rb in the starting solutions as internal standard for the fluid inclusions (see discussion). Great care was taken to open the inclusions in a controlled manner, such that no daughter crystals were lost during analysis. Overall uncertainties are about 10-20% relative for elements well above the detection limit, but may be higher for elements close to the detection limit (Heinrich et al., 2003). More details about the instrument and the quantification procedure can be found in Günther et al. (1998) and Heinrich et al. (2003).

#### 6.4.4 Results

Primary fluid inclusions recovered after the re-equilibration experiments looked optically the same as before the re-equilibration, except that they contained a small, opaque daughter crystal. There is no evidence that these inclusions leaked, as they do not contain any of the

elements that were present in the external fluid, except for Cu which was gained through diffusion (see below). Also, they are not surrounded by cracks or halos of secondary inclusions.

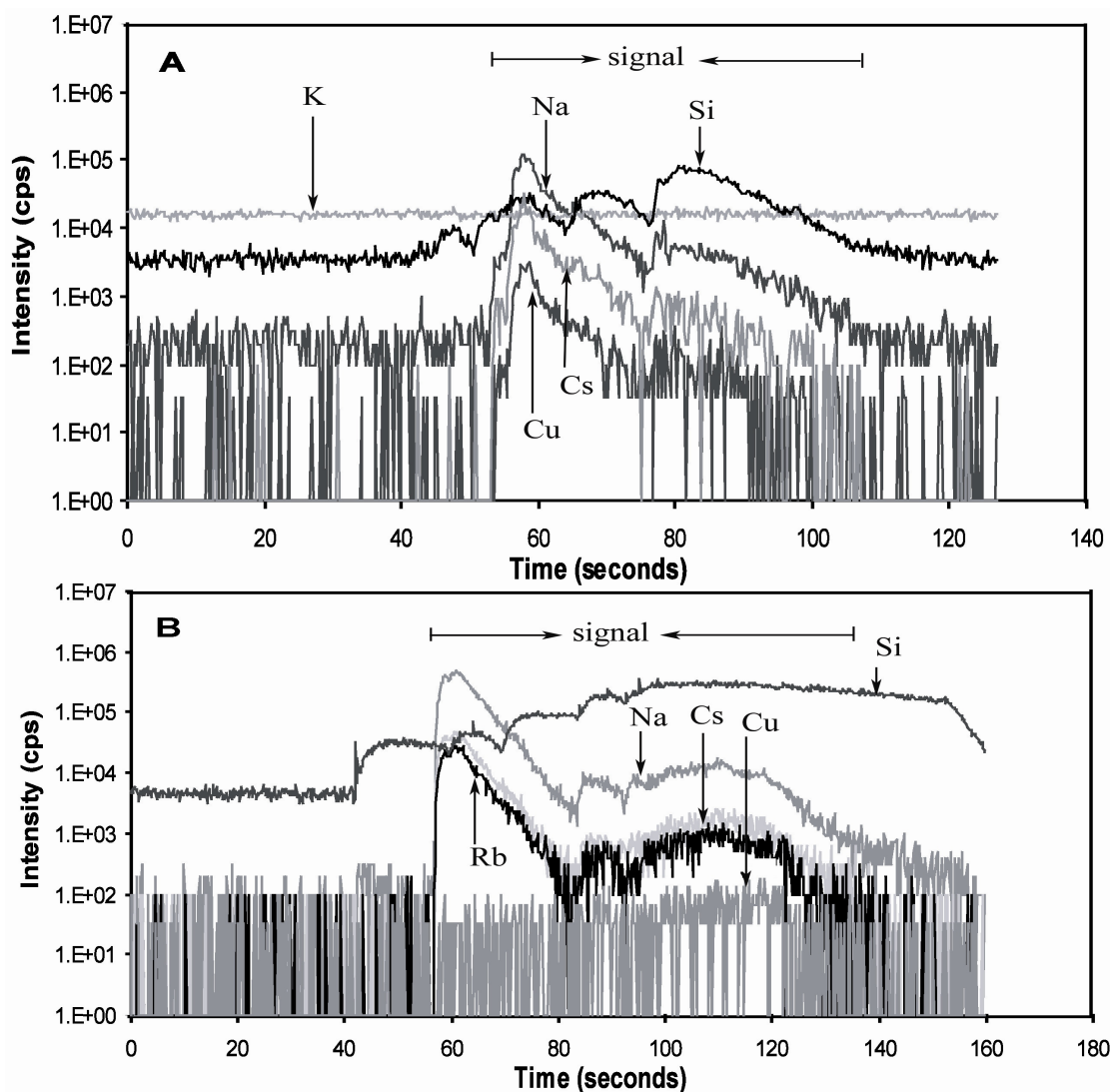


**Figure 6.4.1**

Typical LA-ICP-MS signals of two primary fluid inclusions. A from Set1, B from Set2. Note that no K but strong Cu, Na, and Cs signals are detected in A; in B, the Cu signal is very small compared to the Cu signal in A.

Ice melting temperatures ( $T_{m_{ice}}$ ) and liquid–vapor homogenization temperatures ( $T_{h_{tot}}$ ) of re-equilibrated fluid inclusions reveal the following apparent changes in fluid salinity (expressed as  $NaCl_{equiv}$ ) and fluid density (calculated from  $NaCl_{equiv}$  and  $T_{h_{tot}}$ ): Inclusions of Set 1 show a salinity of  $5.3 \pm 0.2$  wt%  $NaCl_{equiv}$  and a density of  $0.63 \pm 0.01$  g/cm<sup>3</sup> (compared

to 5.0 wt% NaCl and 0.50 g/cm<sup>3</sup> during the pre-run), those of Set 2 a salinity of 10.0 ± 0.5 wt% NaCl<sub>equiv</sub> and a density of 0.57 ± 0.01 g/cm<sup>3</sup> (compared to 9.45 wt% NaCl and 0.61 g/cm<sup>3</sup> during the pre-run), and those of Set 3 a salinity of 5.7 ± 0.1 wt% NaCl<sub>equiv</sub> and a density of 0.57 ± 0.02 g/cm<sup>3</sup> (compared to 5.0 wt% NaCl and 0.50 g/cm<sup>3</sup> during the pre-run). Between 12 and 18 re-equilibrated fluid inclusions and 9-15 secondary fluid inclusion of each set were analyzed by LA-ICP-MS. Typical signals are shown in Figure 6.4.1, and calculated compositions are listed in Table 6.4.2. Re-equilibrated fluid inclusions of Set 1 contain only Na, Rb, Cs and Cu, but no detectable K and Fe despite the fact that the latter two elements were major components in the external fluid (Table 6.4.1 and Figure 6.4.1). The lowest detection limit of 410 ppm K means that if there was any contamination by external fluid it must have been less than 2 % by weight. Based on 464 ppm Cs or 463 ppm Rb as internal standard a Na content of 3300 - 18440 ppm is calculated for these inclusions, which is 6-83 % lower than the 5.0 wt% NaCl present in the solution of the pre-run. On the other hand, they now contain 120 - 5660 ppm Cu, which element was not contained in the solution of the pre-run.

Re-equilibrated fluid inclusions analyzed from Set 2 contain 3-12 % higher Na concentrations than their original content of 9.5 wt% NaCl. Since the external fluid in this experiment contained 20 wt% NaCl, the observed increase in Na is not surprising. The amount of gained Cu is much lower than in Set 1 fluid inclusions, varying from 72 to 140 ppm.

In Set 3, in which fluid inclusions containing 5 wt% NaCl were reequilibrated in an external fluid containing 5 wt% KCl and ~20 ppm Cu at the same P-T-conditions as in the pre-run, 28-83 % of the Na were lost and 20-200 ppm Cu were gained.

**Table 6.4.2** LA-ICP-MS analyses of primary fluid inclusions

	Size (µm)	Na (ppm)	Fe <sup>+</sup> (ppm)	K <sup>+</sup> (ppm)	Cu (ppm)	Rb (ppm)	Sr (ppm)	Cs (ppm)	Na-loss (ppm)	Na-loss <sup>▼</sup> (%)
<b>Set1</b>	35	18440	<4220	<3280	120	480	n.a	464*	1230	6
	30	16050	<5300	<3290	170	440	n.a	464*	3620	18
	30	13710	<2600	<1980	770	400	n.a	464*	5960	30
	30	16990	<1860	<1620	220	470	n.a	464*	2680	14
	20	9190	<8940	<8920	2320	480	n.a	464*	10480	53
	25	15330	<1900	<1530	670	470	n.a	464*	4340	22
	30	15900	<790	<590	410	470	n.a	464*	3770	19
	40	10470	<600	<500	2300	480	n.a	464*	9200	47
	45	15490	<580	<410	1120	470	n.a	464*	4180	21
	40	16570	<2260	<1470	1340	460	n.a	464*	3100	16
	45	12930	<3320	<2510	590	580	n.a	464*	6740	34
	23	3460	<14790	<13230	5660	463*	<70	480	16210	82
	25	3300	<5600	<5720	4890	463*	<30	450	16370	83
	30	3710	<9900	<9340	3380	463*	<50	440	15960	81
	20	4370	<19360	<10730	5470	463*	<40	470	15300	78
30	6230	<11570	<10150	2330	463*	<40	440	13440	68	
25	11300	<10400	<8730	1320	463*	<30	450	8370	43	
	Size (µm)	Na (ppm)	Fe <sup>+</sup> (ppm)	K <sup>+</sup> (ppm)	Cu (ppm)	Rb (ppm)	Sr (ppm)	Cs (ppm)	Na-loss (ppm)	Na-loss <sup>▼</sup> (%)
<b>Set2</b>	25	41000	n.a	n.a	93	859*	900	830	3840	10
	30	40390	n.a	n.a	100	859*	880	780	3230	9
	35	39100	n.a	n.a	140	859*	900	840	1940	5
	32	38230	n.a	n.a	86	859*	870	860	1070	3
	25	39770	n.a	n.a	85	859*	910	840	2610	7
	20	41640	n.a	n.a	94	859*	930	870	4480	12
	45	40940	n.a	n.a	72	859*	920	850	3780	10
	30	38180	n.a	n.a	66	859*	880	830	1020	3
	23	40980	n.a	n.a	97	859*	920	840	3820	10
	22	38780	n.a	n.a	91	859*	920	840	1620	4
	40	41070	n.a	n.a	74	859*	950	880	3910	11
	25	39910	n.a	n.a	90	859*	1000	840	2750	7
		Size (µm)	Na (ppm)	Fe <sup>+</sup> (ppm)	K <sup>+</sup> (ppm)	Cu (ppm)	Rb (ppm)	Sr (ppm)	Cs (ppm)	Na-loss (ppm)
<b>Set3</b>	45	10440	n.a	<3460	88	501*	<9	467	9230	47
	45	3590	n.a	<3120	96	501*	<8	460	16080	82
	45	3310	n.a	<1780	115	501*	<7	459	16360	83
	35	4160	n.a	<4650	104	501*	<17	457	15510	79
	45	4150	n.a	<4360	204	501*	<22	485	15520	79
	30	4070	n.a	<4880	86	501*	<17	539	15600	79
	40	9150	n.a	<3810	44	501*	<13	446	10520	54
	40	7830	n.a	<6340	55	501*	<22	452	11840	60
	40	7900	n.a	<5250	153	501*	<14	435	11770	60
	80	9810	n.a	<1650	98	501*	<6	461	9860	50
	80	14200	n.a	<950	22	501*	<3	501	5470	28
	50	6730	n.a	<2480	69	501*	<10	495	12940	66
	30	12270	n.a	<3550	39	501*	<13	466	7400	38
	25	8950	n.a	<9460	140	501*	<33	537	10720	55
	20	9180	n.a	<10840	84	501*	<42	490	10490	53
30	8610	n.a	<2880	61	501*	<11	442	11060	56	
30	4610	n.a	<14430	142	501*	<24	492	15060	77	

<sup>+</sup> Below detection limit; \* internal standard; <sup>▼</sup> relative to the original Na concentration of 19670 ppm (Set 1, Set 3) and 37160 ppm (Set 2).

## 6.4.5 Discussion

### 6.4.5.1 *Accuracy of LA-ICP-MS quantification*

In order to transform the element concentration ratios determined by LA-ICP-MS into absolute concentrations, the absolute concentration of one element in each fluid inclusion has to be known. For this reason, known amounts of Rb and Cs have been added to the solutions used in the pre-runs. Due to the large ionic radius of these elements they are unlikely to have diffused through quartz in significant amounts at our experimental conditions (e.g., Zajacz, 2009). However, they could have been incorporated into precipitating mineral phases during the pre-run, or their concentrations could have changed as a result of gains or losses of water, sodium or other major fluid components. Fluid inclusions analyzed after the pre-runs of Set 2 and Set 3 contain Rb/Cs/Na-ratios that are slightly different from those in the starting solutions, suggesting that ~10 % of Rb and Cs were lost during the pre-run of Set 2 (Li & Audétat, 2009) and ~10 % Cs were lost during the pre-run of Set 3. Although this situation certainly is not perfect we like to point out that an uncertainty of 10 % is negligible compared to the up to 10-fold changes in element concentrations observed during re-equilibration.

In view of the large amounts of Na lost from fluid inclusions during the re-equilibration in Set 1 and Set 3 (up to 81 % Na lost in Set 1; up to 83 % lost in Set 3) and the observed changes in fluid density we need to discuss the possibility that the concentrations of Rb and Cs changed indirectly due to gains or losses of major elements. As shown above, fluid densities in these two sets increased relative to the starting density by 0.07-0.13 %, which means that 0.07-0.13 % of mass would have been gained if the volume of the inclusion stayed constant. Replacing the lost Na<sup>+</sup> by H<sup>+</sup> (see below) has no significant effect on fluid density. Thus, if the increase in fluid density were due to the gain of mass (most likely H<sub>2</sub>O), then the fluid salinity and the concentrations of Rb and Cs should have decreased by 0.07-0.13 % relative. However, apparent fluid salinities in re-equilibrated fluid inclusions in Set 1 and Set 3 are slightly higher than after the pre-run. The shift to higher apparent fluid salinities can be explained by a replacement of Na<sup>+</sup> ions by H<sup>+</sup> ions (see below), as the ice melting temperature of a 0.9 molal HCl solution ( $T_{m_{ice}} = -3.7$  °C; Marion, 2002; corresponding to 6.0 wt% NaCl<sub>equiv</sub>) is slightly higher than that of a 0.9 molal

(5.0 wt%) NaCl solution ( $T_{m_{ice}} = -3.0\text{ }^{\circ}\text{C}$ ). The replacement of 30-80%  $\text{Na}^+$  by  $\text{H}^+$  results in apparent fluid salinities of 5.3-5.8 wt%  $\text{NaCl}_{equiv}$ , which is in agreement with the observed values. If there were an additional gain of 0.07-0.13 %  $\text{H}_2\text{O}$  the apparent fluid salinities should be all below 5.2 wt%  $\text{NaCl}_{equiv}$ , which is not the case. Thus, our preferred interpretation of the microthermometric data of Set 1 and Set 3 is that the mass of fluid contained in the inclusions stayed approximately constant, but that the inclusion volume slightly decreased during the exchange of  $\text{Na}^+$  by  $\text{H}^+$ .

In Set 2 the apparent fluid salinity, the fluid density and the Na/X concentration ratios all changed by less than 10 %, so there is no reason to assume that absolute element concentrations changed by more than this value.

Taken together with the apparent loss of 10 % Cs ( $\pm\text{Rb}$ ) during the pre-runs and uncertainties associated with the external standardization, overall uncertainties in calculated absolute element concentrations are considered to be  $\pm 10\text{-}20\text{ }%$  relative.

#### *6.4.5.2 Cu, Na diffusion in primary fluid inclusions*

Experimental studies (Verhoogen, 1952; Kats, 1962; Rybach & Laves, 1967; Frischat, 1970) have shown that small, single-charged ions such as  $\text{H}^+$ ,  $\text{Li}^+$ ,  $\text{Na}^+$ ,  $\text{Cu}^+$ , and  $\text{Ag}^+$  have very high diffusion coefficients in quartz and can be mobilized due to concentration gradients (Rybach & Laves, 1967) as well as electric fields (Verhoogen, 1952; Kats, 1962). Recent experimental studies on quartz-hosted silicate melt inclusions and fluid inclusions (Kamenetsky & Danyushevsky, 2005; Zajacz et al., 2009) confirm rapid diffusion of  $\text{H}^+$ ,  $\text{Li}^+$ ,  $\text{Na}^+$ ,  $\text{Cu}^+$ , and  $\text{Ag}^+$  under hydrothermal and magmatic conditions. Kamenetsky & Danyushevsky (2005) performed heating experiments with quartz-hosted melt inclusions from the Taupo rhyolites in a muffle furnace and analyzed both unheated and heated inclusions by LA-ICP-MS. Re-heated melt inclusions were found to contain systematically higher Cu and Ag contents than unheated ones, with Cu contents having risen from 2.76 ppm to 396 ppm and Ag contents from  $< 1$  ppm to 97 ppm. Similar experiments performed by Zajacz et al. (2009) in cold seal pressure vessels showed that Li, Na, Cu and Ag concentrations in silicate melt inclusions can be increased by more than two orders of magnitude if homogenized in a Li, Na, Cu, and Ag-rich environment, and can be depleted

in these elements by up to two orders of magnitude if homogenized in a metal-free environment. A similar behavior was observed with re-equilibrated fluid inclusions. In one experiment in which natural fluid inclusions containing  $7 \pm 4$  ppm Cu were equilibrated in an external fluid containing 5 wt%  $\text{CuCl}_2$ , they subsequently were found to contain  $2000 \pm 400$  ppm Cu.

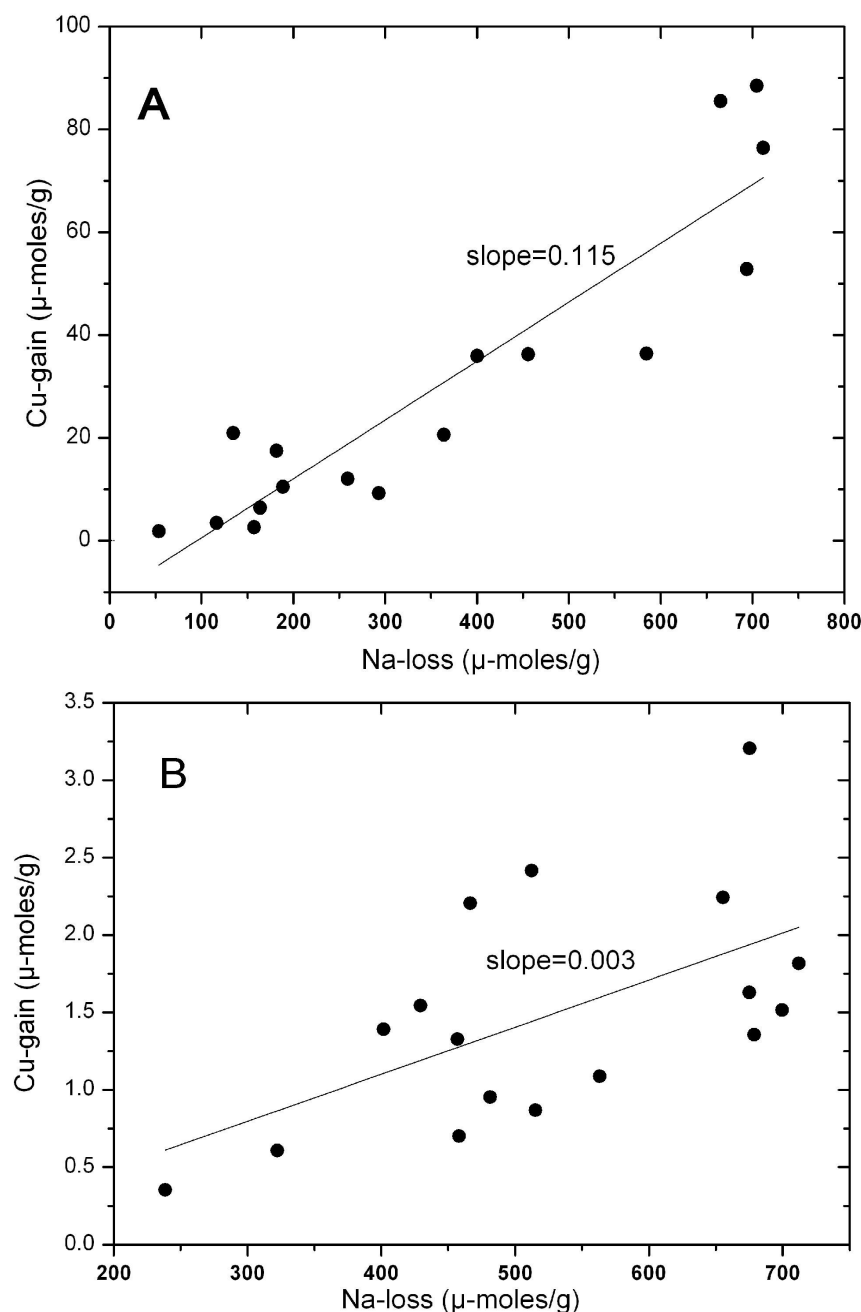


**Figure 6.4.2**

Na loss versus Cu gain in primary fluid inclusions in (A) Set 1 and (B) Set 3. Linear regression of the data (ppm converted into  $\mu\text{-moles/g}$ ) gives slopes of about 0.115 and 0.0028, respectively, which means that another cation (e.g.,  $\text{H}^+$ ) is needed to satisfy the charge balance in the inclusions.

In our experiments, fluid inclusions equilibrated in an external fluid containing zero NaCl, lost 6-83 % of their original Na content in Set 1, and 28-83 % of their original Na content in Set 3. At the same time, 120-5660 ppm Cu were gained in Set 1 (which external fluid contained excess Cu in form of copper iron sulfides), and 20-200 ppm Cu in Set 3 (which external fluid contained a small amount of dissolved CuCl). Remarkably, the amount of Cu gained in re-equilibrated inclusions is often higher than the Cu concentration in the external fluid. In Set 3 the external fluid contained  $19 \pm 6$  ppm dissolved Cu (some Cu was lost to the Pt-capsule; Table 6.4.1), whereas re-equilibrated fluid inclusions contained up to 204 ppm Cu (average: 94 ppm Cu). The same qualitative behavior can be observed in Set 1, although things are complicated by the fact that the external fluid was in the two-phase field. Copper contents of re-equilibrated fluid inclusions range from 120 ppm to 5660 ppm. In contrast, the vapor phase of the external fluid (which made up 97 vol% of the bulk fluid) contained only 200 ppm to 600 ppm Cu. No brine inclusions were found in this experiment, but a later experiment performed under identical conditions produced brine inclusion containing 3000 ppm to 3500 ppm Cu and vapor inclusions containing 200 ppm to 1000 ppm Cu. Thus, even if the 3000 ppm to 3500 ppm Cu in the brine is taken as reference, there must have been uphill Cu diffusion to explain the highest Cu contents observed in re-equilibrated inclusions. The large variation in diffusional gains/losses of Na and Cu in different inclusions from the same experiment may be related to the different depths and volumes of the analyzed fluid inclusions (Hall & Sterner, 1993). If the amounts of Cu gained during Set 1 and Set 3 are plotted against the amounts of Na that were lost (Figure 6.4.2), a positive correlation is evident, with a linear regression slope of  $\sim 0.1$  (Set 1) and  $\sim 0.003$  (Set 3) on a molecular basis. Thus, the processes of Na-loss and Cu-gain were coupled to each other. However, the slopes of the linear regressions suggest that maximal 10 % of the lost  $\text{Na}^+$  ions were replaced by  $\text{Cu}^+$  ions, implying that the inclusions would have become negatively charged if no other positively charged ions were gained to satisfy the charge balance. The most likely source of other positively charged ions is  $\text{H}^+$ , which was available in the external fluid and can easily diffuse through quartz (Kats, 1962). Sodium would thus have been exchanged by  $\text{Cu}^+$  and  $\text{H}^+$ , with the latter recombining with left behind  $\text{Cl}^-$  to form HCl. This interpretation is supported by

the microthermometric data discussed above. In this scenario, the driving force for  $H^+$  and  $Cu^+$  diffusion is electrochemical potential, and the uphill Cu diffusion could be the result of a change in pH, which in turn controls Cu solubility. In Set 2, in which fluid inclusions containing 10 wt% NaCl were equilibrated in an external fluid containing about 20 wt% NaCl, primary fluid inclusions gained both Na (3-12 % relative) and Cu (72-140 ppm). In this case, the amount of gained Cu is much lower than that amount of Cu dissolved in the external fluid (300 ppm to 600 ppm Cu in the vapor; 1500 ppm to 4000 ppm Cu in the brine), and no correlation exists between Na-gain and Cu-gain (Figure 6.4.3). Thus, in contrast to Set 1 and Set 3, Cu diffusion in this set was simply driven by a concentration gradient rather than by interdiffusion.

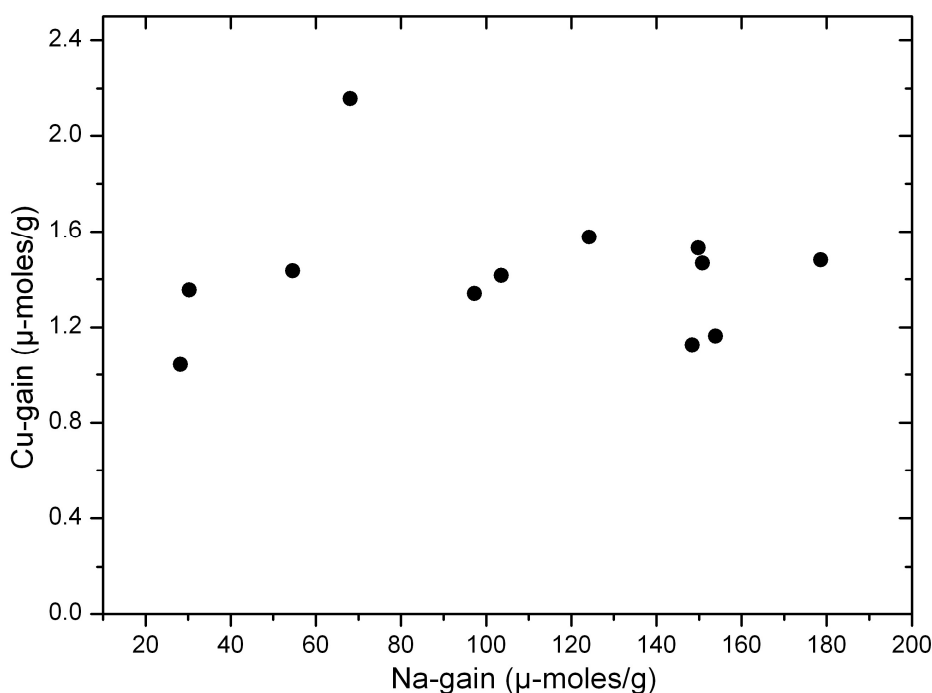


**Figure 6.4.3**

Na-gain versus Cu-gain in primary fluid inclusions of Set 2. Notice that there is no correlation between the two elements (ppm converted into  $\mu$ -moles/g).

#### 6.4.6 Implications

Our experiments confirm recent results of Kamenetsky & Danyushevsky (2005) and Zajacz et al. (2009), which demonstrate that the concentration of Na and Cu (and that of other small, single-charged cations such as Li and Ag) in fluid inclusions can easily be modified by

diffusional processes. Our results additionally demonstrate that the diffusion of trace elements can be linked to the diffusion of major elements into the opposite direction. LA-ICP-MS analyses of natural fluid inclusion assemblages (i.e., populations of fluid inclusion that were trapped at the same time) commonly show a larger variation in Cu concentrations than other elements of similar or higher abundance (e.g., Günther et al., 1998; Ulrich et al., 2002; Landtwing et al., 2005; Klemm et al., 2007, 2008). For example, of 19 major, minor and trace elements analyzed in 39 brine inclusions along a pseudosecondary trail in quartz from the Mole Granite (Australia), all concentrations were reproducible within  $\leq 21\%$  standard deviation except for Cu (721 % stdev), Ag (25 % stdev), Mg (151 % stdev; at detection limit) and Ce (25 % stdev; at detection limit) (Günther et al., 1998). Although part of this large variation could be explained by co-entrapment of Cu-rich vapor (as the analyzed brine inclusions were trapped in the two-phase field and Cu fractionates into the vapor phase), it cannot explain a more than 10-fold enrichment of Cu without significant impact on fluid salinity. To increase the Cu content from 100 ppm Cu in a 50 wt% NaCl<sub>equiv</sub> brine inclusion to 1000 ppm Cu by addition of 3 wt% NaCl<sub>equiv</sub> vapor containing 3000 ppm of Cu (estimated from Audétat et al., 2000) 33 % vapor (by weight) would have to be admixed to 67 % brine, which would result in a fluid salinity of 35 wt% NaCl<sub>equiv</sub> in the mixed inclusion. However, microthermometric measurements demonstrate that fluid salinities of brine inclusions with high Cu concentrations are the same as neighboring brine inclusions with low Cu concentrations. Similarly large variations in Cu concentrations relative to that of other elements well above the detection limit are observed also in populations of supercritical fluids, where co-entrapment of a Cu-rich vapor phase is not possible. Another explanation for anomalously high Cu concentrations in natural fluid inclusions is accidental entrapment of Cu-bearing solids, which may not be detectable in other elements if the Cu-content of the solid is high (such as in intermediate solid solutions, for example). Finally, Cu contents can vary if Cu-bearing daughter crystals are lost during analysis. While some inclusions indeed may have lost some Cu by this process the most anomalous Cu values are higher than the majority of the inclusions rather than too low, requiring another explanation. Although we cannot rule out that accidental entrapment of Cu-rich solids lead to variable Cu contents in certain natural fluid inclusion assemblages we

believe that Cu-diffusion due to concentration gradients and/or electrochemical potentials is more common considering the long re-equilibration times available in nature. However, Na–Cu interdiffusion of the type observed in our experimental Set 1 and Set 3 does not seem to be widespread in nature, as measured Na/X-concentration ratios (with X representing any other major or minor cation except for Cu<sup>+</sup> and maybe Li<sup>+</sup> and Ag<sup>+</sup>) typically are rather constant and in agreement with solubility constraints from fluid–rock equilibria.

#### **6.4.7 Conclusions**

- 1) Given large enough concentration gradients or electrochemical potentials, large amounts of Cu and Na can diffuse into or out of fluid inclusions at 600–800 °C within a few days.
- 2) The positive correlation between Na loss and Cu gain observed in fluid inclusions equilibrated in Na-free external fluids suggests a direct link between the two phenomena. Since the number of lost Na<sup>+</sup> ions is about 10 times higher than the number of gained Cu<sup>+</sup> ions we propose that Cu-diffusion was accompanied by large amounts of H<sup>+</sup> diffusion to satisfy the charge balance.
- 3) The amount of Cu gained in some re-equilibrated inclusions was higher than the amount of Cu present in the surrounding fluid, which could be due to a coupling with H<sup>+</sup> via fluid pH.
- 4) Reproducibilities of element concentrations in natural fluid inclusion assemblages suggest that diffusional gain or loss of Cu may be a common phenomenon also in nature, but so far no evidence for interdiffusion with Na was found.

#### **6.4.8 Acknowledgements**

We like to thank Thomas Pettke and Kirill Shmulovich for their constructive reviews, and Sumit Chakraborty and Hans Keppler for helpful comments regarding diffusion processes. This work was supported by grants from Bayerisches Geoinstitut, Universität Bayreuth, Germany, the NBRP of China (2007CB411303) and the NNSF of China (90714011,

40825010).

#### 6.4.9 References

- Audétat A, Günther D (1999) Mobility and H<sub>2</sub>O-loss from fluid inclusions in natural quartz crystals. *Contributions to Mineralogy and Petrology*, **137**, 1-14.
- Audétat A, Günther D, Heinrich CA (2000) Causes for large-scale metal zonation around mineralized plutons: Fluid inclusion LA-ICP-MS evidence from the Mole Granite, Australia. *Economic Geology*, **95**, 1563-81.
- Bakker RJ, Jansen JBH (1991) Experimental post-entrapment water loss from synthetic CO<sub>2</sub>-H<sub>2</sub>O inclusions in natural quartz. *Geochimica et Cosmochimica Acta*, **55**, 2215-30.
- Barker AJ (1995) Post-entrapment modification of fluid inclusions due to overpressure: evidence from natural samples. *Journal of Metamorphic Geology*, **13**, 737-50.
- Danyushevsky LV, Della-Pasqua FN, Sokolov S (2000) Re-equilibration of melt inclusions trapped by magnesian olivine phenocrysts from subduction-related magmatism: petrological implications. *Contributions to Mineralogy and Petrology*, **138**, 68-83.
- Duc-Tin Q, Audetat A, Keppler H (2007) Solubility of tin in (Cl, F)-bearing aqueous fluid at 700 °C, 140 MPa: A LA-ICP-MS study on synthetic fluid inclusions. *Geochimica et Cosmochimica Acta*, **71**, 3323-35.
- Frischat GH (1970) Sodium diffusion in natural quartz crystals. *Journal of the American Ceramic Society*, **53**, 357.
- Goldstein, R. H. and Reynolds, T. J., (1994) Systematics of fluid inclusions in diagenetic minerals. *Society for Sedimentary Geology Short Course Notes* **31**, 199.
- Gratier JP, Jenatton L (1984) Deformation by solution-deposition, and re-equilibration of fluid inclusions in crystals depending on temperature, internal pressure and stress. *Journal of Structure Geology*, **6**, 189-200.
- Günther D, Audétat A, Frischknecht R, Heinrich CA (1998) Quantitative analysis of major, minor and trace elements in fluid inclusions using Laser Ablation-Inductively Coupled Plasma-Mass Spectrometry (LA-ICP-MS). *Journal of Analytical Atomic Spectrometry*, **13**, 263-70.
- Hall DL, Bodnar RJ (1990) Methane in fluid inclusions from granulites: A product of hydrogen diffusion? *Geochimica et Cosmochimica Acta*, **54**, 641-51.
- Hall DL, Sterner SM (1993) Preferential water-loss from synthetic fluid inclusions. *Contributions to Mineralogy and Petrology*, **114**, 489-500.
- Hall DL, Sterner SM (1995) Experimental diffusion of hydrogen into synthetic fluid inclusions in quartz. *Journal of Metamorphic Geology*, **13**, 345-55.
- Heinrich CA, Pettke T, Halter W, Aigner-Torres M, Audétat A, Günther D, Hattendorf B, Bleiner D, Guillong M, Horn I (2003) Quantitative multi-element analysis of minerals, fluid and melt inclusions by laser-ablation inductively-coupled-plasma mass-spectrometry.

- Geochimica et Cosmochimica Acta*, **67**, 3473-96.
- Kamenetsky VS, Danyushevsky LV (2005) Metals in quartz-hosted melt inclusions: Natural facts and experimental artifacts. *American Mineralogist*, **90**, 1674-78.
- Kats A (1962) Hydrogen in alpha-quartz. *Philips Research Reports*, **17**, 133-95.
- Klemm L, Pettke T, Heinrich CA (2007) Hydrothermal evolution of the El Teniente deposit, Chile: porphyry Cu-Mo ore deposition from low-salinity magmatic fluids. *Economic Geology*, **102**, 1021-45.
- Klemm L, Pettke T, Heinrich CA (2008) Fluid source and magma evolution of the Questa porphyry Mo deposit, New Mexico, USA. *Mineralium Deposita*, **43**, 533-52.
- Landtwing MR, Pettke T, Halter WE, Heinrich CA, Redmond PB, Einaudi MT, Kunze K (2005) Copper deposition during quartz dissolution by cooling magmatic-hydrothermal fluids: The Bingham porphyry. *Earth and Planetary Science Letters*, **235**, 229-43.
- Li Y, Audéat A (2009) A method to synthesize large fluid inclusions in quartz at controlled times and under unfavorable growth conditions. *American Mineralogist*, **94**, 367-71.
- Marion GM (2002) A molal-based model for strong acid chemistry at low temperature (<200 to 298 K). *Geochimica et Cosmochimica Acta*, **66**, 2499-516.
- Massare D, Metrich N, Clocchiatti R (2002) High-temperature experiments on silicate melt inclusions in olivine at 1 atm: inference on temperatures of homogenization and H<sub>2</sub>O concentrations. *Chemical Geology*, **183**, 87-98.
- Matthews W, Linnen RL, Guo Q (2003) A filler-rod technique for controlling redox conditions in cold-seal pressure vessels. *American Mineralogist*, **88**, 701-7.
- Mavrogenes JA, Bodnar RJ (1994) Hydrogen movement into and out of fluid inclusions in quartz: experimental evidence and geologic implications. *Geochimica et Cosmochimica Acta*, **58**, 141-8.
- Morgan GB, Chou IM, Pasteris JD, Olsen SN (1993) Re-equilibration of CO<sub>2</sub> fluid inclusions at controlled hydrogen fugacities. *Journal of Metamorphic Geology*, **11**, 155-64.
- Pecher A (1981) Experimental decrepitation and re-equilibration of fluid inclusions in synthetic quartz. *Tectonophysics*, **78**, 567-83.
- Portnyagin M, Almeev R, Matveev S, Holtz F (2008) Experimental evidence for rapid water exchange between melt inclusions in olivine and host magma. *Earth and Planetary Science Letters*, **272**, 541-52.
- Qin Z, Alfred FL, Anderson JR (1992) Diffusive reequilibration of melt and fluid inclusions. *American Mineralogist*, **77**, 565-76.
- Ridley J, Hagemann SG (1999) Interpretation of post-entrapment fluid-inclusion re-equilibration at the Three Mile Hill, Marvel Loch and Griffins Find high-temperature lode-gode deposits, Yilgarn Craton, Western Australia. *Chemical Geology*, **154**, 257-78.
- Rybach L, Laves F (1967) Sodium diffusion experiments in quartz crystals. *Geochimica et Cosmochimica Acta*, **31**, 539-46.

Severs MJ, Azbej T, Thomas JB, Mandeville CV, Bodnar RJ (2007) Experimental determination of H<sub>2</sub>O loss from melt inclusions during laboratory heating: Evidence from Raman spectroscopy. *Chemical Geology*, **237**, 358-71.

Sterner SM, Bodnar RJ (1989) Synthetic fluid inclusions VII. Re-equilibration of fluid inclusions in quartz during laboratory-simulated metamorphic burial and uplift. *Journal of Metamorphic Geology*, **7**, 243-60.

Sterner SM, Hall DL, Keppler H (1995) Compositional re-equilibration of fluid inclusions in quartz. *Contributions to Mineralogy and Petrology*, **119**, 1-15.

Ulrich T, Günther D, Heinrich CA (2002) The evolution of a porphyry Cu-Au deposit, based on LA-ICP-MS analysis of fluid inclusions: Bajo de la Alumbrera, Argentina. *Economic Geology*, **97**, 1889-920.

Verhoogen J (1952) Ionic diffusion and electrical conductivity in quartz. *American Mineralogist*, **37**, 637-55.

Zajacz Z, Halter WE, Pettke T, Guillong M (2008) Determination of fluid/melt partition coefficients by LA-ICPMS analysis of co-existing fluid and silicate melt inclusions: Controls on element partitioning. *Geochimica et Cosmochimica Acta*, **72**, 2169-97.

Zajacz Z, Hanley J, Heinrich CA, Halter WE, Guillong M (2009) Diffusive reequilibration of quartz-hosted silicate melt and fluid inclusions: Are all metal concentrations unmodified? *Geochimica et Cosmochimica Acta*, **73**, 3013-27.

## ACKNOWLEDGEMENTS

First, I want to express my gratitude to my ad- and super-visor Andreas Audétat, who set up this project, raise the DFG-money, made it possible for me to work and study at BGI, and introduced me to the great world of ore deposits. I especially thank him for his abundance of patience, helpfulness, and his persistency in his idea, even if others were of another opinion. Furthermore, I have to thank Prof. Hans Keppler for scientific advice and especially for extra funding, which gave me the opportunity to stay a few months longer and finish my work finally with great outcome.

Lydia, Uwe, Detlef, Hubert, Stefan, Sven, Gerti, and Petra thank you for all your help and making every day a little bit nicer! Sincere thanks are also given to my officemates Vincenzo, Willem, Dennis, Kostya, Sushant, Julien, and Ana who always had some good advice. The same applies to Antje, Martha, Geertje, Vojtěch, Clemens, Diego, Davide, Stephan, Giacomo, Valerio, Jochen and Markus. Thank you for all the wonderful weekends out climbing, hiking, and biking, for all the funny parties and lunch breaks and above all, for your friendship!

Vicky, Christine, Nessi, and Nic, with your friendship and support you made a great contribution to the completion of my work. You always jollied me along, even in the darkest days. I also want to thank all my friends back in Vienna who were always there, ready for a beer, as soon as I got off the train.

Der größte Dank gilt jedoch meiner Familie in Mallnitz und Dölsach. Papa und Mama, ich danke euch aus tiefstem Herzen für all die Unterstützung ohne die ich heute nicht hier wäre. Oma, danke, dass du mich immer daran erinnerst, was wirklich wichtig ist und worauf es ankommt im Leben.

Abschließend möchte ich meinem Freund und Gefährten Gerd für sein Vertrauen, seine bedingungslose Unterstützung und die aufmunternden Worte und Taten danken, die mich sicher durch diese schwierigen Jahre gebracht haben. DANKE!

## ERKLÄRUNG

Hiermit erkläre ich, dass ich die vorliegende Arbeit selbständig verfasst und keine anderen als die von mir angegebenen Quellen und Hilfsmittel benutzt habe. Die aus fremden Quellen direkt oder indirekt übernommenen Gedanken sind als solche kenntlich gemacht.

Ferner erkläre ich, dass ich nicht anderweitig versucht habe, mit oder ohne Erfolg, eine Dissertation einzureichen und auch keine gleichartige Doktorprüfung an einer anderen Hochschule endgültig nicht bestanden habe.

Bayreuth, Mai 2012

Linda Lerchbaumer